AD-A119 084 AIR FORCE INST OF TECH WRIGHT-PATTERSON AFB OH F/G 1/3
COMMAND AUGMENTATION INCORPORATING DIRECT SIDE FORCE CONTROL AN--ETC(U)
MAY 82 S L BRUNWALD
UNCLASSIFIED AFIT/CI/NR/82-39T NL

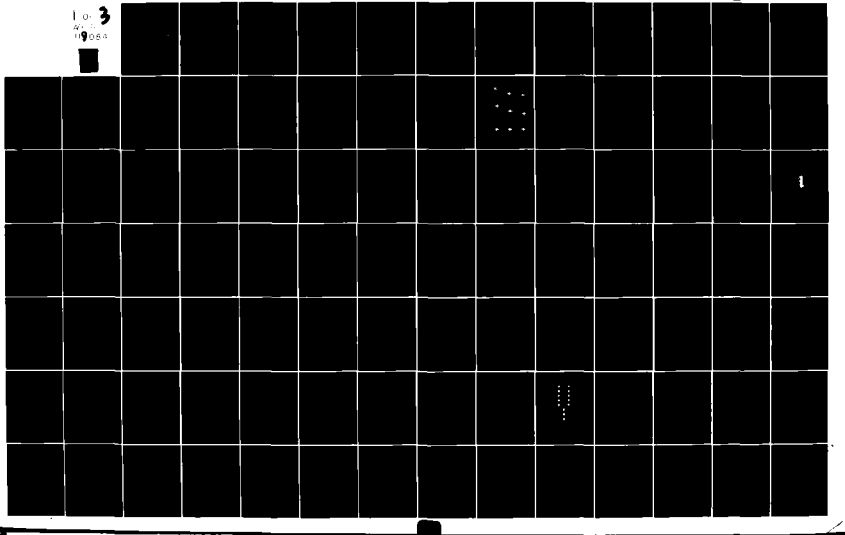

UNCLASS

SECURITY CLASSIFICATION OF THIS PAGE *(When Data Entered)*

REPORT DOCUMENTATION PAGE	READ INSTRUCTIONS BEFORE COMPLETING FORM
1. REPORT NUMBER: AFIT/CI/NR/82-39T	2. GOVT ACCESSION NO.: AD A119084
3. RECIPIENT'S CATALOG NUMBER	
4. TITLE *(and Subtitle)*: Command Augmentation Incorporating Direct Side Force Control and Microprocessor Technology	5. TYPE OF REPORT & PERIOD COVERED: THESIS/DISSERTATION
	6. PERFORMING ORG. REPORT NUMBER
7. AUTHOR(s): Scott L. Grunwald	8. CONTRACT OR GRANT NUMBER(s)
9. PERFORMING ORGANIZATION NAME AND ADDRESS: AFIT STUDENT AT: Princenton University	10. PROGRAM ELEMENT, PROJECT, TASK AREA & WORK UNIT NUMBERS
11. CONTROLLING OFFICE NAME AND ADDRESS: AFIT/NR WPAFB OH 45433	12. REPORT DATE: May 1982
	13. NUMBER OF PAGES: ?
14. MONITORING AGENCY NAME & ADDRESS *(if different from Controlling Office)*	15. SECURITY CLASS. *(of this report)*: UNCLASS
	15a. DECLASSIFICATION/DOWNGRADING SCHEDULE

16. DISTRIBUTION STATEMENT *(of this Report)*

APPROVED FOR PUBLIC RELEASE; DISTRIBUTION UNLIMITED

17. DISTRIBUTION STATEMENT *(of the abstract entered in Block 20, if different from Report)*

18. SUPPLEMENTARY NOTES

APPROVED FOR PUBLIC RELEASE: IAW AFR 190-17

30 AUG 1982

LYNN E. WOLAVER
Dean for Research and
Professional Development
AFIT, Wright-Patterson AFB OH

19. KEY WORDS *(Continue on reverse side if necessary and identify by block number)*

20. ABSTRACT *(Continue on reverse side if necessary and identify by block number)*

ATTACHED

DTIC
ELECTE
SEP 9 1982

AD A119084

FILE COPY

DD FORM 1 JAN 73 1473 EDITION OF 1 NOV 65 IS OBSOLETE

UNCLASS

SECURITY CLASSIFICATION OF THIS PAGE *(When Data Entered)*

DTIC

82 09 07 425

ABSTRACT

Designs of aircraft for the near future exhibit the desire for a greater amount of maneuverability. Direct force control enables the decoupling of the aircraft's motion from its attitude, providing significant benefits to both civilian and military planes. And with the advent of the highly capable microcomputer, the control law incorporating this increase in maneuverability will most likely be implemented digitally. However, the information and results in the areas of direct force control and digital flight control are deficient.

This project was undertaken to increase the data base in these areas through the use of a microcomputer mounted aboard the Variable-Response Research Aircraft. An Equivalent Stability Derivitive matching control law was developed digitally to enable the following modes: flat turn, lateral translation or acceleration, fuselage pointing, pure roll, and coordinated turn. A method was devised to command an aircraft motion whose integral is included as a state in the dynamic equation of motion. Controller-to-command pairings were varied for evaluation.

The control law was coded in Assembly Language for use on the microcomputer. The resulting program, entitled CAS-6, used a nominal sampling rate of 10 samples-per-second (sps) although 4 and 20 sps were also included for testing. The modes were satisfactorly verified in a hybrid simulation which closely resembled

conditions during flight testing.

During the initial flight tests instabilities were encountered, attributed to external disturbances and the lack of weathercock stability (N_β) in the control law model. New modes including a stabilizing N_β term were developed and readied for flight. These new modes performed significantly better in flight than their previous counterparts, although pilot ratings showed that some deficiencies still existed compared to the open-loop dynamics. Two pilots preformed a tracking and an approach-to-landing exercise.

It is apparent from flight testing that probably as much attention must be devoted to human factors considerations as to the control law itself in order to develop an effective digital flight control system incorporating direct force control.

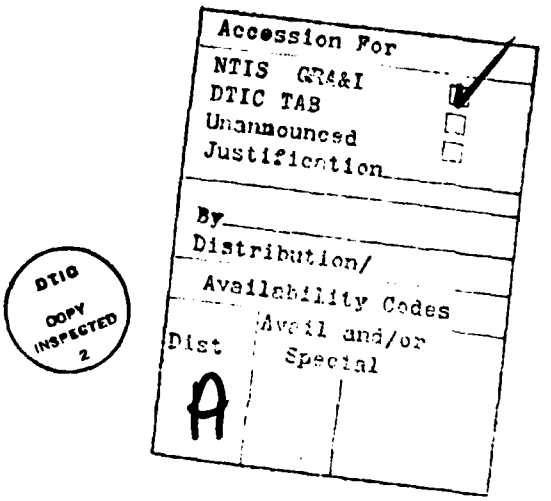

AFIT/CI/NR/82-39T

AFIT RESEARCH ASSESSMENT

The purpose of this questionnaire is to ascertain the value and/or contribution of research accomplished by students or faculty of the Air Force Institute of Technology (ATC). It would be greatly appreciated if you would complete the following questionnaire and return it to:

AFIT/NR
Wright-Patterson AFB OH 45433

RESEARCH TITLE: Command Augmentation Incorporating Direct Side Force Control and Microprocessor Technology

AUTHOR: Scott L. Grunwald

RESEARCH ASSESSMENT QUESTIONS:

1. Did this research contribute to a current Air Force project?

( ) a. YES ( ) b. NO

2. Do you believe this research topic is significant enough that it would have been researched (or contracted) by your organization or another agency if AFIT had not?

( ) a. YES ( ) b. NO

3. The benefits of AFIT research can often be expressed by the equivalent value that your agency achieved/received by virtue of AFIT performing the research. Can you estimate what this research would have cost if it had been accomplished under contract or if it had been done in-house in terms of manpower and/or dollars?

( ) a. MAN-YEARS _____ ( ) b. $_____

4. Often it is not possible to attach equivalent dollar values to research, although the results of the research may, in fact, be important. Whether or not you were able to establish an equivalent value for this research (3. above), what is your estimate of its significance?

( ) a. HIGHLY SIGNIFICANT ( ) b. SIGNIFICANT ( ) c. SLIGHTLY SIGNIFICANT ( ) d. OF NO SIGNIFICANCE

5. AFIT welcomes any further comments you may have on the above questions, or any additional details concerning the current application, future potential, or other value of this research. Please use the bottom part of this questionnaire for your statement(s).

NAME GRADE POSITION

ORGANIZATION LOCATION

STATEMENT(s):

COMMAND AUGMENTATION

INCORPORATING DIRECT SIDE FORCE

CONTROL AND MICROPROCESSOR TECHNOLOGY

by

Scott L. Grunwald

Princeton University
School of Engineering and Applied Science
Department of Mechanical and Aerospace Engineering

Submitted in partial fulfillment of the requirements for the degree of Master of Science in Engineering from Princeton University, 1982

Prepared by:

Scott L. Grunwald
Scott L. Grunwald

Approved by:

Robert F. Stengel
Professor Robert F. Stengel
Thesis Advisor

H. C. Curtiss, Jr.
Professor H. C. Curtiss, Jr.
Thesis Reader

May 1982

ABSTRACT

Designs of aircraft for the near future exhibit the desire for a greater amount of maneuverability. Direct force control enables the decoupling of the aircraft's motion from its attitude, providing significant benefits to both civilian and military planes. And with the advent of the hightly capable microcomputer, the control law incorporating this increase in maneuverability will most likely be implemented digitally. However, the information and results in the areas of direct force control and digital flight control are deficient.

This project was undertaken to increase the data base in these areas through the use of a microcomputer mounted aboard the Variable-Response Research Aircraft. An Equivalent Stability Derivitive matching control law was developed digitally to enable the following modes: flat turn, lateral translation or acceleration, fuselage pointing, pure roll, and coordinated turn. A method was devised to command an aircraft motion whose integral is included as a state in the dynamic equation of motion. Controller-to-command pairings were varied for evaluation.

The control law was coded in Assembly Language for use on the microcomputer. The resulting program, entitled CAS-6, used a nominal sampling rate of 10 samples-per-second (sps) although 4 and 20 sps were also included for testing. The modes were satisfactorly verified in a hybrid simulation which closely resembled

conditions during flight testing.

During the initial flight tests instabilities were encountered, attributed to external disturbances and the lack of weathercock stability (N_β) in the control law model. New modes including a stabilizing N_β term were developed and readied for flight. These new modes performed significantly better in flight than their previous counterparts, although pilot ratings showed that some deficiencies still existed compared to the open-loop dynamics. Two pilots preformed a tracking and an approach-to-landing exercise.

It is apparent from flight testing that probably as much attention must be devoted to human factors considerations as to the control law itself in order to develop an effective digital flight control system incorporating direct force control.

ACKNOWLEDGMENTS

I wish to express my gratitude to those at the Flight Research Laboratory who helped make this thesis a reality. I thank my advisor, Professor Robert Stengel, for keeping me working in the proper direction to the end. Then there is George Miller who was always available to provide the practical insight in dealing with the microcomputer and the research aircraft. I appreciate the computer help Tom Williams gave me and the effort Bart Reavis displayed in keeping the airplane flying. Finally, I thank Barry Nixon for his expertise during flight testing and Marion Sandvik for typing this thesis.

I would also like to acknowledge the Office of Naval Research, the Guggenheim Fellowship Foundation, and the United States Air Force for their funding during this yearlong project.

This thesis carries number 1553-T in the records of the Department of Mechanical and Aerospace Engineering.

TABLE OF CONTENTS

TABLE OF CONTENTS (contd)

LIST OF FIGURES

LIST OF FIGURES (contd)

LIST OF TABLES

LIST OF SYMBOLS

Variables	Description
A	Matrix describing relationship of control to state
C	Gain matrix
C_B	Feedback gain matrix
C_F	Forward gain matrix
C'_F	Singular equilibrium forward gain matrix
C_I	Singular equilibrium gain matrix
e	Naperian base (2.71828...)
$\underline{f}$	Nonlinear functions
F	System dynamics matrix
g	Gravitational acceleration (32.2 ft/sec^2)
G	Control effects matrix (continuous time)
H_x	State observation matrix
H_u	Control observation matrix
I	Identity matrix
K	Gearing between pilot's controls and commands
$L_{()}$	Roll moment derivative
$N_{()}$	Yaw moment derivative
n_y	Lateral acceleration, g's
p	Roll rate, deg/sec
r	Yaw rate, deg/sec
t	Time, sec
T	Sampling interval, sec
$\underline{u}$	Control vector
V	Velocity, ft/sec
$\underline{w}$	Disturbance vector
$\underline{x}$	State vector
y	Lateral position
$\underline{y}$	Output vector
$Y_{()}$	Side force derivative
$\underline{y}_p$	Pilot control vector

Variables (Greek)

β	Sideslip, deg
Γ	Control effects matrix (discrete time)
δA	Aileron deflection, deg
δP	Pedal deflection, in
δR	Rudder deflection, deg
δS	Lateral stick deflection, in
δSF	Side force surface deflection, deg
δT	Thumb lever deflection, deg
Δ	Perturbation
ζ	Damping ratio
θ	Nonsingular equilibrium compound matrix
λ	Eigenvalue
Λ	Matrix with cross-product terms of state transition matrix
μ	One millionth or micro ($\times 10^{-6}$)
ξ	Lateral flight path angle, deg
τ	• Time constant, sec • Integration variable, sec
ϕ	Roll Angle, deg
Φ	State transition matrix
ψ	Yaw angle, deg
ω_n	Natural frequency, rad/sec
Ω	Singular equilibrium compound matrix

Subscripts

c	Commanded
CL	Closed-loop
i	Index
k	Sampling instant
max	Maximum
M	Model
N	Nonsingular equilibrium
o	Initial condition
S	Singular equilibrium
4	Fourth-order system

Superscripts

T	Matrix transpose
-1	Matrix inverse
#	Pseudoinverse
*	Equilibrium value

Punctuation

$(\dot{\cdot})$	Derivative with respect to time
$(\tilde{\cdot})$	Nonzero set-point
!	Factorial
$\lvert\ \rvert$	Determinant

Abbreviations and Acronyms

A/D	Analog-to digital
AGL	Above ground level
APL	A Programming Language
APU	Arithmetic Programming Unit
CAS	Command augmentation system
CCV	Control configured vehicle
CDU	Control display unit
CPU	Central processing unit
CRT	Cathode ray tube
D/A	Digital-to-analog
DOF	Degree(s) of freedom
DSF	Direct side force
EPROM	Erasable programmable read-only memory
ESD	Equivalent Stability Derivative
F	Farad
FBW	Fly-by-wire
FCCU	Flight control computer unit
FM	Frequency-modulated
FRL	Flight Research Laboratory
Hz	Hertz
I/O	Input/output
K	One thousand (x 103)

KIAS	Knots indicated airspeed
In	Natural logarithm
LQ	Linear-quadratic
Micro-DFCS	Microprocessor-based digital flight control system
NACA	National Advisory Committee for Aeronautics
PROM	Programmable read-only memory
RAM	Random access memory
RF	Radio frequency
RPM	Revolutions per minute
sps	Samples per second
USART	Universal Synchronous/Asynchronous Receive/Transmit
VRA	Variable-Response Research Aircraft

1. INTRODUCTION

Control systems which allow a pilot to command an aircraft's motions rather than its aerodynamic surfaces have the potential for improving maneuverability and safety as well as reducing pilot workload. This is particularly true for aircraft that incorporate direct force control in addition to the more conventional angular controls. Nevertheless, the choice of command variables is not obvious, and flight data are required to determine desirable control structures. Princeton's Variable-Response Research Aircraft (VRA), which is equipped with direct lift and side force surfaces, has the capability of independent control about all six rigid-body degrees of freedom (DOF), so it is capable of performing experiments related to this issue. Furthermore its digital flight control system can execute the logic that is required to investigate advanced control concepts, such as decoupling, stability augmentation, and the use of unconventional control surfaces.

The research reported here is part of a continuing investigation of digital flight control using microprocessor technology at Princeton's Flight Research Laboratory (FRL). In the first phase of study, a single-input, single-output, Type 0 control law was developed using a reduced-order longitudinal dynamic model, and it was flight-tested in the VRA (Ref. 1). The CAS-1 control law demonstrated that off-the-shelf microprocessor components could be used as a flexible basis for digital flight control research. In the next phase, dual-input dual-output lateral-directional control laws involving a Type 0 and equivalent Type 1 structures were investigated (Ref. 2). The command augmentation system (CAS-2) was flown in the VRA using four-state feedback linear-quadratic sampled-data regulator theory, and, in one part of the testing, a side-slip estimator. Only the conventional control surfaces (ailerons and rudder) were commanded by CAS-2.

The Model 1 microprocessor-based digital flight control system (Micro-DFCS) used in these tests was based on the Intel 8085 central processing unit (CPU). During the first two years, Navy and Princeton University pilots accomplished sixty hours of flight tests. The piloting tasks involved tracking at altitude, field carrier landing practice, and conventional approach and landing, and there was emphasis on determining the effects of sampling rate, control resolution, and computation delay.

The present investigation constitutes the third phase of this research. Building on the prior work, its overall objective is to develop new methodologies for digital control system design and test them in flight, with the particular emphasis on the incorporation of direct side force control in the system. Additional details of this goal are given in the next section.

1.1 OBJECTIVES

This thesis considers the control of an aircraft's lateral-directional modes of motion; the research on which it is based has three main parts:

- Analysis of advanced control modes employing direct side force control
- Implementation of the necessary digital control laws using microprocessor-based technology
- Flight testing of these advanced control concepts

1.1-1 Advanced Control Modes

An aircraft such as the VRA with full moment and force control can respond in a manner which has only recently been investigated. Potential applications can be found for civilian (Ref. 3-5) and military (Ref. 6-12) aircraft, and further work must be accomplished. New (unconventional) modes may improve such operations as approach and landing, air-to-air

engagements, and air-to-ground tasks. Three of the more significant advanced lateral-directional control modes are described in further detail.

The flat turn (Fig. 1-1a) involves a heading change with no excursion in either sideslip or roll. In this fashion, a pilot can correct an azimuth error with one command. A conventional roll-to-turn airplane requires two distinct inputs--one, a bank into the turn and another, to return to straight-and-level flight once the proper heading is achieved. This normal technique not only can add to maneuver time and pilot workload, but it could serve to disorient the pilot because of the additional axis of motion involved. The flat turn mode has shown promise in ground target tracking and air-to-ground weapon delivery, where the control of the velocity vector and the elimination of the roll pendulum effect is critical. In control configured vehicle (CCV) flight tests, F-16 pilots reported that up to .7 g of lateral acceleration was tolerable during the maneuver (Ref. 13).

A second control mode unique to aircraft with direct side force control is lateral translation (Fig. 1-1b). This capability features the ability to control lateral velocity (or sideslip) without any deviation in heading or roll angles. Lateral translation can be beneficial in offsetting cross-wind effects or small lateral displacements during either landing or ground target tracking. It also can be used to track vehicles on winding roads or roads running nearly perpendicular to the flight path.

The third advanced control mode is fuselage pointing (Fig. 1-1c). During this maneuver, the aircraft's nose is pointed laterally while the horizontal flight path and roll angles remain unchanged. Possible uses of this technique include cancelling tracking errors in an air-to-air environment and increasing the tracking duration.

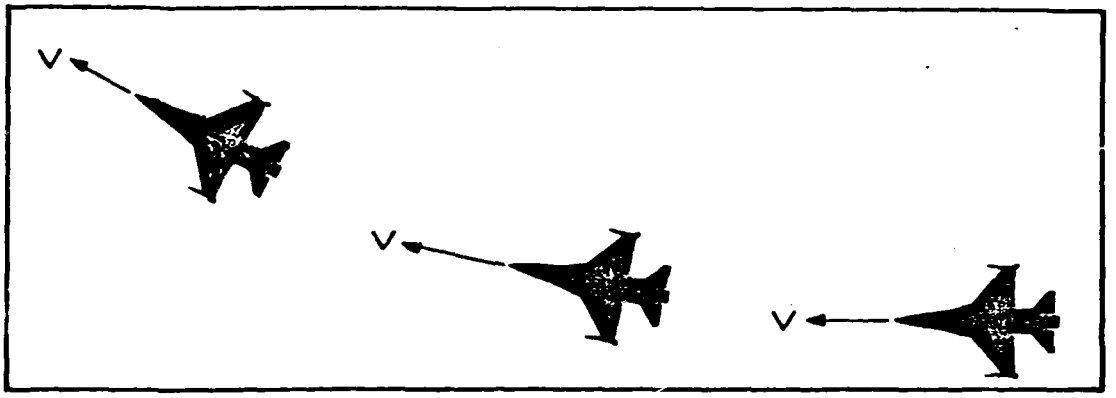

a) Flat Turn

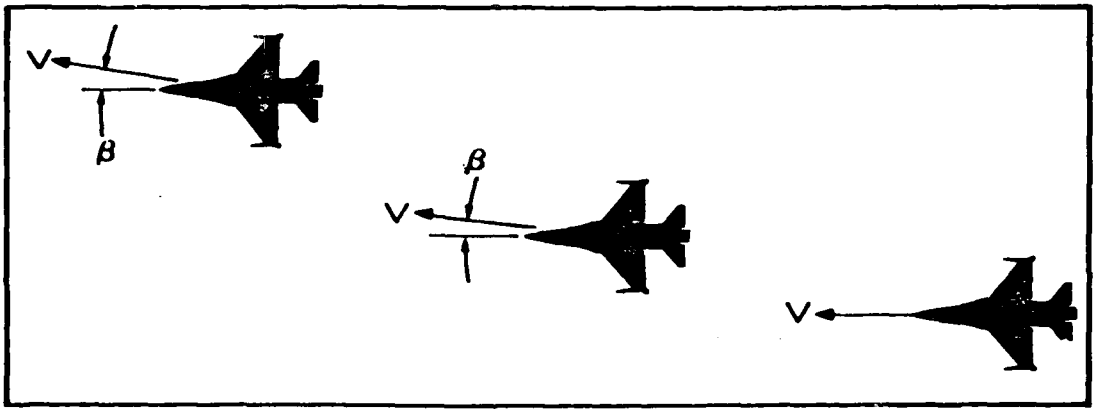

b) Lateral Translation

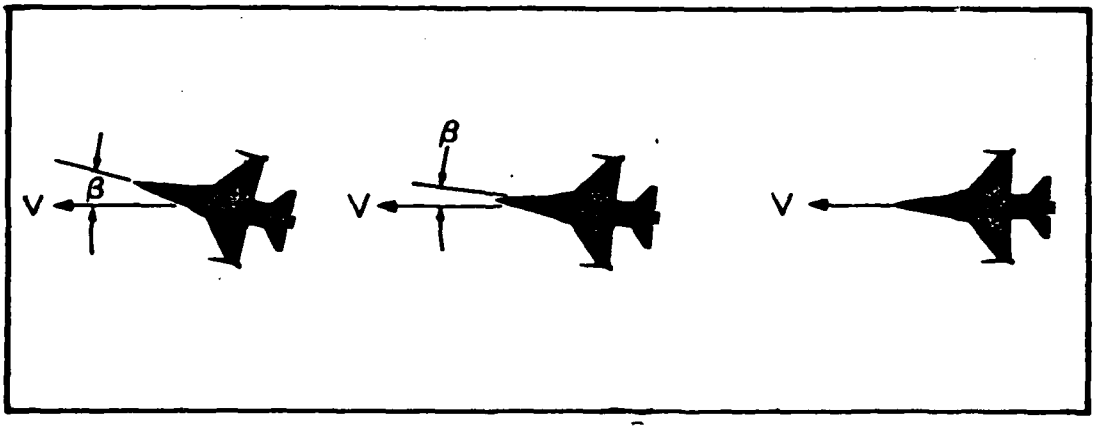

c) Fuselage Pointing

Figure 1-1. Lateral-Directional Advanced Control Modes.

1.1-2 Digital Control Laws

Recent advances in computer technology have made digital flight control possible. Digital computers are well-suited to the matrix manipulation associated with modern control laws. Microprocessor-based technology gives the capability of having a small on-board computer process signals in the short time between sampling instants. The flexibility of digital computers allows for control program modifications or gain changes without hardware alteration. Through redundancy management, flying safety can be improved by the use of these computers. Since control systems of this type are beginning to appear in operational aircraft, alternative designs must be analyzed, including their effect on flying qualities.

1.1-3 Flight Tests

Analytical results of an aircraft control law cannot be satisfactorily verified without flight tests. The resulting handling qualities are major factors in a pilot's evaluation of the aircraft, and the traditional airplane handling specifications guide, MIL-F-8785B (Ref.14), requires new information concerning both advanced control modes using direct force, and sampling effects associated with digital flight control routines. Studies, including that of Ref. 15, are being conducted to improve the specifications in this area. The VRA, with a microprocessor-based flight control system (Micro-DFCS) capability, is ideally suited to conducting this type of evaluation.

1.2 OVERVIEW

This thesis follows the logical order of developing the digital flight control system for testing in the research aircraft. Chapter 2 develops the digital control law and presents the resulting computer simulations. Chapter 3 shows the development of the microcomputer

program along with results of a hybrid simulation. Chapter 4 decribes the flight tests and the corresponding pilot evaluations. Finally, Chapter 5 discusses the results of the study, along with conclusions and recommendations.

2. CONTROL LAW DEVELOPMENT

This study begins with the development of a flight control law for implementation on the microcomputer. After the derivation of the lateral-directional dynamic model, command vectors are determined based on task-oriented considerations and steady-state responses. The problem of which cockpit manipulator should command each of the seclected aircraft motions is then addressed. Control laws suited to these command vectors are determined, and the associated gains are calculated. Computer simulations of the closed-loop time responses are presented.

2.1 AIRCRAFT DYNAMICS

Although the control law is to be implemented digitally, the aircraft dynamic equations of motion are derived in the continuous-time domain and then transformed to the discrete-time domain.

2.1-1 Continuous-Time Dynamic Model

The aircraft's rigid-body motions are described by a twelfth-order, nonlinear, differential equation of the form,

$$\dot{\underline{x}}(t) = \underline{f}[\underline{x}(t),\underline{u}(t),\underline{w}(t),t] \qquad (1)$$

where $\underline{x}$ is a vector containing the aircraft states, $\underline{u}$ the controls, $\underline{w}$ the disturbances, and t is time.

For control law development, the equations of motion are simplified by

- Neglecting unsteady aerodynamic effects
- Neglecting disturbances
- Retaining only the lateral-directional modes of motion
- Linearizing about a nominal point with a first-order Taylor Series expansion.

These simplifications give the sixth-order expression,

$$\Delta\dot{\underline{x}}(t) = F(t)\Delta\underline{x}(t) + G(t)\Delta\underline{u}(t) \tag{2}$$

where the Δ signifies perturbations about the nominal, or trim, condition. F and G are determined by partial differentiation of the equations of motion with respect to $\Delta\underline{x}$ and $\Delta\underline{u}$, respectively. The state vector consists of lateral position, yaw angle, yaw rate, sideslip angle, roll rate, and roll angle,

$$\Delta\underline{x} = [\Delta y \ \Delta\psi \ \Delta r \ \Delta\beta \ \Delta p \ \Delta\phi]^T \tag{3}$$

where the superscript T denotes the transpose of the vector. The deflections of the three aerodynamic surfaces--rudder, side force panels, and ailerons--comprise the control vector,

$$\Delta\underline{u} = [\Delta\delta R \ \Delta\delta SF \ \Delta\delta A]^T \tag{4}$$

With the further assumption that

- Δy and $\Delta\psi$ can be neglected since they provide little dynamic information
- The equations apply only at one flight condition (i.e., F and G are time-invariant)

the fourth-order lateral-directional, continuous-time equations of motion (which neglect actuator dynamics) for use in this study are written,

$$\begin{bmatrix} \Delta\dot{r} \\ \Delta\dot{\beta} \\ \Delta\dot{p} \\ \Delta\dot{\phi} \end{bmatrix} = \begin{bmatrix} N_r & N_\beta & N_p & 0 \\ Y_r/V^{-1} & Y_\beta/V & Y_p/V & g/V \\ L_r & L_\beta & L_p & 0 \\ 0 & 0 & 1 & 0 \end{bmatrix} \begin{bmatrix} \Delta r \\ \Delta\beta \\ \Delta p \\ \Delta\phi \end{bmatrix} + \begin{bmatrix} N_{\delta R} & N_{\delta SF} & N_{\delta A} \\ Y_{\delta R}/V & Y_{\delta SF}/V & Y_{\delta A}/V \\ L_{\delta R} & L_{\delta SF} & L_{\delta A} \\ 0 & 0 & 0 \end{bmatrix} \begin{bmatrix} \Delta\delta R \\ \Delta\delta SF \\ \Delta\delta A \end{bmatrix} \tag{5}$$

or,

$$\dot{\Delta x} = F\Delta x + G\Delta u \tag{6}$$

with the initial condition, $\Delta x(0)=\Delta x_o$. (Note that Δx and Δu still are functions of time, although the notation (t) has been dropped.) The F matrix describes the aircraft's stability and modes of motion, while the G matrix contains the effects of control on the dynamics.

Based on the advanced control modes to be implemented, two straight-and-level flight speeds were selected:

- VRA cruise speed (105 KIAS)
- VRA final approach speed (75 KIAS)

The F and G matrices for the above flight conditions are given in Table 2-1. The stability and control derivatives of the VRA have been obtained from various sources, both published (Ref. 16-17) and unpublished. Some differences were noted, so the values of Table 2-1 should be considered approximate.

Table 2-1 presents the corresponding eigenvalues (λ) of the lateral-directional modes of motion: Dutch roll, spiral, and roll. These are based on the determinant,

$$|\lambda_i I - F| = 0 \tag{7}$$

where I is the identity matrix.

Defining the system output, Δy, as the pilot command, the equation,

$$\Delta y = H_x \Delta x + H_u \Delta u \tag{8}$$

also is required. The pilot command, Δy has the same dimension as Δu, and H_x and H_u are the state observation matrix and the control observation matrix, respectively. This relation allows the command vector to

Table 2-1. VRA Stability Characteristics
(All angles in radians or degrees.)

V = 105 Knots

$$F = \begin{bmatrix} -0.75 & 5.3 & -0.260 & 0 \\ -1. & -0.400 & 0 & 0.181 \\ 1.16 & -11.5 & -6.5 & 0 \\ 0 & 0 & 1. & 0 \end{bmatrix} \quad G = \begin{bmatrix} -6.10 & 2.1 & -0.222 \\ 0.0935 & 0.38 & 0 \\ 0.6 & 0 & 21. \\ 0 & 0 & 0 \end{bmatrix}$$

$\omega_{n_{DR}}$ = 2.51 rad/sec, ζ_{DR} = 0.212

λ_r = -6.576 rad/sec

λ_s = -0.0108 rad/sec

V = 75 Knots

$$F = \begin{bmatrix} -0.685 & 2.99 & -0.199 & 0 \\ -1. & -0.416 & 0 & 0.254 \\ 1.6 & -6.096 & -4.6 & 0 \\ 0 & 0 & 1. & 0 \end{bmatrix} \quad G = \begin{bmatrix} -4.12 & 1.54 & -1.09 \\ 0.047 & 0.25 & 0 \\ 0.392 & 0 & 11.4 \\ 0 & 0 & 0 \end{bmatrix}$$

$\omega_{n_{DR}}$ = 1.97 rad/sec, ζ_{DR} = 0.264

λ_r = -4.672 rad/sec

λ_s = 0.00857 rad/sec

represent states, state rates, controls, or linear combinations thereof. Equations 6 and 8 represent the aircraft's continuous-time dynamics and output.

2.1-2 Discrete-Time Dynamic Model

Sampled-data regulator theory (Ref. 18) transforms the continuous-time domain equations for control system design to the discrete-time domain, allowing "direct digital synthesis". In a sampled-data system, the input occurs at discrete instants, but it drives a continuous-time system. Observations of the state and output variables are available only at these discrete times. With the discrete-time transformation, eq. 6 becomes,

$$\Delta \underline{x}_{k+1} = \Phi \Delta \underline{x}_k + \Gamma \Delta \underline{u}_k \tag{9}$$

The subscript k is a non-negative integer that represents the sampling instant. Φ, the state transtion matrix, is expressed,

$$\Phi = e^{FT} \tag{10a}$$

$$= I + FT + \frac{(FT)^2}{2!} + \frac{(FT)^3}{3!} + \ldots \tag{10b}$$

where T is the sampling interval, $t_{k+1} - t_k$. The relation for the control effects matrix, Γ, is,

$$\Gamma = \int_{t_k}^{t_{k+1}} \Phi(\tau) G d\tau \tag{11a}$$

$$= (\Phi - I) F^{-1} G \tag{11b}$$

Equation 11b follows from the fact that the control is assumed to change only at the sampling points, i.e.,

$$\Delta\underline{u}(t) = \Delta\underline{u}_k \quad , \quad t_k \leq t < t_{k+1} \tag{12}$$

Equation 12 is characteristic of a zero-order hold system.

The pilot command in eq. 8 transforms to the discrete-time domain as

$$\Delta\underline{y}_k = H_x \Delta\underline{x}_k + H_u \Delta\underline{u}_k \tag{13}$$

where H_x and H_u remain the same as in the continuous case.

2.1-3 Fifth-Order System

The preceding discussion presupposes a fourth-order state vector. However, in order to implement a command mode like fuselage pointing, in which both lateral flight path angle and sideslip angle are controlled independently, the state vector must be augmented to include the yaw angle. The yaw angle is a better choice for the fifth component than the flight path angle, because a heading gyro (which measures yaw attitude) is available for control feedback. Since the yaw angle is pure integral of the yaw rate at the nominal flight condition, the fifth-order model becomes,

$$F = \begin{bmatrix} 0 & 1 & 0 & 0 & 0 \\ 0 & & & & \\ 0 & & F_4 & & \\ 0 & & & & \\ 0 & & & & \end{bmatrix} \quad , \quad G = \begin{bmatrix} 0 & 0 & 0 \\ & G_4 & \\ & & \end{bmatrix} \tag{14}$$

where the subscript 4 denotes the fourth-order model described in Table 2-1. The state vector now includes yaw angle in the first row, and the original components are shifted down one position. The dynamics and output equations remain in the same form, but, F is singular, i.e., it can not be inverted because there is an eigenvalue equal to zero (a pure integration mode). Consequently, eq. 11b is not defined; however F^{-1} can be eliminated (Ref. 19) if it is represented in series notation. The control effects matrix is then,

$$\Gamma = \Phi T[I - \frac{FT}{2!} + \frac{(FT)^2}{3!} - \ldots] G \qquad (15)$$

2.2 COMMAND VECTORS

The command augmentation system (CAS) is designed to implement a command vector selected on the basis of practicality and feasibility. Practicality involves those command modes which are dictated by an operational, or task-oriented, need, while feasibility considerations are based on steady-state responses to command.

2.2-1 Task-Oriented Modes

Some modes which allow for practical tasks have already been described as advanced control modes. For example, a logical flat turn command vector is,

$$\Delta \underline{y} = [\Delta r \ \Delta\beta \ \Delta p]^T \qquad (16)$$

since yaw rate is commanded while maintaining sideslip and roll rate perturbations near zero. This command vector also facilitates a lateral translation mode in which sideslip is commanded without excursions in the other two command variables. A command of only roll rate produces a pure, or "knife-edge", roll which is of questionable value, as yaw rate remains zero, so the aircraft does not turn.

Substituting roll angle, $\Delta\phi$, for roll rate in the command vector provides an alternative mode. In a coordinated turn (a turn in which lateral acceleration is zero), steady state yaw rate is related to steady-state roll angle by,

$$\Delta r^* \cong \frac{g}{V}\Delta\phi^* \qquad (17)$$

where $(\,)^*$ denotes a variable that has reached equilibrium (Ref. 20).

If this desired yaw rate is commanded through an interconnect, the turning maneuver will be coordinated.

If instead, the command vector in eq. 16 is changed to include sideslip rate, $\Delta\dot{\beta}$, rather than sideslip angle, a lateral acceleration translation mode results. This mode could prove useful for energy management, or for "jinking", an evasive maneuver in air-to-air combat.

In order to have the ability to point the fuselage, a command vector like,

$$\Delta\underline{y} = [\Delta\xi \ \Delta\beta \ \Delta p]^T \tag{18}$$

must be chosen. ($\Delta\xi$ is the lateral flight path angle, which is defined as $\Delta\psi + \Delta\beta$.) This selection would allow a flat turn of a desired angle.

2.2-2 Steady-State Responses

Command augmentation is concerned not only with satisfactory stability and transient behavior but with equilibrium response to command (Ref. 21). Steady-state response is determined by the aircraft dynamics and the desired command vector, and it is independent of the feedback control law. Given a desired command vector alone, the resulting steady-state control and state variables of an aircraft can be calculated.

In the steady state, all transients have died out, so,

$$\Delta\underline{x}_{k+1} = \Delta\underline{x}_k = \Delta\underline{x}^* \tag{19}$$

and upon substitution, eq. 9 becomes,

$$\Delta\underline{x}^* = -(\Phi - I)^{-1}\Gamma\Delta\underline{u}^* \tag{20a}$$

$$= (I - \Phi)^{-1}\Gamma\Delta\underline{u}^* \tag{20b}$$

This equation gives the relation between steady-state control and state, but the command vector, $\Delta\underline{y}$, is not included. Assuming the output is in steady-state when the state and control are in equilibrium, i.e.,

$$\Delta\underline{y}^* = H_x\Delta\underline{x}^* + H_u\Delta\underline{u}^* \tag{21}$$

and solving eq. 20 and 21 simultaneously leads to the single matrix equation,

$$\begin{bmatrix} \Delta\underline{x}^* \\ \Delta\underline{u}^* \end{bmatrix} = \begin{bmatrix} \Phi-I & \Gamma \\ H_x & H_u \end{bmatrix}^{-1} \begin{bmatrix} 0 \\ \Delta\underline{y}^* \end{bmatrix} \tag{22a}$$

$$\triangleq \theta^{-1} \begin{bmatrix} 0 \\ \Delta\underline{y}^* \end{bmatrix} \tag{22b}$$

In general, eq. 22 describes the steady-state response of an aircraft's motion variables and controls to a pilot command. The relationship, however, does not apply if the compound matrix, θ, is either non-square or singular (i.e., its determinant is zero).

In this study, θ is square since the number of controls is equal to the number of commands. On the other hand, θ may be singular for certain choices of the command vector. Specifically, when a state variable is the integral of another component that is chosen as a command variable, the former state variable does not remain constant when the latter has reached steady state. For example, if roll rate is commanded, a steady-state roll rate implies a steadily increasing roll angle, and similar results pertain to the command and state pairings of $\Delta\dot{r}$ and Δr, $\Delta\dot{\beta}$ and $\Delta\beta$, etc.

In the event of this singular command equilibrium, a quasi-steady relationship in which forces and moments are momentarily balanced, can be derived by partitioning vectors and matrices in the following manner:

$$\Delta\underline{x} = \begin{bmatrix} \Delta\underline{x}_N \\ \hline \Delta\underline{x}_S \end{bmatrix}, \quad \Phi = \left[\begin{array}{c|c} \Phi_N & \Lambda_N \\ \hline \Lambda_S & \Phi_S \end{array}\right], \quad \Gamma = \begin{bmatrix} \Gamma_N \\ \hline \Gamma_S \end{bmatrix}, \quad H_x = \left[\begin{array}{c|c} H_{x_N} & H_{x_S} \end{array}\right] \quad (23a,b,c,d)$$

The subscript S denotes terms causing the singular equilibrium, while all other terms are denoted by the subscript N, for "nonsingular"; the Λ matrices represent cross-product terms in the state-transition matrix. Then, there is a reduced-order model for which a steady equilibrium truly exists, and it has the form,

$$\begin{bmatrix} \Delta\underline{x}_N^* \\ \Delta\underline{u}^* \end{bmatrix}_k = \begin{bmatrix} \Phi_N - I & \Gamma_N \\ H_{x_N} & H_u \end{bmatrix}^{-1} \begin{bmatrix} -\Lambda_N \Delta\underline{x}_S^* \\ \Delta\underline{y}^* - H_{x_S} \Delta\underline{x}_S^* \end{bmatrix}_k \quad (24a)$$

$$\triangleq \begin{bmatrix} \Omega_{11} & \Omega_{12} \\ \Omega_{21} & \Omega_{22} \end{bmatrix} \begin{bmatrix} -\Lambda_N \Delta\underline{x}_S^* \\ \Delta\underline{y}^* - H_{x_S} \Delta\underline{x}_S^* \end{bmatrix}_k \quad (24b)$$

The nonsteady terms, appearing as external disturbances to the new model, are described by a summation involving the steady states, i.e.,

$$\Delta\underline{x}_{S_k}^* = \Lambda_S \Delta\underline{x}_{N_{k-1}}^* + \Phi_S \Delta\underline{x}_{S_{k-1}}^* + \Gamma_S \Delta\underline{u}_{k-1}^* \quad (25)$$

This analysis enables the determination of the maximum amount of aircraft motion that can be commanded in steady state. For a particular command vector, the maximum amount of a command variable that can be generated by the VRA is dictated by the control surface whose steady-state deflection reaches the VRA's maximum capability (Table A-1) first. (It should be noted that although the maximum deflection of the VRA's side force panels is ±35 deg, the panels stall at ±15 deg in the zero-side-slip condition.)

Based on the presentation in this section, steady-state response to commands were calculated. Numerous command vectors were tried, but

only those vectors deemed practical and feasible (shown in Table 2-2, along with the corresponding steady-sate responses and maximum command capability) were selected for further consideration.

The possibility of using lateral acceleration, Δn_y, as a state should be considered. Lateral acceleration, in g units, can be expressed as (Ref. 22),

$$\Delta n_y = \frac{V}{g}(\Delta r + \Delta\dot{\beta}) - \Delta\phi \tag{26}$$

where all angles are expressed in radians. Substitution of the first two rows of eq. 5 into eq. 26 gives,

$$\Delta n_y = \frac{1}{g}(Y_r\Delta r + Y_\beta\Delta\beta + Y_p\Delta p + Y_{\delta R}\Delta\delta R + Y_{\delta SF}\Delta\delta SF + Y_{\delta A}\Delta\delta A) \tag{27}$$

In order to use Δn_y as a state in the form of eq. 6, its derivative must be calculated; from eq. 27 (ignoring terms which are zero for the VRA),

$$\Delta\dot{n}_y = \frac{Y_\beta}{g}\Delta\dot{\beta} + \frac{Y_{\delta R}}{g}\Delta\dot{\delta R} + \frac{Y_{\delta SF}}{g}\Delta\dot{\delta SF} \tag{28a}$$

$$= -\frac{Y_\beta}{g}\Delta r + \frac{Y_\beta}{g}\Delta n_y + \frac{Y_\beta}{g}\Delta\phi + \frac{Y_{\delta R}}{g}\Delta\dot{\delta R} + \frac{Y_{\delta SF}}{g}\Delta\dot{\delta SF} \tag{28b}$$

This equation clearly shows that without augmenting the state vector to include actuator dynamics, the use of Δn_y as a state will not give a true dynamic representation. (This was verified in time response comparison using $\Delta\beta$ and then substituting Δn_y as a state.) However, in nonsingular equilibrium,

$$\Delta n_y^* = \frac{V}{g}\Delta r^* - \Delta\phi^* \tag{29}$$

so lateral acceleration could be used to replace sideslip angle as a state in steady-state analyses. In addition, when the command vector includes yaw rate, as well as roll rate or roll angle, the command of

Table 2-2. Steady-State Analysis of Command Vectors

	$\Delta\underline{y}$				$\begin{bmatrix}\Delta r\\ \Delta\beta\\ \Delta p\end{bmatrix}$ 105[x]		$\begin{bmatrix}\Delta r\\ \Delta\beta\\ \Delta\phi\end{bmatrix}$ 105	$\begin{bmatrix}\Delta\xi\\ \Delta\beta\\ \Delta p\end{bmatrix}$ 105	$\begin{bmatrix}\Delta r\\ \Delta\dot{\beta}\\ p\end{bmatrix}$ 105	
	$\Delta\underline{y}^*$	$\begin{bmatrix}1\\0\\0\end{bmatrix}$	$\begin{bmatrix}0\\1\\0\end{bmatrix}$	$\begin{bmatrix}0\\0\\1\end{bmatrix}$			$\begin{bmatrix}0\\0\\1\end{bmatrix}$ $\begin{bmatrix}.181\\0\\1\end{bmatrix}$	$\begin{bmatrix}1\\0\\0\end{bmatrix}$ $\begin{bmatrix}0\\1\\0\end{bmatrix}$	$\begin{bmatrix}0\\1\\0\end{bmatrix}$	
				t=0 sec	t=1 sec				t-0 sec	t=1 sec
$\Delta\Psi^*(°)$		-	-	-	-	-	-	1 -1	-	-
$\Delta r^*(°/s)$		1	0	0	0	0	.181	0 0	0	0
$\Delta\beta^*(°)$		0	1	0	0	0	0	0 1	1	.98
$\Delta p^*(°/s)$		0	0	1	1	0	0	0 0	0	0
$\Delta\phi^*(°)$		0	0	0	1	1	1	0 0	0	.009
$\Delta ny^*(g)$		.096	0	-.001	-.018	-.017	0	0 0	0	.096
$\Delta\delta R^*(°)$		.72	1.12	-.057	-.21	-.15	-.020	0 1.12	.87	1.97
$\Delta\delta SF^*(°)$		2.45	.78	-.010	-.45	-.44	.005	0 .78	2.42	3.18
$\Delta\delta A^*(°)$		-.076	.52	.31	.32	.004	-.009	0 .52	.005	.51
	$\Delta\underline{y}^*_{max}$		$\begin{bmatrix}4.9\\13.4\\5.43^+\end{bmatrix}$			$\begin{bmatrix}4.9\\13.4\\27.3\end{bmatrix}$ $\begin{bmatrix}4.9\\13.4\\750\end{bmatrix}$		$\begin{bmatrix}\infty\\13.4\\5.43^+\end{bmatrix}$	$\begin{bmatrix}4.9\\1.93^+\\5.43^+\end{bmatrix}$	

+ signifies the maximum command authority after 5 seconds

x denotes velocity (in knots) at which equilibrium occurs

Table 2-2. Steady-State Analysis of Command Vectors (contd)

$\Delta\underline{y}$	$\Delta\delta R$ $\Delta\delta SF$ $\Delta\delta A$ 105			Δr $\Delta\beta$ $\Delta\phi$ 75				$\Delta\delta R$ $\Delta\delta SF$ $\Delta\delta A$ 75		
	1	0	0	1	0	0	.254	1	0	0
$\Delta\underline{y}^*$	0	1	0	0	1	0	0	0	1	0
	0	0	1	0	0	1	1	0	0	1
$\Delta r^*(°/s)$	-27.0	9.75	43.9	1	0	0	.254	39.4	-15.4	-45.1
$\Delta\beta^*(°)$	2.68	.98	6.25	0	1	0	0	10.4	-4.05	-9.97
$\Delta p^*(°/s)$	0	0	0	0	0	0	0	0	0	0
$\Delta\phi^*(°)$	-156	53.9	256	0	0	1	1	172	-68.4	-194
$\Delta ny^*(g)$	.11	-.002	-.24	.069	0	-.017	0	-.30	.14	- .95
$\Delta\delta R^*(°)$	1	0	0	1.29	1.14	-.36	-.031	1	0	0
$\Delta\delta SF^*(°)$	0	1	0	3.76	1.45	-.95	.006	0	1	0
$\Delta\delta A^*(°)$	0	0	1	-.18	.50	.012	-.035	0	0	1
$\Delta\underline{y}^*_{max}$		15			3.19		3.19		15	
		35			13.2		13.2		35	
		30			12.6		484		30	

Δn_y creates a singularity, because setting Δr and $\Delta\phi$ to zero in eq. 26 implies a $\Delta\dot{\beta}$ command.

2.3 CONTROLLER-TO-COMMAND PAIRINGS

Even though possible command vectors have been determined, the problem of which cockpit controller, or manipulator, should direct which command motion remains. Prior studies involving tests of direct side force (DSF) have employed such manipulators as a "coolie hat" switch or thumb wheel atop the control stick, in addition to conventional foot pedals and lateral stick motion. These studies showed that pilots have varying opinions as to which manipulator/command pairs are best. Reference 3 found that pilots preferred to use a proportional thumb lever uncoupled from the conventional controls for direct side force command, having tested a number of alternatives in flight. Foot pedals were used to achieve a flat turn in Ref. 6, while side force effects were geared to the lateral stick for the approach-and-landing simulations of Ref. 4. A throttle-mounted controller was used in the simulation of Ref. 9 to command sideslip, while the pedals commanded a flat turn and the lateral stick commanded a coordinated turn. Reference 7 points out that pilots preferred the foot pedals for the command of all of the DSF advanced maneuvers during the F-16 CCV test flights. The thumb button was considered useful only for precise changes in pipper position during the flat turn mode.

The VRA's spring-loaded, stick-mounted, thumb lever (Fig. 2-1), which has a lateral travel of 15 deg (about one inch at the apex), was used in this investigation. It was decided to test the following nominal controller-to-command pairings in flight:

- Foot pedals--yaw rate or flight path angle
- Thumb lever--sideslip angle or rate
- Lateral stick--roll angle or rate

These pairings were thought to be the most natural for the pilot; the

two directional motions are commanded by the two directional manipulators, and roll is commanded by lateral stick deflection. Two variations of the baseline pairings also were considered for further possible testing. In the first case, each directional motion is controlled by the other directional manipulator.

- Pedals--sideslip
- Thumb lever--yaw rate
- Lateral stick--roll rate

In the second case, the pure roll mode, which may be of limited value, is commanded by the less conventional thumb lever, and the stick, which conventionally commands a banked turn, commands a flat turn.

- Pedals--sideslip
- Thumb lever--roll rate
- Lateral stick--yaw rate

2.4 CONTROL LAW

With the choice of command vectors and controller-to-command pairings complete, a closed-loop control law that can produce the decoupled motions, as selected by the command vector, must be determined. A number of control design possibilities exist, including implicit and explicit model following (Ref. 23-26), or the linear-quadratic (LQ) regulator, with variations such as state-rate or control-rate weighting (Ref. 27-28). A relatively simple algebraic control design approach was pursued in the present investigation, as detailed below.

2.4-1 Equivalent Stability Derivative Matching

Equivalent Stability Derivative (ESD) Matching (Ref. 29) enables the VRA's closed-loop response to closely match the open-loop dynamics of some chosen model. In the continuous-time case with three controls (rudder, ailerons, and side force panels) for the three lateral directional

rigid-body degrees of freedom (yaw and roll moments plus side force), perfect model following, in the sense of Erzberger (Ref. 30), can be achieved within the constraints of the VRA's control deflection, rate, and bandwidth limits. With direct side force available, ESD Matching enables the control law to be calculated algebraically. The resulting gains are identical to those that would be calculated by the more sophisticated implicit model following technique.

For microcomputer implementation, the ESD control law derivation must proceed in the discrete-time domain. The mathematical model of the aircraft to be followed is assumed to have the same dimensions, form, and initial conditions as the VRA's equation (eq. 9), i.e.,

$$\Delta\underline{x}_{k+1_M} = \Phi_M \Delta\underline{x}_{k_M} + \Gamma_M \Delta\underline{u}_{k_M} \tag{30}$$

where the subscript M denotes the model. If the VRA and the model are stable systems, the two will be matched when,

$$\Delta\dot{\underline{x}} = \Delta\dot{\underline{x}}_M \qquad \text{and} \qquad \Delta\underline{x} = \Delta\underline{x}_M \tag{31,32}$$

With these two conditions, the control for the VRA is,

$$\Delta\underline{u}_k = \Gamma\#[(\Phi_M - \Phi)\Delta\underline{x}_k + \Gamma_M \Delta\underline{u}_{M_k}] \tag{33a}$$

$$\triangleq C_B \Delta\underline{x}_k + C_F \Delta\underline{u}_{M_k} \tag{33b}$$

where,

$$C_B = \Gamma\#(\Phi_M - \Phi) \tag{34}$$

$$C_F = \Gamma\#\Gamma_M \tag{35}$$

Choosing the C_B and C_F for Fig. 2-2 in this way will enable the VRA to behave like the model aircraft. $\Gamma\#$, the Moore-Penrose pseudoinverse

Figure 2-1. VRA Thumb Switch.

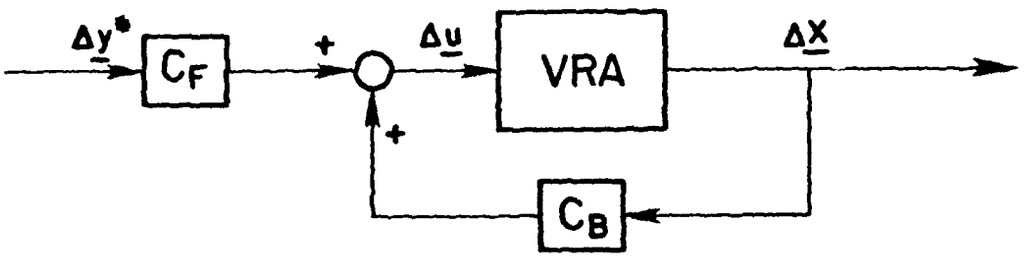

Figure 2-2. Equivalent Stability Derivative Matching Control Law.

is defined as (Ref. 31),

$$\Gamma\# = (\Gamma^T\Gamma)^{-1}\Gamma^T \tag{36}$$

The pseudoinverse is useful when the inverse of a matrix does not exist due to the fact that there are more equations than unknowns (in this case, four and three, respectively). It is precisely because of this control overdetermination--which can be circumvented in the continuous case--that the model following is not guaranteed to be perfect. The discrete-time model is controllable (Ref. 32), so perfect model following is attainable at the sampling instants. Because the control law uses the pseudoinverse, the VRA follows the model in a least-square fashion.

Since the model aircraft is fictitious, and it is desired that its inputs be the pilot's commands, the ESD law of eq. 33 is appropriately modified. If Φ_M and Γ_M can be selected so that the model's controls will produce the corresponding aircraft motions desired in the constant command vector, i.e.,

$$\Delta\underline{u}_M = \Delta\underline{y}^* \tag{37}$$

the ESD control law becomes,

$$\Delta\underline{u}_k = C_B\Delta\underline{x}_k + C_F\Delta\underline{y}^* \tag{38}$$

as depicted in Figure 2-2. Equation 38 is now identical to the general control law with a nonzero set-point, of the form (Ref. 22),

$$\Delta\tilde{\underline{u}}_k = -C\Delta\tilde{\underline{x}}_k \tag{39}$$

The aircraft states are fed back through the matrix C_B, while the pilot commands are transmitted through C_F. Although this is a Type 0 system--there is no pure integration or summation in the forward loop--zero

error still can be attained if the aircraft parameters are known exactly, and no disturbances are present.

If a command vector is selected such that singular equilibrium results, at least one of the aircraft states will be in quasi-steady equilibrium, and eq. 38 no longer applies. A solution is developed for the command vector that includes yaw rate, sideslip, and roll rate.

To begin, eq. 39 is expanded so that,

$$\Delta\underline{u}_k = \Delta\underline{u}^*_k = C(\Delta\underline{x}_k - \Delta\underline{x}^*_k) \tag{40}$$

Upon substitution of eq. 24b,

$$\Delta\underline{u}_k = \Omega_{21}\Lambda_N\Delta\underline{x}^*_s + \Omega_{22}\Delta\underline{y}^* - C\left[\Delta\underline{x}_k - \begin{pmatrix}\Delta\underline{y}^*_k \\ \Delta\underline{x}^*_{S_k}\end{pmatrix}\right] \tag{41}$$

Because of the particular command vector chosen, some terms appearing in eq. 24b simplify: $H_{x_S} = 0$, and since $H_u = 0$, $\Omega_{11} = 0$ and $\Omega_{12} = I$. Then, grouping terms in eq. 41,

$$\Delta\underline{u}_k = (\Omega_{22} + C_N)\Delta\underline{y}^* - C\Delta\underline{x}_k + (-\Omega_{21}\Lambda_N + C_S)\Delta\underline{x}^*_{S_k} \tag{42}$$

where the gain matrix, C, is appropriately subdivided as,

$$C = \left[C_N \,\vdots\, C_S\right] \tag{43}$$

Finally, eq. 42 is rewritten as,

$$\Delta\underline{u}_k \triangleq C'_F\Delta\underline{y}^* + C_B\Delta\underline{x}_k + C_I\Delta\underline{x}^*_{S_k} \tag{44}$$

C'_F denotes a forward gain matrix that is different from that calculated when nonsingular equilibrium exists. C_B, on the other hand, is computed as before (eq. 34). Note that,

$$C_B = -C \tag{45}$$

An additional term, C_I, is required in the ESD Matching control law equation to account for quasi-steady equilibrium.

The need to make adjustments in the control law for quasi-steady equilibrium was not understood until late in the research. Consequently, the modes which involve the command of roll rate initially were developed using eq. 33 as the control law equation. Computer simulations were performed using the correct equation developed late in the investigation. These verified the suitability of eq. 44 during quasi-steady equilibrium. Comparison figures are presented in Section 4.3-2. The use of the modified control law equation practically negated any steady-state yaw rate or sideslip when roll rate was commanded. However, for certain choices of the aircraft model (e.g., when f_{24} is zero) no difference arises between the two equations. Also, the difference is not apparent when either yaw rate or sideslip is commanded.

The closed-loop response can be calculated to ensure that the control law is enabling the VRA to follow the model. An equivalent continuous-time closed-loop system dynamics matrix is solved,

$$F_{CL} = \frac{1}{T} \ln \Phi_{CL} \tag{46a}$$

$$= \frac{1}{T}\left[(\Phi_{CL} - I) - \frac{1}{2}(\Phi_{CL} - I)^2 + \frac{1}{3}(\Phi_{CL} - I)^3 - \ldots\right] \tag{46b}$$

where the closed-loop state transition matrix is,

$$\Phi_{CL} = \Phi + \Gamma C_B \tag{47}$$

The eigenvalues of the continuous-time closed-loop system are computed as before, by solving for the roots of the characteristic equation:

$$| \lambda I - F_{CL} | = 0 \tag{48}$$

2.4-2 Model Selection

Steady-state equations can be used to make the relation in eq. 37 hold. The equivalent continuous-time expression of eq. 20 is, for the model,

$$\Delta \underline{x}_M^* = -F_M^{-1} G_M \Delta \underline{u}_M^* \tag{49}$$

The continuous-time relationship is used because the F and G matrices provide more physical dynamic insight than their discrete counterparts. F_M dictates the model's transient behavior, while both F_M and G_M determine the amount of motion coupling in steady-state. If the decoupled commands are aircraft state variables, the following method is used:

1) Select F_M so that the states are decoupled as much as practicable and with satisfactory transient behavior.

2) Chose G_M based on the following:

   a) Equation 49 is written

$$\Delta \underline{x}_M^* = A_M \Delta \underline{u}_M^* \tag{50}$$

   b) A_M (a 4 x 3 matrix), which describes the steady-state relationship between the model's control and state vectors, is determined by the choice of command vector.

   c) From eq. 49 and 50,

$$G_M = -F_M A_M \tag{51}$$

3) Calculate Φ_M and Γ_M using eq. 10 and 11.

4) Calculate C_B and C_F using eq. 34 and 35.

In choosing F_M and G_M, some constraints were heeded so that the model would fly like a "real aircraft". (Ref. 33) Roll angle is dynamically the pure integration of roll rate, so the bottom row of F_M and G_M must be identical to the VRA's. It is not clear whether the "g/V" term (f_{24}) must be present in the model. With this in mind, various model F matrices were chosen to give a satisfactory, decoupled transient response of the command variables. Reference 14 is not a satisfactory guide in this instance. The model has decoupled lateral-directional response modes, whereas Ref. 14 is primarily concerned with normal modes of motion (i.e., Dutch roll, roll, and spiral) and aerodynamic surface commands.

VRA pilots provided a guideline for the desired response behavior of the command motions. It was thought that a time constant of 0.1 sec and 0.5 sec would be sufficient for the yaw rate and sideslip response, respectively, while the roll rate response should be at least as good as that of the open-loop VRA (a time constant of 0.154 seconds at 105 KIAS and 0.217 seconds at 75 KIAS). In order to command roll angle, a coupling term, L_ϕ, must be introduced in F_M. Similarily, an N_ψ term is added when the command vector contains flight path angle. Based on Ref. 34, a nominal damping ratio (ζ) of 0.7 is selected for the angle command, while the natural frequency (ω_n) is varied to affect rise time. The amount of roll or flight path angle commanded has a great impact on the proper value of ω_n to be chosen for good handling qualities. For example, a pilot probably would desire a slower rise time when commanding a larger roll angle. One final consideration in choosing a model is the resulting initial control deflections, because actuator dynamics have been ignored and the ESD method does not include control rate restraint. A heuristic approach is followed: the initial control deflections to a command, which are determined by inspection of the corresponding column of C_F, should be reasonable and comparable to those of the unaugmented VRA.

Using the method of this section, various models were selected, associated gains were calculated, and time histories were generated.

Sampling rates used are based on the discussion in the next section. Tables 2-3 and Fig. 2-3 to 2-9 depict the resulting modes. Modes vary because of differences in the selected model, sampling rate, and command vector. (Refer to Appendix B for the computer programs that correspond to the ESD Matching technique.)

In Figure 2-3a, the open-loop response to control of the VRA at 105 KIAS is shown. The Dutch roll mode is prevalent throughout the plots while the snappy roll mode, accompanied by a slight amount of adverse yaw, is seen with a $\Delta\delta A$ input.

Mode 01 is depicted in Figure 2-4(a-c). All of the states commanded represent first-order responses (Δr has a τ = 0.1 sec, $\Delta\beta$ a τ = 0.5 sec, and Δp a τ = 0.1 sec). With a Δr command of 1 deg/sec, Δp is nulled, and a miniscule hangoff of .00009 deg exists in $\Delta\beta$. To enable the quick rise time of Δr, $\Delta\delta R$ is initially deflected in the opposite direction of its equilibrium value. When 1 deg of $\Delta\beta$ is commanded, an initial $\Delta\delta SF$ of 4.45 deg is required--a possible problem considering the VRA's actuator rate and limit. This large initial control deflection is due to the inherent properties of the VRA; $\Delta\delta SF$ is required immediately to negate the strong tendency of the aircraft to yaw with the sideslip-producing $\Delta\delta R$. However it is seen also that the steady-state control required, as is the case for all the examples, agrees with the equilibrium response to command previously computed. The lateral translation creates an initial Δn_y of 0.18 g per degree of $\Delta\beta$. Finally, as a result of using the improper control law gains for this singular equilibrium case, a continuously increasing $\Delta\beta$ results when Δp is commanded.

Mode 02 (Fig. 2-4(d-f)) is similar to Mode 01. The speed of response has been diminished so that τ = 1 sec for Δr and $\Delta\beta$, and τ = 0.154 sec for Δp. The initial $\Delta\delta SF$ required for 1 deg of $\Delta\beta$ is reduced to 2.4 deg and the initial Δn_y is now only 0.09 g.

Table 2-3. Description of Modes Developed

MODE	(knots) AIR-SPEED	CONTROL PAIRINGS ΔδP ΔδT ΔδS	F_M	G_M	C_B	C_F
00	105 or 75	ΔδR ΔδSF ΔδA	DIRECT ELECTRICAL LINKAGE NO CONTROL LAW CALCULATED			
01	105	Δr Δβ Δp	-10 0 0 0 0 -2 0 .181 0 0 -10 0 0 0 1 0	10 0 0 0 2 0 0 0 10 0 0 0	1.44 -.49 -.024 -.0056 1.43 -3.67 .0003 -.037 -.080 .51 -.099 .0052	-.72 1.61 -.026 1.02 4.45 .011 .0039 .0097 .410
02	105	Δr Δβ Δp	-1 0 0 0 0 1 0 .181 0 0 -6.5 0 0 0 1 0	1 0 0 0 1 0 0 0 6.5 0 0 0	.83 .27 -.030 .0017 2.30 -1.56 .0041 -.0164 -.077 .51 .0011 .0052	-.11 .845 -.020 .15 2.34 .0076 .0006 .0051 .31
03	105	Δβ Δr Δp	same as Mode 01		1.43 -3.67 .0003 -.037 1.44 -.49 -.024 -.0056 -.080 .51 -.099 .0052	1.02 4.45 .011 -.72 1.61 -.026 .0039 .0097 .410
04	105	Δβ Δp Δr	same as Mode 01		1.43 -3.67 .0003 -.037 -.080 .51 -.099 .0052 1.44 -.49 -.024 -.0056	1.02 4.45 .011 .0039 .0097 .410 -.72 1.01 -.026
05	105	Δr Δβ Δp	-10 0 0 0 0 -2 0 0 0 0 -10 0 0 0 1 0	10 0 0 0 2 0 0 0 10 0 0 0	1.44 -.49 -.029 -.15 1.43 -3.67 -.015 -.44 -.078 .51 -.099 .0043	-.72 1.61 -.028 1.02 4.45 .0051 .0039 .0097 .41
06	105	Δr Δβ Δϕ+ .181Δr	-10 0 0 0 0 -2 0 .181 0 0 -10 -51 0 0 1 0	10 0 1.81 0 2 -.181 0 0 51 0 0 0	1.44 -.49 -.018 .12 1.43 -3.67 -.0008 -.090 -.080 .51 -.18 -1.92	-.72 1.61 -.40 1.02 4.45 -.16 .0039 .0098 1.92
07	105	Δr Δβ Δϕ+ .181Δr	-1 0 0 0 0 -1 0 .181 0 0 -5 -12.7 0 0 1 0	1 0 .181 0 1 -.181 0 0 12.7 0 0 0	.83 .27 -.031 .043 2.30 -1.56 .0053 -.032 -.077 .51 .027 -.63	-.11 .85 -.21 .15 2.34 -.38 .0006 .0051 .63

Table 2-3. Description of Modes Developed (contd)

MODE	(knots) AIR SPEED	CONTROL PAIRINGS ΔδP	ΔδT	ΔδS	F_M	G_M	C_B	C_F
09	105	Δξ	Δβ	Δp	0 1 0 0 0 -5 0 0 0 0 -2 0 0 0 0 -10 0 0 0 1	6 0 0 0 0 12.7 -12.7 0 .181 0 2 0 0 0 1 10 0 0 0 0	1.11 1.22 -.49 -.024 -1.59 1.74 -3.67 .0003 - .0060 -.079 .51 -.099	-.0056 -1.11 2.72 -.026 -.037 1.59 2.86 .011 .0052 .0060 .0037 .41
11	75	Δr	Δβ	Δϕ	-6 0 0 0 0 -1 0 .254 0 0 -10 -51 0 0 1 0	6 0 0 0 1 -.254 0 0 51 0 0 0	2.02 -.25 .078 .86 2.70 -2.16 -.021 -.23 -.18 .52 -.43 -3.27	-.73 1.39 -1.22 1.06 3.61 -.72 -.0072 -.020 3.28
12	75	Δr	Δβ	Δϕ	-1 0 0 0 0 -1 0 .254 0 0 -5 -125 0 0 1 0	1 0 0 0 1 -.254 0 0 12.5 0 0 0	1.44 -.75 -.017 .28 3.54 -2.16 -.0002 -.091 -.18 .52 -.075 -1.06	-.15 1.39 -.64 .22 3.61 -.86 -.0015 -.070 1.07
16	75	Δr	Δβ	Δϕ+ .254Δr	Same as Mode 11	6 0 1.524 0 1 -.254 0 0 51 0 0 0	2.02 -.25 .078 .86 2.70 -2.16 -.021 -.23 -.18 .52 -.43 -3.27	.73 1.39 -1.41 1.06 3.61 -.45 -.0072 -.020 3.27
17	75	Δr	Δβ	Δϕ+ .254Δr	Same as Mode 12	1 0 .254 0 1 -.254 0 0 12.5 0 0 0	1.44 -.25 -.017 .28 3.54 -2.16 -.0002 -.091 -.18 .52 -.075 -1.06	-.15 1.39 -.68 .22 3.61 -.80 -.0015 -.020 1.07
18	75	Δr	Δβ	Δϕ+ .254Δr	Same as Mode 16 except at 20 sps		2.31 .26 .079 1.00 3.04 -2.22 -.017 -.21 -.20 .53 -.46 -3.89	-1.02 1.40 -1.62 .71 3.68 -.56 .017 -.035 3.91
19	75	Δr	Δβ	Δϕ+ .254Δr	Same as Mode 16 except at 4 sps		1.46 -.21 .046 .37 2.09 -1.96 -.052 -.43 -.13 .47 -.30 -1.64	-.17 1.35 -.77 1.66 3.41 -.094 -.051 .026 1.64

Mode 05 (Fig. 2-4(g-i) also is identical to Mode 01, except the "g/V" term in F_M is zero. This alters the last column of C_B and C_F and serves to precisely null $\Delta\beta^*$ when either Δr or Δp is commanded. The command of Δp illustrates the necessity of a quasi-steady equilibrium analysis: $\Delta\phi$ (not shown), Δn_y, and all three controls are changing at each sampling stant.

A coordinated turn capability is included in Modes 06 and 07 (Fig. 2-5). The responses to the command of Δr and $\Delta\beta$ are similar to those of Modes 01 and 02. Again, because of the inclusion of L_ϕ in F_M, $\Delta\beta^* = 0$ when Δr is commanded. For the coordinated turn capability, the second-order $\Delta\phi$ response is quicker in Mode 06 (ω_n = 7 rad/sec, ζ = 0.7) than in Mode 07 (ω_n = 3.5 rad/sec, ζ = 0.7). Accordingly, Δp, Δr, and Δn_y reach their steady-state values faster in Mode 06. Note also that the steady-state control deflections are zero in the coordinated turn.

Mode 09 (Fig. 2-6), the last mode that is designed for 105 KIAS, commands $\Delta\xi$ for a fuselage pointing capability. The second-order $\Delta\xi$ response has ω_n = 3.5 rad/sec and ζ = 0.7. The large extent of transient behavior in all the responses is a result of $\Delta\xi$ not being a state. Rather, the control law is attempting to control the sum of $\Delta\psi$ (not shown) and $\Delta\beta$.

The remainder of the modes illustrated are designed to operate at 75 KIAS. Figure 2-7 depicts Mode 00 operating at the slower airspeed. The Dutch roll mode is longer. More adverse yaw and less roll damping are evident in the response to a $\Delta\delta A$ input.

Because of the importance of bank angle during final approach, Modes 11 and 12 (Fig. 2-8) incorporate the command of $\Delta\phi$ rather than Δp. Mode 11 is quicker with ω_n = 7 rad/sec, compared to ω_n = 3.5 rad/sec in Mode 12. Also, Δn_y is not nulled. Although both modes have a τ = 1 second for a $\Delta\beta$ command (causing an initial Δn_y of 0.07 g per degree of $\Delta\beta$),

Mode 11 uses a time constant of 0.107 seconds for Δr, while τ = 1 second in Mode 12. Like all of the 75 KIAS modes, more control deflection for the same amount of command is required than at 105 KIAS.

A coordinated turn is also included for use at 75 KIAS. Modes 16 and 17 (Fig. 2-9) are similar to Modes 11 and 12, respectively. Mode 16 has the quicker coordinated turn capability.

2.5 SAMPLING RATE

A final consideration in the control law development is the sampling rate to be used for the digital implementation. The sampling interval, T, is used in the computation of eq. 9 and all subsequent related equations.

In general, the sampling rate should be fast enough compared to the aircraft dynamics so that the error remains tolerable between samples, when the system is running open-loop. Also, the longer the sampling interval, the longer, on the average, the time for the digital system to sense a pilot command (called sampling delay). Because the control law is a direct digital design, the high sampling rates that have been used in the past to mimic analog systems are not necessary (Ref. 35).

A previous study (Ref. 24) concluded that 10 samples per second (sps) is acceptable for rigid-body control. Reference 35 employed a 20 sps rate in its direct digital design for a fighter aircraft. Past research with the VRA (Ref. 1-2) used a sampling rate of 10 sps and found that rates as low as 4 sps can be used, particularily during landing, when the controls normally are more sluggish than in cruising flight. Though response features remain largely unaffected, the use of low sampling rates degrades handling qualities rating due to the sampling delay of the pilot inputs.

With these results as a basis, a nominal sampling rate of 10 sps was picked. For evaluation purposes, variations of Mode 16 were designed

with sampling rates of 20 sps (Mode 18) and 4 sps (Mode 19). These time responses, using newly calculated gains, are shown in Figure 2-9 (g-x). As expected, less staircasing is apparent with the higher sampling rate of Mode 18 and there is a slight decrease in the amount of transient behavior. For example, the peak Δp transient during a 1 degree $\Delta\beta$ command is -0.023 deg/sec at 4 sps, -0.004 deg/sec at 10 sps, and -0.001 deg/sec at 20 sps. However, this may be of no practical significance.

This chapter has presented a method of designing a digital command augmentation system. Computer simulations of the closed-loop time responses of a variety of modes, based on the ESD Matching control law, have been presented. As the next step toward flight testing, the control law must be effectively implemented on the microcomputer.

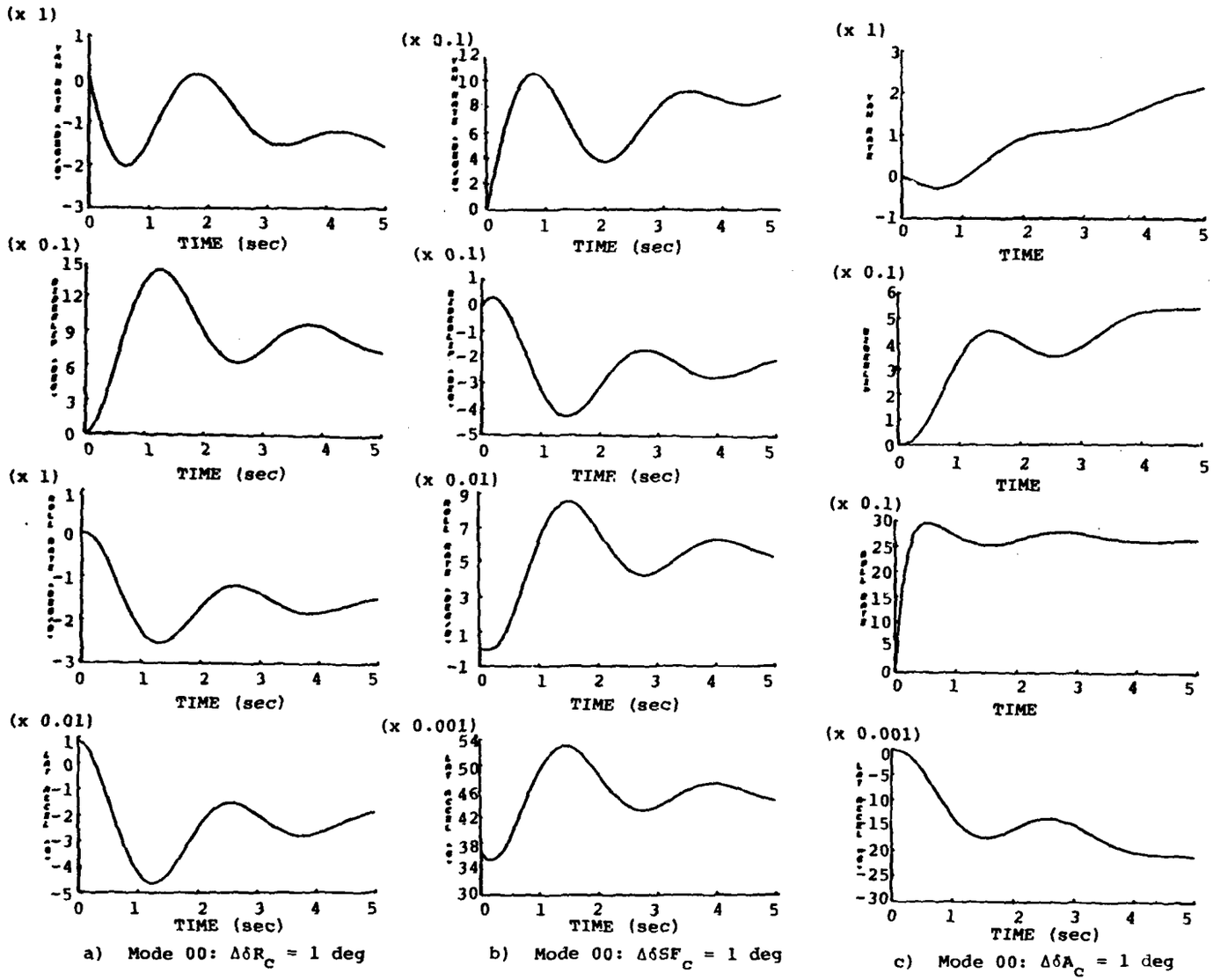

a) Mode 00: $\Delta\delta R_c$ = 1 deg

b) Mode 00: $\Delta\delta SF_c$ = 1 deg

c) Mode 00: $\Delta\delta A_c$ = 1 deg

Figure 2-3. Digital Simulation of Unaugmented VRA Response, V=105 KIAS

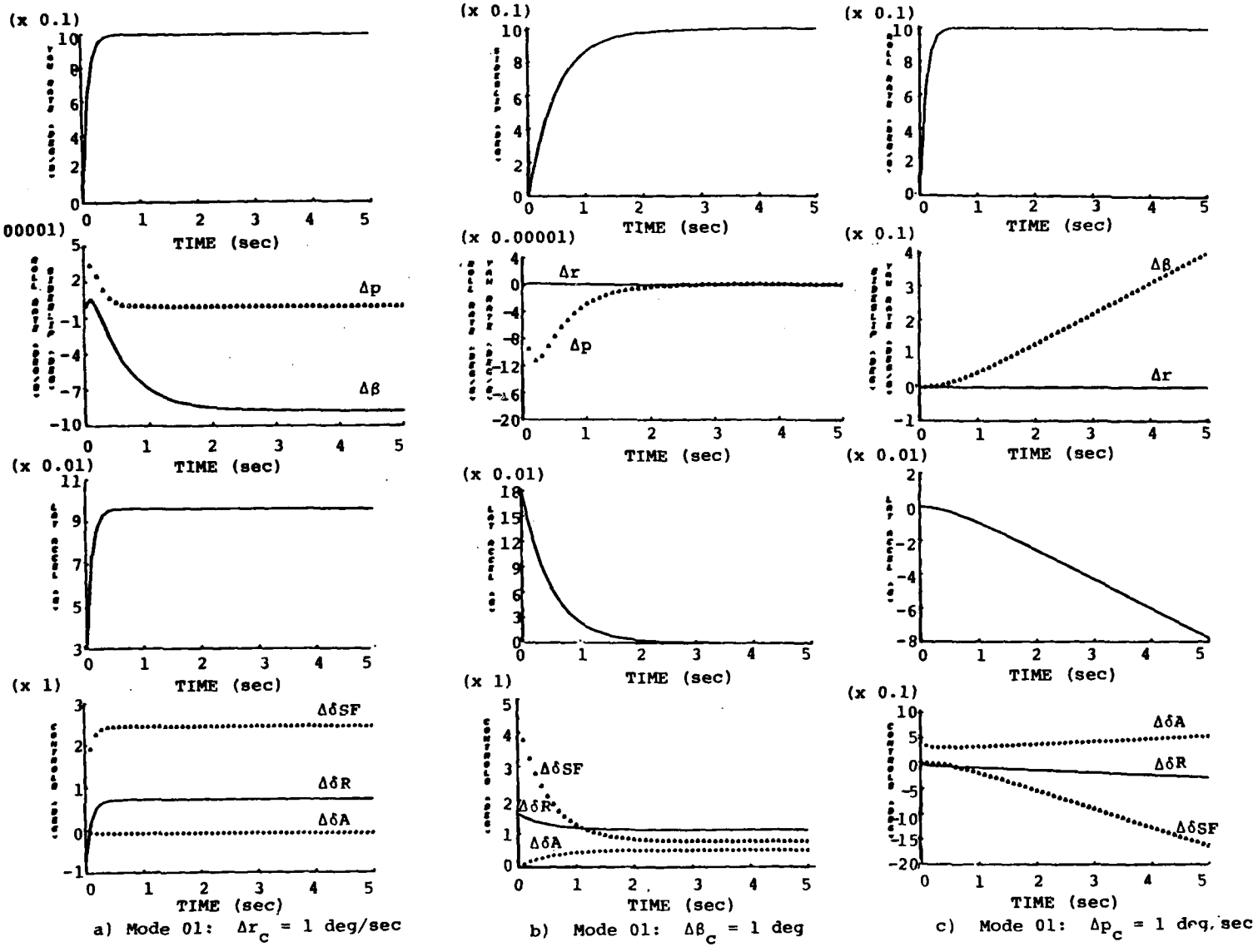

a) Mode 01: Δr_c = 1 deg/sec

b) Mode 01: $\Delta \beta_c$ = 1 deg

c) Mode 01: Δp_c = 1 deg/sec

Figure 2-4. Digital Simulations of (r, β, p) Mode Response, V = 105 KIAS.

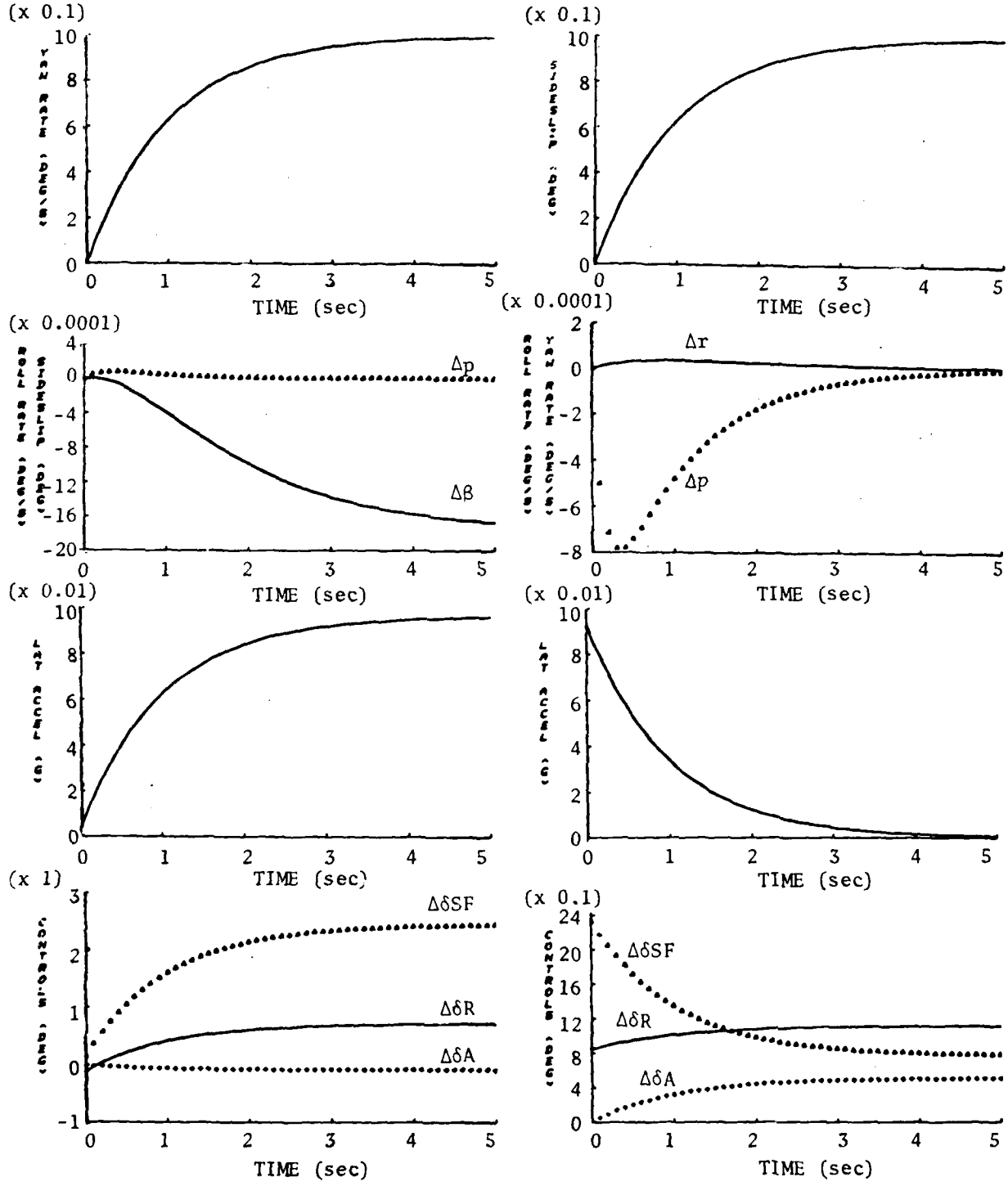

d) Mode 02: Δr_c = 1 deg

e) Mode 02: $\Delta \beta_c$ = 1 deg

Figure 2-4. (continued)

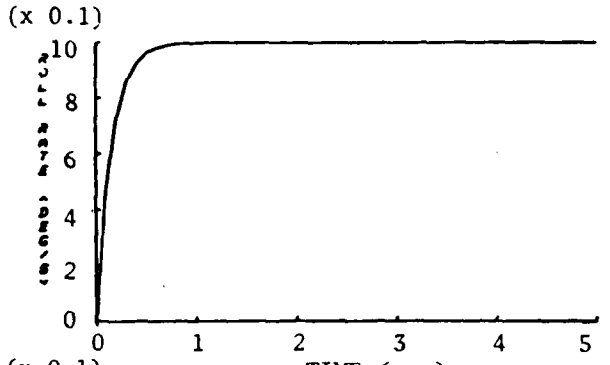

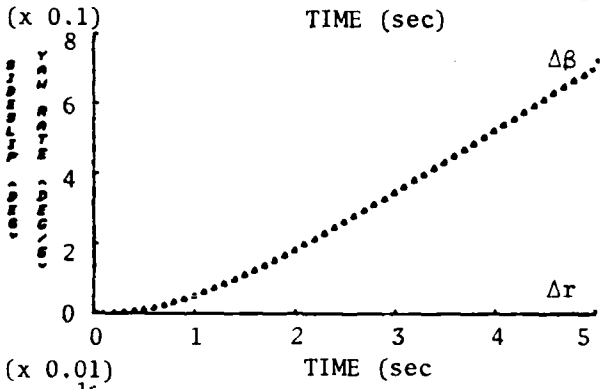

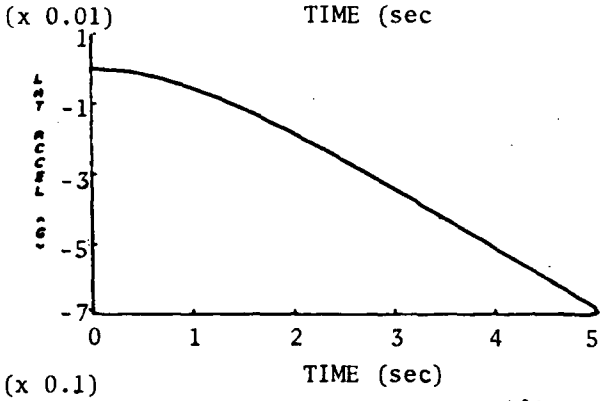

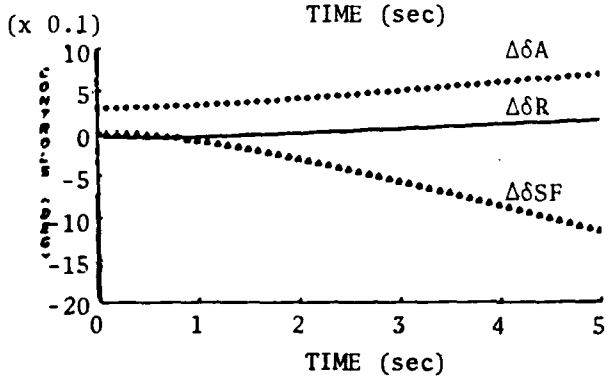

f) Mode 02: Δp_c = 1 deg/sec

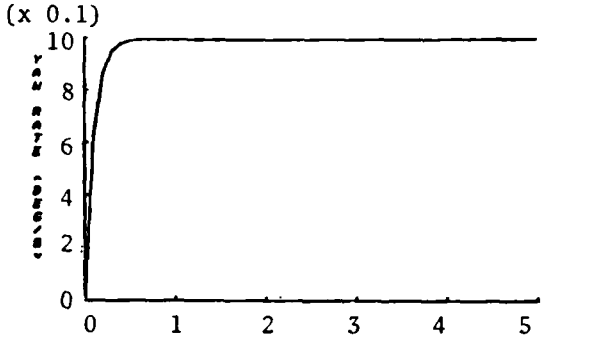

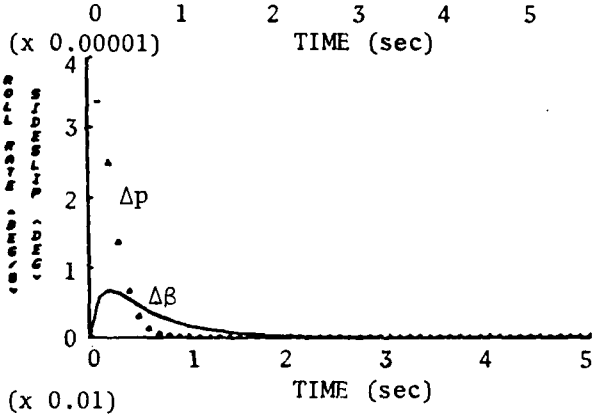

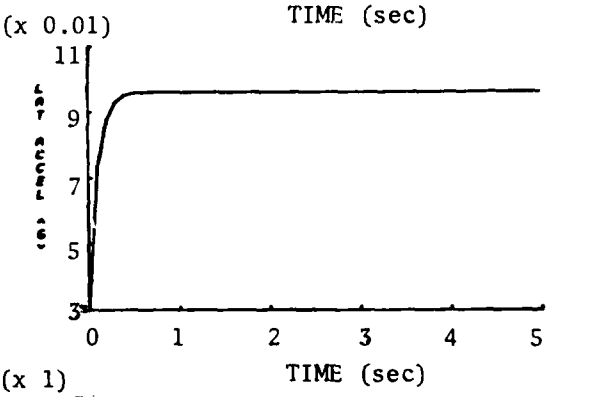

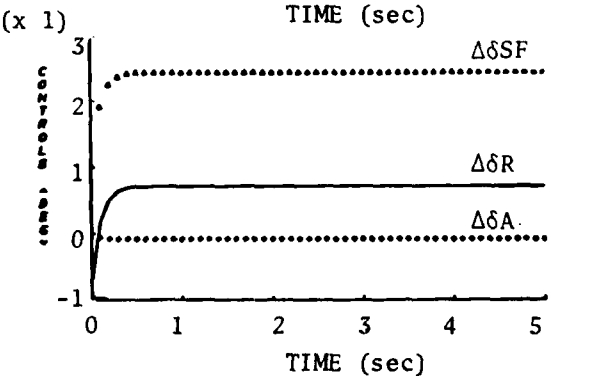

g) Mode 05: Δr_c = 1 deg/sec

Figure 2-4. (continued)

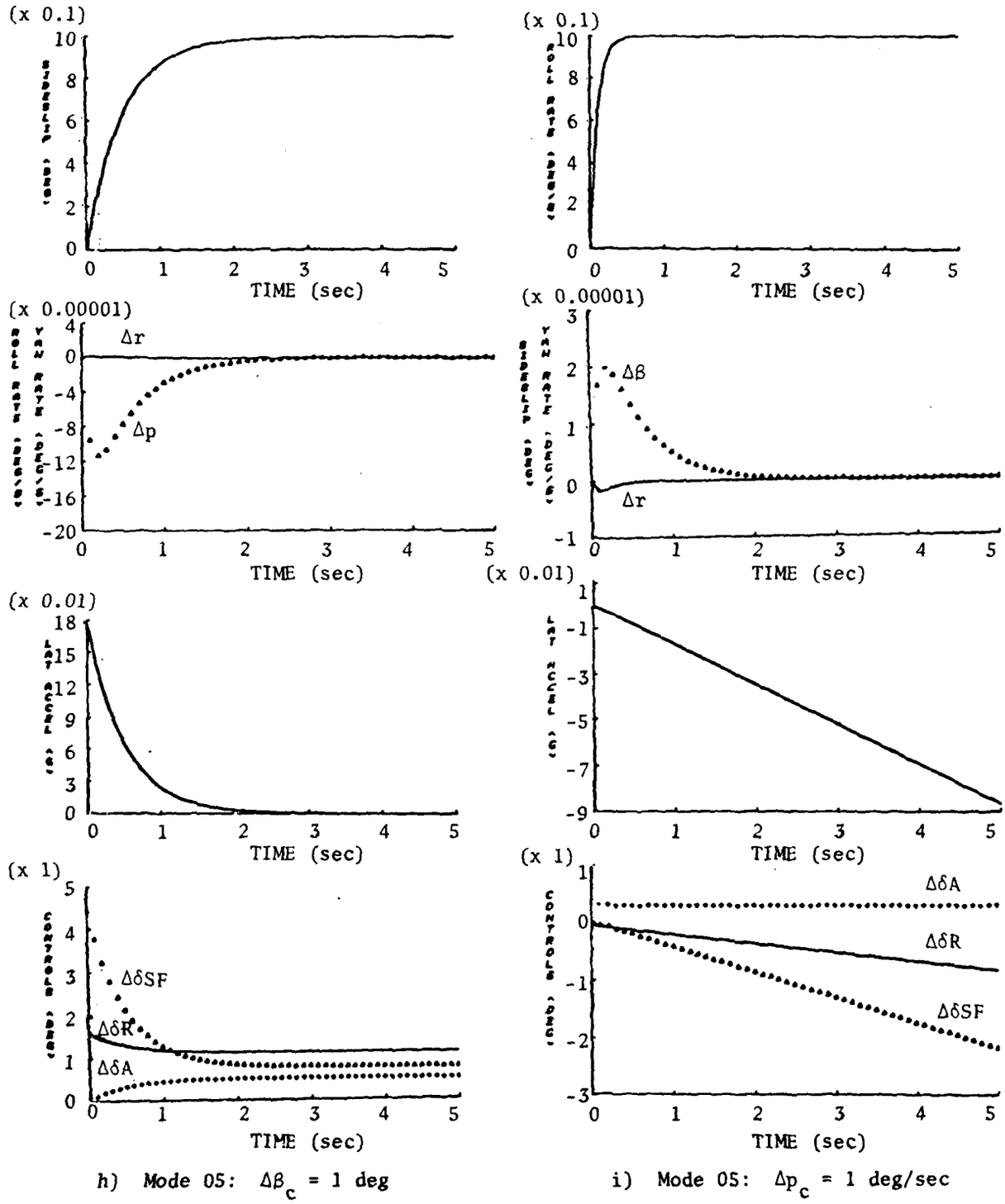

h) Mode 05: $\Delta\beta_c$ = 1 deg

i) Mode 05: Δp_c = 1 deg/sec

Figure 2-4. Continued.

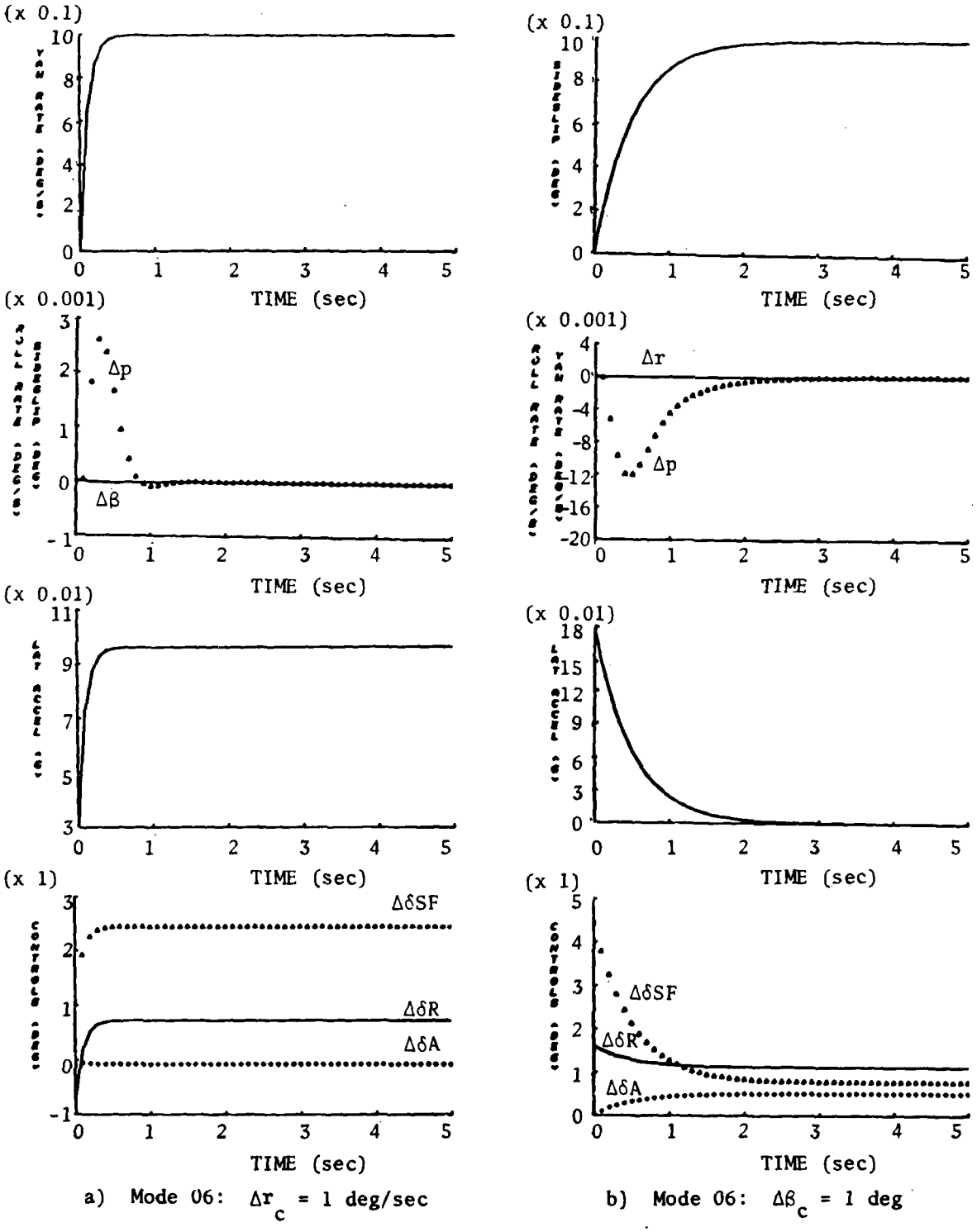

a) Mode 06: Δr_c = 1 deg/sec

b) Mode 06: $\Delta \beta_c$ = 1 deg

Figure 2-5. Digital Simulations of Coordinated (r, β, ϕ) Mode Response, V = 105 KIAS.

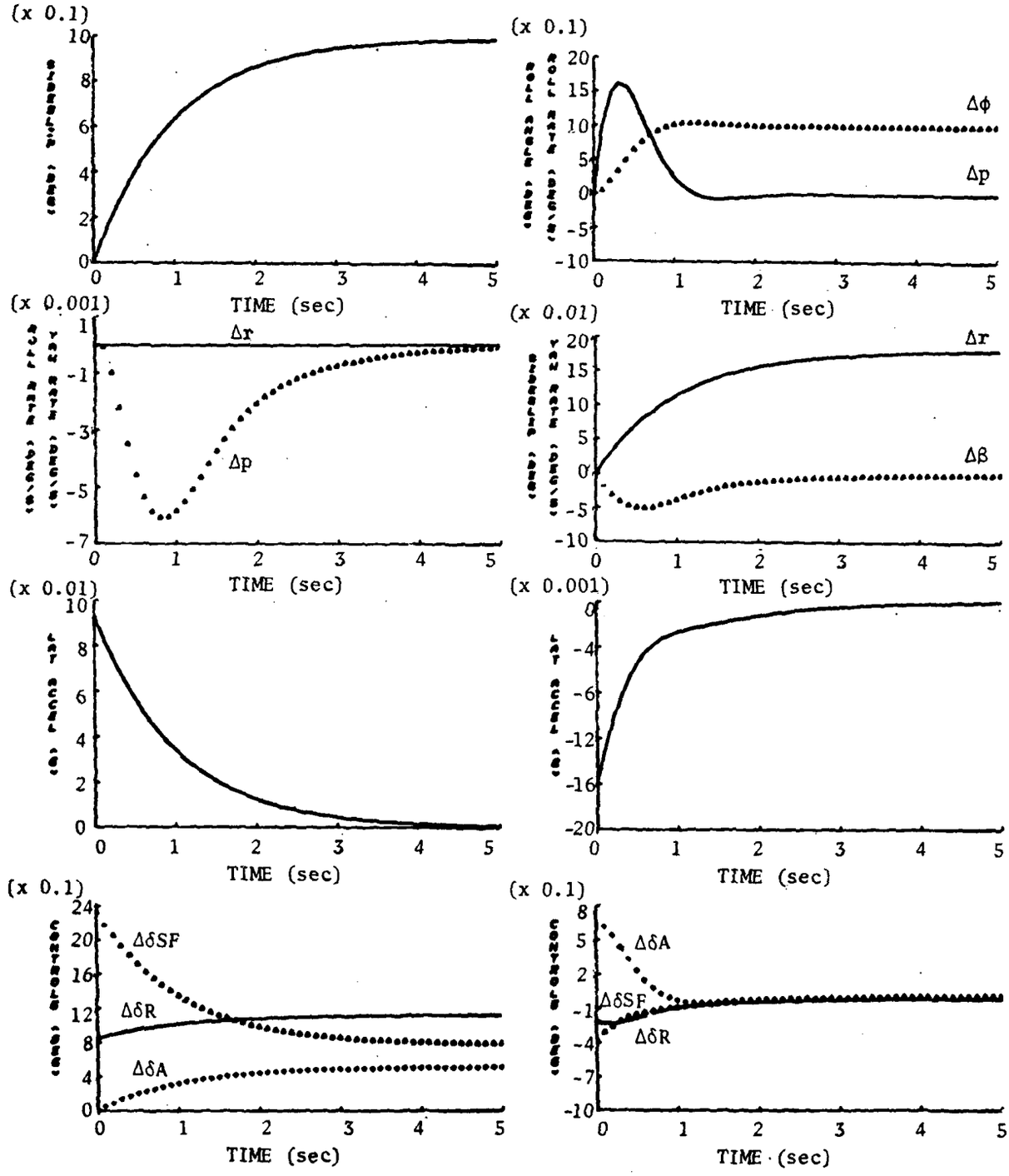

e) Mode 07: $\Delta\beta_c$ = 1 deg

f) Mode 07: $\Delta\phi_c$ = 1 deg, Δr_c =.181 deg/sec

Figure 2-5. Continued.

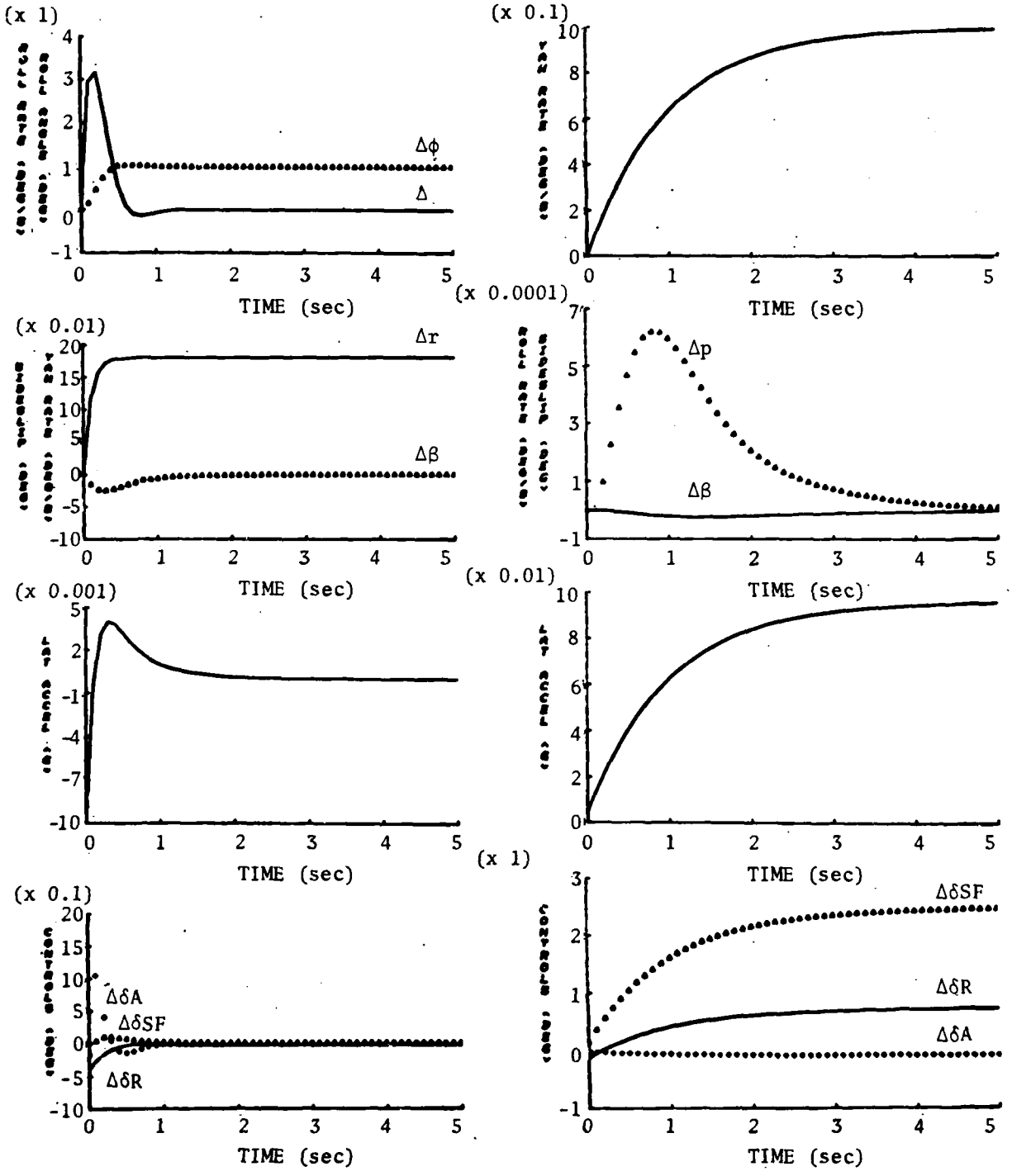

c) Mode 06: $\Delta\phi_c$ = 1 deg,
Δr_c = .181 deg/sec

d) Mode 07: Δr_c = 1 deg/sec

Figure 2-5. Continued

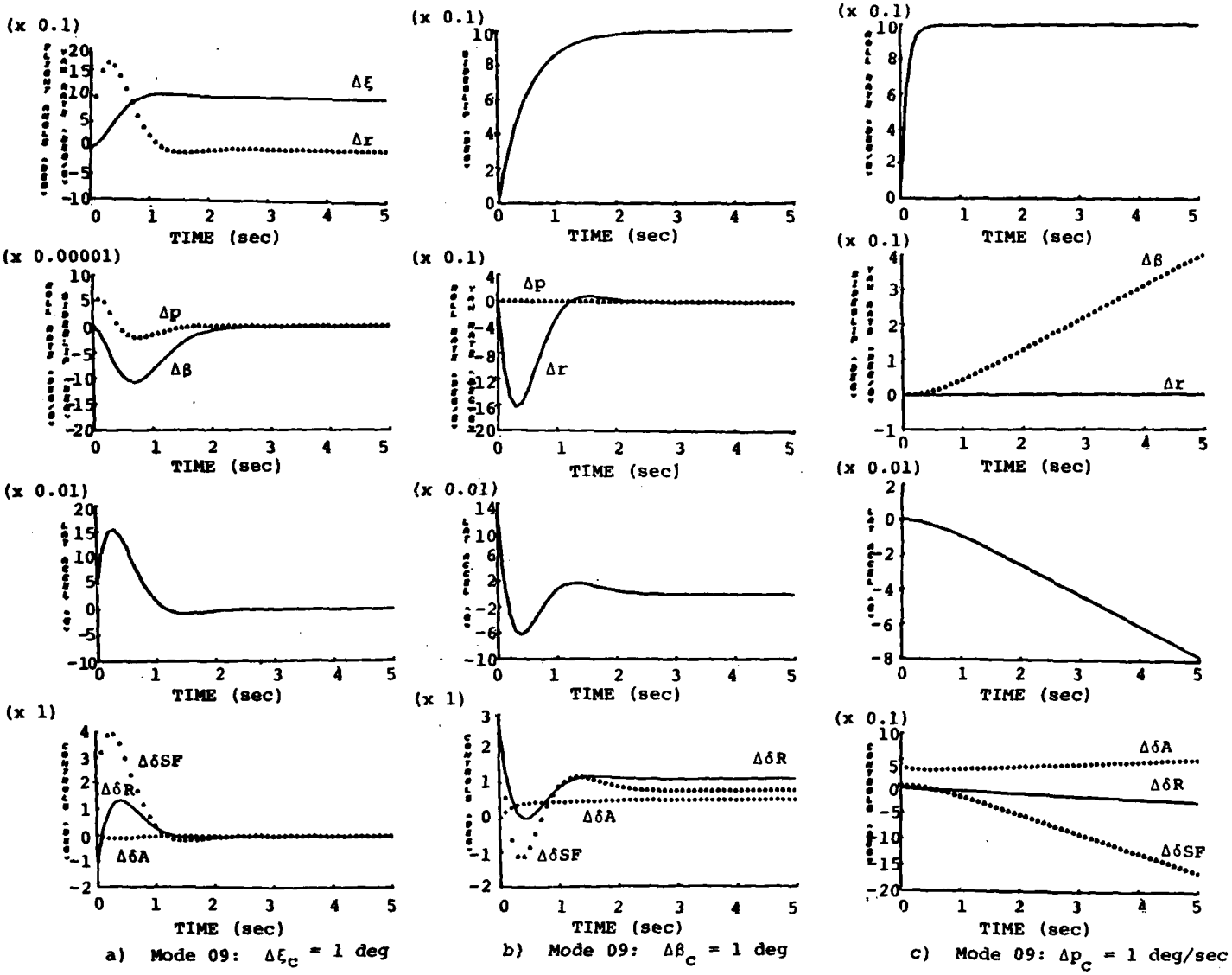

a) Mode 09: $\Delta\xi_c$ = 1 deg

b) Mode 09: $\Delta\beta_c$ = 1 deg

c) Mode 09: Δp_c = 1 deg/sec

Figure 2-6. Digital Simulations of (ξ, β, p) Mode Response, V = 105 KIAS.

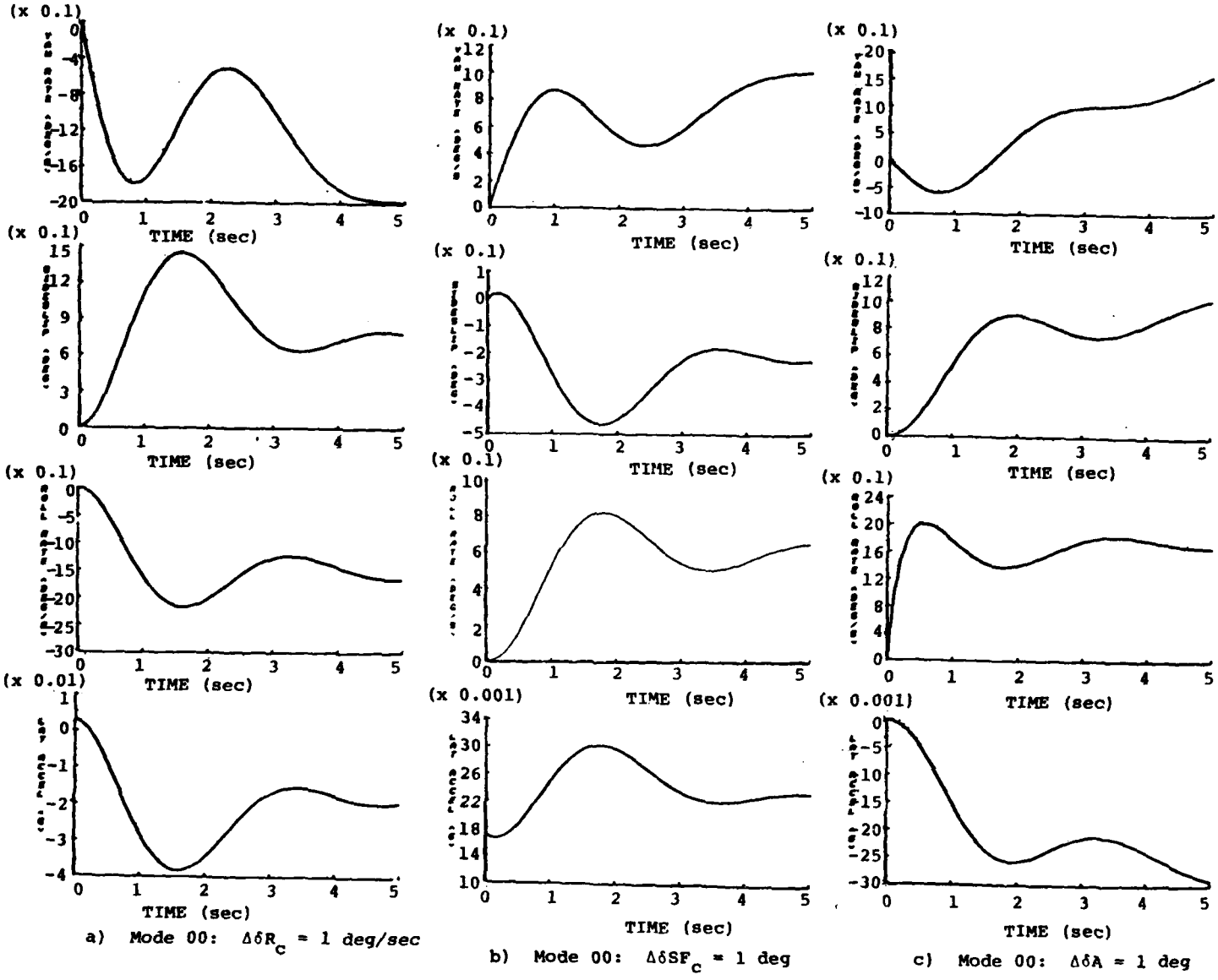

a) Mode 00: $\Delta\delta R_c$ = 1 deg/sec

b) Mode 00: $\Delta\delta SF_c$ = 1 deg

c) Mode 00: $\Delta\delta A$ = 1 deg

Figure 2-7. Digital Simulations of Unaugmented VRA Response, V = 75 KIAS.

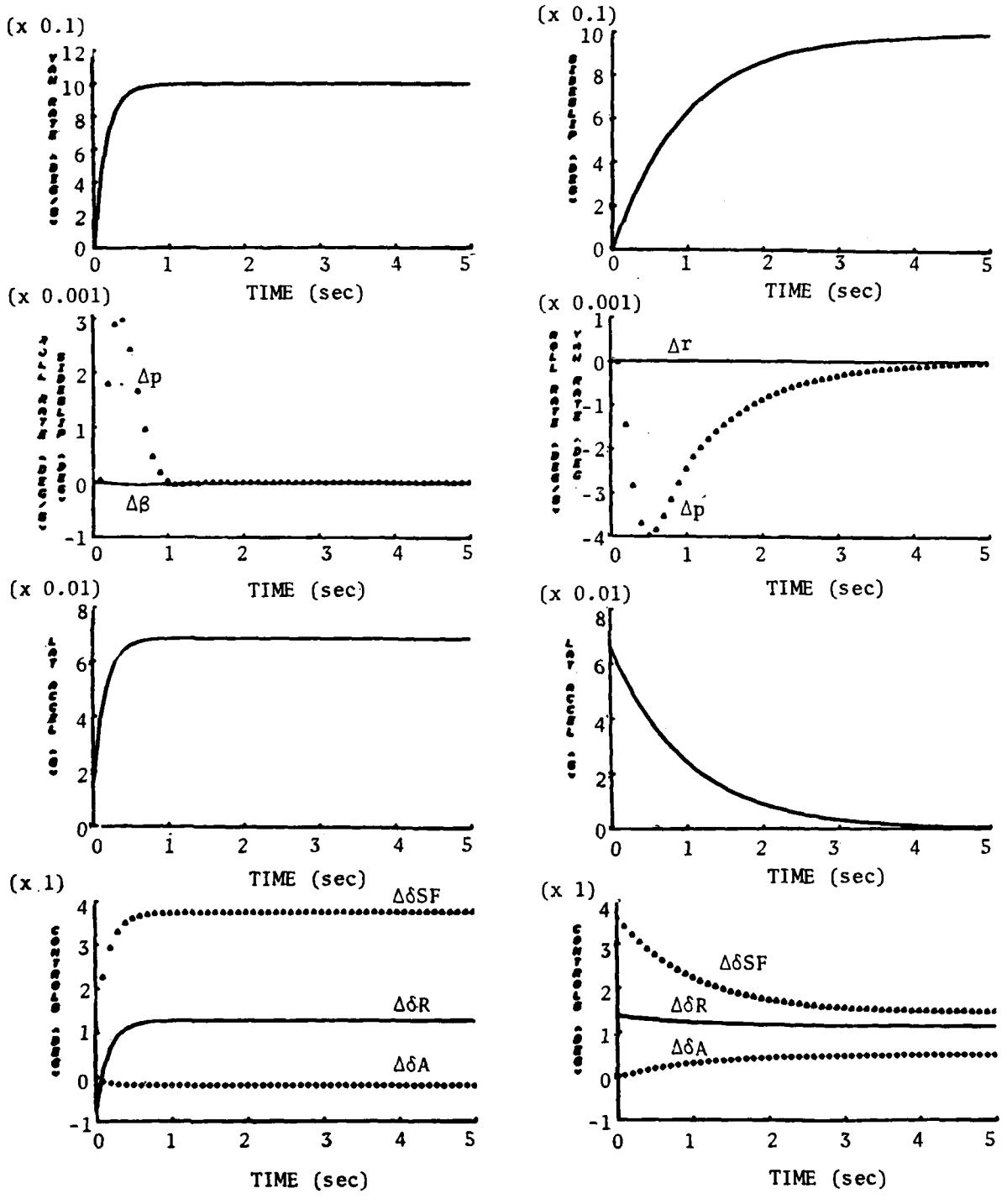

a) Mode 11: Δr_c = 1 deg/sec

b) Mode 11: $\Delta \beta_c$ = 1 deg

Figure 2-8. Digital Simulations of Uncoordinated (r, β, θ) Mode Response, V = 75 KIAS.

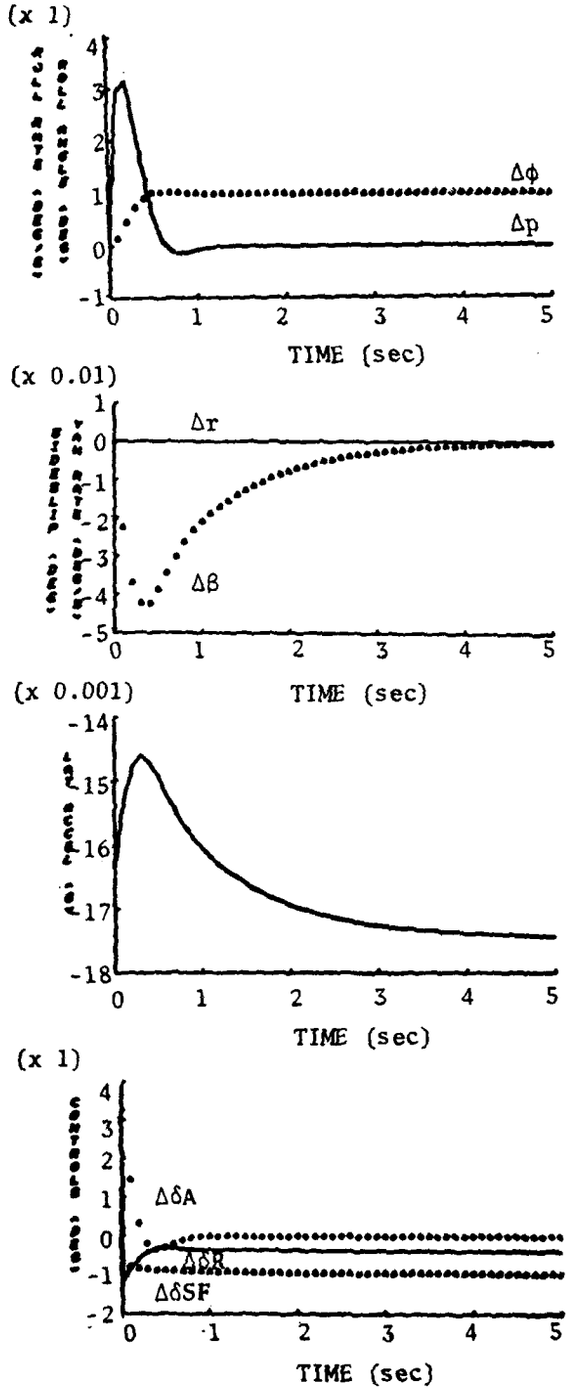

c) Mode 11: $\Delta\phi_c$ = 1 deg

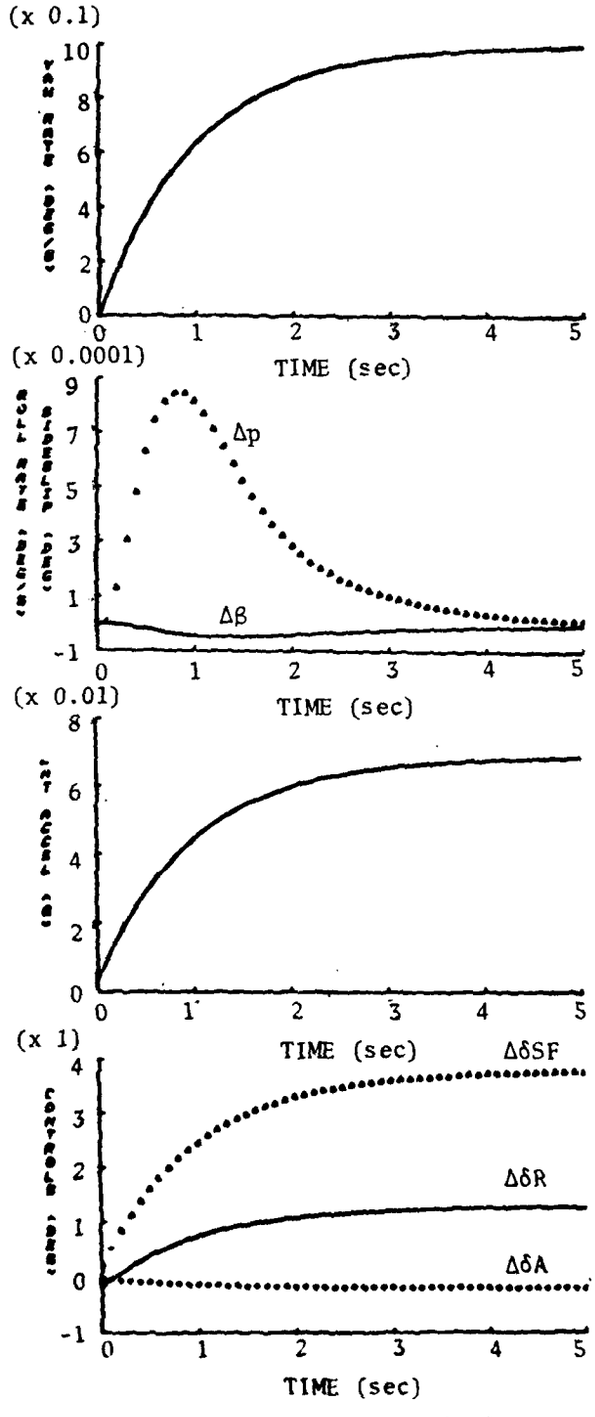

d) Mode 12: Δr_c = 1 deg/sec

Figure 2-8. Continued

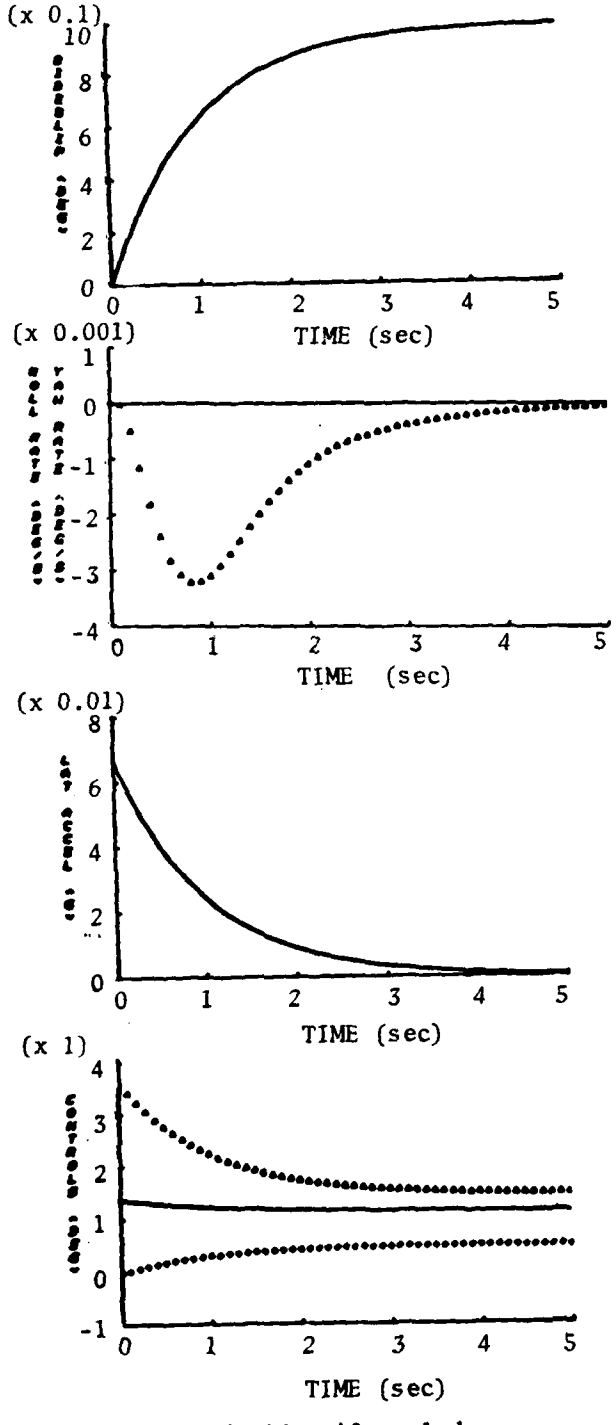

e) Mode 12: $\Delta\beta_c$ = 1 deg

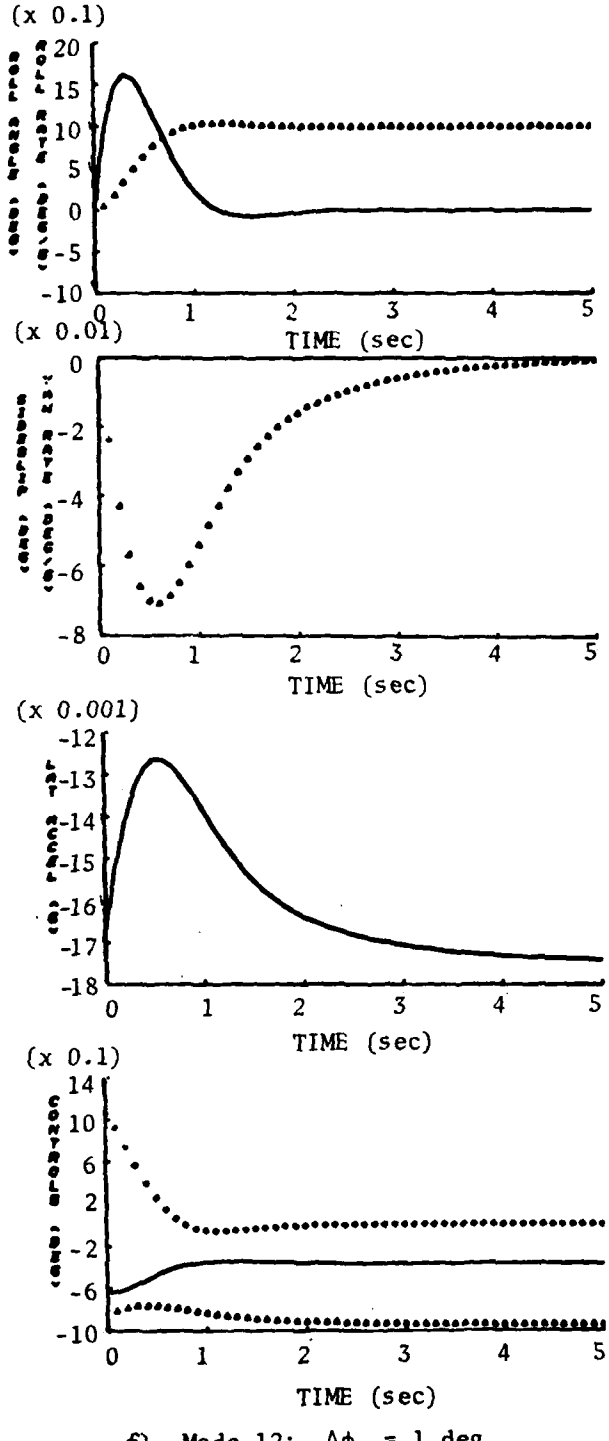

f) Mode 12: $\Delta\phi_c$ = 1 deg

Figure 2-8. Continued.

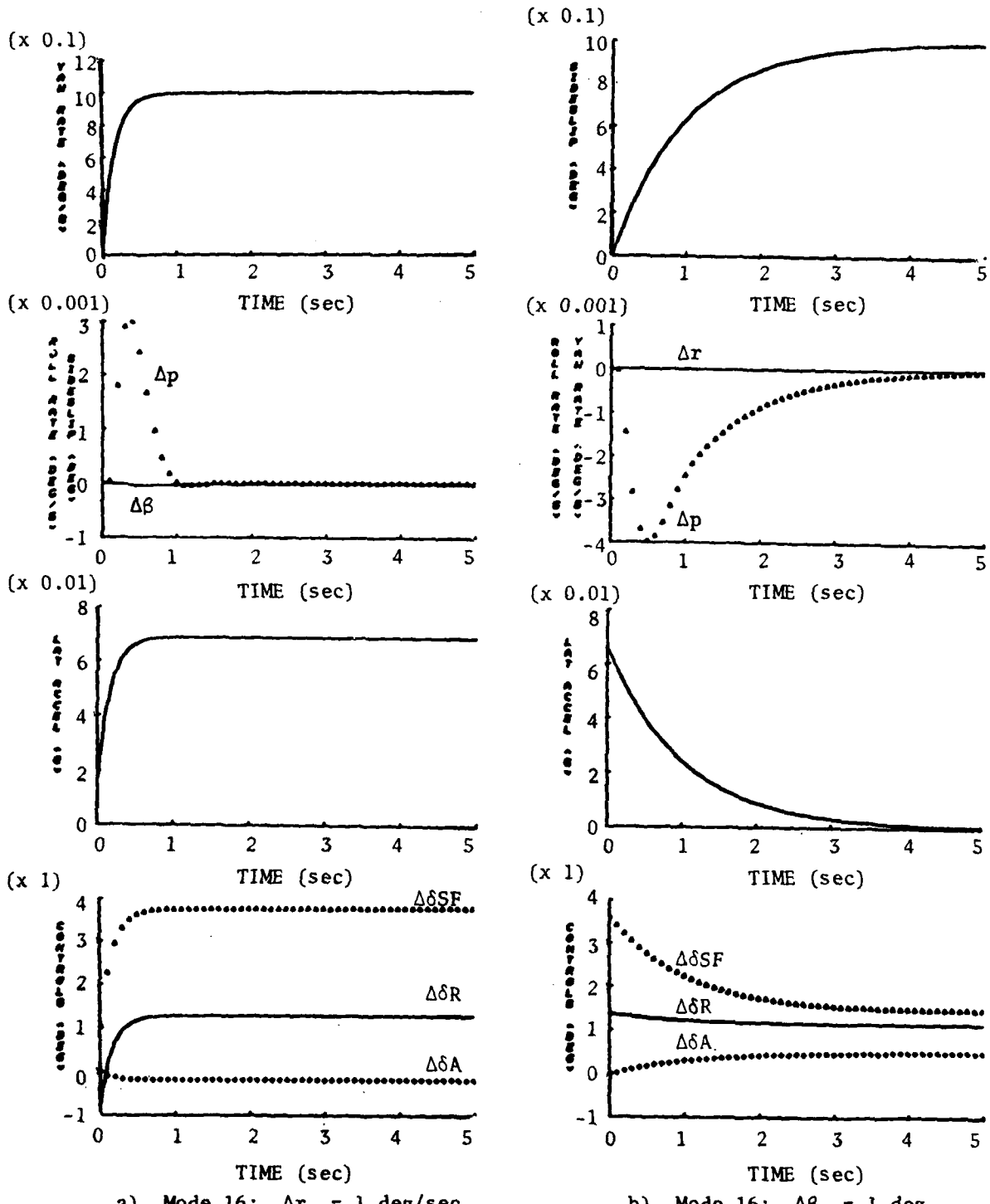

a) Mode 16: Δr_c = 1 deg/sec

b) Mode 16: $\Delta \beta_c$ = 1 deg

Figure 2-9. Digital Simulations of Coordinated (r, β,ϕ) Mode Response, V = 75 KIAS.

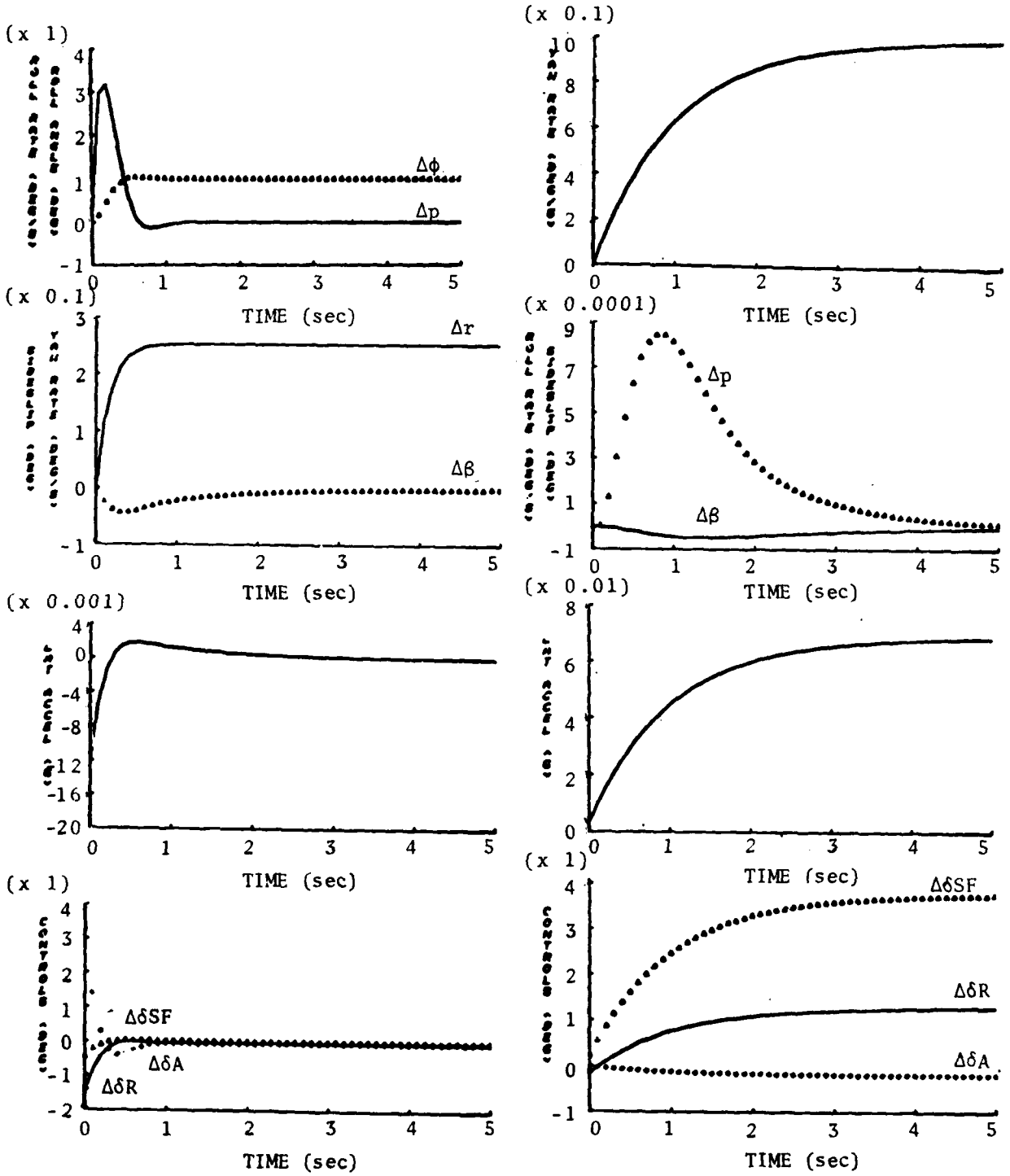

c) Mode 16: $\Delta\phi_c$ = 1 deg, Δr_c = .254 deg/sec

d) Mode 17: Δr_c = 1 deg/sec

Figure 2-9. Continued

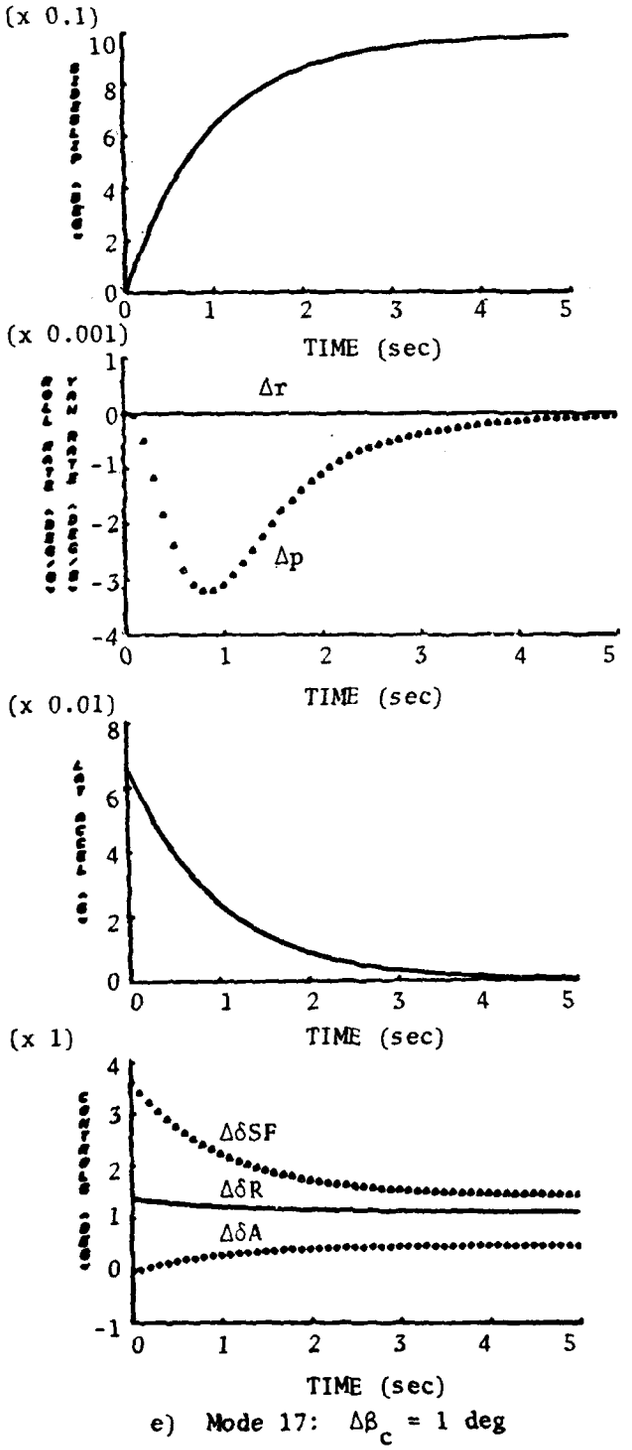

e) Mode 17: $\Delta\beta_c$ = 1 deg

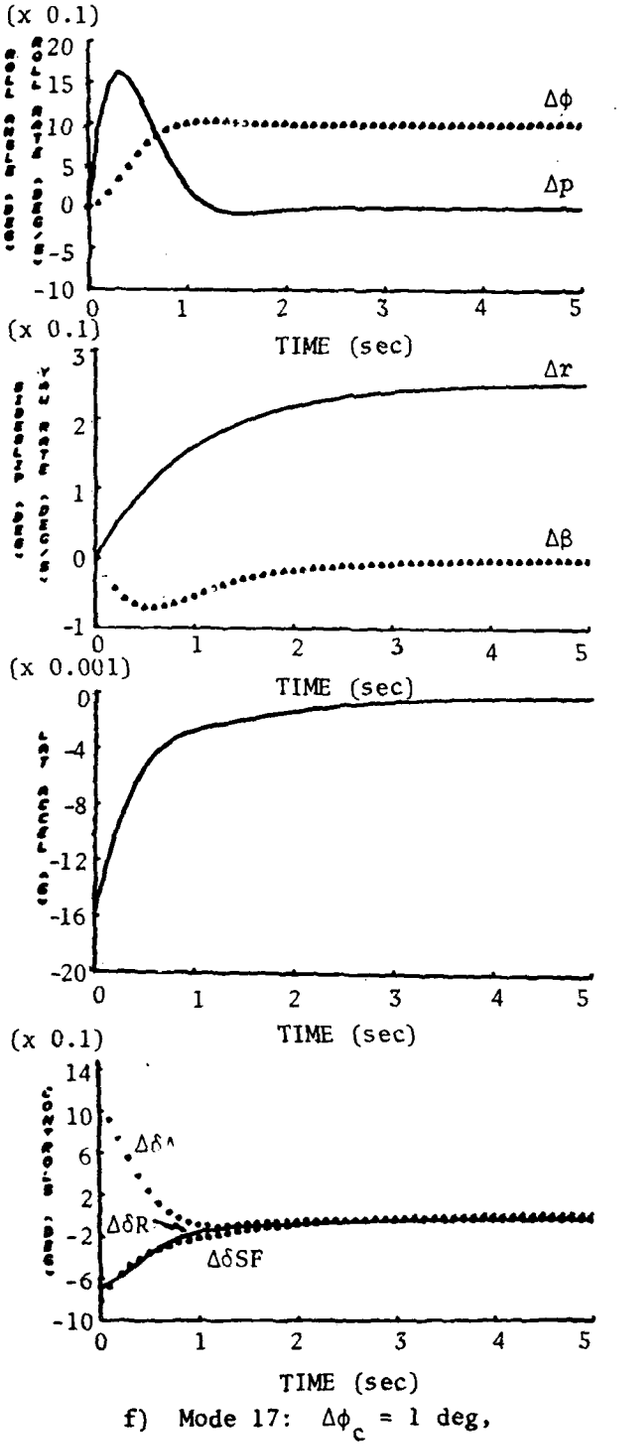

f) Mode 17: $\Delta\phi_c$ = 1 deg, Δr_c = .254 deg/sec

Figure 2-9. Continued

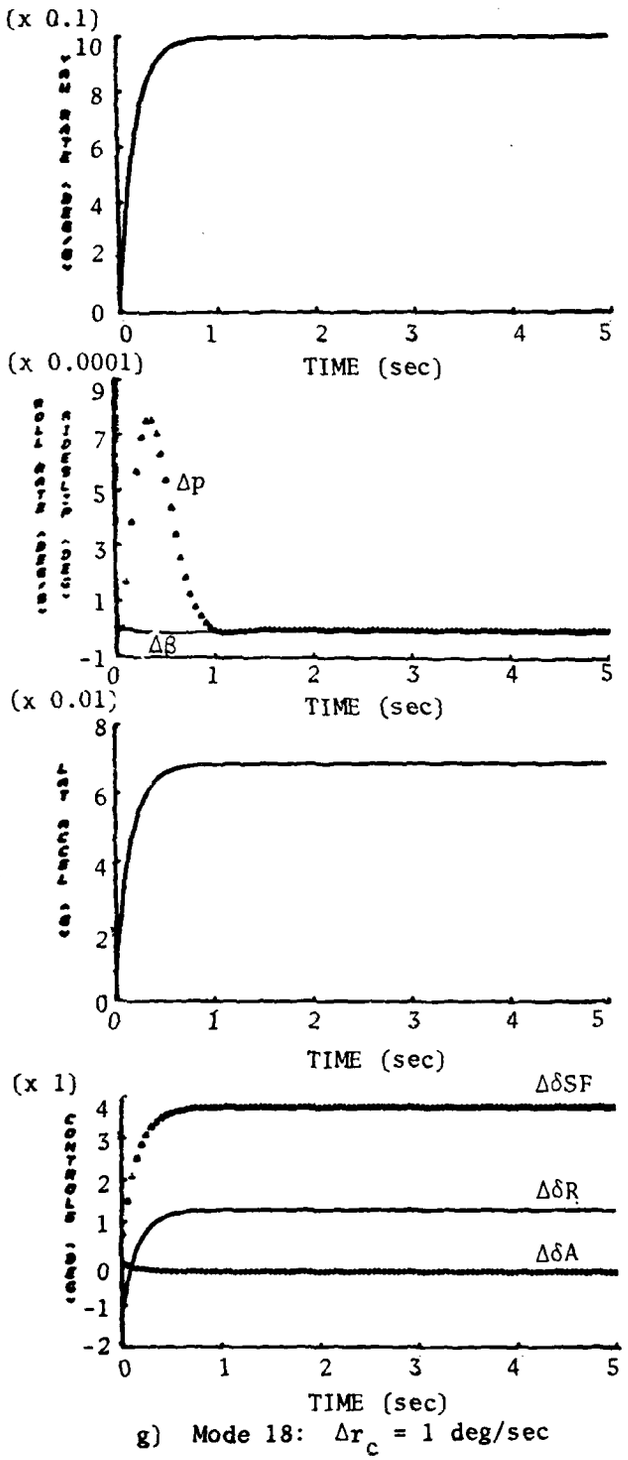

g) Mode 18: Δr_c = 1 deg/sec

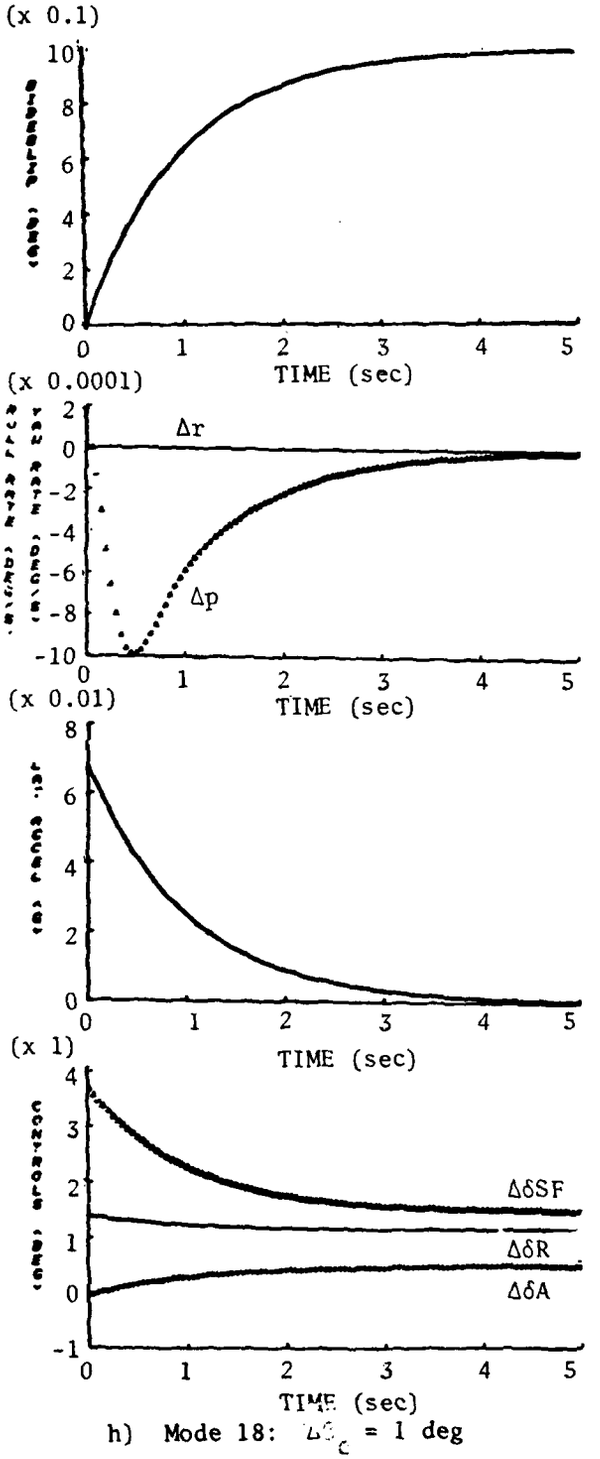

h) Mode 18: $\Delta\delta_c$ = 1 deg

Figure 2-9. Continued

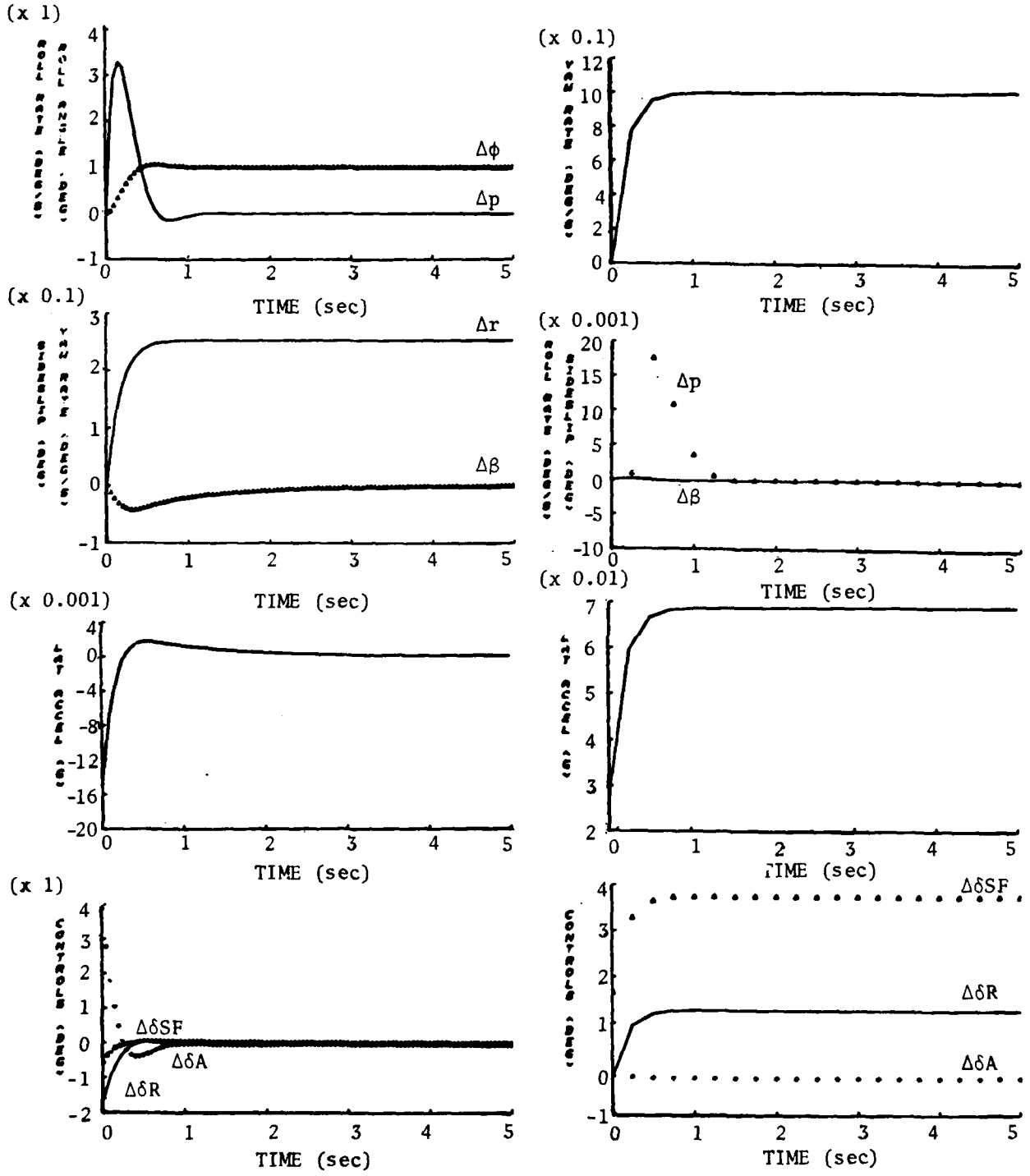

i) Mode 18: $\Delta\phi_c$ = 1 deg,
Δr_c = .254 deg/sec

j) Mode 19: Δr_c = 1 deg/sec

Figure 2-9. Continued

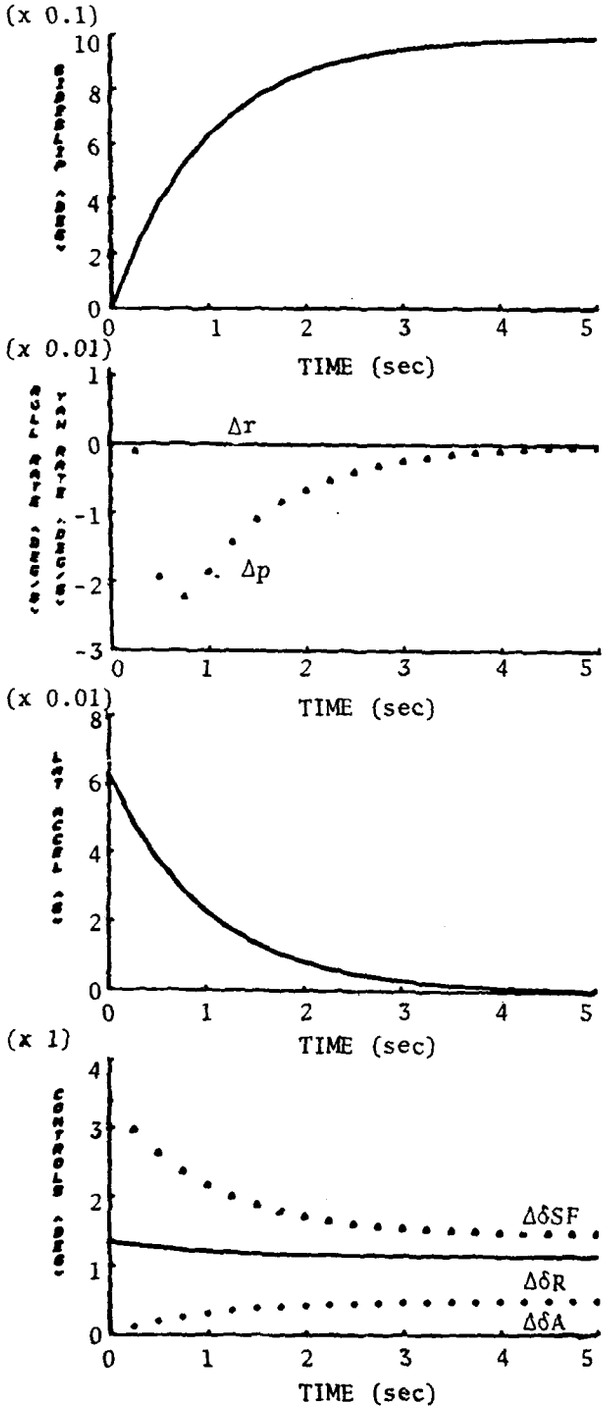

k) Mode 19: $\Delta\beta_c$ = 1 deg

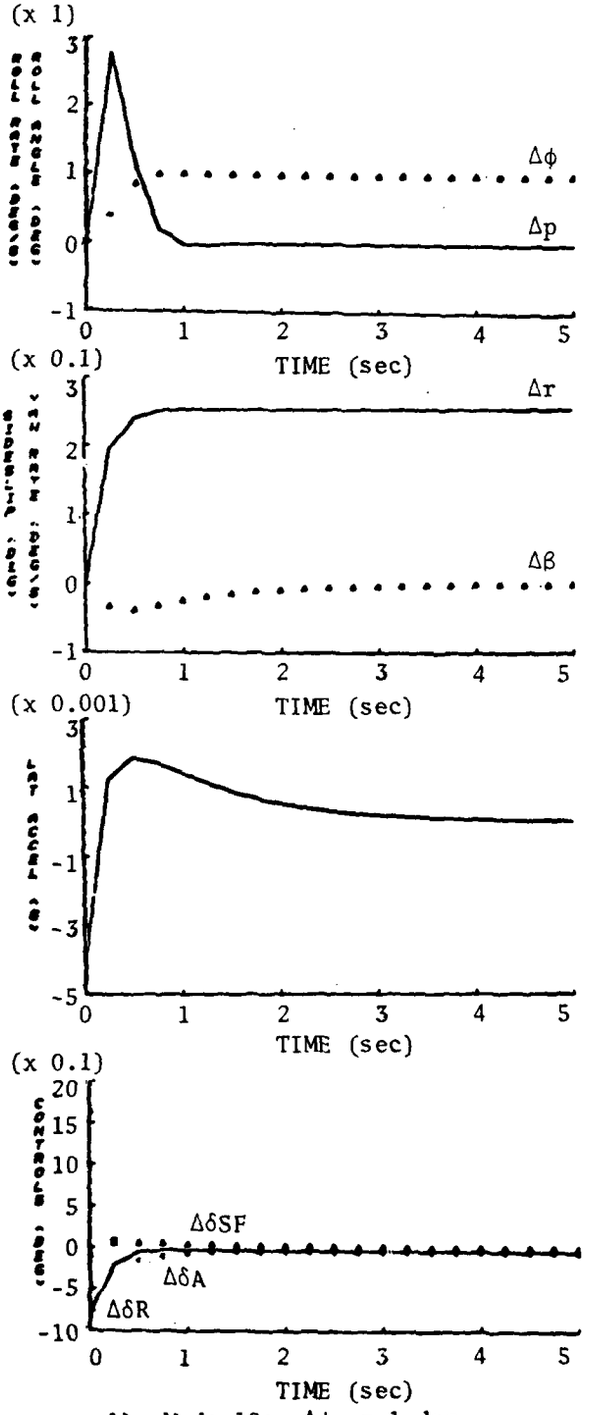

l) Mode 19: $\Delta\phi_c$ = 1 deg, Δr_c = .254 deg/sec

Figure 2-9. Continued.

3. MICROCOMPUTER IMPLEMENTATION

Once the digital control law for the CAS is developed, its logic must be transformed to the microcomputer for subsequent use in flight testing. The microcomputer used is a small digital computer with a modular board design that contains a microprocessor--a CPU housed in one chip. A Micro-DFCS was developed to implement the ESD Matching control law of the previous chapter. Its purpose is to accept analog information from the aircraft's sensors, and output analog signals calculated by the control law to each aircraft control actuator at periodic instants in time. The structure of the Model 2 Micro-DFCS was designed with flexibility in mind so that it could be used for other microprocessor-based systems, including a redundant system.

3.1 FLIGHT CONTROL COMPUTER UNIT

To accomplish the flight control task, the digital computer must have a variety of capabilities, including the following:

- A resettable timer to initiate the control law at precise instants in time
- Memory capacity to store the flight control program
- Analog-to-digital (A/D) and digital-to-analog (D/A) conversions
- Speed to calculate the control law between sampling intervals
- Interface with the pilot

The microcomputer is housed in a card cage unit which can hold up to eight computer boards. Each board contains the hardware to perform a specialized task. The boards used in this investigation are the following:

- Monolithic MSC 8004 Single Board Computer
- Intel iSBC 094 Battery RAM
- Intel iSBC 310 High-Speed Math

- Intel iSBC 724 Analog Output
- Intel iSBC 732 Combination Analog I/O

The MSC 8004 board contains the Zilog Z-80A microprocessor, which operates at 4MHz. The transfer of data between the MSC 8004 and the remainder of the boards uses the Multibus™. The user communicates with the computer by means of a control display unit (CDU)--either a console CRT terminal (when in the laboratory) or the Termiflex HT/4 hand-held CDU (when in the airplane).

The hardware layout of the Micro-DFCS, as used in flight testing, is depicted in Figure 3-1. The iSBC 116 memory board shown in the figure was not needed in the final system layout because the memory capacity of the MSC 8004 was adequate. For a detailed explanation of each piece of equipment, see Appendix C.

3.2 *FLIGHT CONTROL PROGRAM (CAS-6)*

This CAS-6 flight control program provides all of the microprocessor logic necessary to control the lateral-directional dynamics (including direct side force) of the VRA. CAS-6 includes the following routines:

- Flight Control
- Executive
- Utility

As an overview, the execution priority at each sampling instant is as follows:

1) Control law calculation
2) CDU input (on demand)
3) Memory check (every 5 seconds)
4) Wait state for remainder of sampling interval

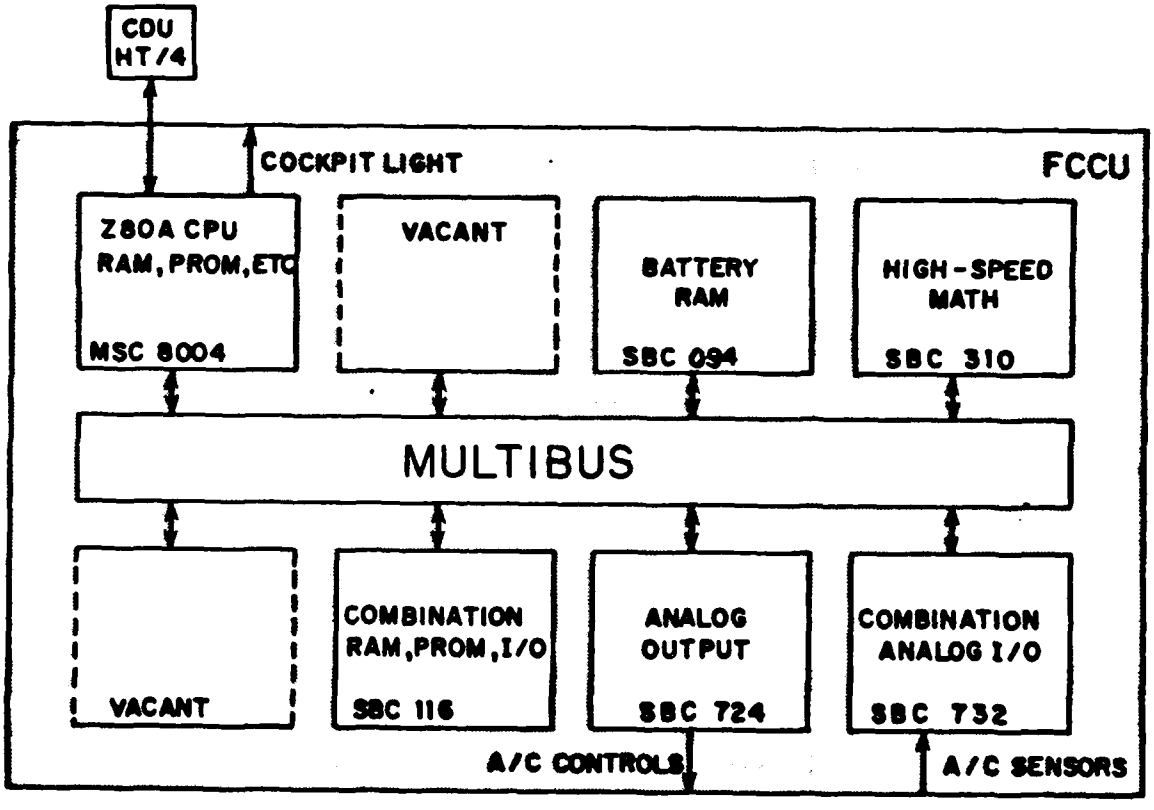

Figure 3-1. Model 2 Micro-DFCS Configuration.

A table of contents for CAS-6 appears in Table 3-1, along with the amount of memory devoted to each subroutine. The entire program is contained in about 6K (6144) bytes of memory. Figure 3-2 depicts the steps which the program logic must perform in order to execute the control law in the Micro-DFCS.

3.2-1 Flight Control Routine

The Flight Control Routine is the section of CAS-6 which is directly involved in the control law calculation. This calculation occurs only at each discrete sampling point (or interrupt), nominally occurring every 100 milliseconds. The Flight Control Routine is divided into subroutines that set up the control law for use and those that actually are serviced for the computation.

The set-up subroutines initialize the Micro-DFCS before the first control law calculation is performed. Specifically, a set-up routine,

- Displays the mode number selected
- Moves the gains and controller-to-command conversions
- Sets the interrupt branch.
- Initializes nominal values and stores them in a floating point format

The mode number chosen by, and then displayed to, the pilot corresponds to the model that the VRA is to follow. The various modes can differ in any of the following ways:

- Command vector
- Airspeed
- Transient response
- Controller-to-command pairings
- Sampling rate

Table 3-1. CAS-6 Table of Contents

Table 3-1. CAS-6 Table of Contents (contd)

		Memory Bytes
2.24	Strip Output	18
2.25	Timer	116
2.26	Move 4 Words (with Wait)	48
2.27	States and Commands Input	57
2.28	States Interpreted	245
2.29	Commands Interpreted	184
2.30	Signal Output	72
3.	FLIGHT CONTROL ROUTINE (3288)	
3.1	Direct Mode Set-Up	96
3.2	Yaw Rate, Sideslip, Roll Rate Set-Up (Modes 01-04)	223
3.3	Yaw Rate, Sideslip, Coordinated Turn Set-Up (Modes 06-08)	61
3.4	Flight Angle, Sideslip, Roll Rate Set-Up (Mode 09)	54
3.5	Yaw Rate, Sideslip, Roll Angle Set-Up at 75 kts (Modes 11-12)	28
3.6	Yaw Rate, Sideslip, Coordinated Turn Set-Up at 75 kts (Modes 16-19)	120
3.7	Direct Mode Service Routine	220
3.8	Yaw Rate, Sideslip, Roll Rate/Angle Service Routine	1114
3.9	Flight Angle, Sideslip, Roll Rate Service Routine	183
3.10	Gains, Messages, Constants	1189
	Total	6133

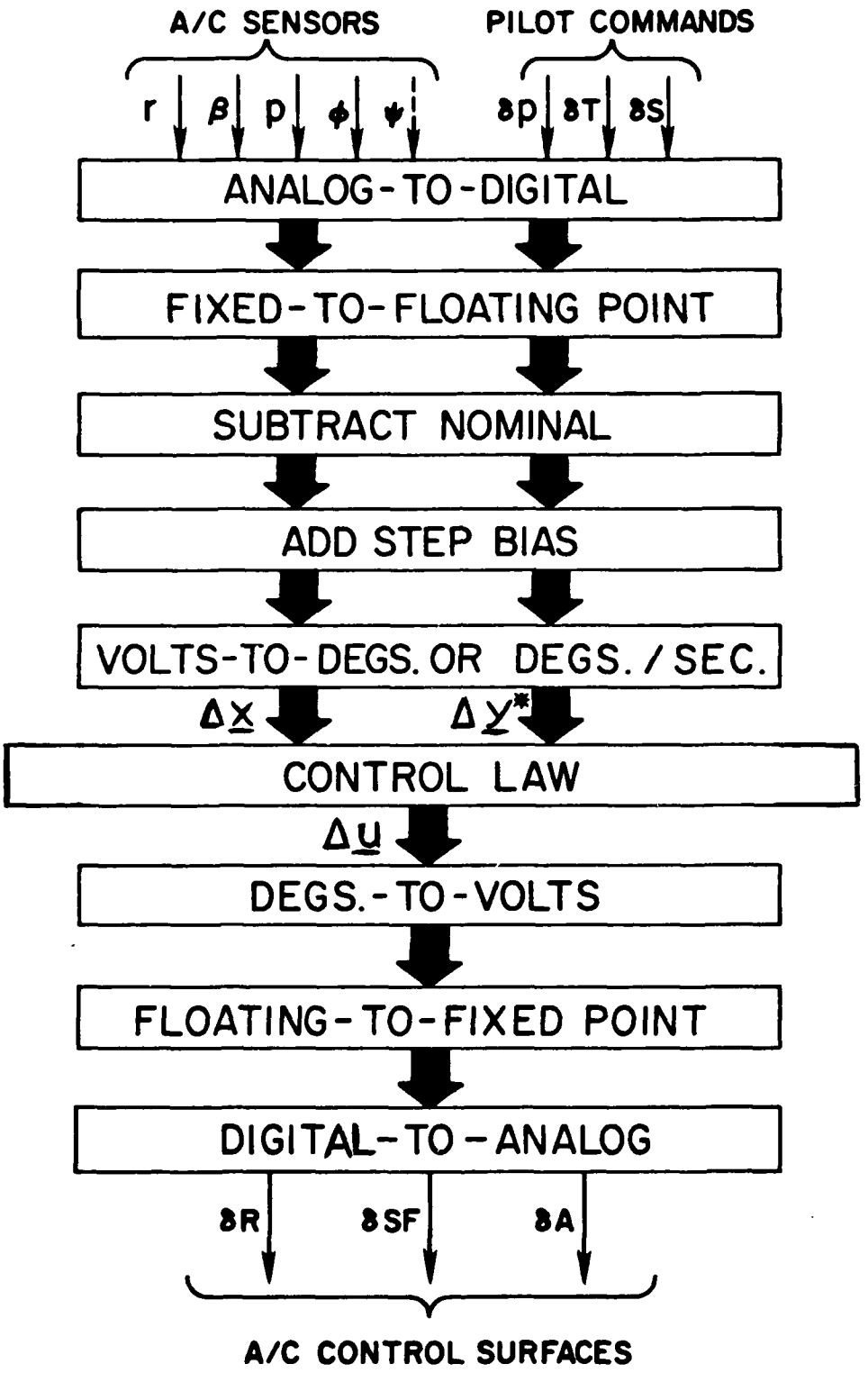

Figure 3-2. Flow Diagram of Control Law Implementation.

Depending on the mode selected, certain ESD gains and controller-to-command conversions are moved to the location where the service routine will use them. Controller-to-command conversions scale the voltage sent by the cockpit manipulators to the corresponding units of command motion. All of the A/D and D/A conversion factors used for CAS-6 are found in Appendix D. The controller-to-command conversions are computed using the relation,

$$\frac{\text{Maximum amount of command variable available on the VRA}}{.5 \times (\text{Volts produced by full deflection of manipulator})} \qquad (52)$$

For example, from the steady-state analysis in section 2.3-2, 13.4 deg of sideslip can be achieved by the VRA in Mode 01. Because the thumb controller produces 2.88 volts from full-right to full-left throw, the thumb-to-sideslip conversion is,

$$\frac{13.4}{.5 \times 2.88} = 9.306 \text{ deg/volt}$$

In addition, the appropriate service subroutine is set up for use at each sampling instant by having its starting address written at the software interrupt location in the system monitor.

The final action that each set-up subroutine takes is to sample the four states and three pilot commands. These are used as the nominal values in the calculation of perturbations in the control law. Furthermore, these values are converted from the 12-bit format of the A/D conversion to a 32-bit floating-point representation for later use by the math unit.

The remaining section of the Flight Control Routine consists of the service subroutines which are executed on each timed interrupt. The function of each is to,

- Input and convert the states and commands
- Calculate the required control deflections by ESD Matching
- Output the appropriate signals to the control actuators
- Increment the interrupt count
- Blink a light in the cockpit

CAS-6 employs two such service subroutines--one for the fourth-order dynamic system and the other for the fifth-order system. The fifth-order subroutine, used only when the command vector includes horizontal flight path angle, jumps to the fourth-order subroutine for completion of the control law calculation.

Each service routine first receives the voltages corresponding to the four states and three commands and converts them to the proper units and format for use in the control law. The subroutine then calculates the surface deflections required at that particular sampling instant using the ESD control law of eq. 33. The calculation of rudder perturbation, $\Delta\delta R$, employs the top row of the equation, $\Delta\delta SF$ the middle row, and $\Delta\delta A$ the bottom row.

The control calculations use floating-point arithmetic with units of degrees, while the control surfaces are driven by an analog voltage, so some conversions are necessary. First, the controls are scaled to units of volts by the D/A conversion factors. Then the main unit converts the digital values to a fixed-point format for the D/A board. The voltage output of the D/A board is sent immediately upon completion of each calculation and conversion. In other words, at each sampling point, the rudder signal is transmitted before either of the other two surface deflections is calculated.

After all three control signals have been sent, the service subroutine increments by one the interrupt count for use by the Executive and Utility Routines. The subroutine also enables an output port on the

8004 board to be turned on-and-off every 10 sampling periods. This is designed to flash a light in the cockpit to let the pilot know that the service subroutine is being entered on every interrupt. In addition to the Flight Control Routine, CAS-6 contains the Executive and the Utility Routine.

3.2-2 Executive Routine

The Executive Routine serves as the overall coordinator of CAS-6, and it consists of the following subroutines:

- Initialization
- CDU interface/command recognition
- Memory check

The initialization subroutine is executed at the start of CAS-6 to enable interface with the Micro-DFCS. When the program is accessed, some of the hardware elements must be initialized, including the following:

- Interrupt Controller
- Stack Pointer
- Timers
- I/O Ports
- Universal Synchronous/Asynchronous Receive/Transmit (USART) Unit
- Math Board
- A/D and D/A boards

The interrupt controller is designed so that the timer interrupt which occurs at each sampling instant possesses the third highest priority. This facilitates the use of higher priority interrupts should CAS-6 be modified for a redundant flight control system. The stack pointer must be initialized to a location that, when data is stored or removed from the stack, will not interfere with the execution steps of the program.

Two timers are used in CAS-6 to provide sampling rates of 4, 10, and 20 sps. One timer employs software to run ten times slower than the clock rate of 1 MHz. This, in conjunction with the second timer, provides a sensible range of sampling rates. The second timer, also software controlled, initially allows for the nominal sampling rate of 10 sps. An I/O port, whose bits are used in the service subroutines for execution timing checks and blinking the cockpit light, is initialized as an output port with zero volts. Next, the USART unit is set up to allow for the serial, asynchronous data transmission between the CDU (i.e. the user) and the CPU (i.e. the computer). In addition, the initialization subroutine defines the memory location where the math unit and analog conversion boards will be accessed.

At any time during program operation, the user may reinitialize CAS-6 to its original configuration. This part of the initialization subroutine performs the following:

- Displays initialization message
- Stores count-up address at interrupt location
- Clears flags, counters, etc.
- Initializes resolution mask
- Sends zero volts to all controls

The one-line initialization message lets the user know that the initialization subroutine has been entered. The count-up subroutine address is stored at the timer interrupt location so that a sequence of integers from one through ten will appear on the CDU--one each sampling instant--thus verifying the proper initialization of the timers and interrupt. The initialization subroutine then clears the memory locations which store the flags, counters, step voltage biases, and control law gains to ensure that a subsequent mode selection has a fresh start. The resolution mask is initialized to allow for the nominal resolution of 12 bits for the Micro-DFCS output signals. Finally, all six VRA controls--elevator, flaps, throttle, rudder, side force panels, and ailerons--are

sent zero volts by this subroutine. This ensures that the fly-by-wire (FBW) system will engage smoothly.

The next subroutine in the Executive Routine provides the interface between the CDU and Micro-DFCS, so that the user's commands can be interpreted. The user can select a variety of alternatives by depressing a single key on the CDU. The following options are presently defined in CAS-6 (with the select letter in parentheses):

- Break to system monitor (B)--jumps out of program and returns the user to the system monitor
- Delay parameters set (D)--allows for delay of sending of output signals
- Halt (H)--halts CPU
- Initialize (I)--enables fresh start of program
- Mode change (M)--allows for the selection of one of the defined modes
- Resolution change (R)--allows for the change in output resolution
- Step input (S)--allows for a voltage bias on any of the state or command variable inputs
- Timer change (T)--allows for a variation in sampling rate by changing the timer frequency

More on the aforementioned options can be found in the Utility Routine discussion.

A memory check feature is also located in the Executive Routine. Every five seconds, this subroutine adds the contents of the memory locations where CAS-6 resides. If the sum changes during execution, the message, "CKSUM ERROR", is displayed while the program is allowed to continue. This memory check feature notifies the pilot of any software alteration and may also be useful in a redundant computer system where the proper operation of each computer needs to be verified.

3.2-3 Utility Routine

The Utility Routine comprises the remainder of the CAS-6 program. This routine contains those generalized subroutines which the Executive and Flight Control Routines often use and which can be adopted in other microprocessor-based work. All of the subroutines in the Utility Routine are listed in Table 3-1; some have been previously described, so an enumeration of them will not be done here. Suffice it to say that the subroutines are used for such things as,

- CDU I/O
- A/D conversions
- D/A conversions that limit the output to ± 10 volts
- Math operations
- Moving and erasing memory
- State and command variable interpretation

In addition, the Utility Routine contains those subroutines necessary for implementation of some of the user-selectable options mentioned in the Executive Routine discussion. Specifically, those subroutines are,

- Set delay/delay output
- Mode change
- Resolution change/strip output
- Step input
- Timer change

The subroutines which set the delay option and then delay the signal output are available only in the Direct Mode. The delay feature is useful for testing the effects of delays--computation, sampling, etc,--between the pilot command and the associated output to the control surface. The set delay subroutine allows the user to delay the output signal to any or all of the three controls.

The mode change subroutine gives the user the choice of any of the defined modes in CAS-6. Presently, Modes 00-07,09,11,12, and 16-19 are available. After the two-digit mode number is entered, a jump is performed to the corresponding set-up routine.

With the resolution change and strip output subroutines, the user may change the resolution of the Micro-DFCS output signal. The user initiates a resolution change by entering a two-digit decimal integer, not greater than twelve. Then, each time the required control outputs are calculated, they are stripped to the desired number of bits and adjusted for the associated bias.

The step input feature in the Utility Routine provides the pilot with the means of adding a calibrated step in voltage to any of the four states or three commands. This provides the capability in testing to input precise commands--as opposed to using the cockpit manipulators--to the Micro-DFCS. The desired input is selected by first entering the two-digit multiplexer channel for the variable, and then the voltage. A carriage return initiates the step, and it is terminated by depressing any CDU key. Changing modes with the mode change option clears all step biases in the system.

The last user-selectable subroutine in the Utility Routine allows for the variation in sampling rate. A timer change places the four-digit hexadecimal entry into the second timer counter to provide sampling rates from nearly continuous to as low as 1.5 sps. This subroutine must be used before Mode 18 (20 sps) and Mode 19 (4 sps) are implemented.

After the entire program is written in Assembly Language, Princeton University's IBM 3033 computer generates the corresponding hexadecimal machine code. This code then can be directly loaded into the micro-computer by the 3033. CAS-6 is too lengthy to list here; the program is available at the Flight Research Laboratory (FRL). As an example of an

Assembly Language program written for the microcomputer, Appendix B shows the program that is used to add the hexadecimal contents of CAS-6 for use in the memory check subroutine.

3.3 DESIGN CONSIDERATIONS

Although the Z-80A microprocessor is fast--a minimum instruction time of 1.25 μsec--additional computational savings can be achieved. CAS-6 includes some features designed to reduce the time between the sampling instant and the output signal to the VRA's control actuators.

The service routines are coded specifically to the task. This means that the calling of subroutines is kept to a minimum, and those subroutines called are specific to the operation. For example, the closed-loop service routines perform all of the instructions necessary to initiate a math operation and retrieve the result. In this manner, while the math unit is busy, the bytes for the next math operations can be readied for transfer. Also, the ESD gains calculated for each mode are coded in floating-point format, thereby eliminating the time that the math unit would take during program execution to convert the gains. Furthermore, by having all of CAS-6 located in memory on-board the MSC 8004, a further time savings is realized, since the data are not put on the bus for use by the CPU. An example of this type of savings is illustrated by the execution of a software timing loop used to generate a 50 msec pulse. (Table 3-2)

As a result of these time-saving designs, the CAS-6 closed-loop service routines use only 20 msec of the sampling interval. Each of the three control calculations is 5 msec long, while the remaining 5 msec is used to input and convert the state and command signals. The direct mode service subroutine, which uses more generalized subroutines but a much lesser number of calculations than the ESD service routines, takes 9 msec to complete.

Table 3-2. Computation Time Savings of On-Board Memory

Test Condition	Program Time (msec)
on-board RAM	50
on-board PROM	50
off-board RAM	79
off-board battery RAM	86

(Tests conducted with 4 MHz Z-80A during the timing loop used to generate 50 msec pulse for the PROM programmer.)

Though CAS-6 performs the control law calculation swiftly enough for accurate tracking, future Micro-DFCS designs could decrease the computational time even more. The Am 9511 Arithmetic Processing Unit (APU) located on the 8004 board performs math operations twice as fast, on the average, as the iSBC 310 math unit. The APU also has additional time-saving benefits because it avoids the access time associated with the data bus. However, the APU was not used because its proper operation had not been sufficiently verified at the time of the CAS-6 design. Also, new software was required for the calculation of gains in the chip's floating-point format (which is different from the iSBC 310's floating-point format).

Another possible method to reduce computational time is to pre-compute the ESD gains taking into account the VRA's sensor input and control output conversion factors. For example, the pilot's controls, $\Delta \underline{y}_p$, are related to his desired commands, $\Delta \underline{y}$, by,

$$\Delta \underline{y}_p = \begin{bmatrix} K_P^Y 1 & 0 & 0 \\ 0 & K_T^Y 2 & 0 \\ 0 & 0 & K_S^Y 3 \end{bmatrix} \Delta \underline{y} \qquad (53)$$

where K_{p1}^{Y} , for instance, is the "gearing" between the pedals and one of the command variables, Δy_1. If this relationship is included in the ESD control law gains, a conversion step in the program would be eliminated. The time-savings associated with this technique may be offset by the increase in complexity and decrease in software flexibility (for example, when a conversion value is in error or needs to otherwise be adjusted).

3.4 HYBRID SIMULATION

In order to verify the Micro-DFCS design, a hybrid simulation was conducted prior to flight testing. This ground simulation consisted of the microcomputer interfaced by trunk lines with the EAI TR-48 analog computer. The analog computer provided the VRA's lateral-directional dynamics. (See Fig. 3-3 for the analog diagram and Table 3-3 for the corresponding potentiometer settings.) The objective of the simulation was to analyze the Micro-DFCS in an environment similar to that of the flight test, so as to reduce the cost, time, and risk of flying a novel system. One thing that is done, therefore, is to include the conversion voltages of the aircraft's motion sensors and control sunfaces on the analog board. As a result, CAS-6 can be interfaced with the analog computer without any software modification.

During the simulation, the states and controls of the analog computer are sent to a six-channel strip chart recorder. Figures 3-4 to 3-10 show the verification of the control modes to be flight tested. The time responses from the hybrid simulation should differ only slightly from those of the digital computer simulation (Fig. 2-3 to 2-9) for the following reasons:

- System noise
- Digital Resolution
- Computation delay
- Continuous-time integration of states
- Zero-order hold (staircasing) of controls

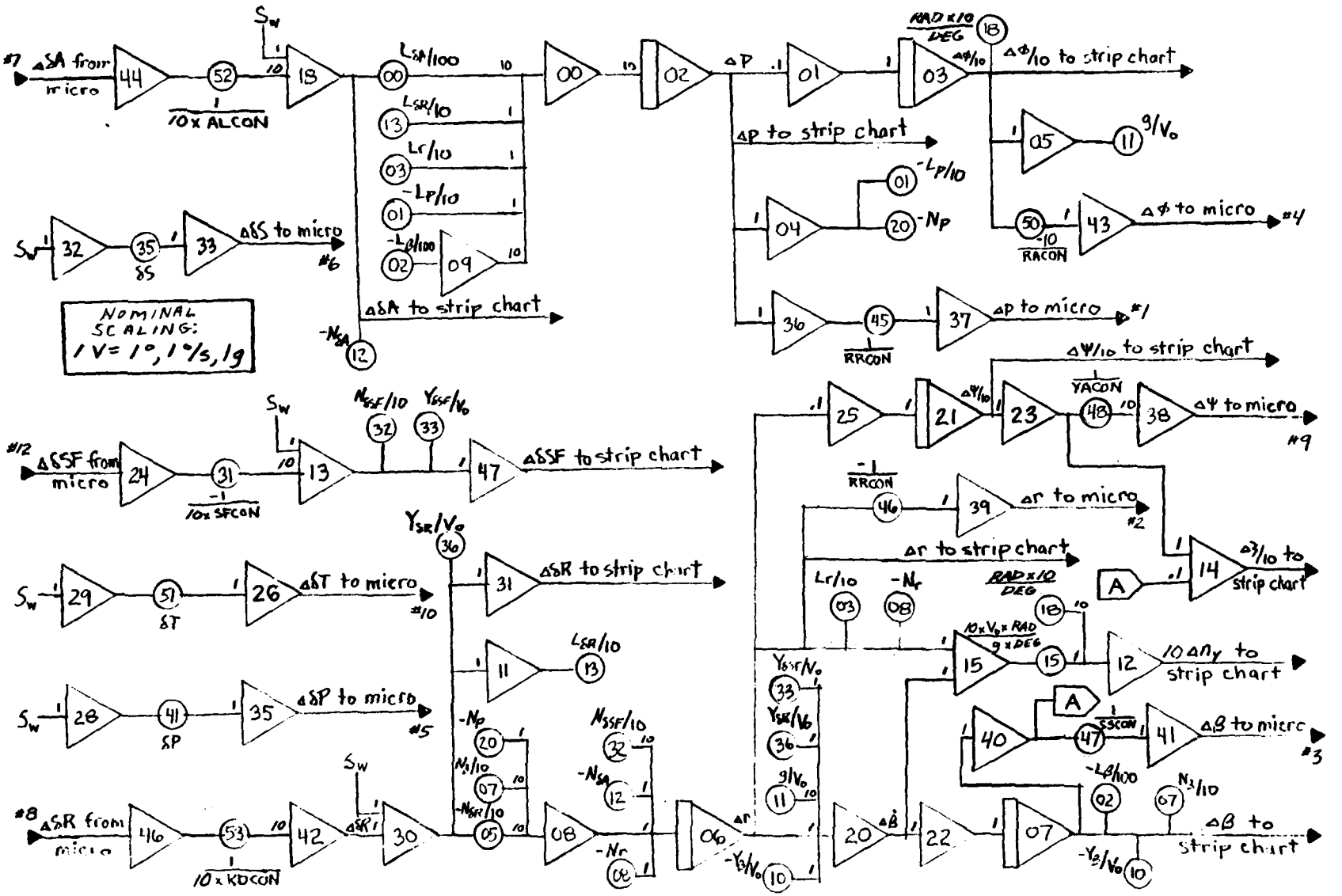

Figure 3-3. Analog Diagram of VRA Lateral-Directional Dynamics.

Table 3-3. Analog Potentiometer Settings

POT	PARAMETER/SCALING	SETTING 105 kts	75 kts
00	$L_{\delta A}/100$	.210	.154
01	$-L_p/10$	.650	.460
02	$-L_\beta/100$	.115	.061
03	Lr/10	.116	.160
05	$-N_{\delta R}/10$	.610	.412
07	$N_\beta/10$	.530	.299
08	-Nr	.750	.685
10	$-Y_\beta/V_o$	.400	.416
11	g/V_o	.181	.254
12	$-N_{\delta A}$	.222	.109(x10)
13	$L_{\delta R}/10$	.060	.039
15	$[(V_o/g)x(rad/deg)]x10$	.962	.687
18	(rad/deg)x10	.175	.175
20	$-N_p$	.260	.199
31	(-1/SFCON)/10	.349	.349
32	$N_{\delta SF}/10$	.210	.114
33	$Y_{\delta SF}/V_o$	.380	.250
35	δS	?	?
36	$Y_{\delta R}/V_o$	.094	.047
41	δP	?	?
45	1/RRCON	.224	.224
46	-1/YRCON	.272	.272
47	1/SSCON	.171	.171
48	1/YACON	?	?
50	(-1/RACON)x10	.832	.832
51	δT	?	?
52	(1/ALCON)/10	.195	.195
53	(1/RDCON)/10	.191	.191

* (? - Signifies variable or undetermined value)

Noise is apparent in the plots of the $\Delta\phi$, $\Delta\delta SF$, and $\Delta\delta A$ traces, thereby affecting the efficiency of the control law. This noise was attributed to the 60-Hz noise on the trunk lines and should not be present during flight testing.

Some other discrepancies in the hybrid simulation verification were noted. When the Δr command is returned to zero in Modes 01, 05, 06 and 07 (Fig. 3-5 and 3-6) the $\Delta\delta SF$ is not quite properly nulled. Additionally, the initial $\Delta\delta SF$ to $\Delta\beta$ command in Modes 02, 05, and 07 (Fig. 3-5 and 3-6) is less than expected. Both of these types of discrepancies have no noticeable effect on the output. For some reason the steady-state Δr is not zero when Δp is commanded in Mode 05 (Fig. 3-5c). In Mode 06 (Fig. 3-6a), Δr is less than the proper coordinating value of 0.181 deg/sec; thus the steady-state controls are nonzero. At 75 KIAS, all of the associated closed-loop modes (Fig. 3-8 to 3-10) show a Δr that is improperly excited by a $\Delta\beta$ command and all three controls are deflected less than the correct amount.

Because of the undesirable discrepencies noted, a comprehensive check of the analog computer configuration and optimal gains was accomplished, but nothing unusual was uncovered. Much later it was discovered that the open-loop response of the analog computer model of the VRA at 75 KIAS to 1 deg $\Delta\delta A$ input was unquestionably too large in state magnitude. This could have caused the difficulties of the modes at 75 KIAS during the hybrid simulation, yet the control law would still work properly on the VRA in actual flight.

The hybrid simulation plots point out some interesting features. The controls do not return to zero when the Δp step command is zeroed in Modes 01 and 02 (Fig. 3-5) because $\Delta\beta$ is not properly nulled in these singular equilibrium examples. $\Delta\xi$ is traced in Mode 09 (Fig. 3-7) to illustrate that the fuselage pointing mode results when $\Delta\beta$ is commanded, and that the foot pedals will simply command a change in heading. At 4 sps,

Mode 19 (Fig. 3-10d) graphically shows the resolution and zero-order hold of the controls, yet the states are not perceptibly degraded. Finally, lateral acceleration (not shown) was monitored on the analog computer to verify that the coordinated turn modes (Modes 06, 07, and 16-19) were properly nulling this acceleration.

With the hybrid simulations completed, the modes were ready to be evaluated in flight.

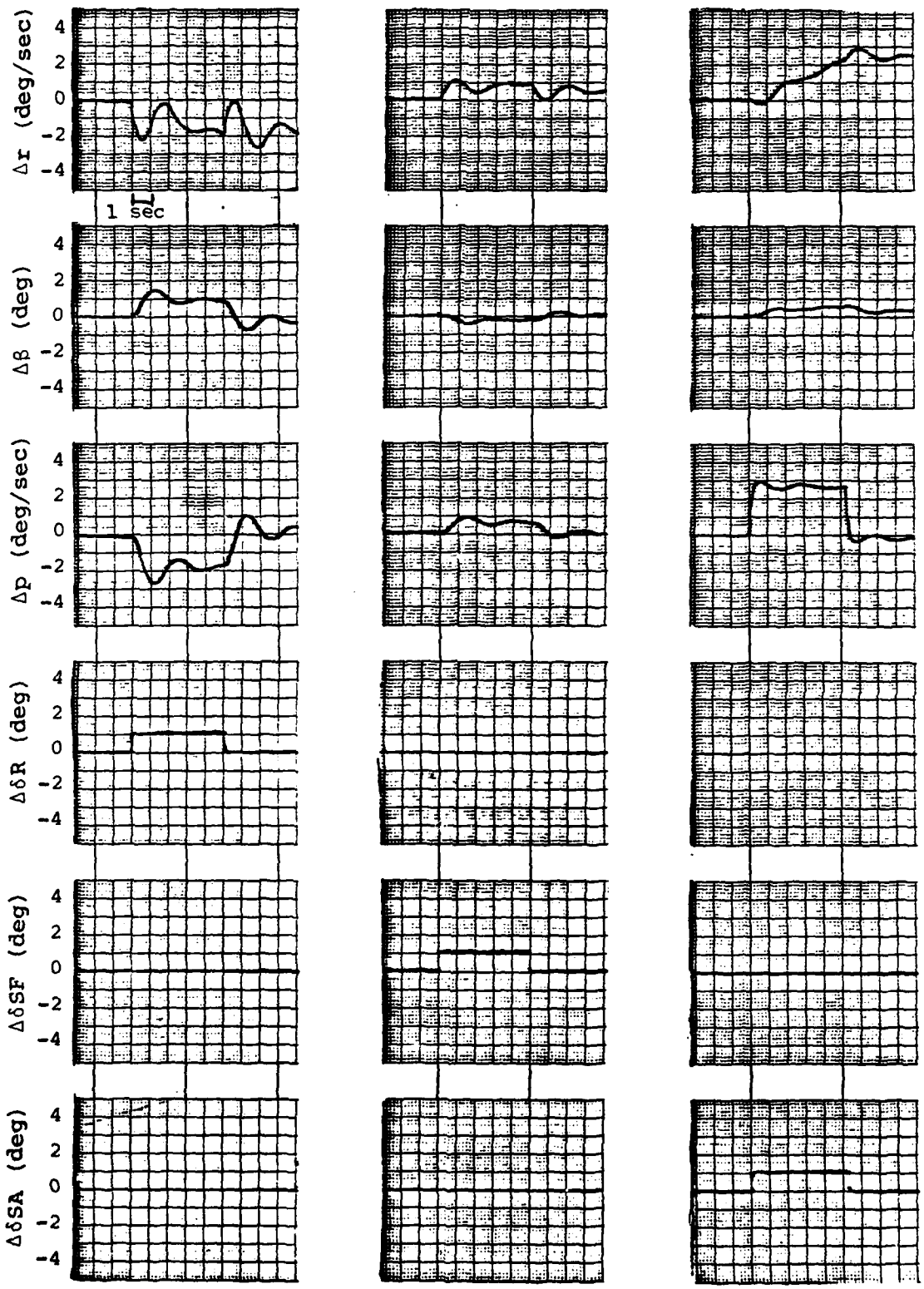

a) $\Delta\delta R_c$ = 1 deg b) $\Delta\delta SF_c$ = 1 deg c) $\Delta\delta A_c$ = 1 deg

Figure 3-4. Hybrid Simulations of Unaugmented VRA Response V = 105 KIAS.

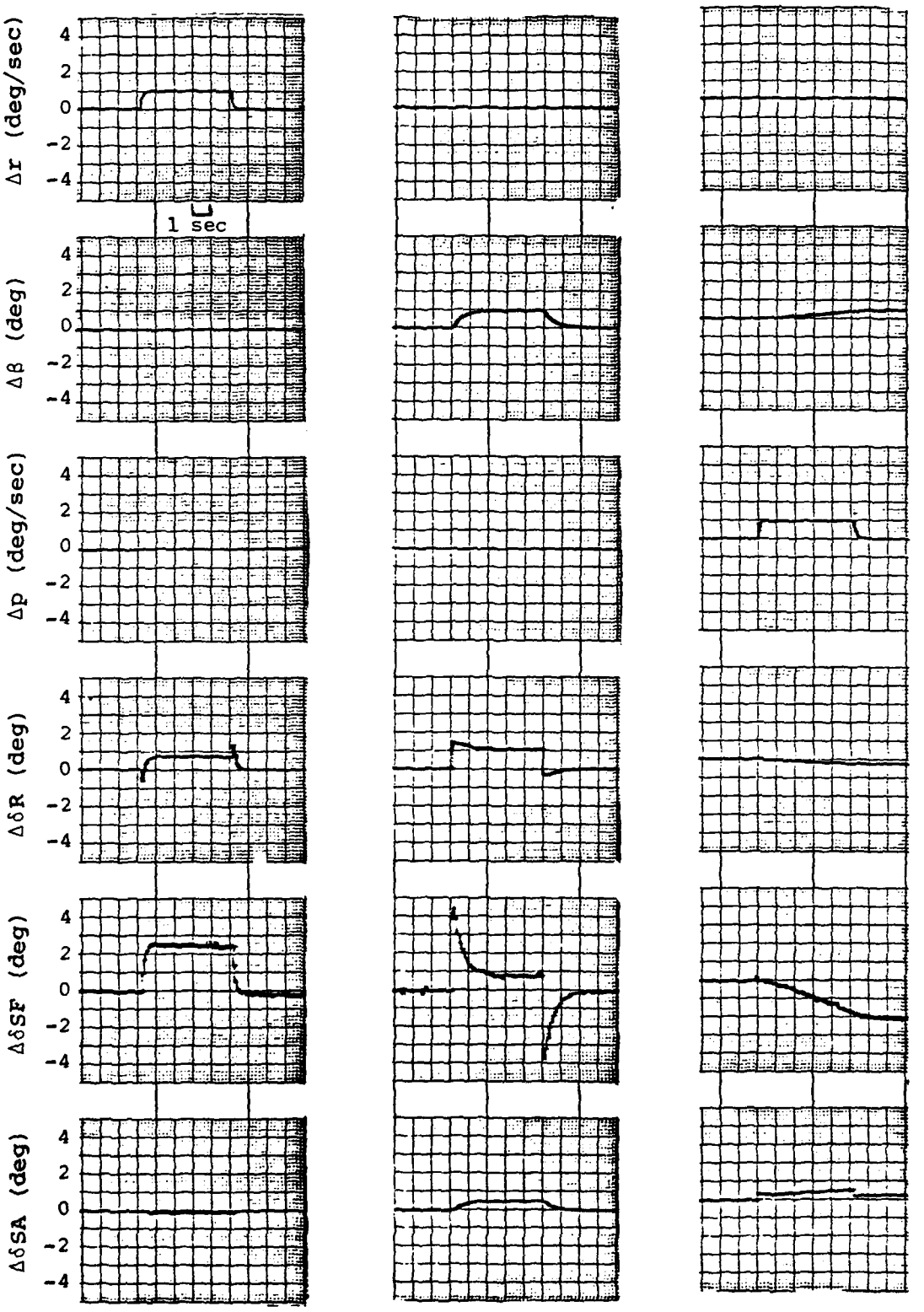

i) Δr_c = 1 deg/sec ii) $\Delta \beta_c$ = 1 deg iii) Δp_c = 1 deg/sec

a) Mode 01

Figure 3-5. *Hybrid Simulations of (r,β,p) Mode Response.* **V = 105 KIAS.**

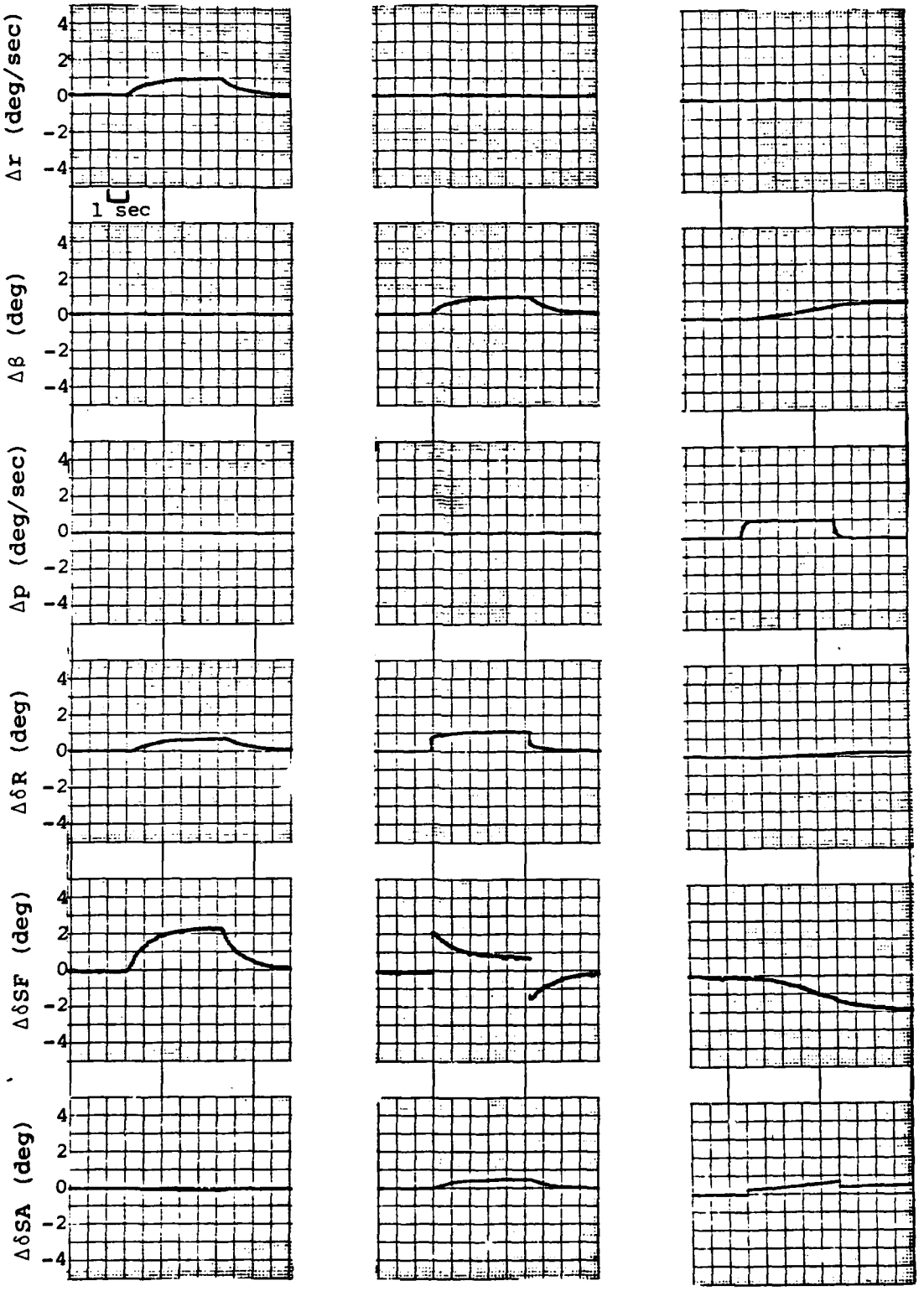

i) Δr_c = 1 deg/sec ii) $\Delta \beta_c$ = 1 deg iii) Δp_c = 1 deg/sec

b) Mode 02

Figure 3-5. Continued

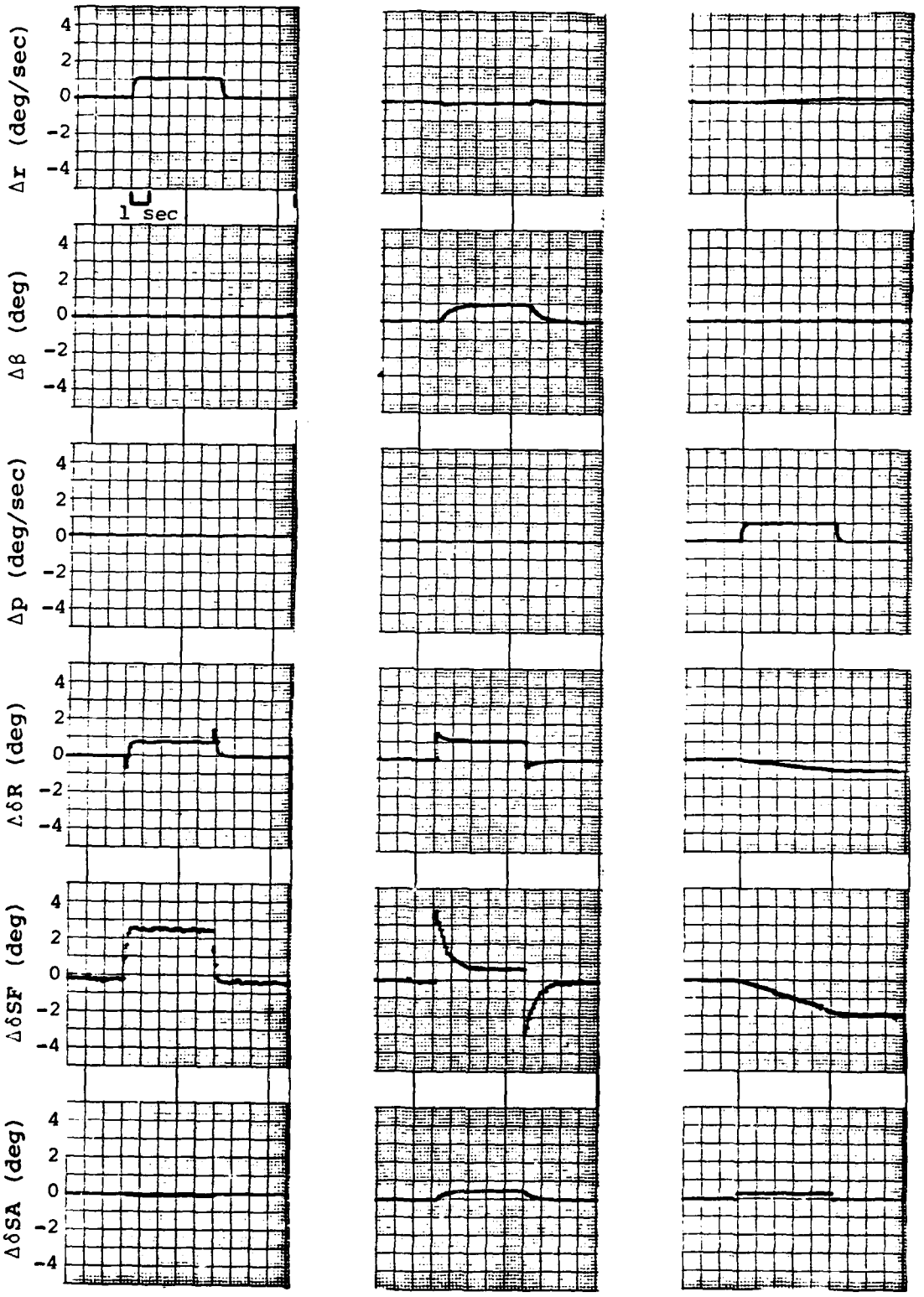

i) Δr_c = 1 deg/sec ii) $\Delta \beta_c$ = 1 deg iii) Δp_c = 1 deg/sec

c) Mode 05

Figure 3-5. Continued

AD-A119 084 AIR FORCE INST OF TECH WRIGHT-PATTERSON AFB OH F/G 1/3
COMMAND AUGMENTATION INCORPORATING DIRECT SIDE FORCE CONTROL AN--ETC(U)
MAY 82 S L GRUNWALD
UNCLASSIFIED AFIT/CI/NR/82-39T NL

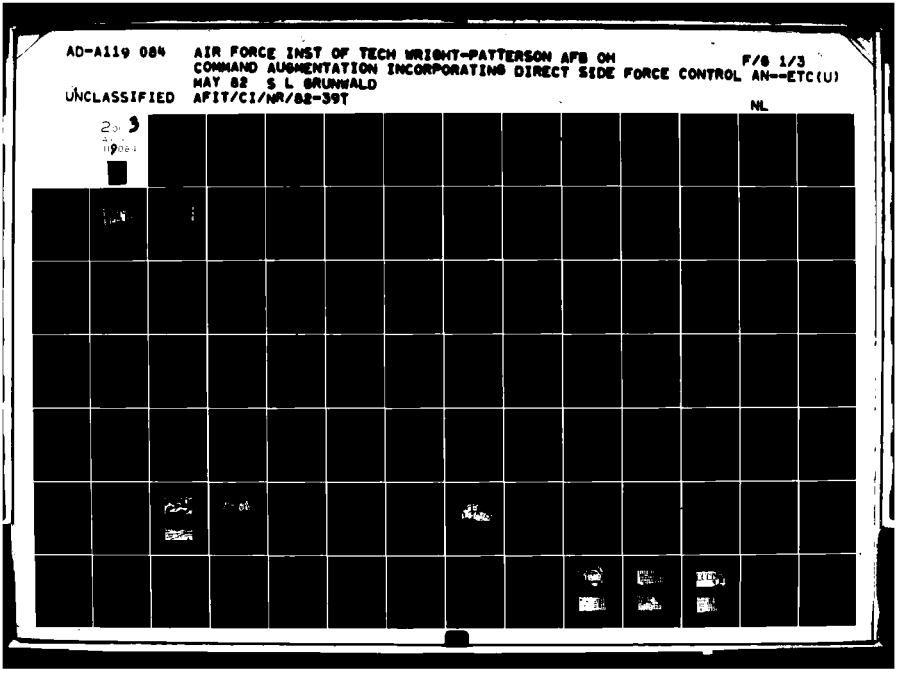

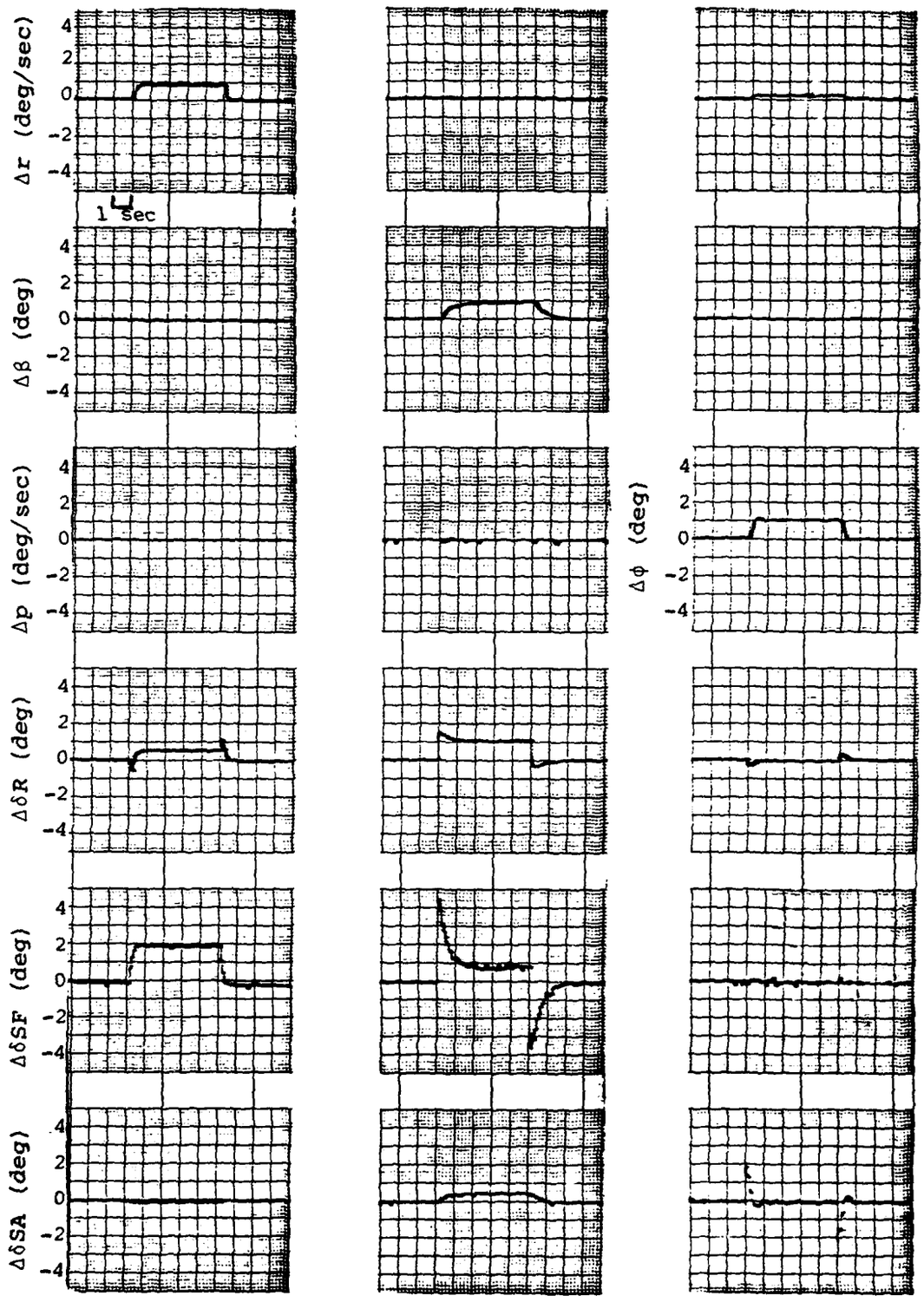

i) Δr_c = 1 deg/sec ii) $\Delta \beta_c$ = 1 deg iii) $\Delta \phi_c$ = 1 deg

a) Mode 06 Δr_c = .181 deg/sec

Figure 3-6. Hybrid Simulations of Coordinated (r,β,φ) Response. V = 105 KIAS.

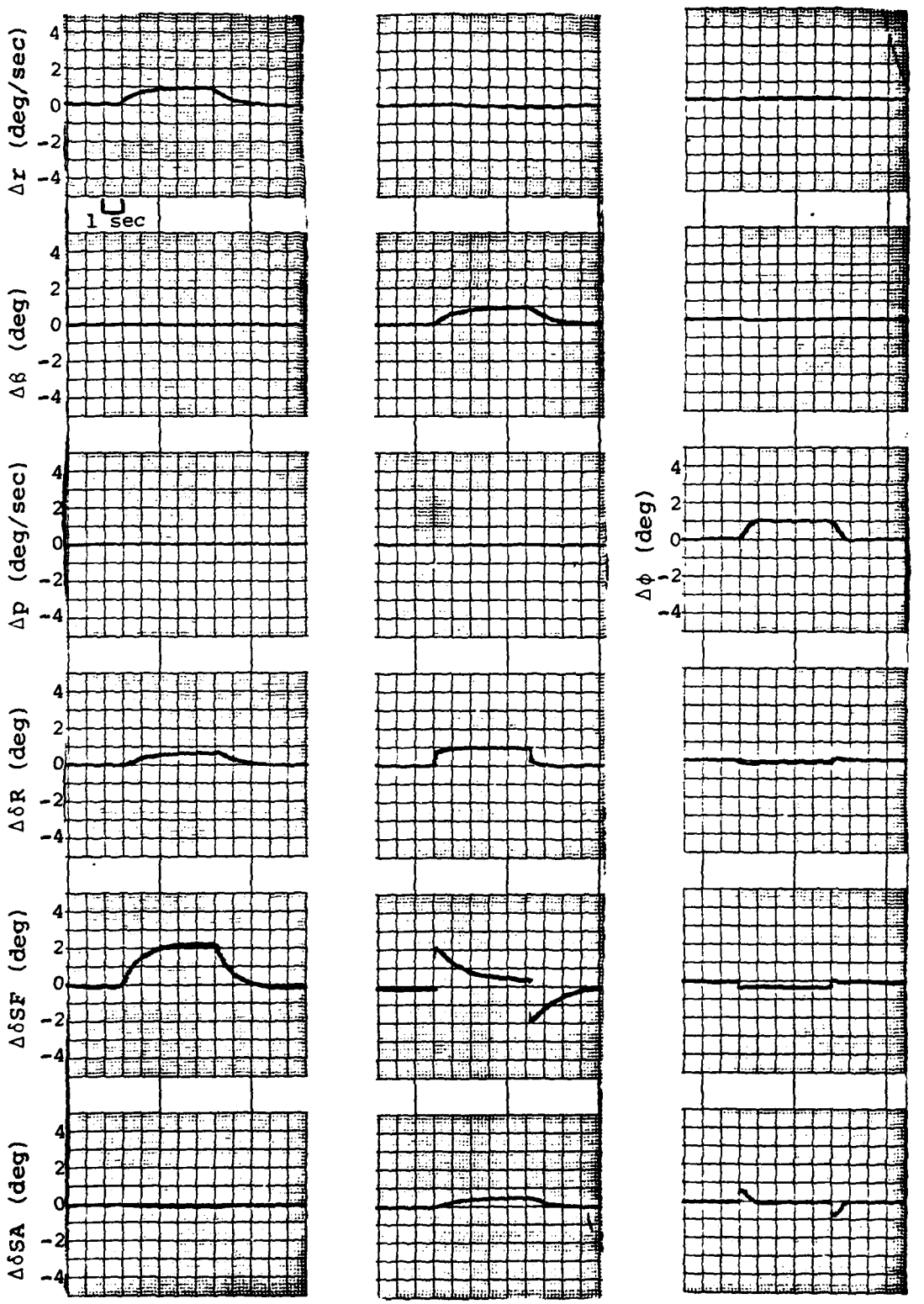

i) Δr_c - 1 deg/sec ii) $\Delta \beta_c$ = 1 deg iii) $\Delta \phi_c$ = 1 deg

b) Mode 07 Δr_c = .181 deg/sec

Figure 3-6. Continued.

5-10

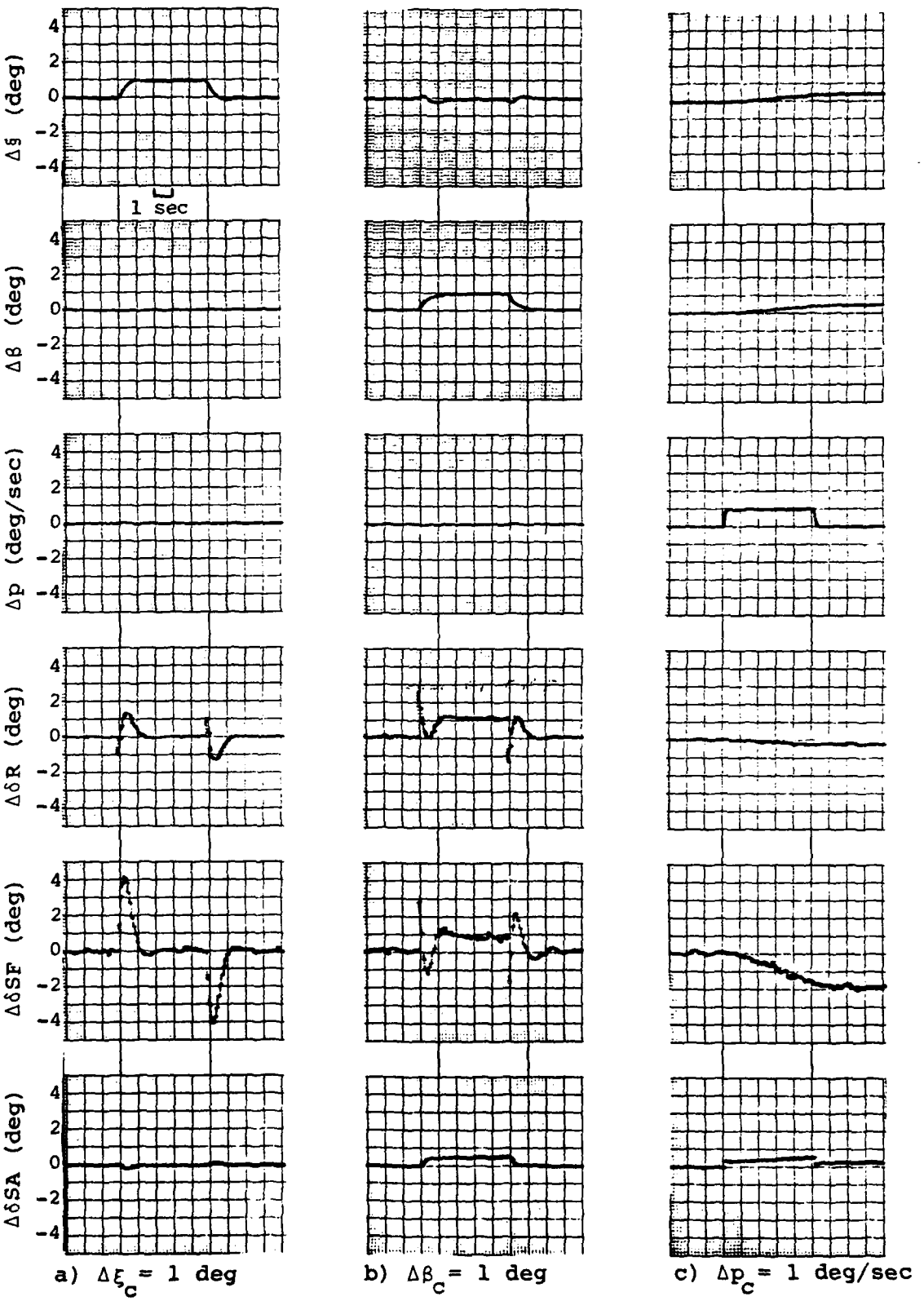

Figure 3-7. Hybrid Simulations of (ξ,β,p) Mode Response. V = 105 KIAS.

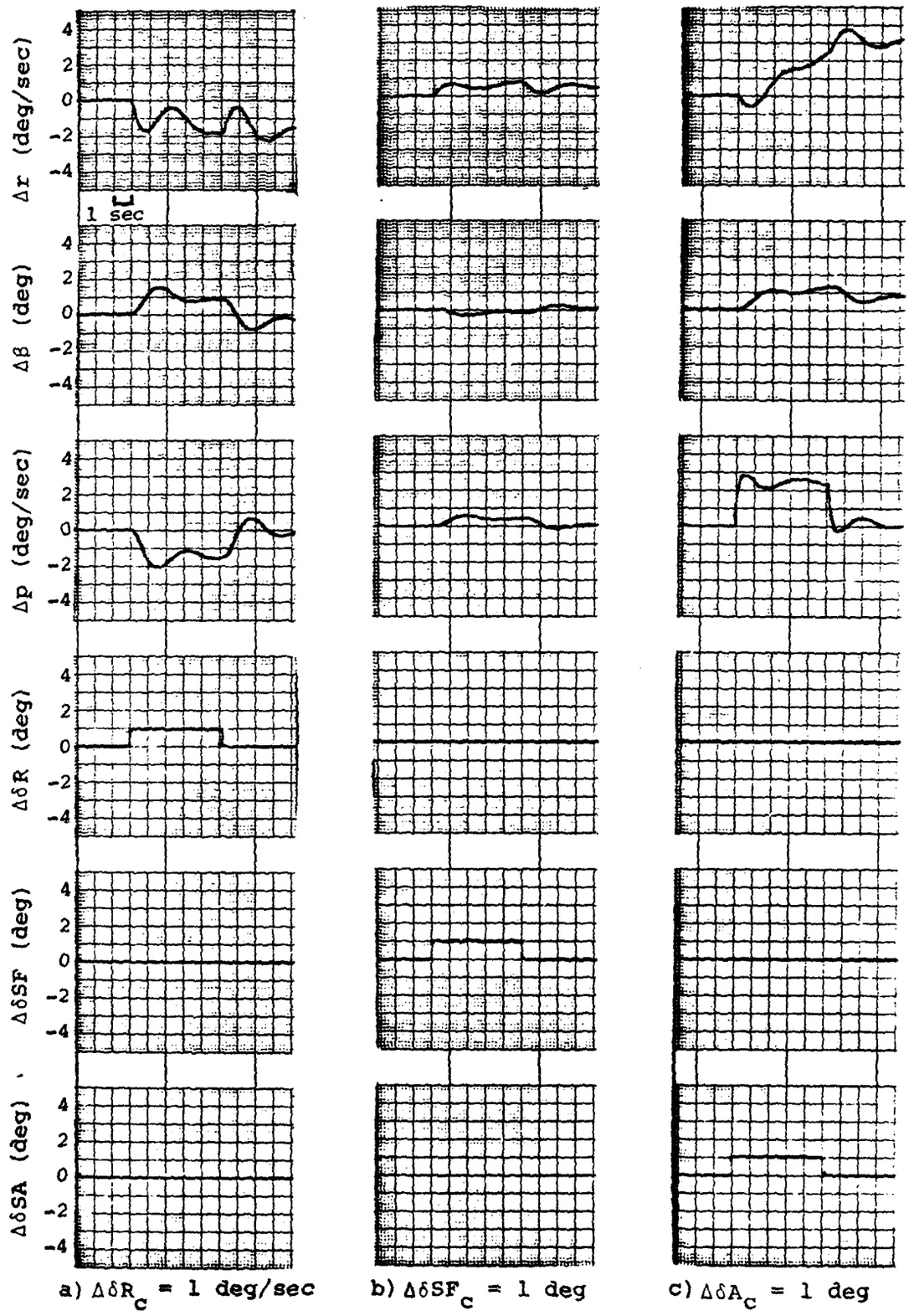

Figure 3-8. Hybrid Simulations of Unaugmented VRA Response. V = 75 KIAS.

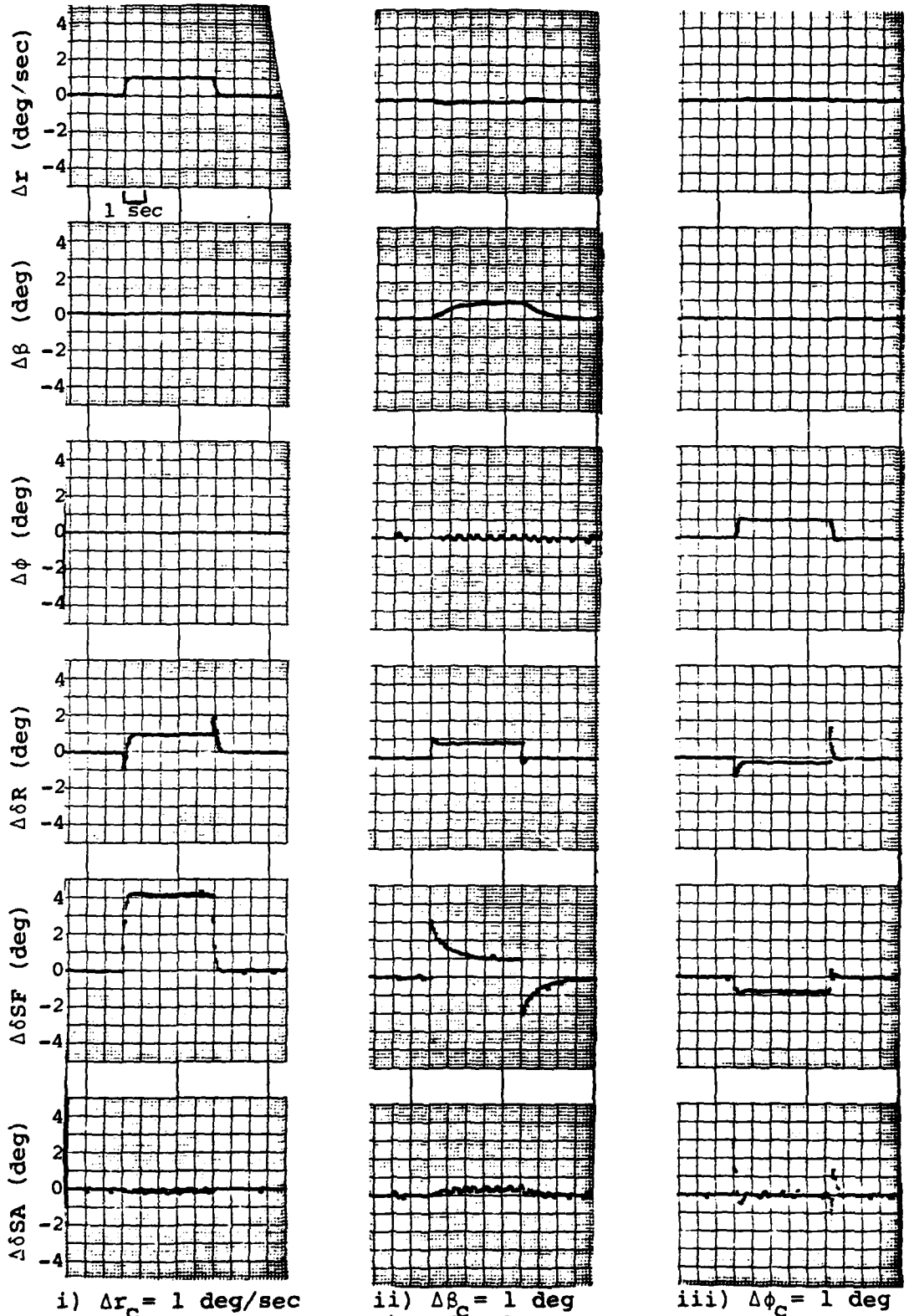

a) Mode 11

Figure 3-9. Hybrid Simulations of Uncoordinated (r,β,φ) Mode Response. V = 75 KIAS.

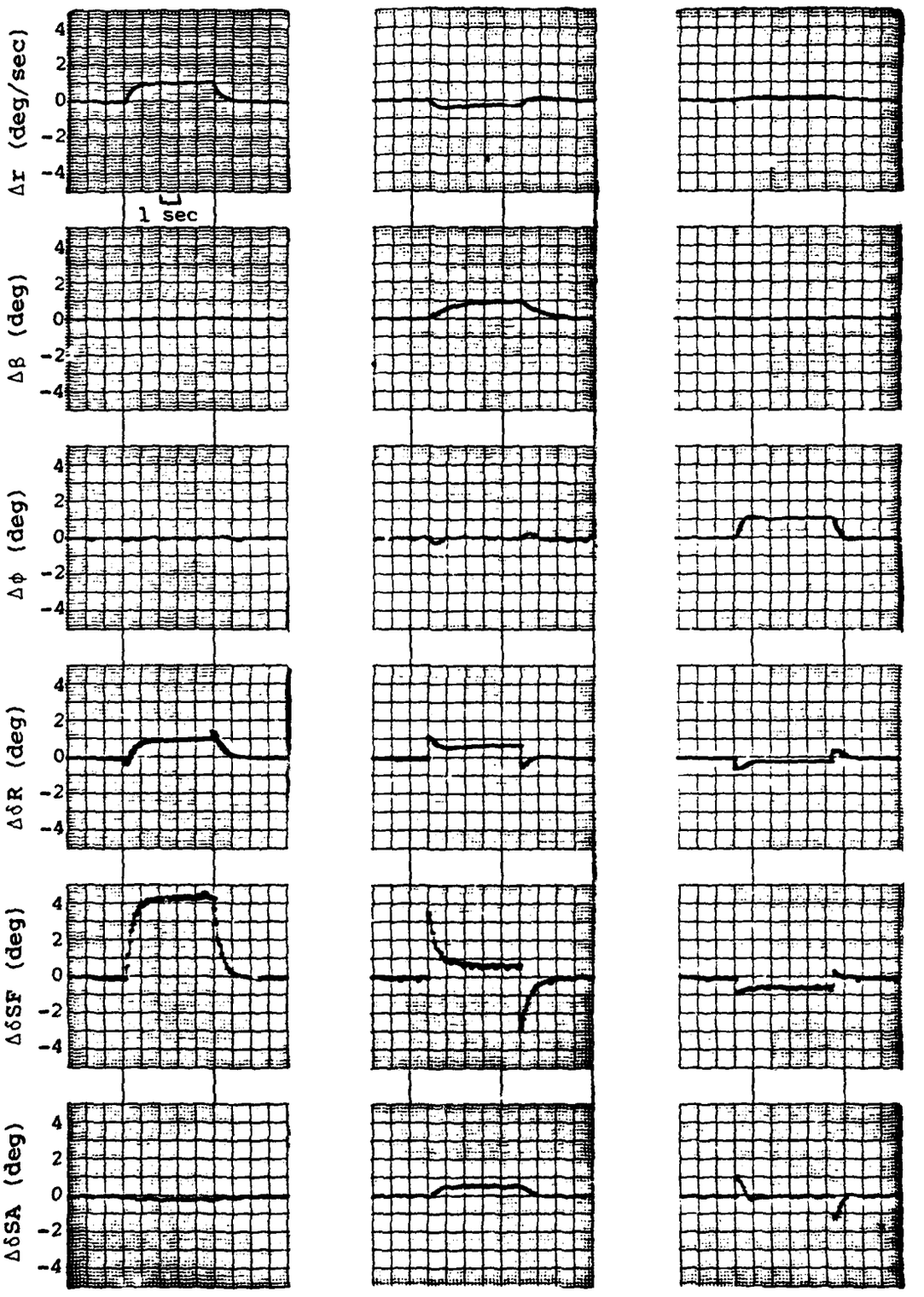

i) Δr_c = 1 deg/sec ii) $\Delta \beta_c$ = 1 deg iii) $\Delta \phi_c$ = 1 deg

b) Mode 12

Figure 3-9. Continued.

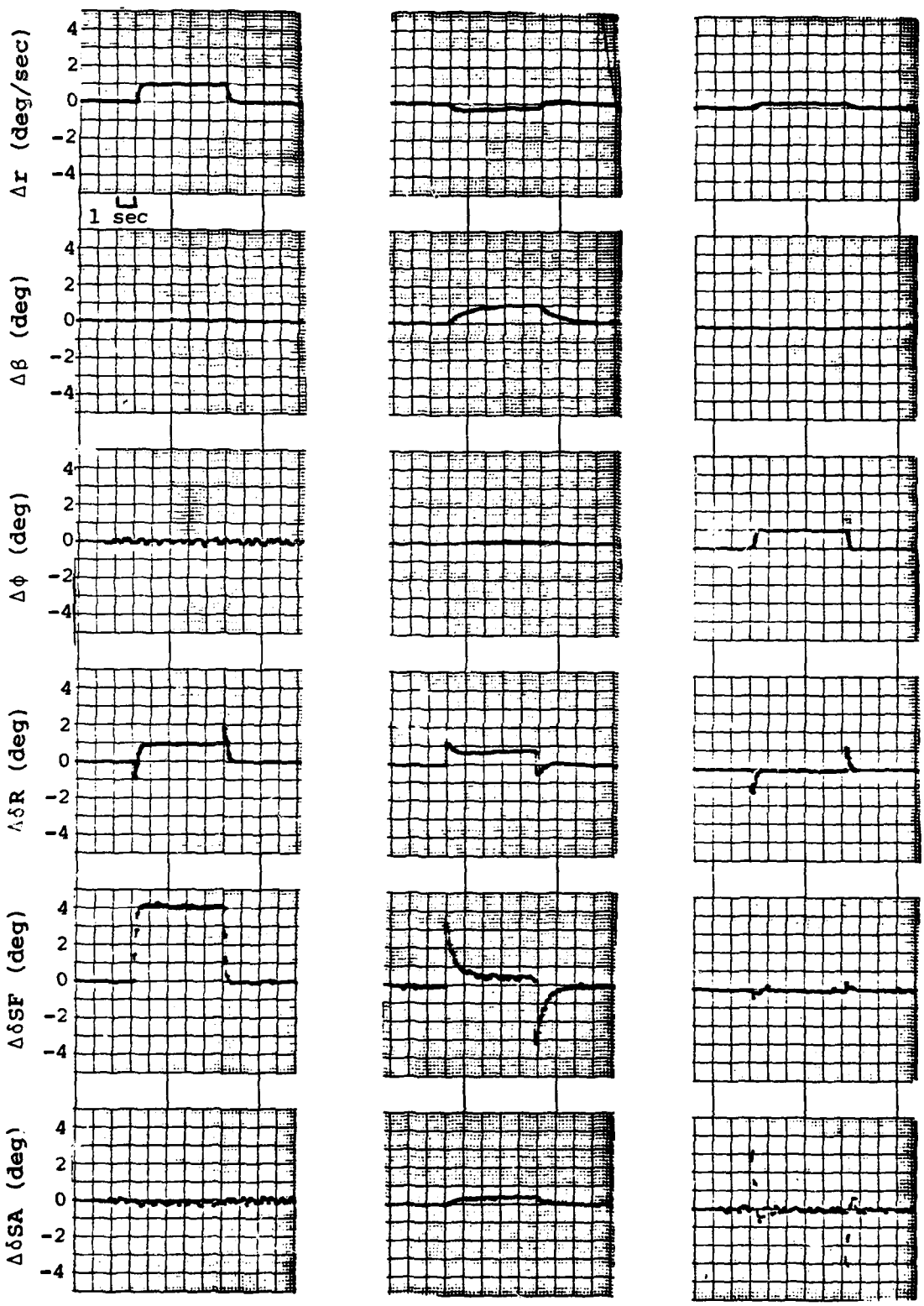

i) Δr_c = 1 deg/sec ii) $\Delta \beta_c$ = 1 deg iii) $\Delta \phi_c$ = 1 deg

Δr_c = .254 deg/sec

a) Mode 16

Figure 3-10. Hybrid Simulations of Coordinated (r,β,φ) Mode Response. V = 75 KIAS.

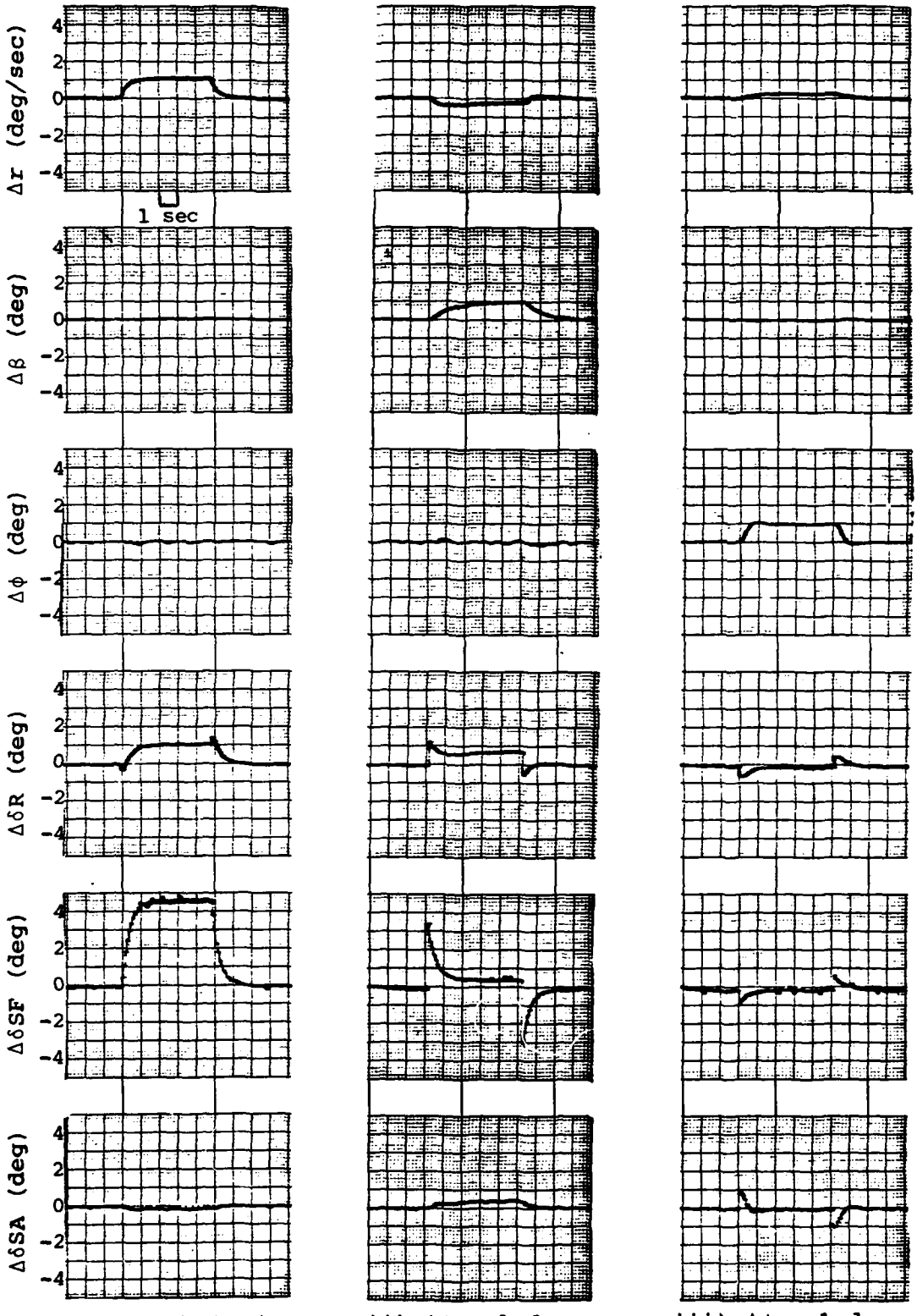

i) Δr_c = 1 deg/sec ii) $\Delta \beta_c$ = 1 deg iii) $\Delta \phi_c$ = 1 deg

Δr_c = .254 deg/sec

b) Mode 17

Figure 3-10. Continued

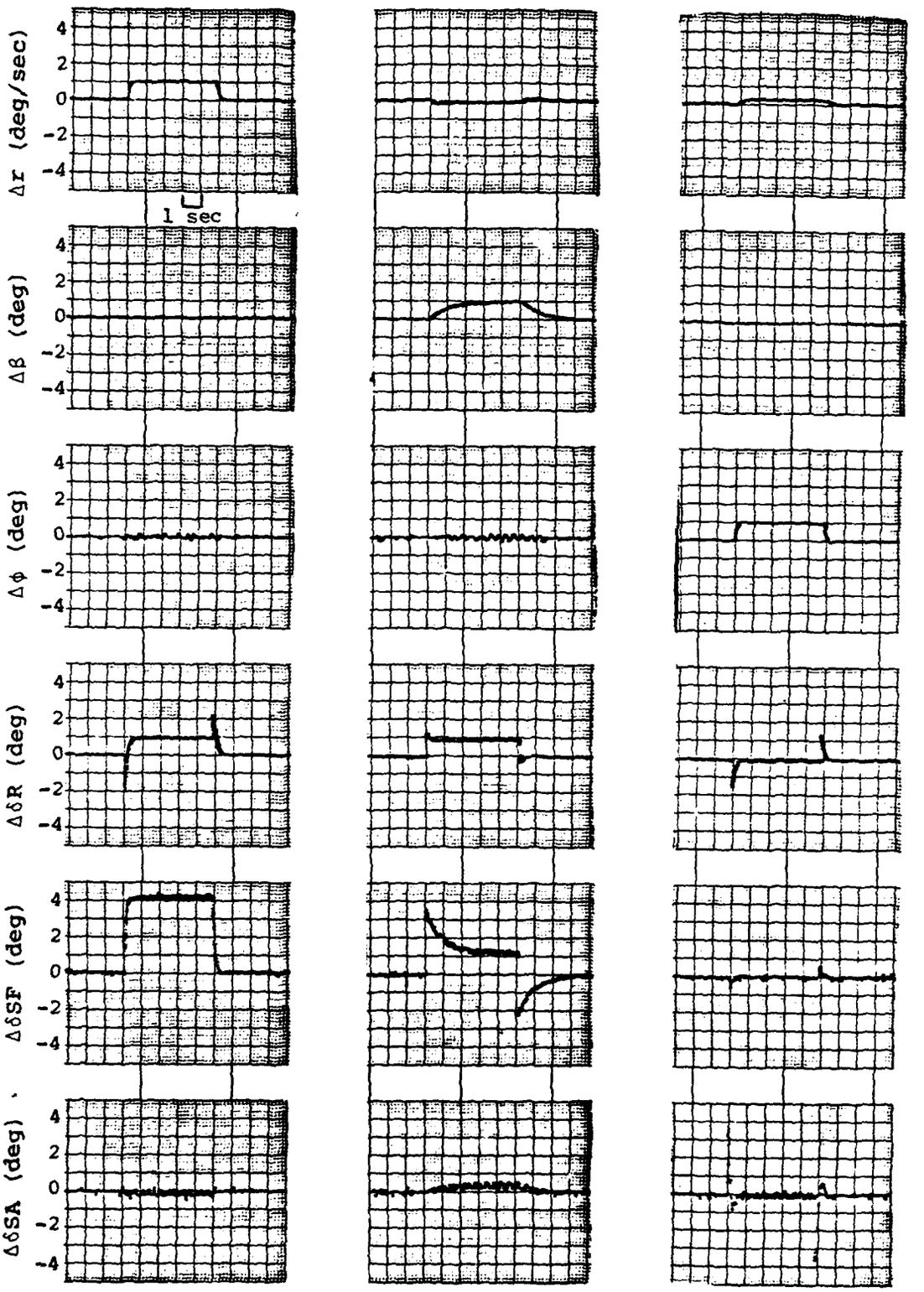

i) Δr_c = 1 deg/sec ii) $\Delta \beta_c$ = 1 deg iii) $\Delta \phi_c$ = 1 deg

c) Mode 18 Δr_c = .254 deg/sec

Figure 3-10. Continued

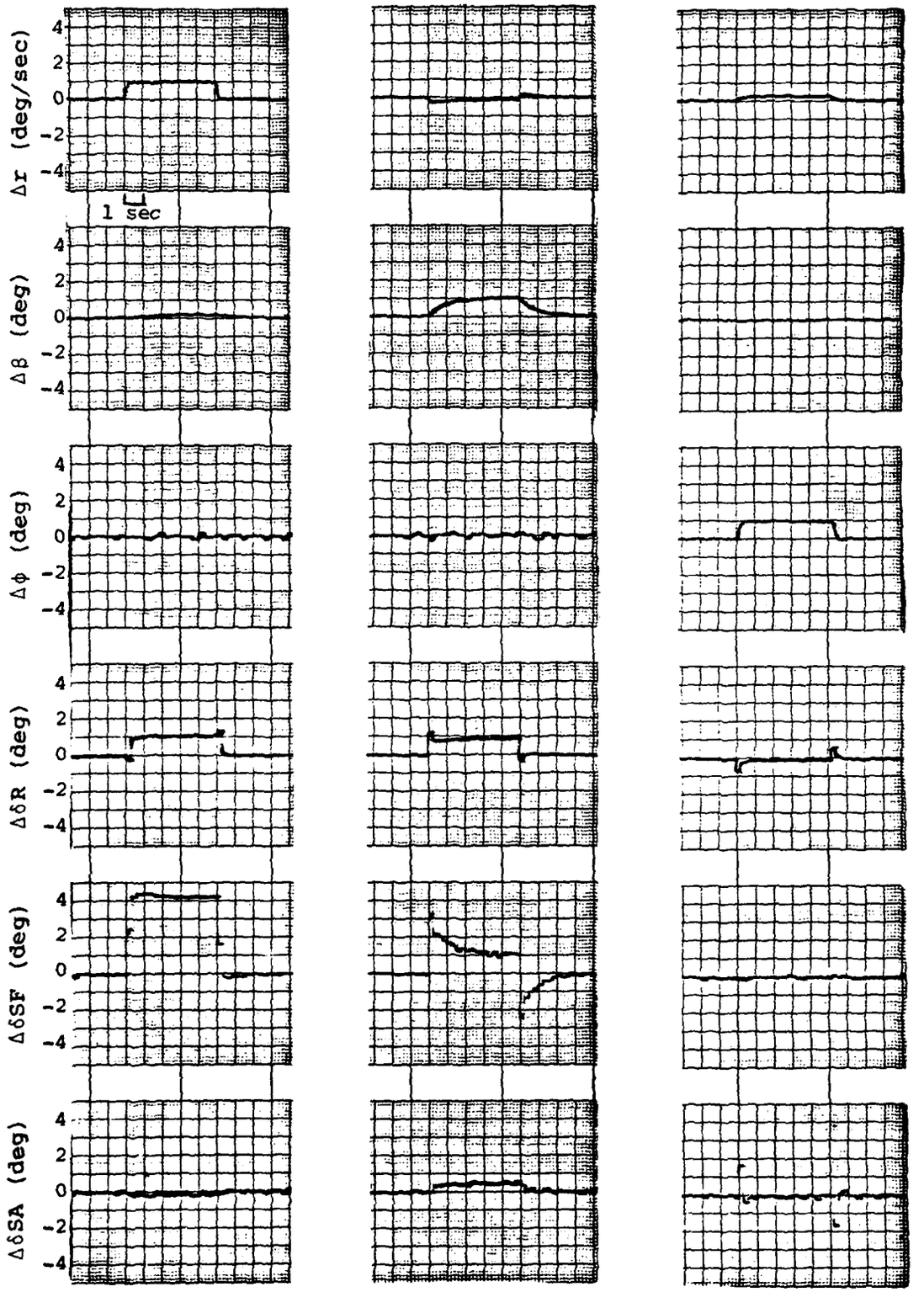

i) Δr_c = 1 deg/sec ii) $\Delta \beta_c$ = 1 deg iii) $\Delta \phi_c$ = 1 deg

d) Mode 19 Δr_c = .254 deg/sec

Figure 3-10. Continued.

4. FLIGHT TESTING

Flight testing the Micro-DFCS was the logical concluding phase of this digital CAS investigation. The purpose of the testing was to verify the ground results and to predict their utility for civilian and military aircraft. The worthiness of the control modes available with direct side force and the effects of a digital flight control system were to be determined.

4.1 MICRO-DFCS SET-UP

The laboratory configuration of the Micro-DFCS was slightly modified for use in the VRA. The microcomputer boards were housed in a RF-shielded, shock-mounted box which required connections for the following:

- Power supply
- Analog inputs and outputs
- CDU
- Cockpit light and CPU halt/reset

Unlike its ground counterpart, the flight control computer unit (FCCU) had no self-contained power source. Instead, the aircraft supplied ±5, ±12, and ±28 volts to power the boards and the unit's cooling fan. A 25-pin connector was used for the analog inputs from the aircraft's motion sensors and cockpit manipulators and for the analog outputs to the control surface actuators. The handheld CDU used a 9-pin connector to enable serial transmission of data between the microcomputer and the pilot. The fourth connector to the FCCU allowed the 20-milliamp light on the instrument panel to be flashed; it also allowed the safety pilot to halt or reset the CPU during flight without using the CDU.

Another consideration before flight testing involved the storage of memory. The machine code for CAS-6 had to be retained during the time between the removal of the computer boards from the ground unit and the application of aircraft power to the FCCU. Therefore, erasable programmable read-only memory (EPROM) and battery-powered random access memory (RAM) were used to store CAS-6. Two 2K EPROM's contained most of the CAS-6 program, while the battery RAM stored the remainder of the program, including conversion factors which were subject to change during the course of testing. After the FCCU gained power, the program was moved from PROM and battery RAM to RAM locations on the 8004 board so that the execution time advantage of on-board memory could be obtained.

As a final precursor to flight testing, a ground check of the Micro-DFCS was performed in the FRL hangar. The direct mode worked properly with the correct magnitude and direction of control surface deflection. Even though the feedback sensors remained motionless, the check confirmed the proper initial surface deflections for the closed-loop modes. One disturbing characteristic was noted: a small amount of chatter existed in the side force panels and rudder while the system was engaged with no command inputs. Time did not permit the installation of the VRA's heading gyro, so the fifth-order fuselage pointing mode was not tested in flight.

4.2 EVALUATION METHODS

The Micro-DFCS was evaluated in flight by two methods:

- Telemetry records of VRA response
- Pilot opinion

Time response data was telemetered from the VRA to the FRL ground station receiver (Fig. 4-1). The system operates under crystal control at 1458.5 MHz in the FM mode. Up to 42 channels, each sampled at 20 sps, can be received by the FRL telemetry system. The signals are demultiplexed

five channels at a time, buffered by the analog computer, and then recorded on the strip chart machine. Signal calibrations used on the analog computer are included in Appendix D. Augmenting the telemetry system is a Honeywell seven-channel tape recorder that can be used for playing back telemetry data for additional strip chart recording after the flight.

The telemetry data was intended to verify the previous time responses obtained in the ground simulations. The calibrated step input subroutine of CAS-6 was used to generate precise command inputs for this purpose.

Pilot opinion represented the other method of evaluating the modes in flight. Two pilots from Princeton University's technical staff evaluated the CAS-6 control modes. Both possessed an MSE degree in aeronautical engineering and have had major responsibilities throughout the history of the variable-stability program at the University. Pilot A, with over 5000 flying hours in a variety of military and civilian aircraft, was the chief test pilot, while Pilot B served chiefly as the engineering test pilot. (See Appendix A for a description of VRA/pilot interfaces.)

The pilots evaluated the advanced modes using the Cooper-Harper Scale (Ref. 36), which is reproduced as Fig. 4-2. This is the definitive handling qualities rating used in flight testing throughout the world. The pilots also provided subjective comments and suggestions for mode improvement.

4.3 FLIGHT TESTS

Flight tests were performed in the VRA at the Princeton University Forrestal Campus airfield. Initial tests showed the need for revamping the models used for ESD model following. New modes were then developed, verified, and subsequently flight tested.

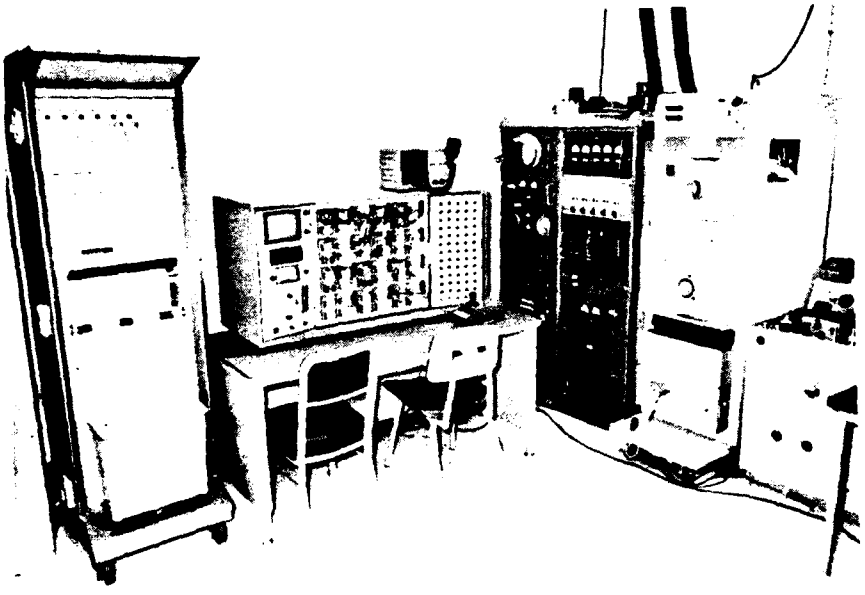

Figure 4-1. FRL Ground Station.

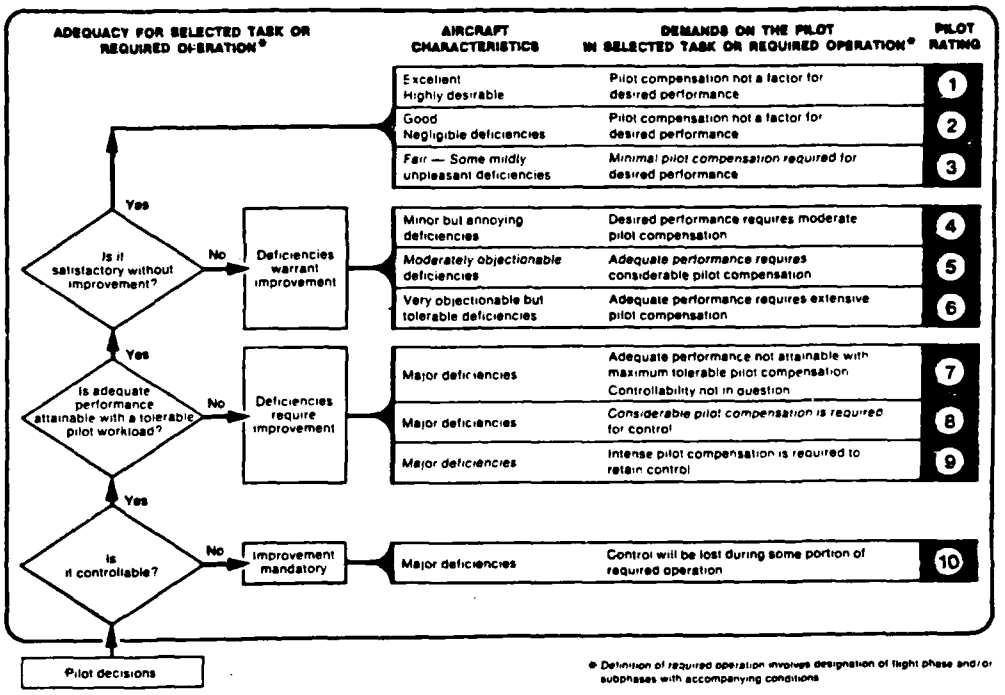

Figure 4-2. Cooper-Harper Handling Qualities Rating Scale.

4.3-1 Initial Flights

Initially tested were the modes developed in Chapters 2 and 3. All modes flight tested were performed in a similar manner. The safety pilot obtained the proper airspeed in straight-and-level flight. He then entered the mode number to be evaluated in the CDU, and when the carriage return was depressed, the mode was engaged. The evaluation pilot then had control of the aircraft through the FBW controls until the mode was disengaged, normally by another CDU input.

Because of familiarity with CAS-6, this writer was allowed to evaluate the modes in flight first, to determine if they were working properly. Every mode was given a quick check by selecting each of the command variables in succession. The directional modes worked well in a basic sense--full deflection of the pilot's manipulators commanded the maximum amount of VRA motion available without stalling the side force panels. The response to a β command was too abrupt: in the transient, an excessive amount of lateral acceleration resulted in order to achieve the snappy sidestep maneuver. In the first test it also was noticed that the lateral modes were seriously deficient. After the flight it was discovered that the roll rate gyro had been mounted backwards in the VRA!

On the next flight, Pilot B evaluated CAS-6. He also noted the degrading effect of the lateral acceleration during the sidestep maneuver. More importantly, after continually seeing the sloppy heading control of the modes and the erratic and inconsistent response to the same input, Pilot B realized that the closed-loop aircraft possessed no directional (weathercock) stability. That is, all of the models used in the ESD Matching control law had an N_β of zero. This explained the divergent heading tendencies of the VRA with the Micro-DFCS engaged when disturbances were included. The net result of the sloppy VRA response characteristics was that new models had to be developed to include the critical N_β term before further meaningful flight tests could be conducted.

4.3-2 New Command Modes

As a result of the first two flight tests, it was apparent that the new ESD models to be followed by the VRA must include a stabilizing (i.e., positive) N_β term. The weathercock stability of each model was selected to be nominally equal to the unaugmented VRA's N_β (5.3 at 105 KIAS and 3.0 at 75 KIAS). This addition to the model's F matrix introduced a transient coupling effect between the yaw rate and sideslip commands. As had been accomplished with the original models, computer simulations of the newly developed models were generated. Among other things, the degree of transient coupling between command variables was analyzed to ensure a tolerable level. See Table 4-1 for all the new modes devised and Fig. 4-3 to 4-6 for the associated digital computer simulations.

Mode 1 (Fig. 4-3a) has a Δr command response with a $\tau \approx 0.1$ sec with a peak $\Delta\beta$ transient of about 0.07 deg after .2 sec. Notice that Δn_y is about 0.97 g per degree of Δr. For a 1 deg $\Delta\beta$ command ($\tau \approx 0.5$ sec) the initial Δn_y is 0.18 g and $\Delta\delta SF$ is 4.4 deg. Additionally, a transient Δr exists, peaking out after 0.2 sec at -.34 deg/sec. This produces a steady-state heading deviation opposite to the direction of the lateral translation. The F_M contains no "g/V" term, so the uncommanded transients die out with a Δp command.

Mode 02 (Fig. 4-3d-f) possesses similar transient coupling. Because of the speed reduction of the $\Delta\beta$ command ($Y_\beta/V = -1$), the initial Δn_y is 0.10 g and $\Delta\delta SF$ is 2.3 deg, but a maximum Δr transient of -.39 deg/sec occurs. When Δp is commanded, Δr and $\Delta\beta$ do not remain nulled because the quasi-steady control law was not used. No responses are presented of Modes 03 and 04. They have the same time histories as Mode 02--only the controller-to-command pairings vary.

Figure 4-4(a-c) shows Mode 06 with a coordinated turn capability. The Δr response is now slower ($\tau \approx 0.2$ sec), and because $Y_r/V = 1$ in F_M

Table 4-1. New Modes Developed

MODE	(knots) AIR SPEED	CONTROL PAIRINGS Δδ$_P$	Δδ$_T$	Δδ$_S$	F_M	G_M	C_B	C_F
01	105	Δr	Δβ	$\dot{\Delta P}$	-10 5.3 0 0 - 1 -2 0 0 0 0 -10 0 0 0 1 0	10 -5.3 0 1 2 0 0 0 10 0 0 0	.96 -.98 -.029 -.15 .037 -3.60 -.015 -.44 -.083 .51 -.099 .0043	-.24 2.10 -.028 2.42 4.38 .0051 .0069 .0088 .41
02	105	Δr	Δβ	Δp	-10 5.3 0 0 - 1 -1 0 .181 0 0 -6.5 0 0 0 1 0	10 -5.3 0 1 1 0 0 0 6.5 0 0 0	.93 -.24 -.030 -.0032 -.044 -1.49 .0042 -.014 -.083 .51 .0011 .0053	-.21 1.36 -.020 2.50 2.27 .0076 .0071 .0041 .31
03	105	Δβ	Δr	Δp	same as Mode 02		.037 -3.60 -.015 -.44 .96 -.98 -.029 -.15 -.083 .51 .0011 .0053	2.42 4.38 .0051 -.24 2.10 -.028 .0071 .0041 .31
04	105	Δβ	ΔP	Δr	same as Mode 02		.037 -3.60 -.015 -.44 -.083 .51 .0011 .0053 .96 -.98 -.029 -.15	2.42 4.38 .0051 .0071 .0041 .31 -.24 2.10 -.028
06	105	Δr	Δβ	Δϕ+ .181Δr	- 5 5.3 0 0 0 -2 0 0 0 0 -5 -12.7 0 0 1 0	5 -5.3 .905 0 2 0 0 0 -12.7 0 0 0	1.17 -.92 -.038 -.11 1.82 -3.06 -.013 -.45 -.078 .51 .026 -.63	-.45 2.04 -.13 .64 3.84 .12 .0024 .0074 .64
07	105	Δr	Δβ	Δϕ+ .181Δr	- 3 3 0 0 - 1 -1 0 0 0 0 -8 -16 0 0 1 0	3 -3 .543 1 1 .181 0 0 16 0 0 0	.31 -.12 -.031 -.10 .012 -1.47 -.014 -.45 -.082 .51 -.077 -.69	.42 1.24 .027 2.44 2.25 .45 .0060 .0043 .70
08	105	Δr	Δβ	Δϕ+ .181Δr	-3.5 4 0 0 -.6 -.6 0 0 0 0 -4 -4 0 0 1 0	3.5 -4 .6335 .6 .6 .1086 0 0 4 0 0 0	.64 .14 -.042 -.14 .76 -.38 -.012 -.44 -.080 .51 .087 -.21	.088 .98 .0011 1.69 1.15 .31 .0045 .0017 .21

Table 4-1. New Modes Developed (contd)

MODE	AIR SPEED (knots)	CONTROL PAIRINGS Δδp	Δδt	Δδs	F_M	G_M	C_B	C_F
11	75	Δr	Δβ	Δφ	-5 3 0 0 -1 -1 0 0 0 0 -5 -12.7 0 0 1 0	5 -3 0 1 1 0 0 0 12.7 0 0 0	.86 -.79 -.032 -.062 -.0071 -2.10 -.040 -.99 .16 .51 -.076 -1.07	.43 1.93 -.30 3.77 3.55 .044 -.022 -.019 1.08
16	75	Δr	Δβ	Δφ+ .254Δr	same as Mode 11	5 -3 1.27 1 1 .254 0 0 12.7 0 0 0	Same as Mode 11	.43 1.93 -.19 3.77 3.55 1.00 -.022 -.019 1.08
17	75	Δr	Δβ	Δφ+ .254Δr	-1.5 3 0 0 -.75 -.5 0 0 0 0 -6 -9 0 0 1 0	1.5 -3 .381 .75 .5 .19 0 0 9 0 0 0	.54 -.17 -.019 -.16 .84 -.16 -.042 -.98 -.17 .50 -.12 -.72	.75 1.30 -.012 2.92 1.61 .77 -.017 -.0081 .73
18	75	Δr	Δβ	Δφ+ .254Δr	same as Mode 16 except at 20 sps		.93 -.87 -.034 -.070 -.11 -2.12 -.018 -1.00 -.17 .54 -.056 -1.10	.36 2.00 -.20 3.86 3.57 1.03 -.016 -.045 1.10
19	75	Δr	Δβ	Δφ+ .254Δr	same as Mode 16 except at 4 sps		.73 -.62 -.025 -.061 .31 -2.01 -.087 -.95 -.15 .44 -.12 -.94	.56 1.75 -.15 3.45 3.46 .88 -.036 .056 .94

(decoupling $\Delta\beta$ from Δr), no $\Delta\beta$ transient occurs. However, Δr coupling still exists with a $\Delta\beta$ command ($\Delta r = -0.58$ at 0.3 sec). The 1 deg $\Delta\phi$ command response, with $\omega_n = 0.5$ rad/sec and $\zeta = 0.7$, reduces lateral acceleration to within 0.001 g in 0.7 sec.

Modes 11, 16, 18, and 19 were designed to operate at 75 KIAS. The Mode 11 Δr command (Fig. 4-5a) has a 5 percent overshoot and a $\tau \approx 0.2$ sec. The $\Delta\beta$ transient reaches a maximum of 0.13 deg after 0.3 sec, but it is nulled in the steady-state (about 0.3 sec). When a 1 deg $\Delta\beta$ is commanded (Fig. 4-5b), Δn_y is initially 0.07 g, $\Delta\delta SF$ is initially 3.5 deg, and Δr reaches -0.37 deg/sec at 0.3 sec before being eliminated.

Mode 16 possesses identical Δr and $\Delta\beta$ responses as Mode 11, so only the coordinated turn capability is presented in Figure 4-6a. The turn is coordinated (Δn_y less than 0.001 g per degree of $\Delta\phi$ commanded) in 1.5 sec.

Modes 18 and 19 replicate Mode 16 at different sampling rates. Their characteristics are analogous to the original modes, so no time histories are presented. Modes 07, 08 and 17 were developed after still more flight testing and will be described a little later.

Figure 4-7 shows the command of roll rate in Mode 02 using the quasi-steady equilibrium control law equation (eq. 44). Although not tested in flight, the example illustrates how the modified equation practically negates any steady-state yaw rate or sideslip. For the example, C_B is as before and,

$$C_F = \begin{bmatrix} -.21 & 1.36 & -.028 \\ 2.50 & 2.27 & -.014 \\ .0071 & .0041 & .31 \end{bmatrix}, \quad C_I = \begin{bmatrix} -.15 \\ -.43 \\ -.0009 \end{bmatrix} \qquad (54,55)$$

The newly selected modes had to be verified in a hybrid simulation prior to flight testing. The flexibility of the Micro-DFCS was displayed by the fact that only the small amount of CAS-6 coding devoted to the control law gains needed to be altered to incorporate the model changes. The strip chart recordings from the hybrid simulation are included in Figure 4-8. The responses are very similar to those of the digital computer simulation. The high frequency noise apparent during the previous hybrid test has vanished.

The only anomaly noticed in the hybrid simulation occured with the 75 KIAS modes (Fig. 4-5f-j). When Δr is commanded, a steady-state $\Delta\beta$ of about 0.4 deg persists. The traces show a steady-state $\Delta\delta SF$ of about 4.4 deg compared to 3.76 deg predicted earlier by the equilibrium analysis. Again, this matter may be attributed to the improper analog computer configuration for the VRA at 75 KIAS. The remaining flight tests were devoted to testing these new modes.

4.3-3 Subsequent Flights

Nine more flight tests, most lasting from one hour to one-and-three quarters hours, were conducted to analyze the new modes containing a stabilizing N_β term. Only once did a problem occur which may be attributed to the interface of the Micro-DFCS with the VRA. In this instance, some memory was altered after initialization, apparently by the engagement of one of the aircraft's systems (probably the telemetry transmitter). Although the modes could still be entered through the CDU, the "CKSUM ERROR" message was displayed every five seconds. A brief period of flight testing confirmed the alteration of a part of CAS-6. A precaution was subsequently taken to make certain that no aircraft equipment was switched on or off while the Micro-DFCS was engaged, and the memory destruction problem was alleviated.

The newly developed modes underwent two phases of flight testing. The pilots first tested each mode by commanding step inputs to ensure adequate

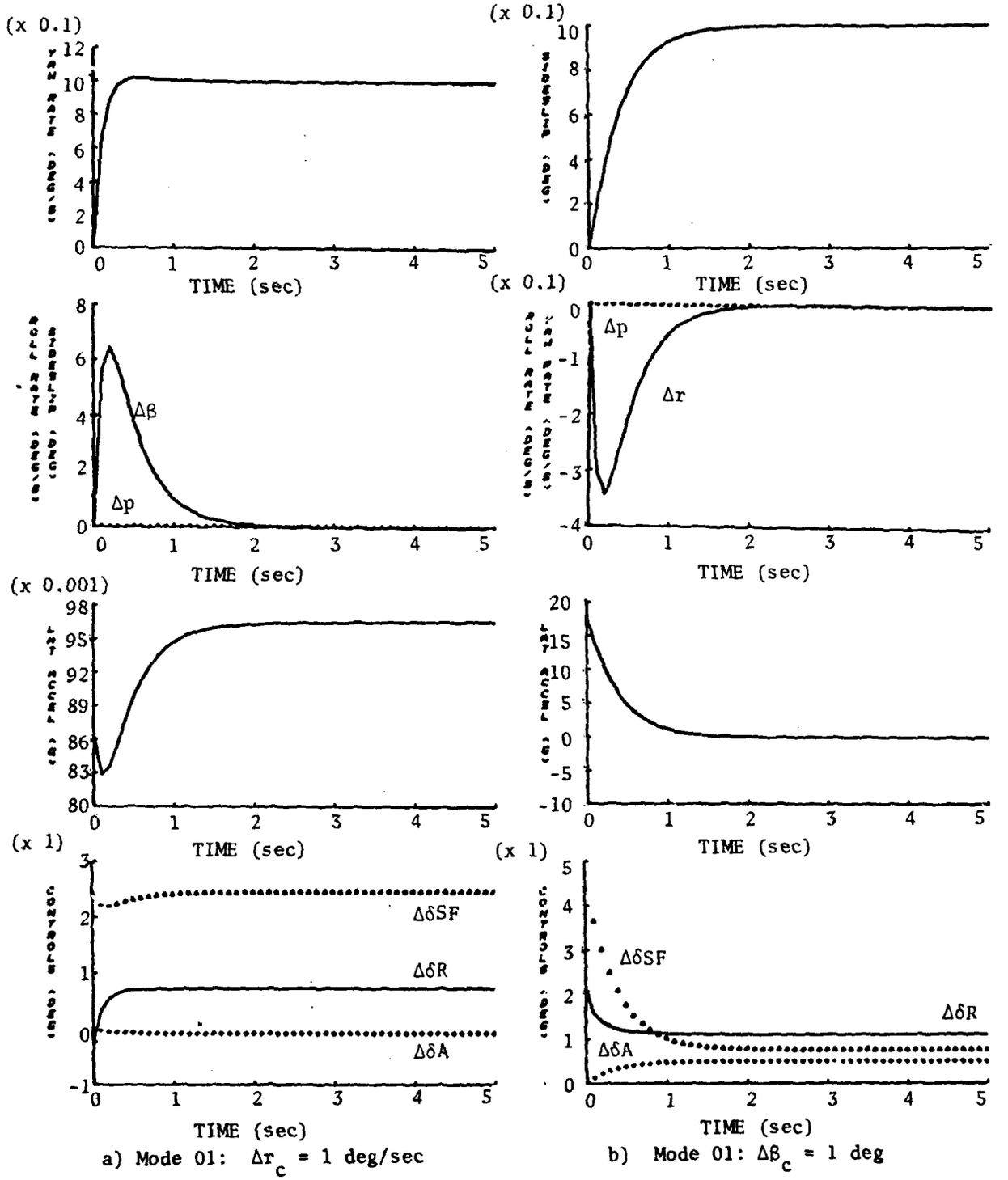

a) Mode 01: Δr_c = 1 deg/sec

b) Mode 01: $\Delta \beta_c$ = 1 deg

Figure 4-3. Digital Computer Simulations of New (r, β, p) Modes. V = 105 KIAS.

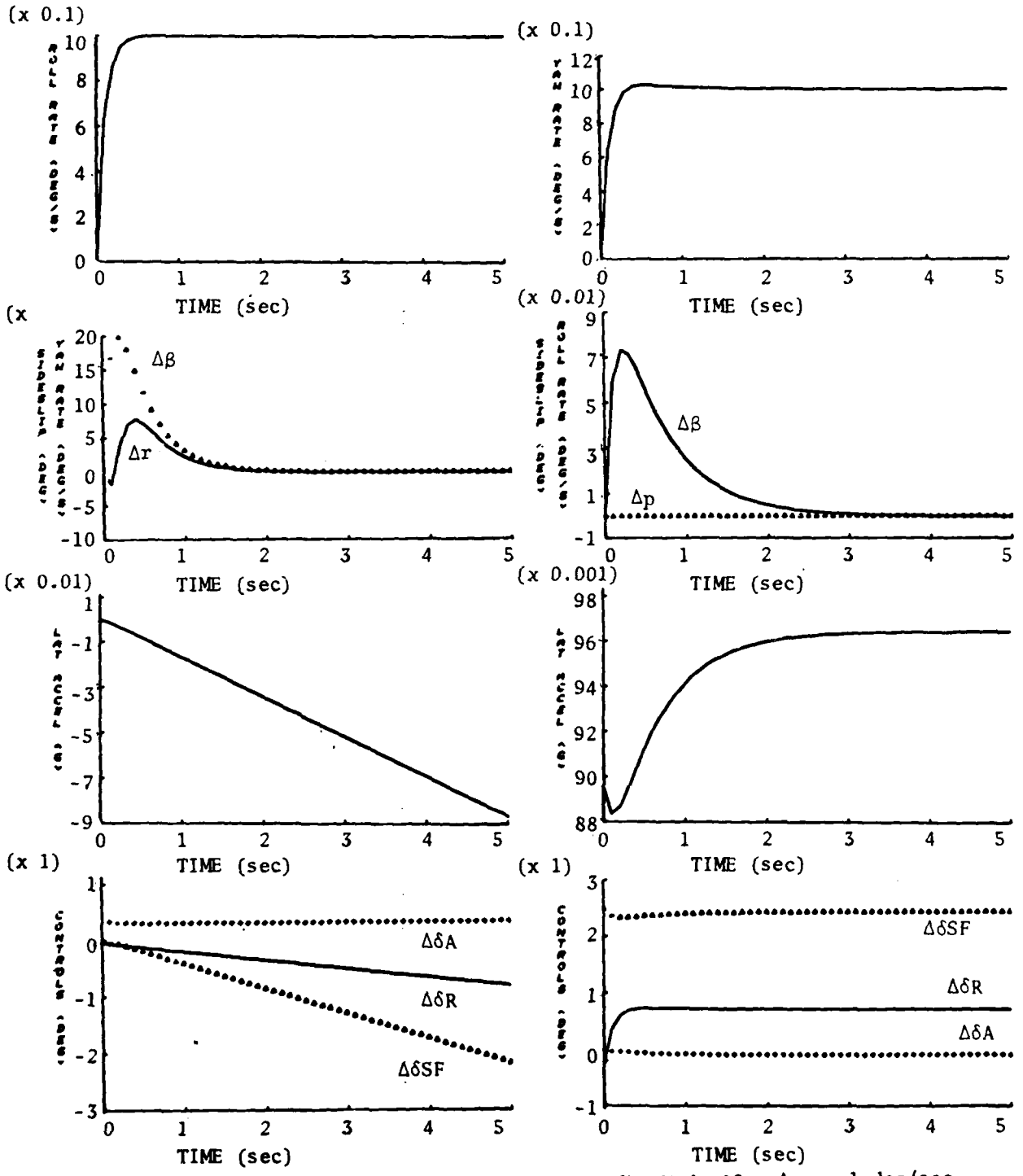

c) Mode 01: Δp_c = 1 deg/sec

d) Mode 02: Δr_c = 1 deg/sec

Figure 4-3. Continued

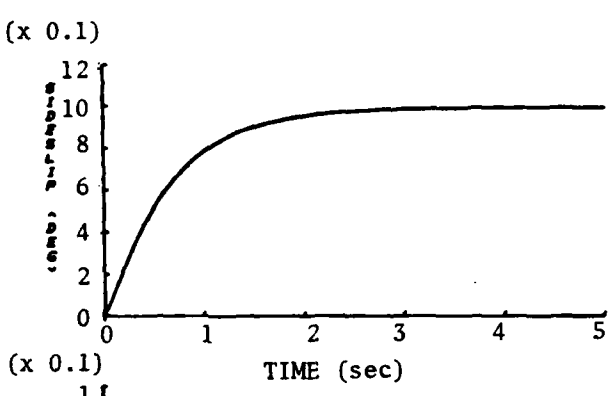

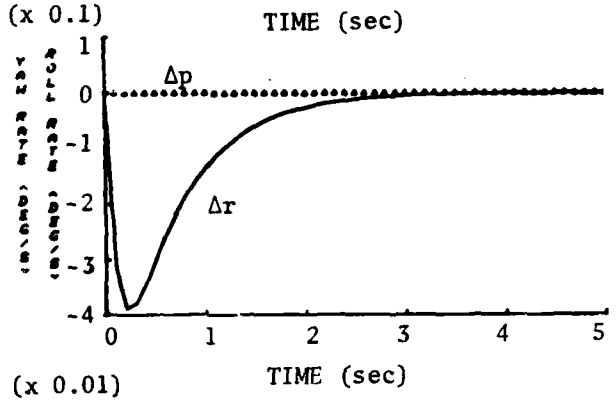

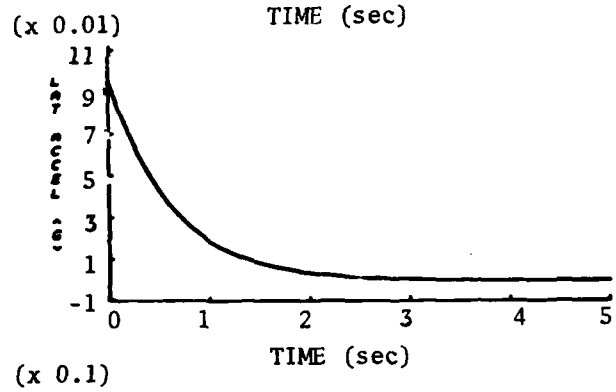

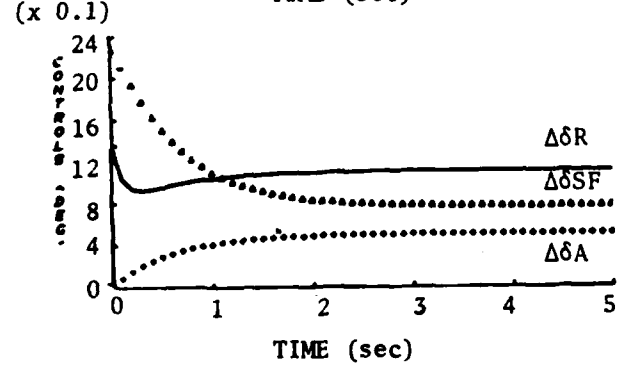

e) Mode 02: $\Delta\beta_c$ = 1 deg

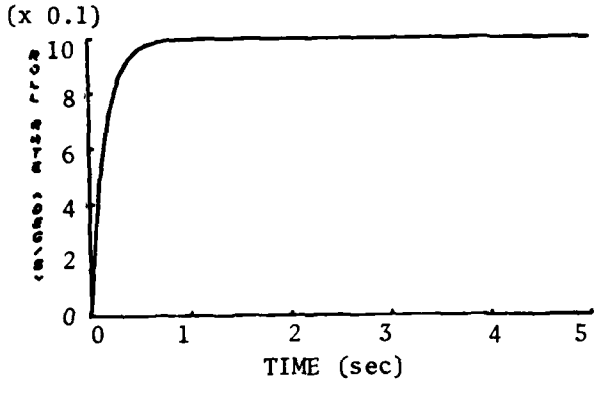

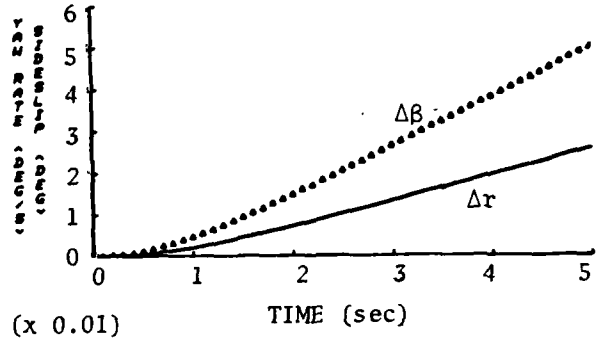

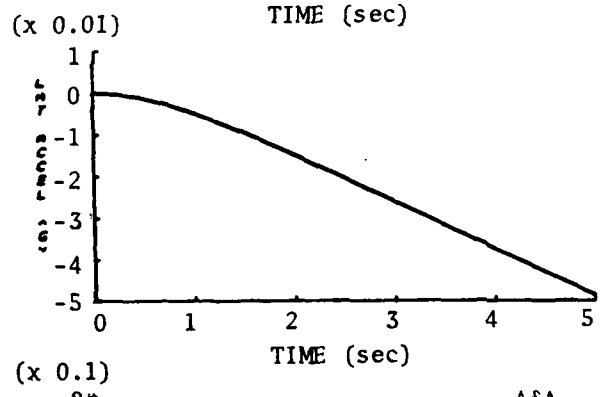

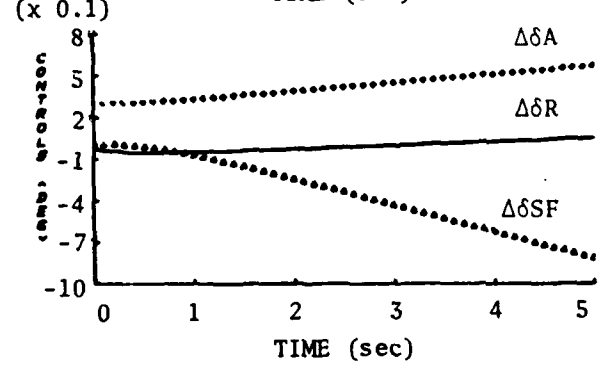

f) Mode 02: Δp_c = 1 deg/sec

Figure 4-3. Continued.

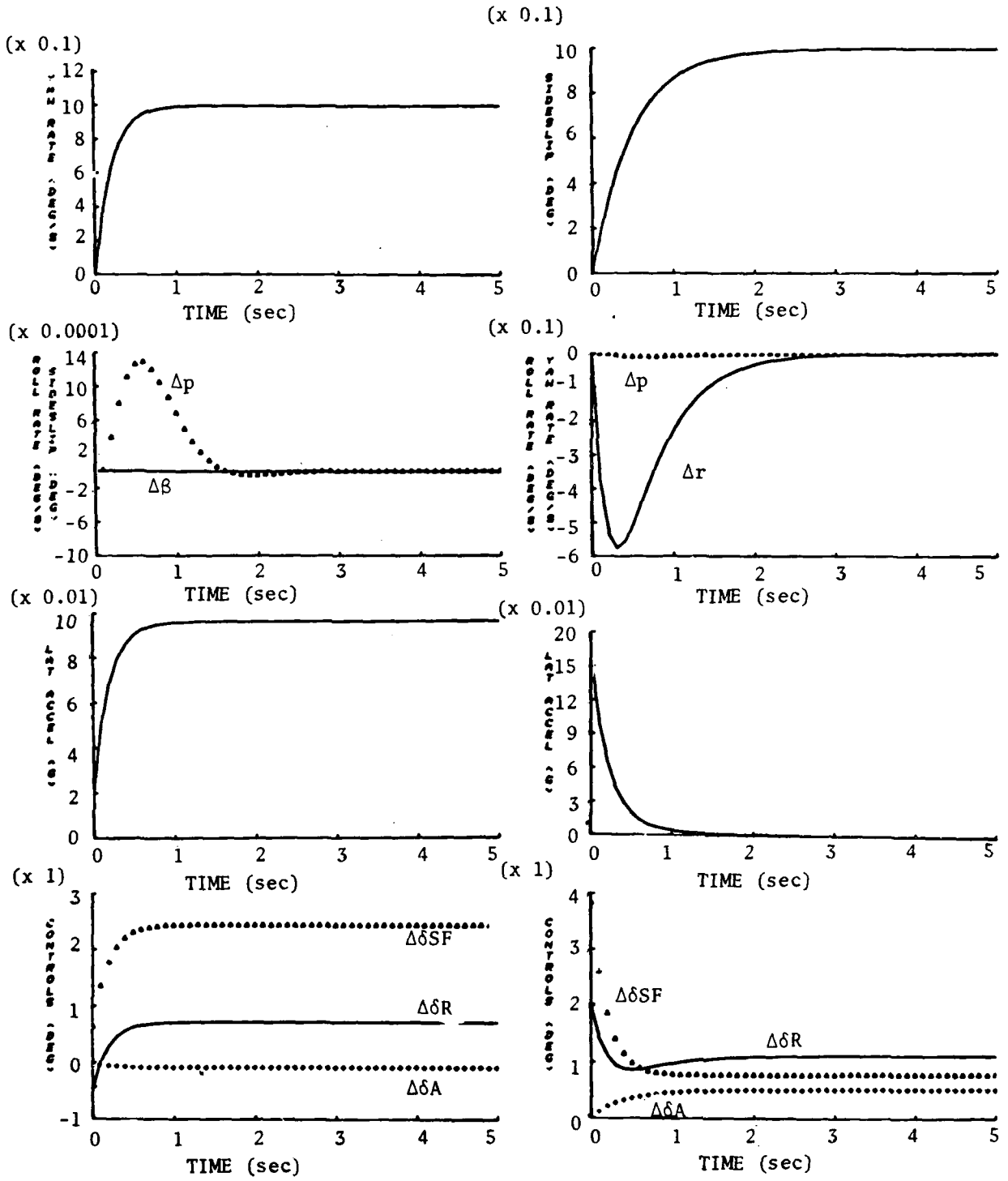

a) Mode 06: Δr_c = 1 deg/sec

b) Mode 06: $\Delta \beta_c$ = 1 deg

Figure 4-4. Digital Computer Simulations of New Coordinated (r, β, ϕ) Modes. V = 105 KIAS.

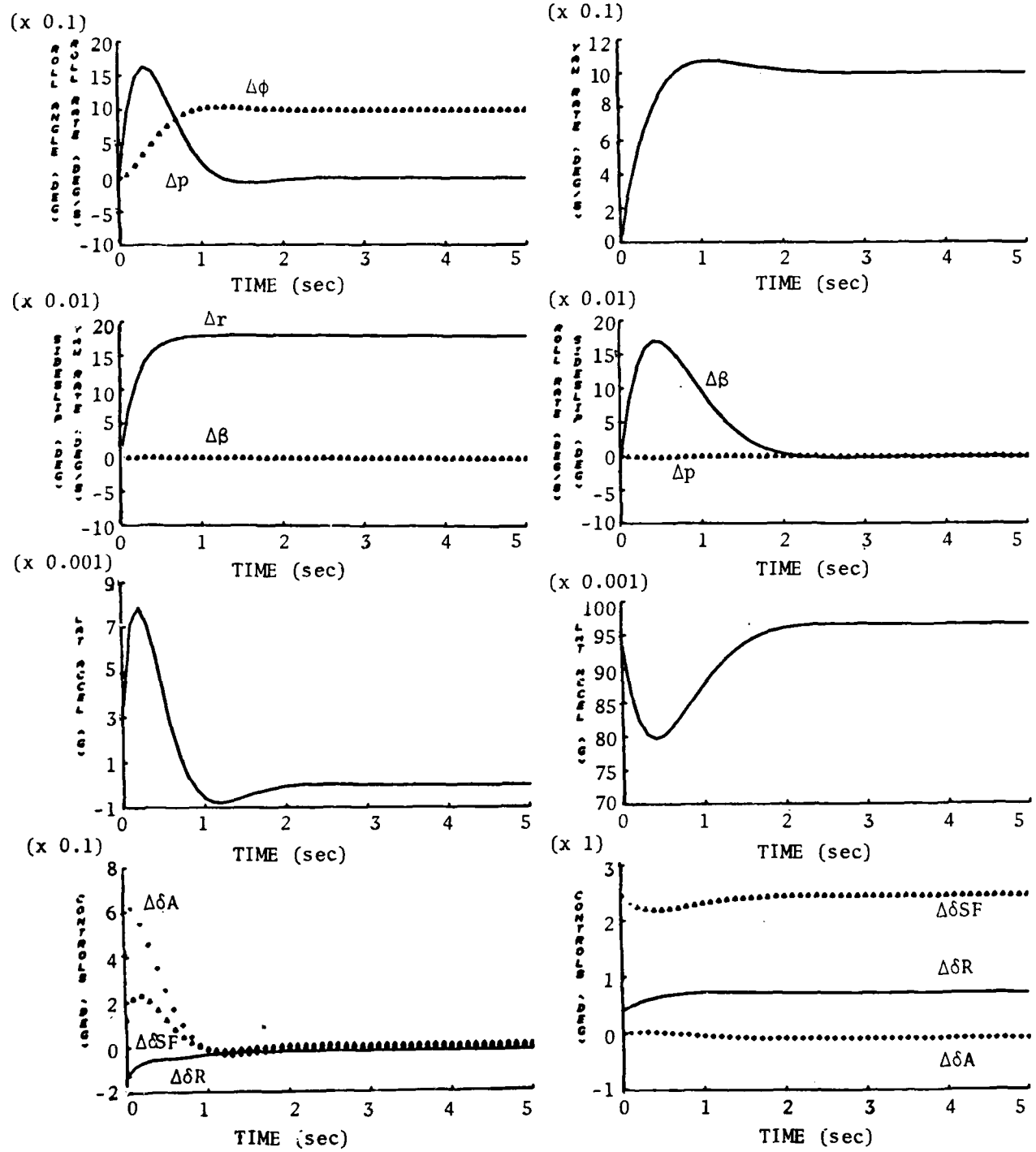

c) Mode 06: $\Delta\phi_c$ = 1 deg, r_c = .181 deg/sec

d) Mode 07: Δr_c = 1 deg/sec

Figure 4-4. Continued

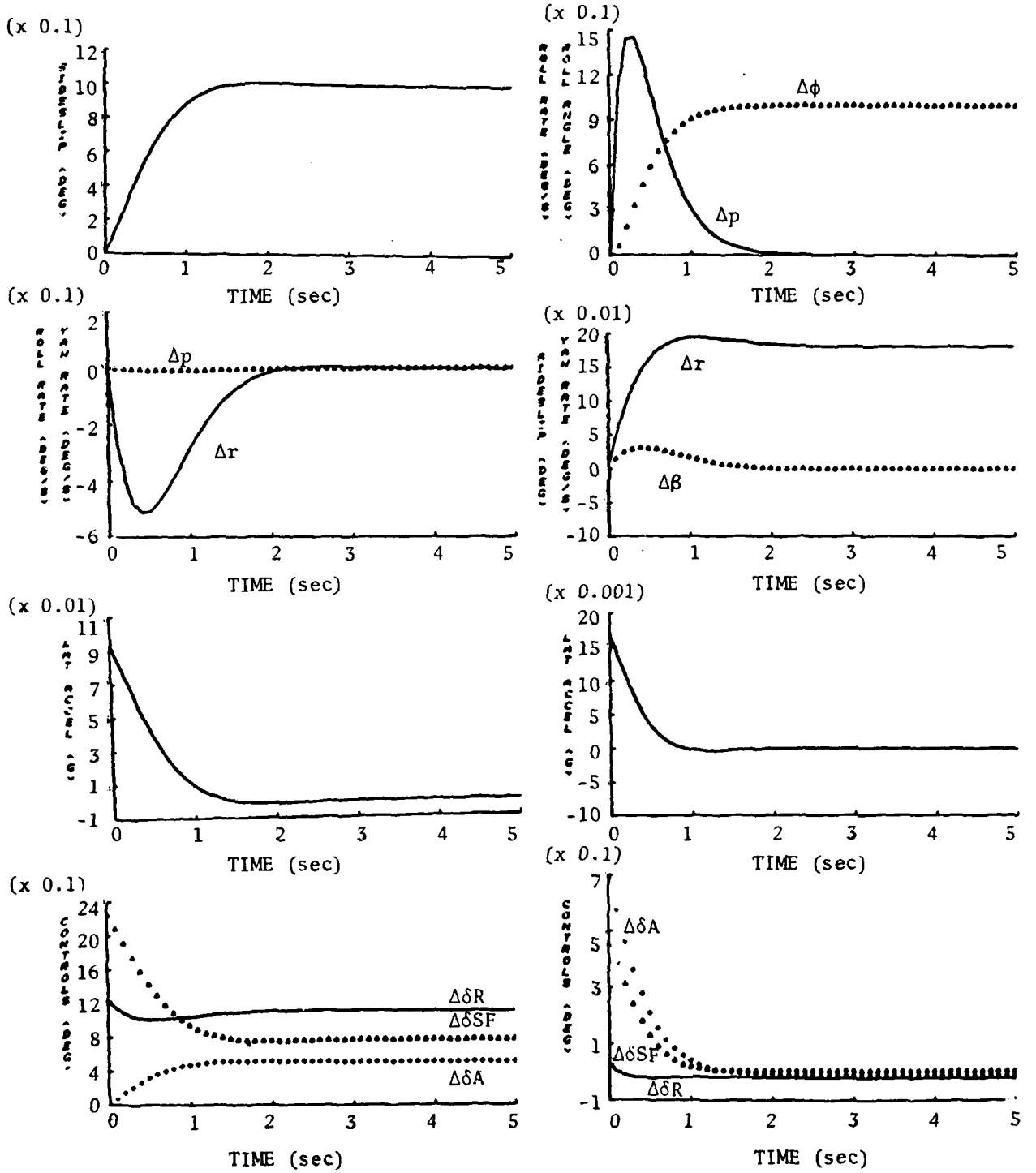

e) Mode 07: $\Delta\beta_c$ = 1 deg

f) Mode 07: $\Delta\phi_c$ = 1 deg, Δr_c = .181 deg/sec

Figure 4-4. Continued

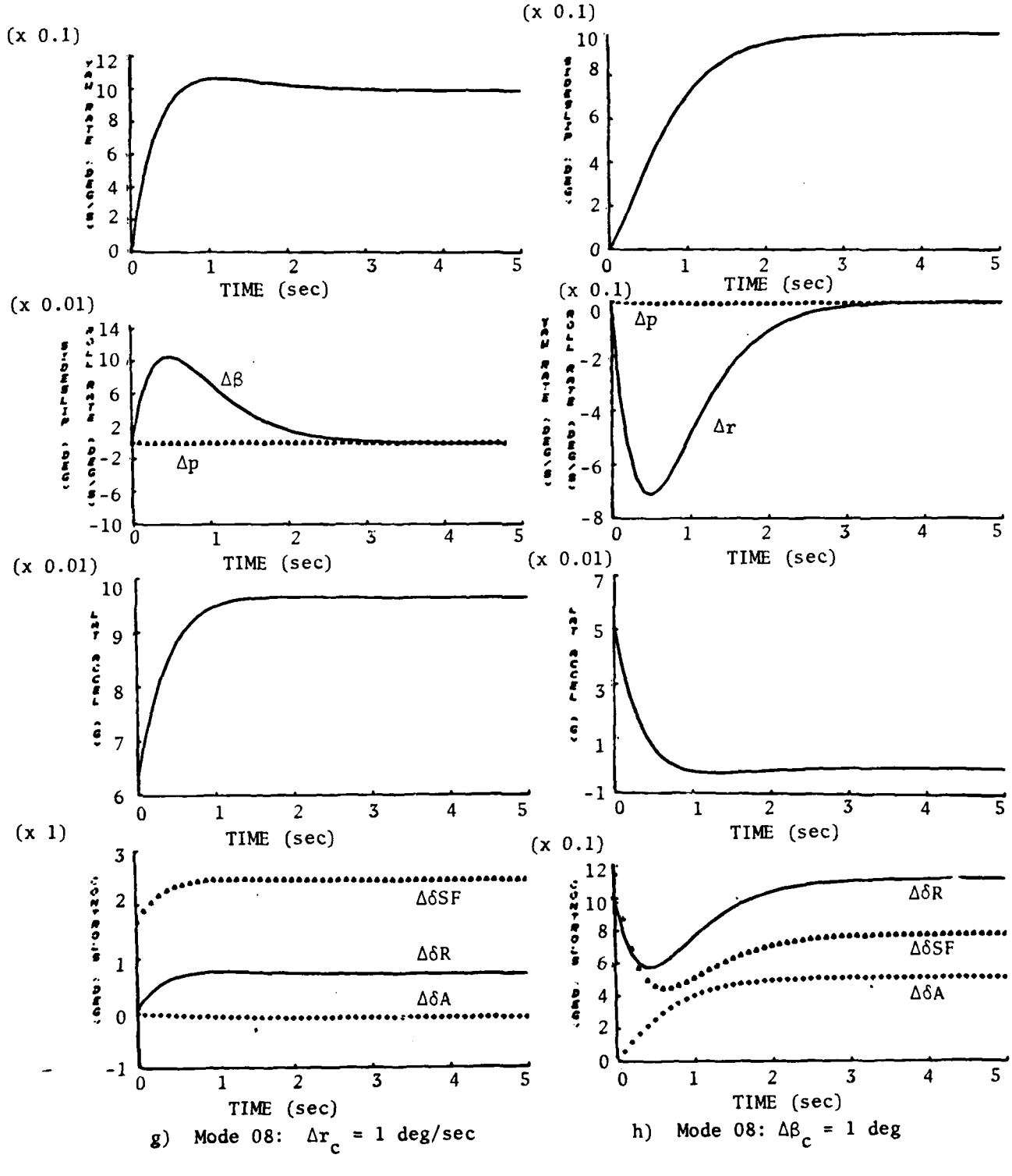

g) Mode 08: Δr_c = 1 deg/sec

h) Mode 08: $\Delta \beta_c$ = 1 deg

Figure 4-4. Continued

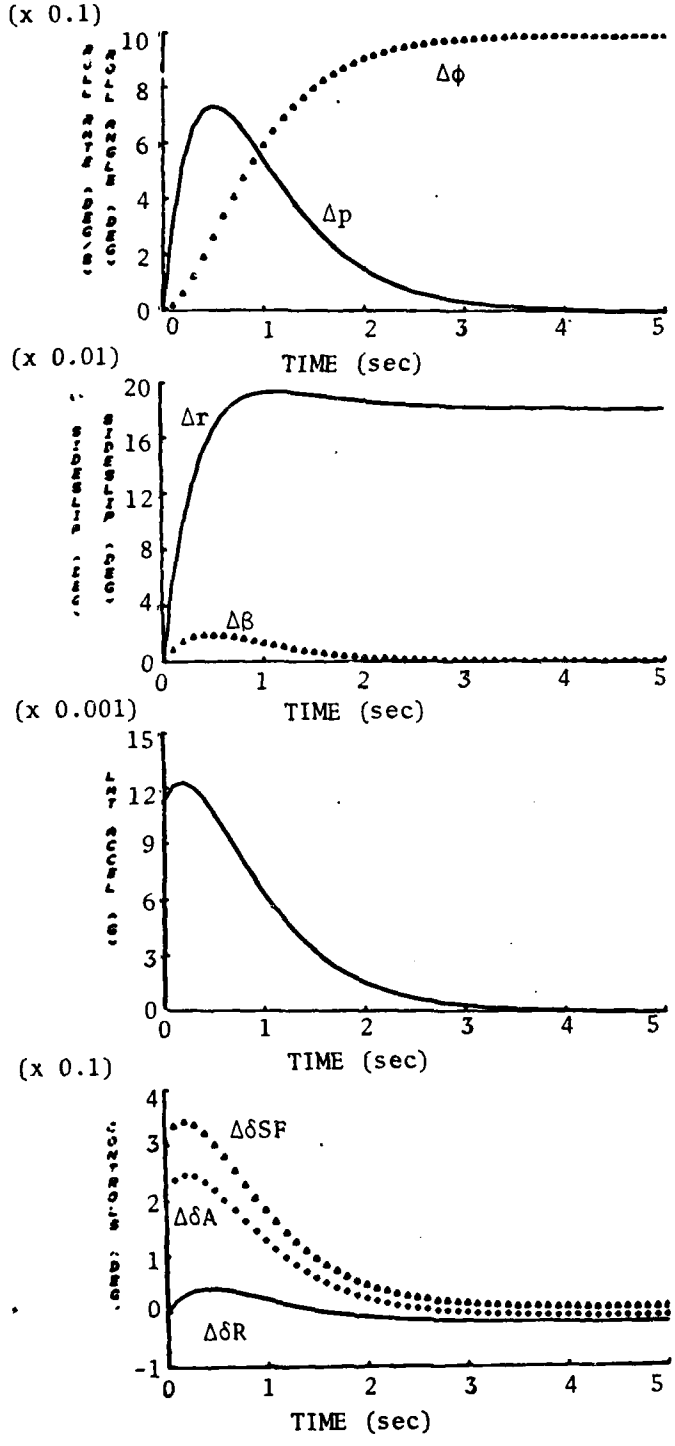

i) Mode 08: $\Delta\phi_c$ = 1 deg,
Δr_c = .181 deg/sec

Figure 4-4. Continued.

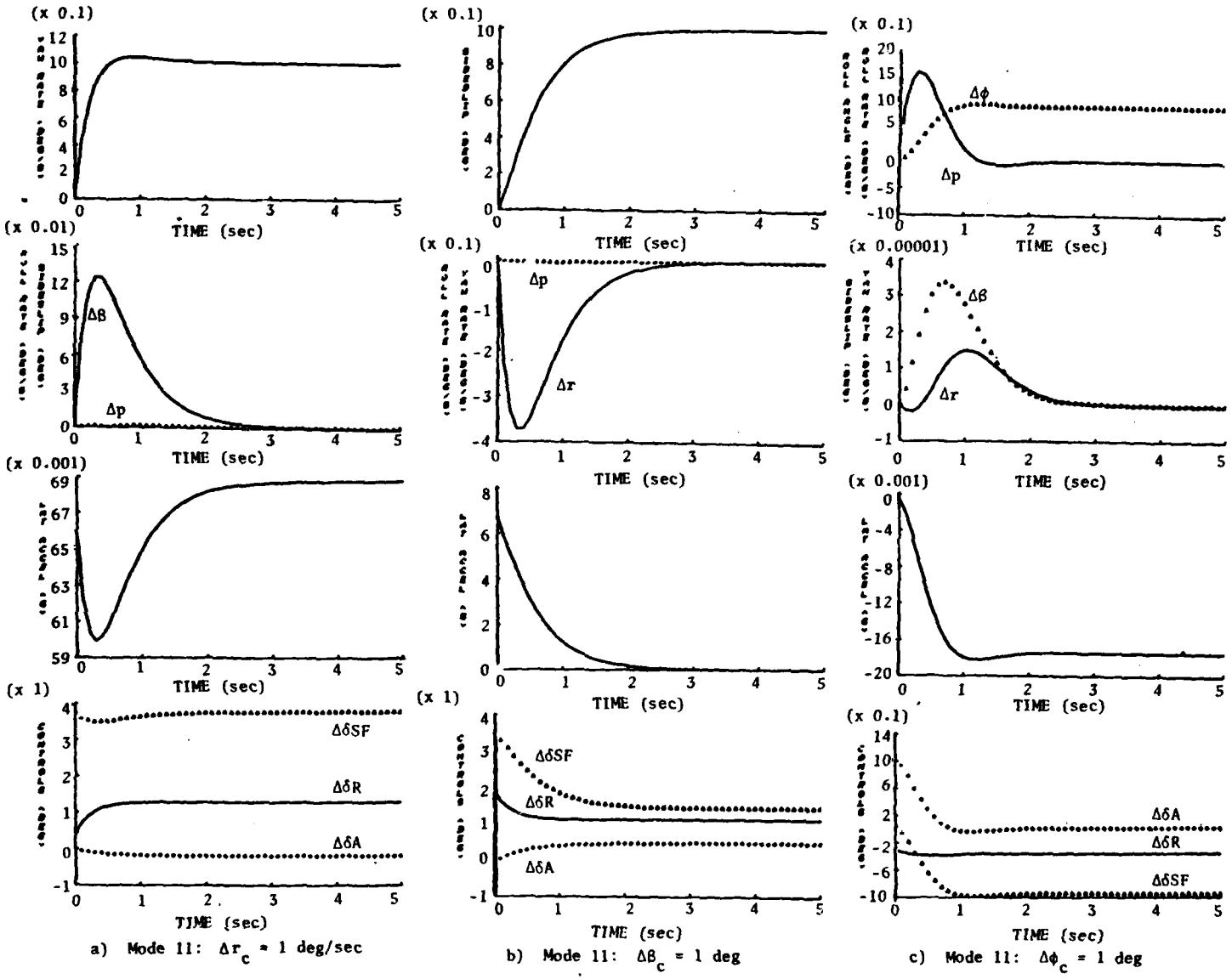

Figure 4-5. Digital Computer Simulations of New Uncoordinated (r,β,ϕ) Mode. V = 75 KIAS.

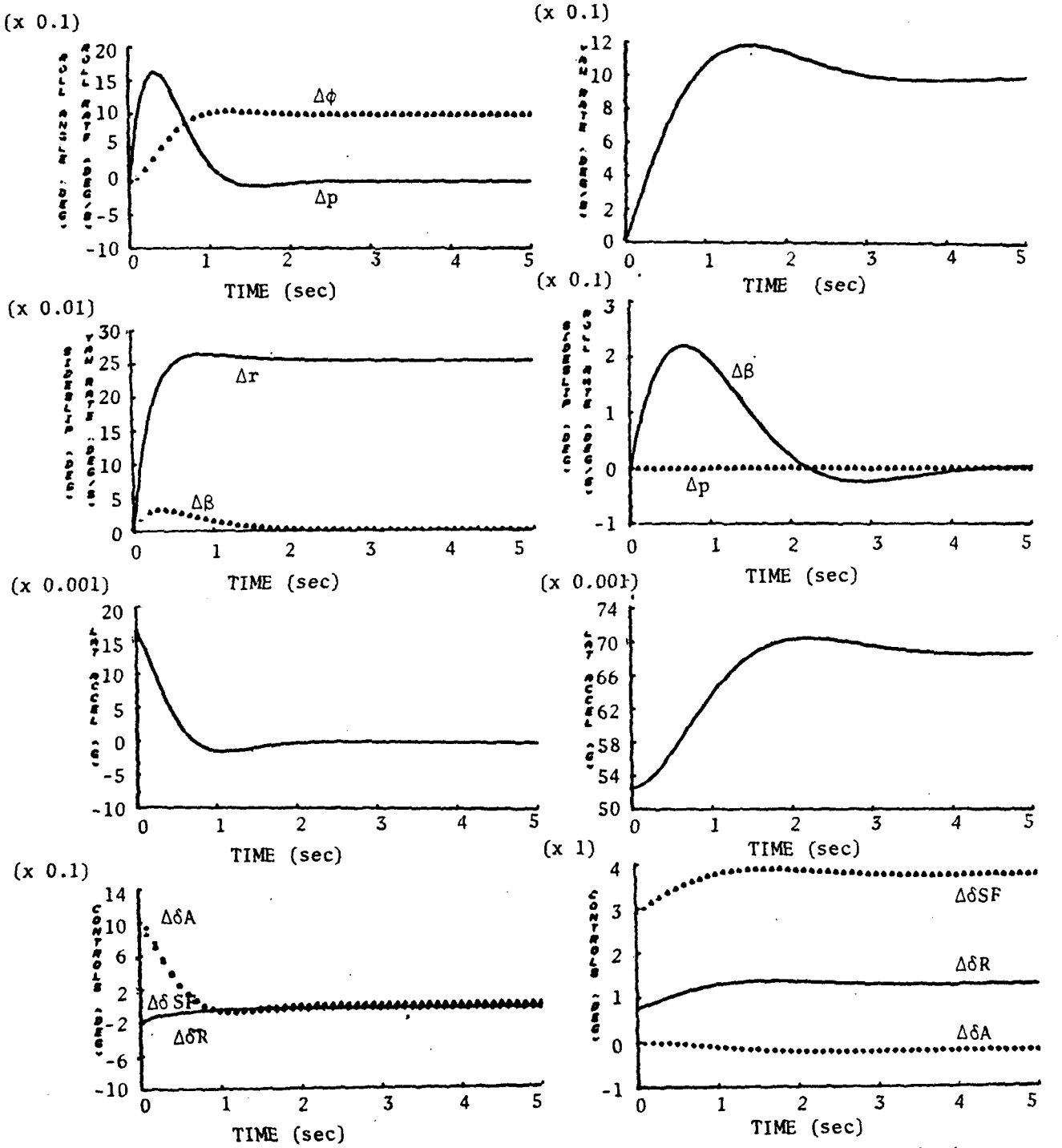

a) Mode 16: $\Delta\phi_c$ = 1 deg,
Δr_c = .254 deg/sec

b) Mode 17: Δr_c = 1 deg/sec

Figure 4-6. Digital Computer Simulations of New Coordinated (r, β, φ) Modes. V = 75 KIAS.

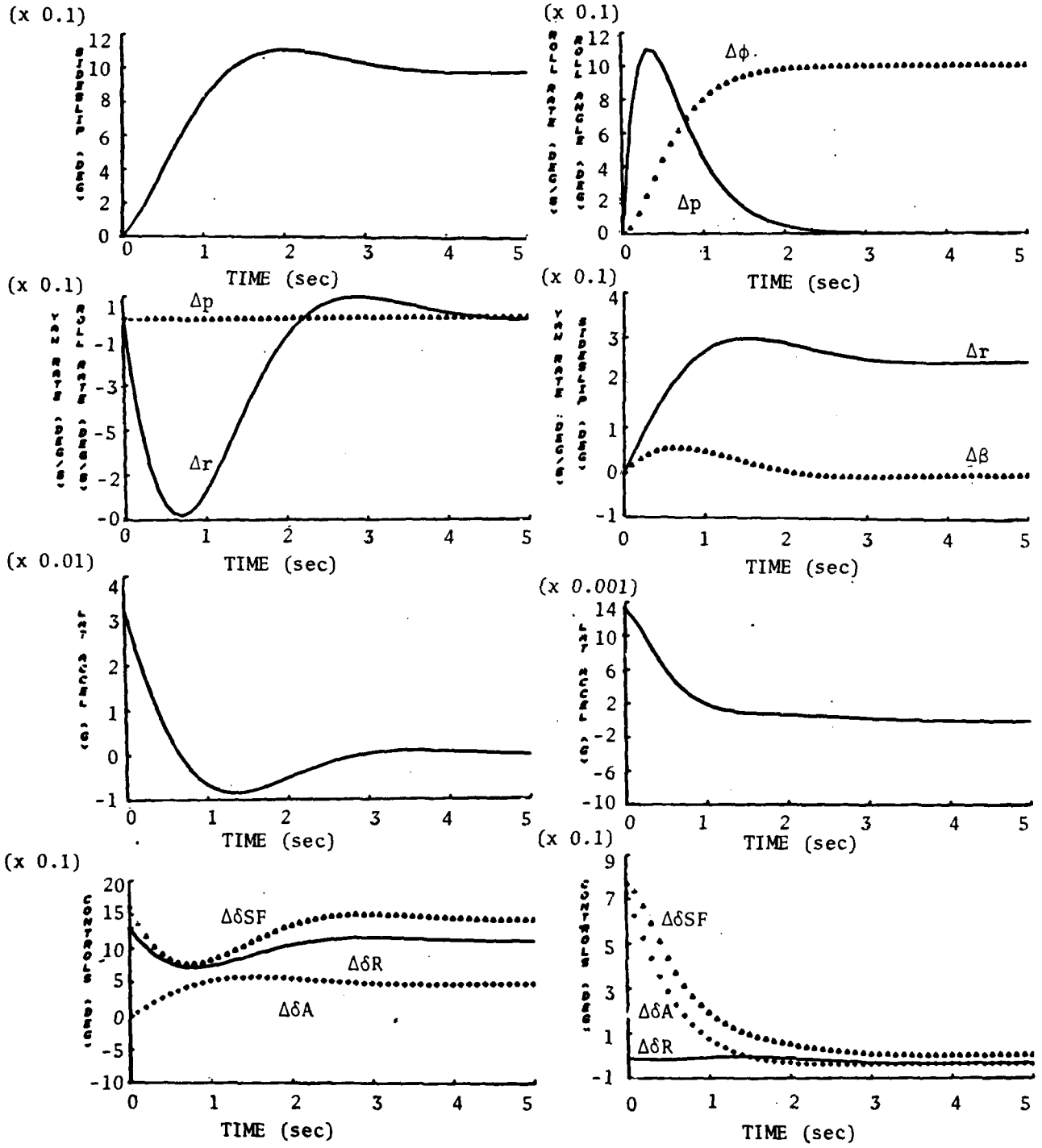

c) Mode 17: $\Delta\beta_c$ = 1 deg

d) Mode 17: $\Delta\phi_c$ = 1 deg, Δr_c = .254 deg/sec

Figure 4-6. Continued.

4-11

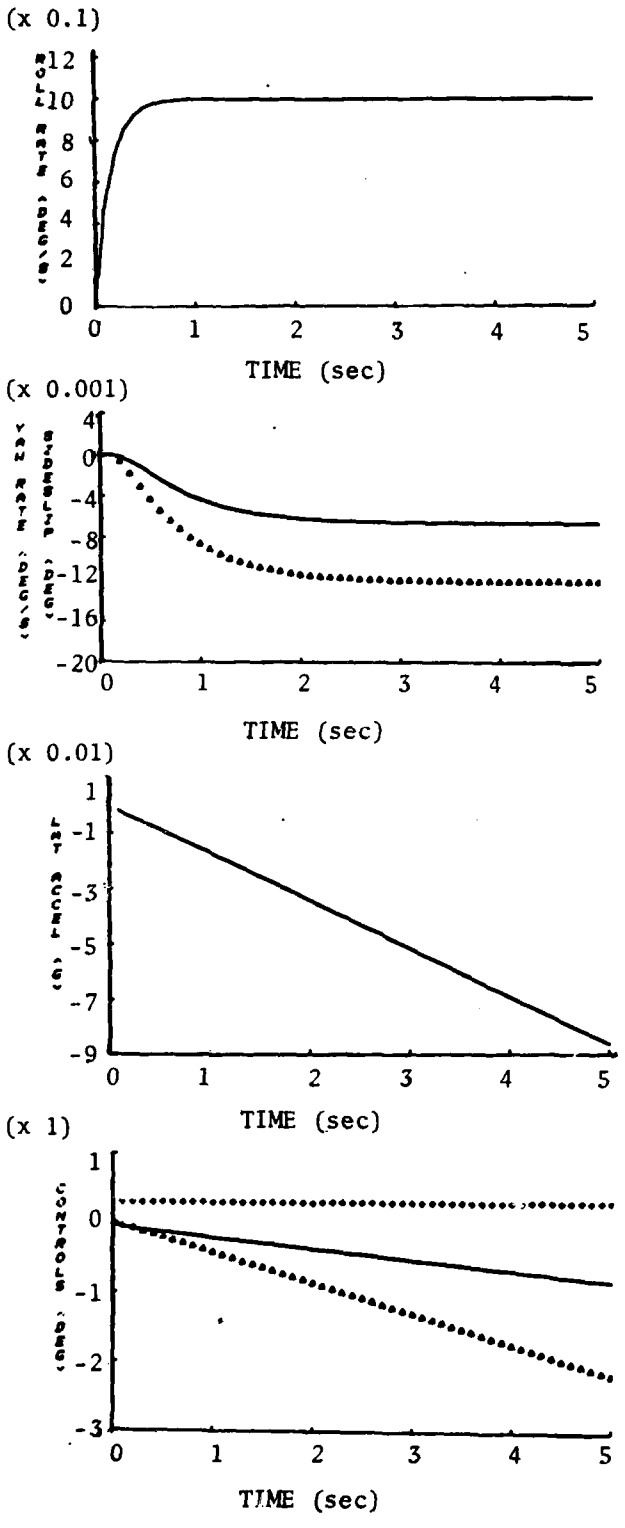

Figure 4-7. Mode 02 Response Using Quasi-Steady Equilibrium (Section 2.2-2): Δp = 1 deg/sec.

4-12

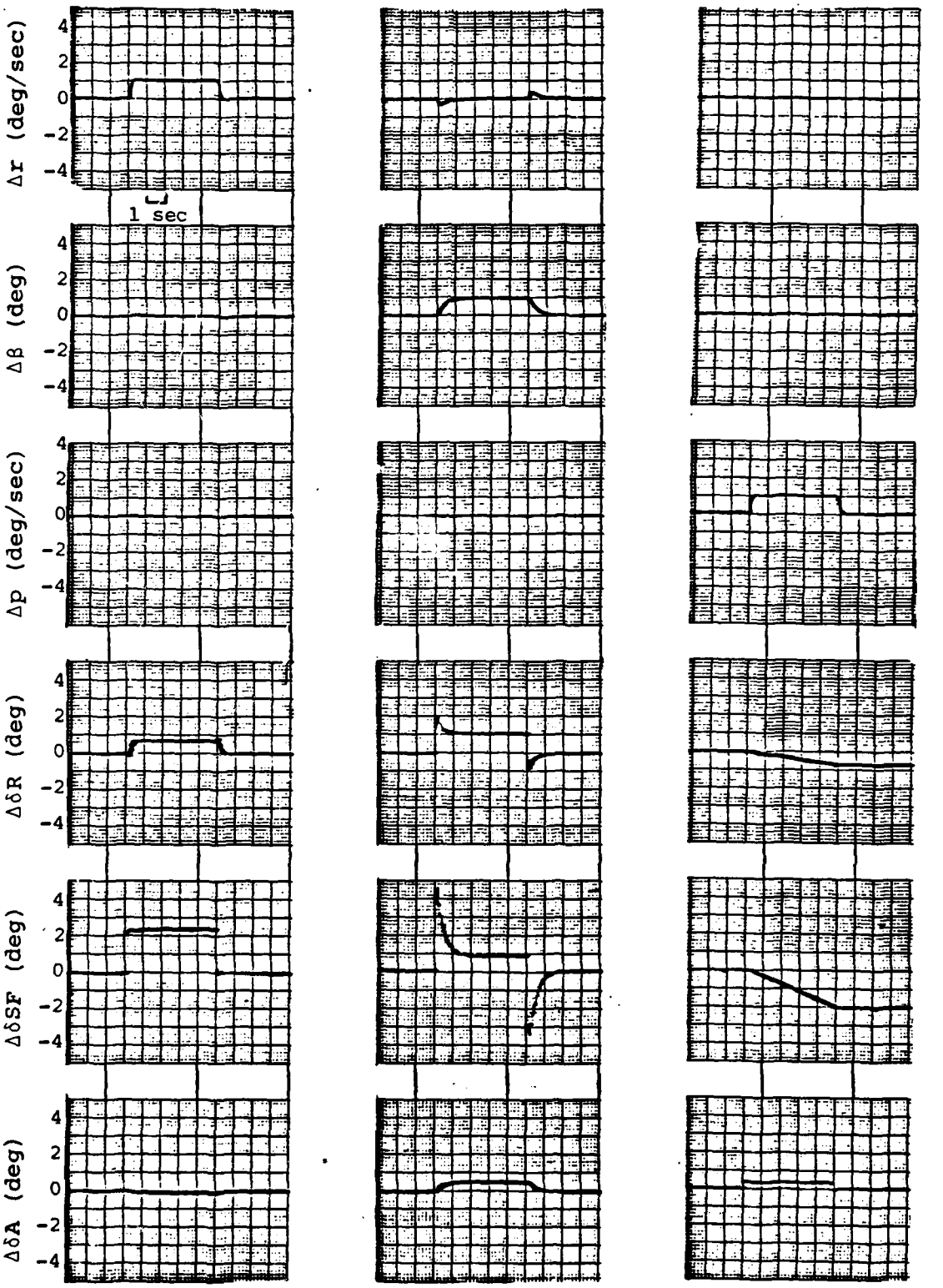

Figure 4-8. Hybrid Simulations of New Modes.

4-13

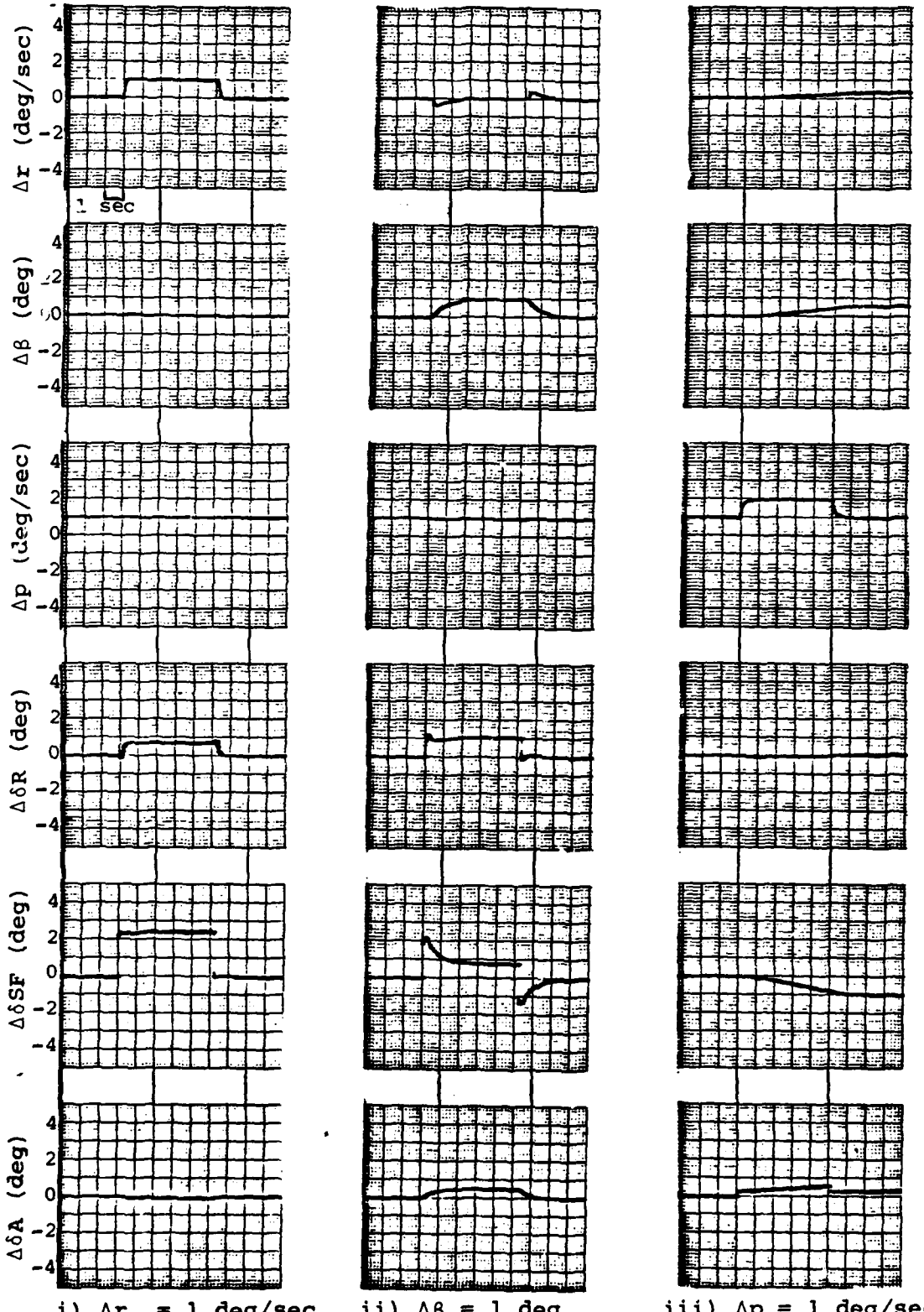

i) Δr_c = 1 deg/sec ii) $\Delta \beta_c$ = 1 deg iii) Δp_c = 1 deg/sec

b) Mode 02

Figure 4-8. Continued

1-14

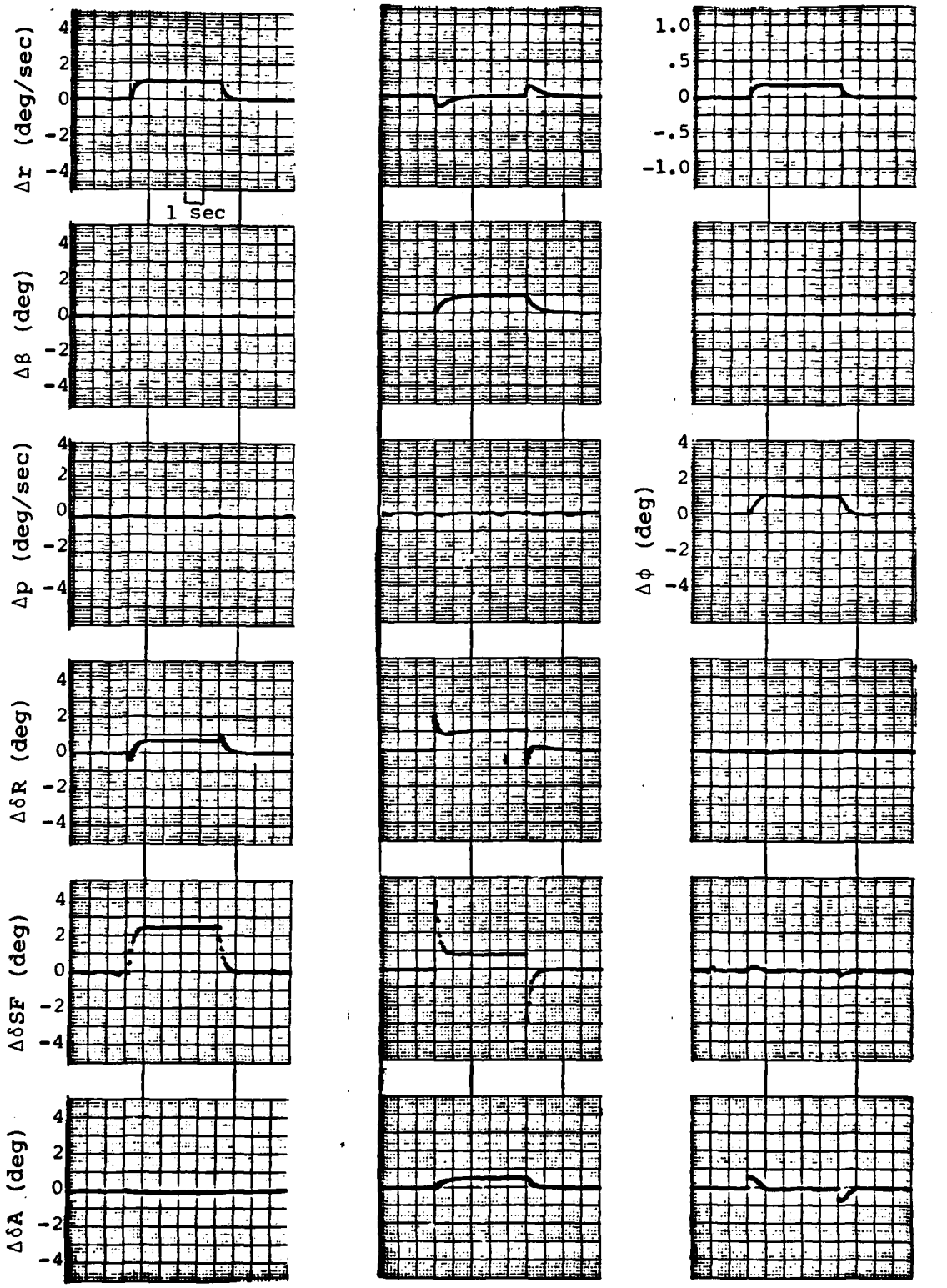

i) Δr_c = 1 deg/sec ii) $\Delta \beta_c$ = 1 deg iii) $\Delta \phi_c$ = 1 deg, Δr_c = .181 deg/sec

c) Mode 06

Figure 4-8. Continued

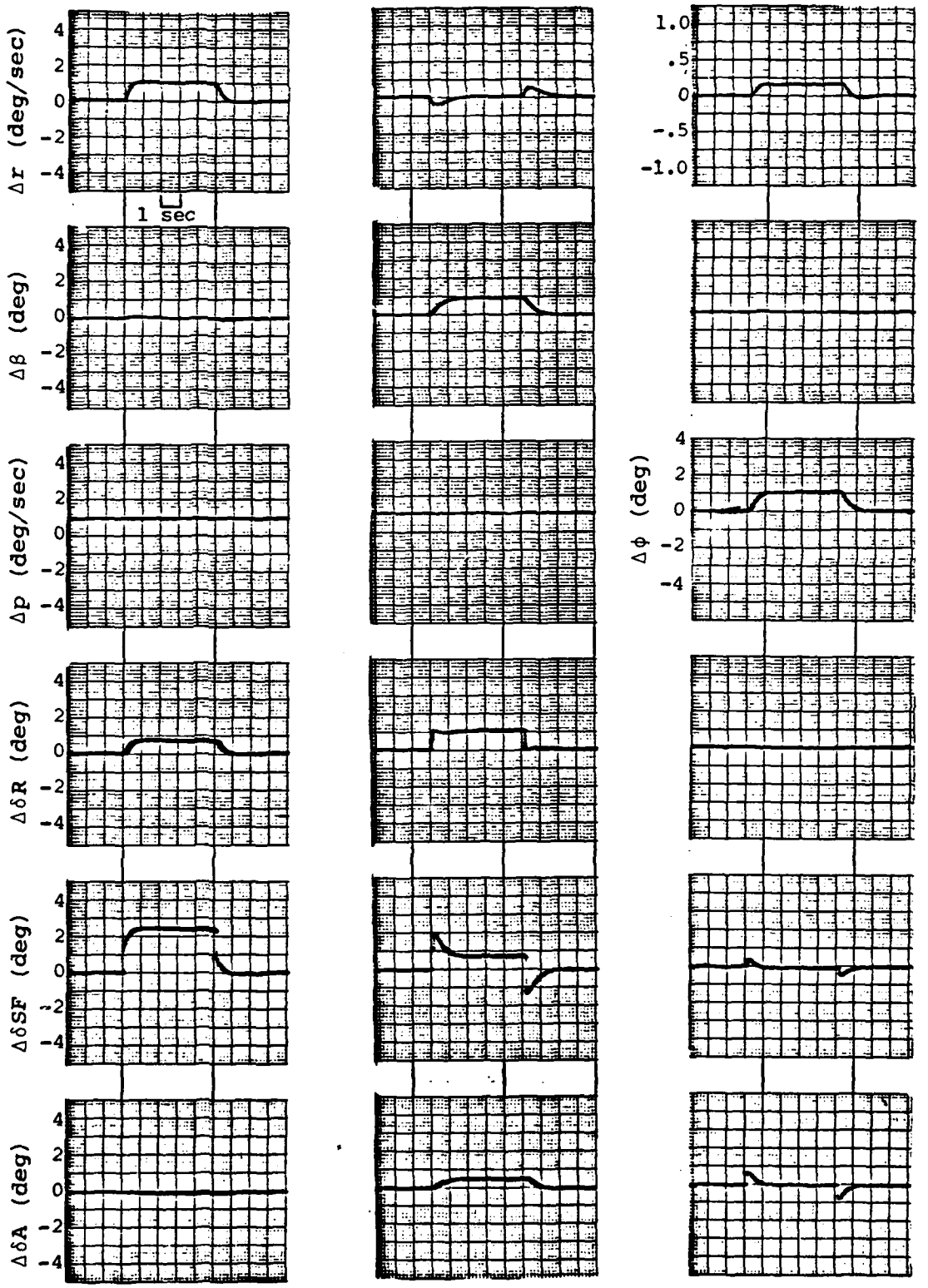

i) $\Delta r_c = 1$ deg/sec ii) $\Delta \beta_c = 1$ deg iii) $\Delta \phi_c = 1$ deg, $\Delta r_c = .181$ deg/sec

d) Mode 07

Figure 4-8. Continued

4-16

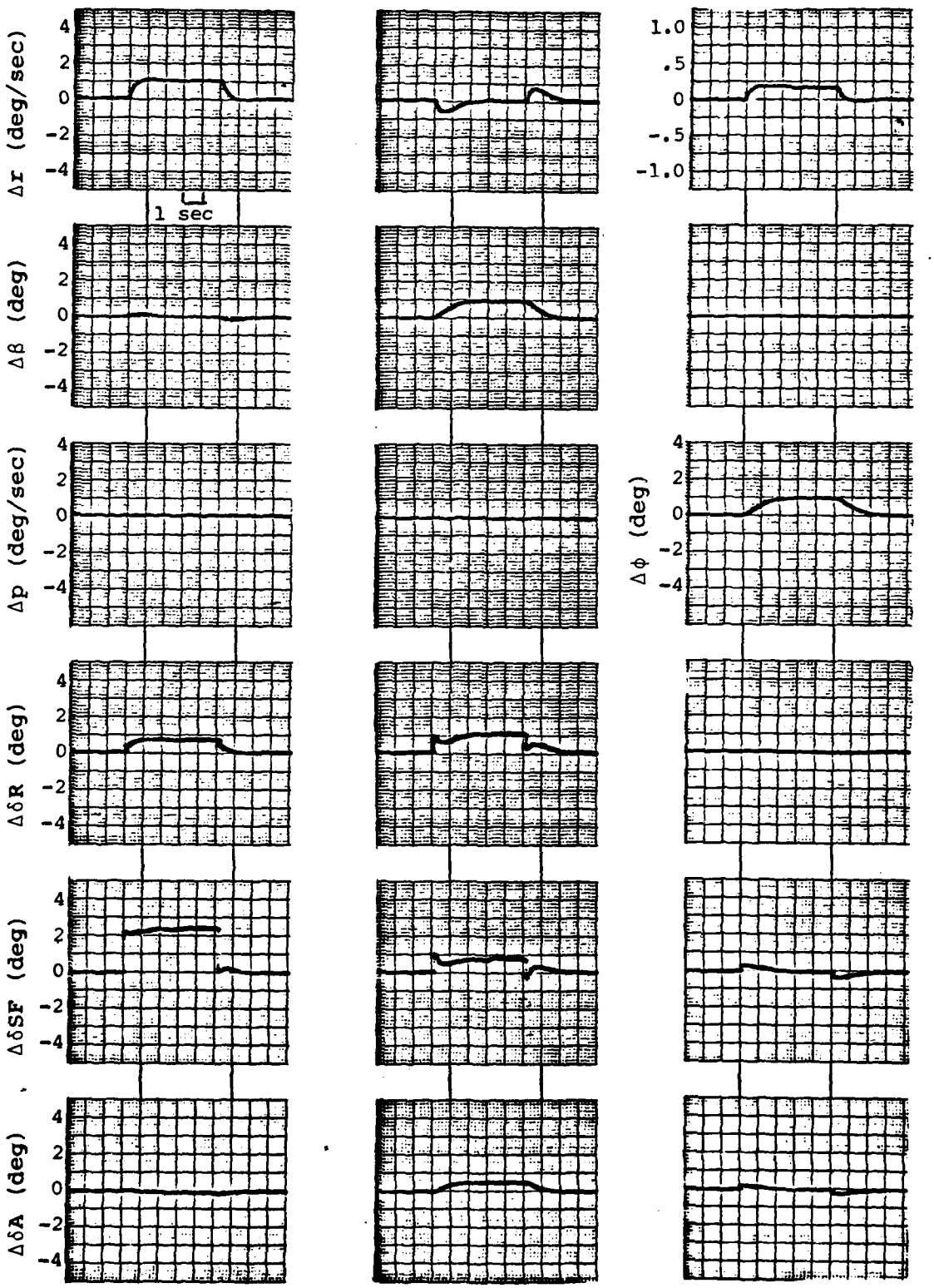

e) Mode 08

Figure 4-8. Continued

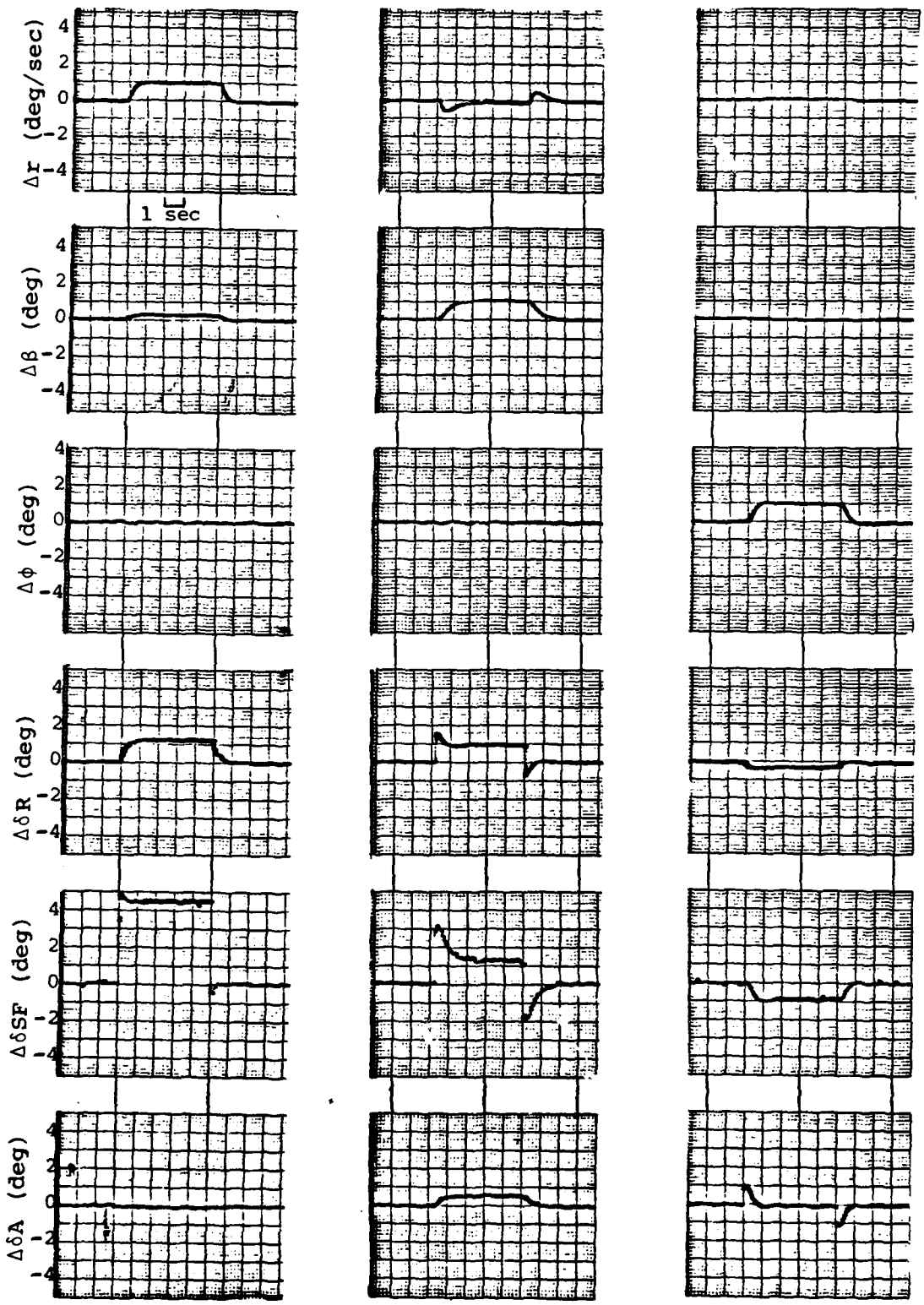

i) Δr_c = 1 deg/sec ii) $\Delta \beta_c$ = 1 deg iii) $\Delta \phi_c$ = 1 deg

f) Mode 11

Figure 4-8. Continued

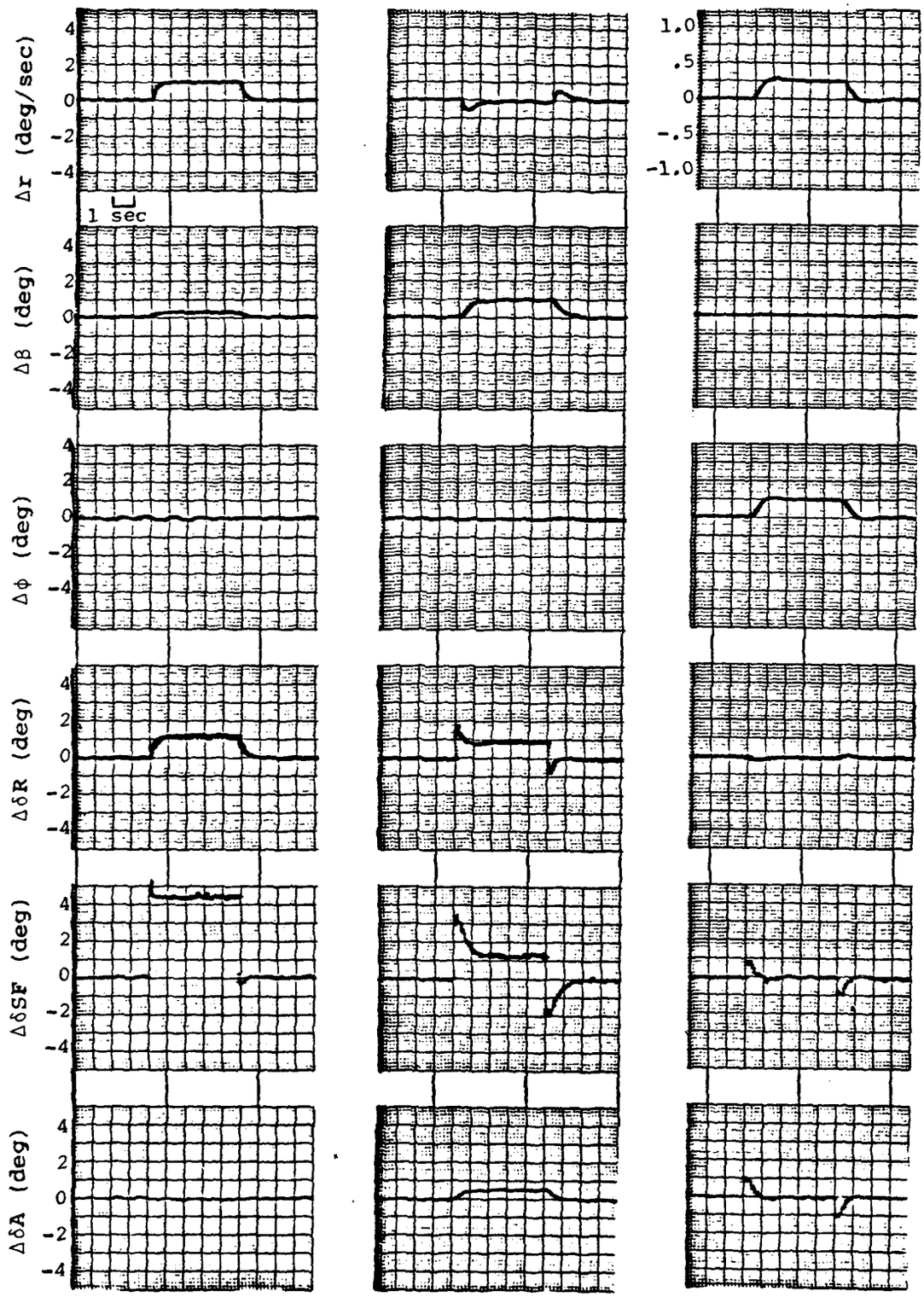

g) Mode 16

Figure 4-8. Continued

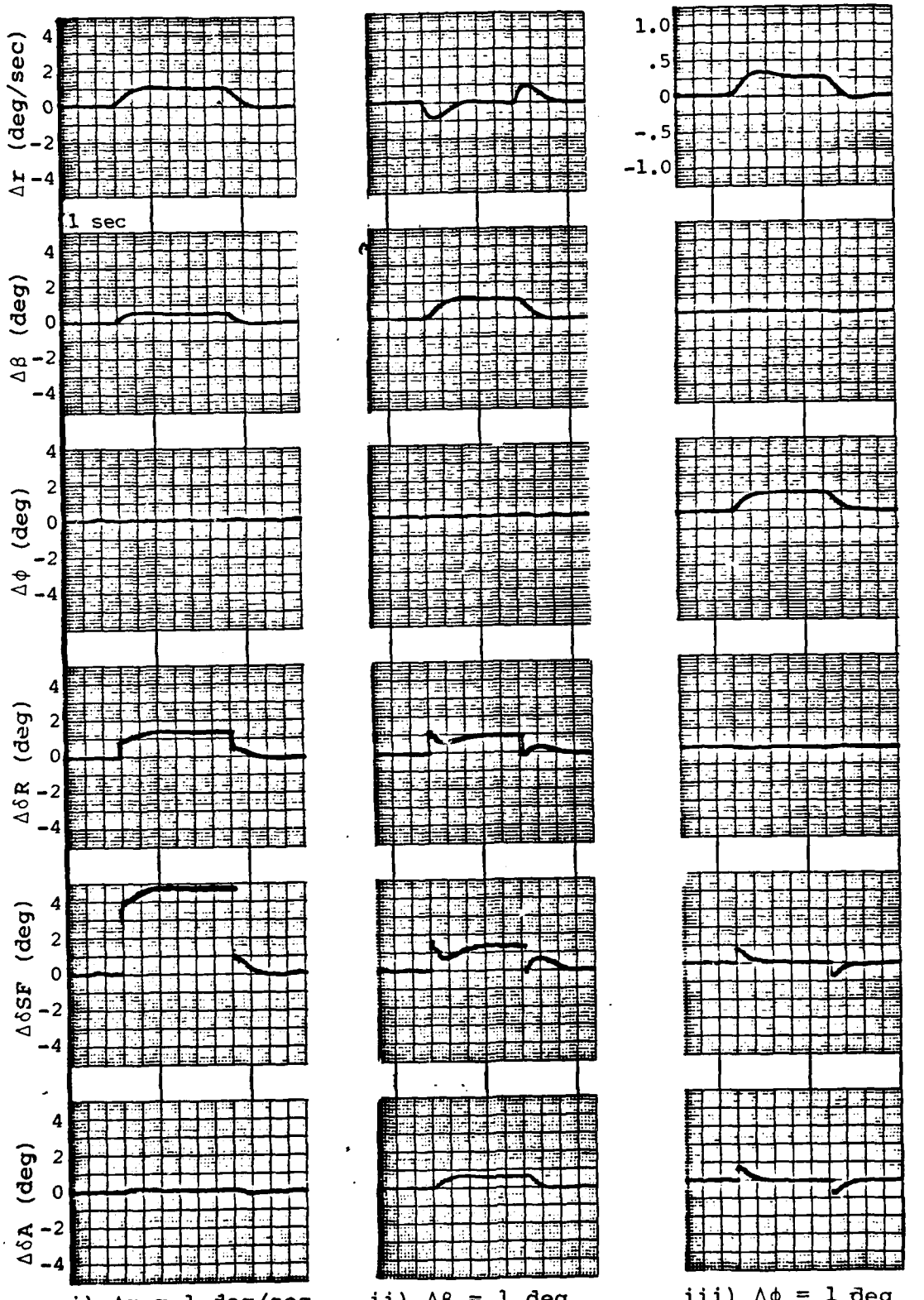

h) Mode 17

Figure 4-8. Continued

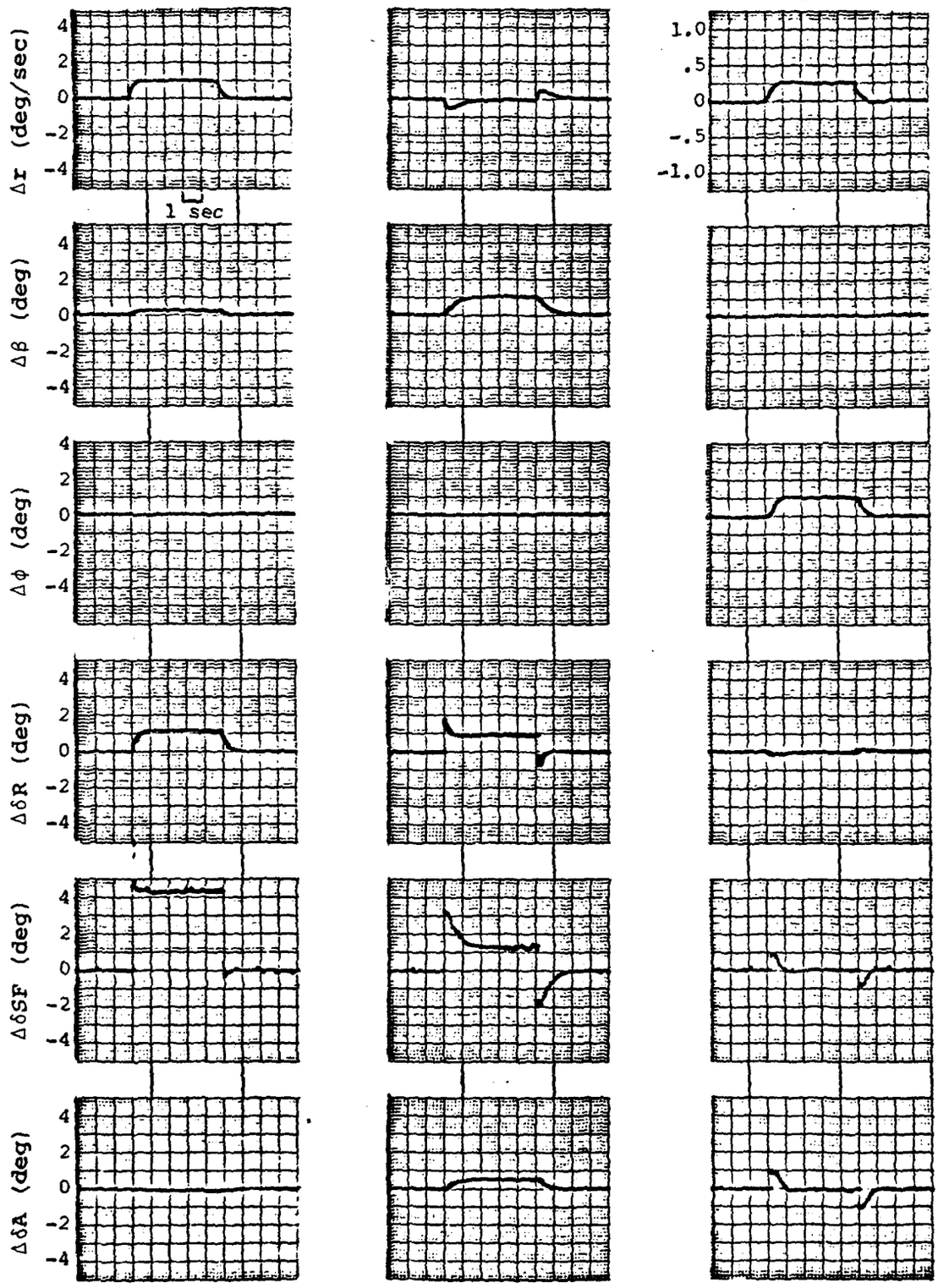

i) Mode 18

Figure 4-8. Continued

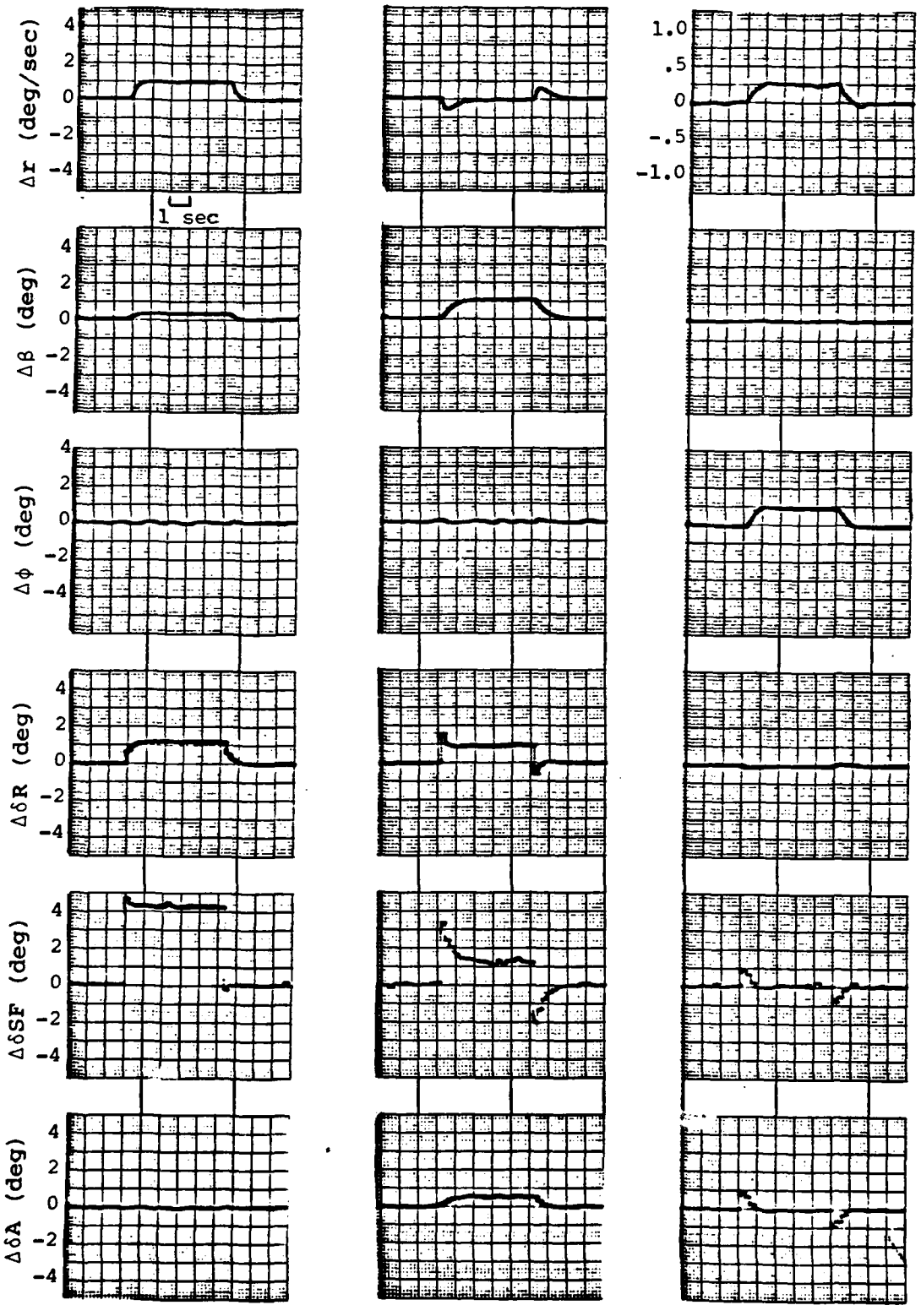

i) Δr_c = 1 deg/sec ii) $\Delta \beta_c$ = 1 deg iii) $\Delta \phi_c$ = 1deg, Δr_c = .254 deg/sec

j) Mode 19

Figure 4-8. Continued.

performance; then an associated task was introduced. As a result of the inclusion of weathercock stability, the new modes performed much better than the previous ones did. The modes tracked consistently, in a manner similar to that predicted by the ground tests. The responses to calibrated step cockpit control inputs of some modes in flight are shown in Figure 4-9. Poor telemetry transmission detracted from recording quality and prevented the documentation of all the modes.

The traces resulting from the flight tests were expected to differ from those generated in the hybrid simulation because of the inclusion of the following new factors:

- Actual VRA nonlinear dynamics
- Control actuators
- Turbulence
- Signal noise
- Sensor accuracy and scaling
- System filters
- Sampling delay of pilot input
- Telemetry scaling

Only five variables could be displayed on the strip chart at a time, so $\Delta\delta A$, which usually has the smallest deflection of any of the controls, is rarely plotted.

Figure 4-9 contains the VRA open-loop response at 105 KIAS, which is similar to that predicted by the linear dynamics of Chapter 2. The response to a 5 deg $\Delta\delta A$ input shows the adverse yaw of the VRA, although the Δp trace is degraded after the proper initial response. This degradation, which prohibited plots for a Δp command in Modes 01 and 02, is caused by telemetry interference when the VRA wing is banked sufficiently far enough.

The $\Delta\beta$ command of Mode 01 (Fig. 4-9b) illustrates the effect of actuator dynamics during flight. The initial $\Delta\delta SF$ is only 10 deg compared to the

theorectical deflection of 22 deg, but this difference does not appear to degrade the response variables. A marginal telemetry signal during the flat turn causes the zero reference line of the Δp and $\Delta\delta SF$ plots to gradually decline. An anomaly occurs during the flat turn of Mode 02 (Fig. 4-9c) in that Δp does not remain zero.

In Mode 06 (Fig. 4-9d), the initial reversal of $\Delta\delta R$ is graphically depicted during the command of Δr. The control deflections are larger than predicted to a 4-deg $\Delta\beta$ command. During the coordinated turn an overshoot in Δr (about 60%) and $\Delta\phi$ (about 15%) is shown, and Δr is proportional to $\Delta\phi$ to allow for the coordination.

Mode 07 (Fig. 4-9d) is also designed to have a coordinated turn capability; however, for some reason, the response to a 20 degree $\Delta\phi$ command shows steady-state control deflections equal to that expected for a simple roll angle mode. Thus the turn is not coordinated.

In all the step inputs of Mode 08 (Fig. 4-9e), the $\Delta\delta SF$ response is predictable, save for the fact that the zero reference line continually decreases. The erratic behavior of $\Delta\beta$ in this mode (when it should be zero), as is the case in many of the other modes flight tested, may be due to the turbulence response of the sideslip vanes.

Finally, Figure 4-9f depicts Mode 11 at 75 KIAS. The time constants of the command responses appear to be similar to those determined during ground simulation.

Overall, when considering the capricious nature of the telemetry system, the plots of the modes flight tested agree in most aspects with those predicted in the ground evaluations.

The major complaints of the two pilots concerned the overly sensitive lateral translation response to thumb lever command, and annoying "kicks",

or chatter, of the rudder and side force panels during the Micro-DFCS operation. One result obtained was that the pilots thought that any more than about 0.5 g (the maximum achievable by the VRA at 105 KIAS) during the flat turn would be disconcerting and would degrade pilot performance.

The annoying control surface kicks, appearing in both the ground check and the flight tests, indicated the presence of an intolerable amount of signal noise. One way to reduce system noise is to diminish the feedback gains of the control law. The magnitude of the gains can be thought of as directly related to the difference between the closed-loop and basic VRA stability derivatives. By using the ESD matching technique, one has a direct effect on the system gains. Additional models were devised which contained stability terms closer in value to the VRA's. Any performance degradation embodied by these new modes was thought to be outweighted by the improvement in control behavior--especially considering that the original modes probably were overly responsive.

By glancing at Table 4-1, one can see the reduction of the control gains in Mode 08 compared to any of the other 105-knot modes. As an example, consider the large gains (those with a magnitude greater than one) of Mode 06: notice that they occur in the calculation of rudder and side force deflection. They are reduced in Mode 08 anywhere from 46 to 88 percent. In the process, though, one new large gain appears in Mode 08. The apparent improvement in Mode 08 is a result of the general reduction of model stability values (especially "Y_{β}/V") to more closely resemble the VRA's. These additional new modes developed, Modes 07 and 08 at 105 KIAS, and Mode 17 at 75 KIAS, illustrated slower command response, decreased damping, and an increase in transient coupling.

In order to more effectively analyze the advanced control modes in flight, certain basic tasks were introduced. The first task-oriented profile involved three phases of flight:

1) 180-degree turn from downwind to final approach
2) Final approach
3) Maintaining runway centerline during low approach

Each phase could be accomplished predominately with a single maneuver: a coordinated banked turn, followed by small flat-turn heading changes for alignment on final approach, and then a lateral translation to maintain the centerline. The approach employed a Navy portable mirror which is used for field carrier landing practice. The pilots determined during practice runs that the flat turn was impractical for accomplishing the 180-deg turn to final due to the inherent lateral g of the maneuver. In addition, the bank of a conventional final turn aids the pilot in visually acquiring the approach environment. As for the final approach, the sidestep capability was of limited value until very near the runway threshold because of the apparent reduced effect of the maneuver at a distance from the runway. It was significant, however, for eliminating lateral ground speed during a crosswind condition--either actual, or simulated by the VRA's analog system.

For the profile, the Micro-DFCS was engaged on the downwind leg at 105 KIAS and an approach power setting. Little trim change is necessary during the approach, so the modes designed at 105 KIAS could be used for the tests with little degradation. Each pilot was able to evaluate several modes with this task-oriented profile. Their Cooper-Harper ratings and comments are included in Table 4-2. Overall, the closed-loop modes do not compare very favorably with the baseline direct mode. Pilot B's ratings are slightly higher than Pilot A's. Of the closed-loop modes tested, Pilot A favored Mode 08 for the turn (rating of 3), Modes 02, 07, and 08 for the approach (rating of 3.5), and Mode 02 for maintaining centerline (rating of 3). Of the modes evaluated by Pilot B, Mode 06 was preferred for the turn (rating of 2.5), Mode 07 for the approach (rating of 2.5), and several modes for maintaining centerline (rating of 3).

Pilot A found some of the flat turn responses too quick. Pilot B did

Table 4-2. Pilot Ratings of Landing Approach Task

MODE	TURN TO FINAL	FINAL APPROACH	MAINTAIN RUNWAY CENTERLINE	COMMENTS
Pilot A				
00	2.5	3	3	OK, normal; nominal
	2.5	3	2.5	
02	4.5	3.5	3	rudder a bit sensitive; δT OK; roll mode odd -- can compensate with rudder, but tough
02	5	3.5	3.5	sensitve rudder for aligning ball, not likeable on final; sidestep dandy but a bit sensitve
07	5	3.5	3.5	roll attitude control no advantage on turn, OK on final; rudder steer still sensitive; sidestep OK
07	5	4	3.5	not rudder sensitive but just a requirement for coordination of ball; wings level turn OK but no great shakes; sidestep handy
08	3	3.5	4	nice coordinated turn; rudder/ flat turn OK but not great; sidestep has adverse yaw--no effect on turn or approach but annoying on maintaining centerline
08	4	4	4	coordinated turn nice but jerky for reversals; have to hold roll attitude--not greatest; rudder steer rather blah; sidestep adverse yaw attentuates it

Table 4-2. Pilot Ratings of Landing Approach Task (con't)

MODE	TURN FINAL	FINAL APPROACH	MAINTAIN RUNWAY CENTERLINE	COMMENTS
03	5	5	6	awkward learning to center ball with thumb; intuitive rudder input sends ball out; roll rate OK but poor coordination; lousy centerline track
03	5	4.5	5.5	hard to coordinate; happy to keep wings level on approach and use thumb; centerline task heading control confusing, upsets δSF position
04	7	8	9	unable to learn new coordination required; when changing ϕ with lever, tend to relax stick to turn and lose heading and ball--then natural instinct is to kick pedals which blows ball and whole setup
04	6	7	6.5	unable to smooth control; only way to fly is feet on floor, roll lever then thumb off, then fly turn stick--crazy!
00	2.5	3.5	3	the way to go; natural control; tried δSF exclusively on approach -- a bit sloppy

Table 4-2. Pilot Ratings of Landing Approach Task (con't)

MODE	TURN FINAL	FINAL APPROACH	MAINTAIN RUNWAY CENTERLINE	COMMENTS
Pilot B				
00	3	3	4	
	3	3	4	
02	4	5	3	more β than needed; coordination required in turn and approach
	4	4	3	(approach more critical); β late in approach OK
06	3	4	3	β too large; uncomfortable "ride" quality; turn better but bothered by turbulence
06	2.5	3.5	3	gain on β too high, otherwise *good type of control; r not much* help; like ϕ
07	4	3	3	
	4.5	2.5	3	
06	4	3	3	uncomfortable ride
03	5	5	3	better than Mode 02; pedals better β control
04	5	5	3	hard to learn; roll δT not hard to control; typical to remember past control pairings
	5	5	4	
00	3	3	4	

not comment on this, perhaps because the small yaw rate command authority (6.2 deg/sec at 105 KIAS) masked the response rise time. Both pilots rated the alternate controller-to-command pairings as inferior to the baseline design. Mode 03 was rated better than Mode 04, showing that the command of lateral translation by the foot pedals (which have a lower sensitivity than the thumb lever) is satisfactory while thumb lever control of roll is not. Pilot A's rating pattern suggests a learning tendency with the alternate pairings, and there is a strong implication that the ratings for all of the modes could improve with pilot experience. Pilot B gave the best combined rating to Mode 06 although is has an uncomfortable ride quality. The poor ride is a result, in part, of surface chatter--particularly during the approach portion of the task where the noise is accentuated in the absence of a need for a large amount of maneuvering. Finally, for maintaining the centerline, Pilot B rated most of the closed-loop modes (which use a single cockpit control) superior to the direct mode (which requires cross-controlling).

In an effort to improve the ride quality of the closed-loop VRA, without altering the control law gains, the thumb lever command on the aircraft's stick was modified. At the suggestion of Pilot B, a first-order, low-pass prefilter, which included a variable capacitor that could be adjusted in flight, was incorporated in the command signal.

Additional improvements made to the thumb controller included a damper, centering spring, and abrasive paper placed on the face of the lever. The damper provided an additional filter to lessen the abruptness of the sidestep maneuver. The spring served as a center detent so that the pilot would consistently have equal command authority in both directions. Although it proved no problem to Pilot B, Pilot A complained of the substantial thumb travel necessary for full command. The sandpaper was added to alleviate thumb slippage throughout the command range. This problem points out the need for human factor considerations in the design of new cockpit controllers.

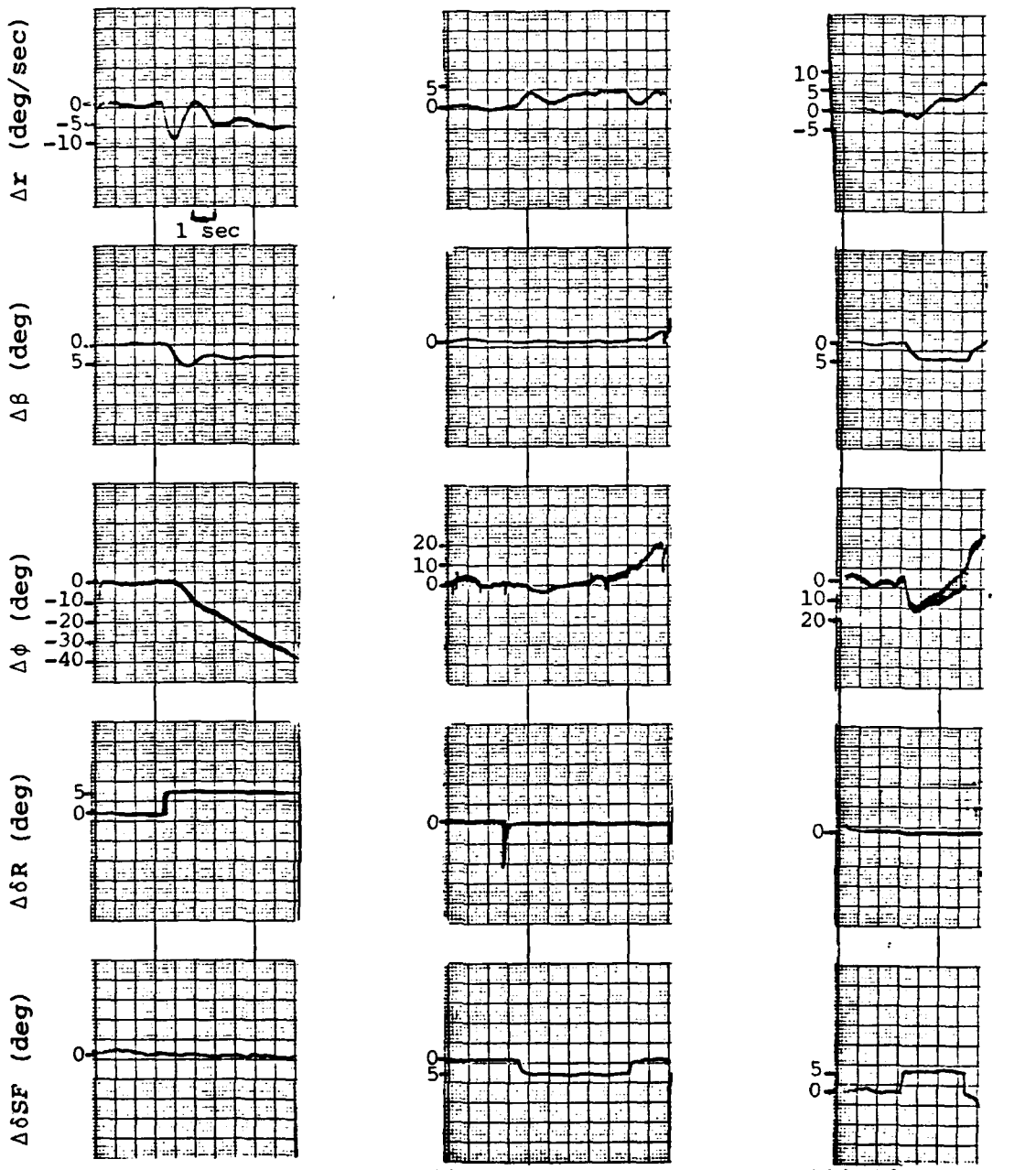

i) $\Delta\delta R_c$ = 1 deg ii) $\Delta\delta SF_c$ = 1 deg iii) $\Delta\delta A_c$=1 deg

a) Mode 00

Figure 4-9. VRA Open-Loop Response at 105 KIAS.

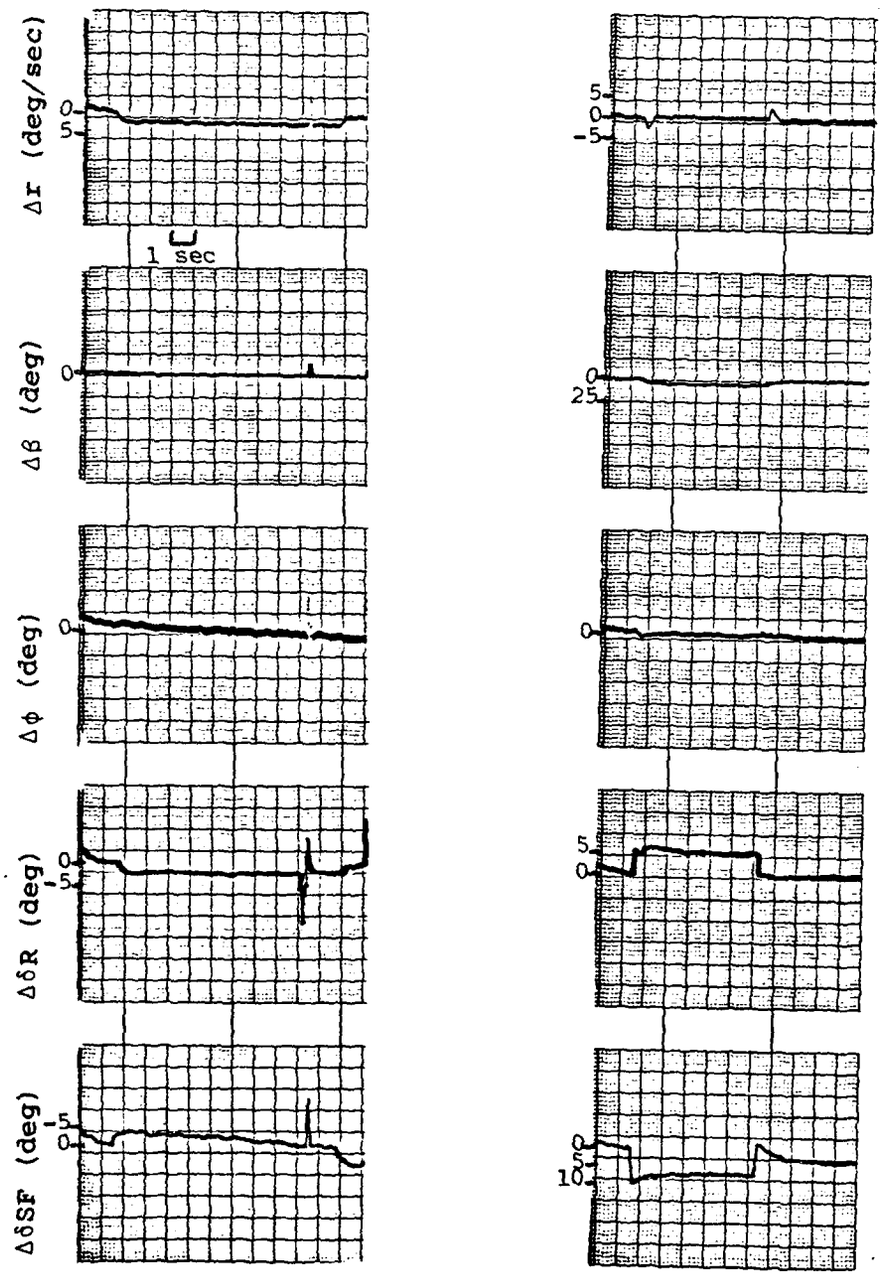

i) Δr_c = -2 deg/sec ii) $\Delta \beta_c$ = 5 deg

b) Mode 01

Figure 4-9. Continued

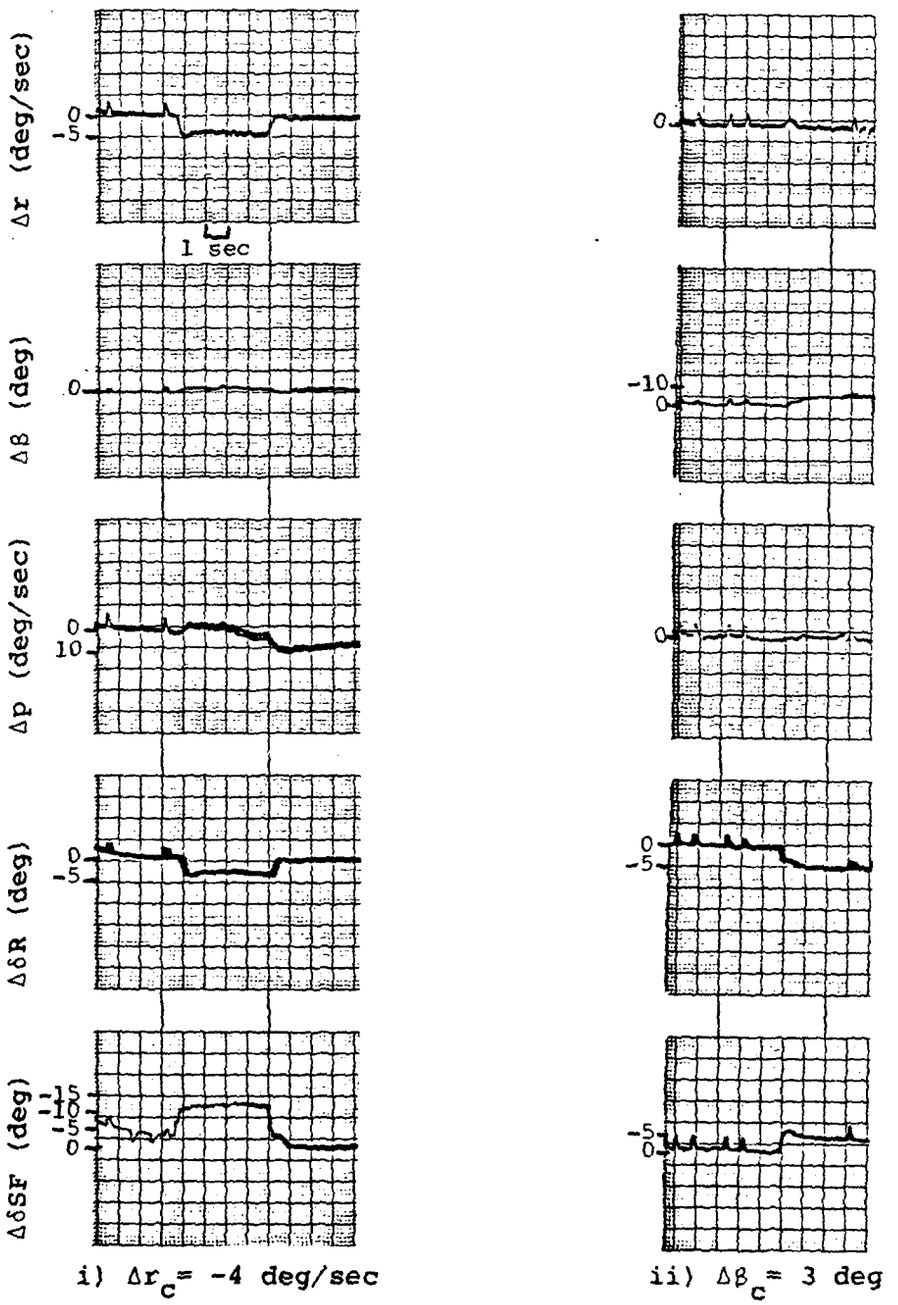

i) Δr_c = -4 deg/sec ii) $\Delta \beta_c$ = 3 deg

c) Mode 02

Figure 4-9. Continued

4.25

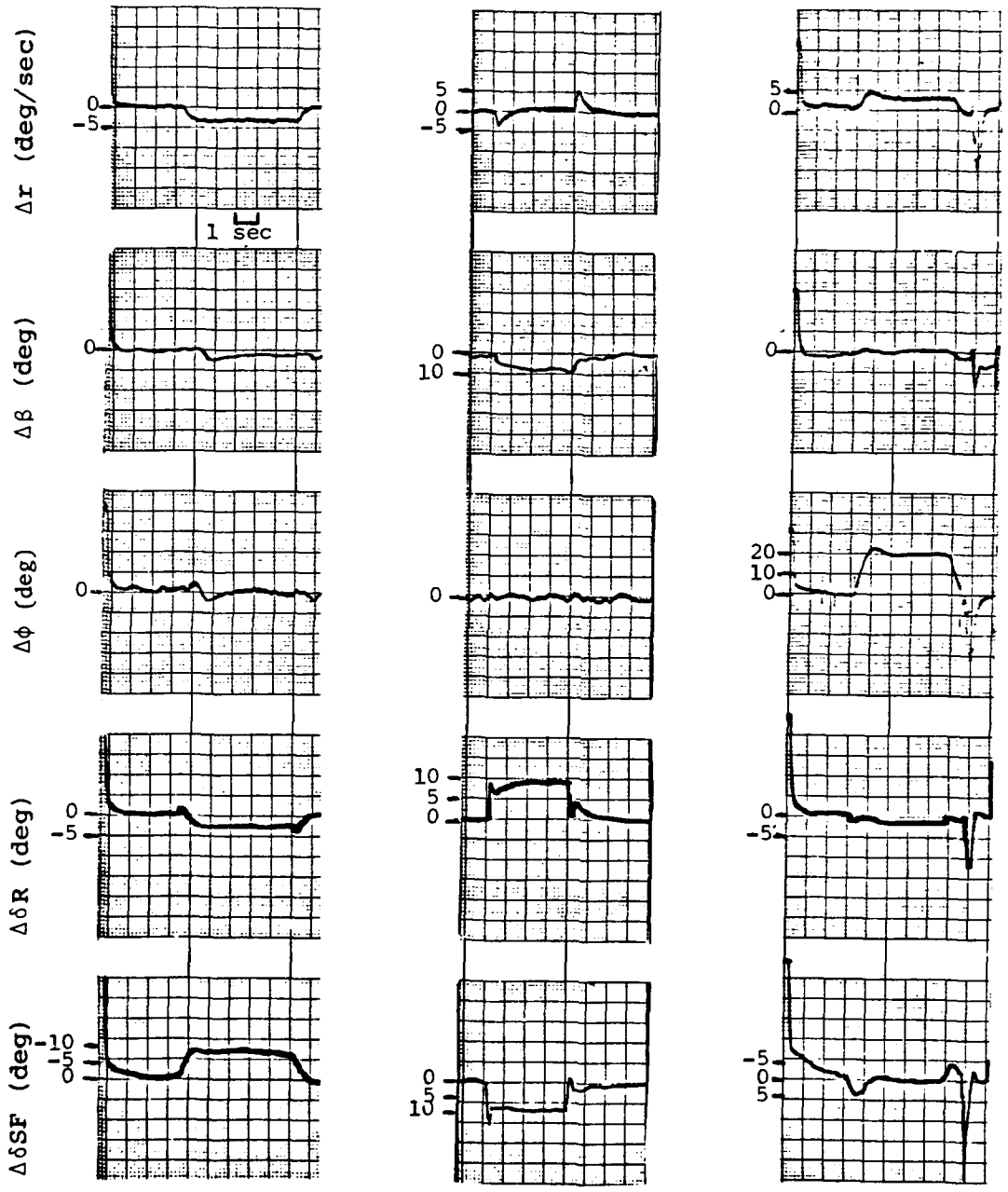

d) Mode 06

Figure 4-9. Continued

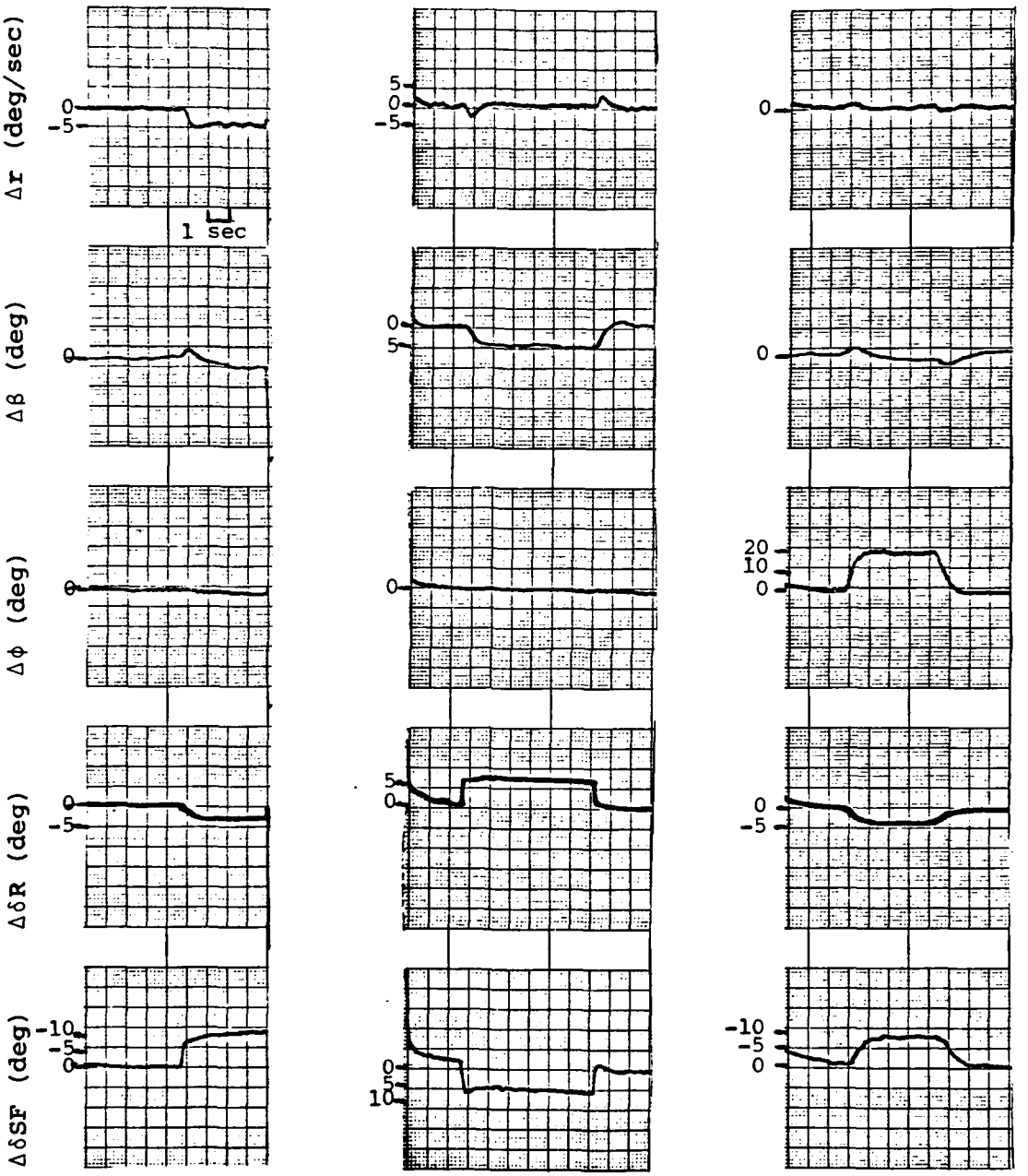

i) Δr_c=-4 deg/sec ii) $\Delta \beta_c$= 4 deg iii) $\Delta \phi_c$= 20 deg, Δr_c= 3.6 deg/sec

e) Mode 07

Figure 4-9. Continued

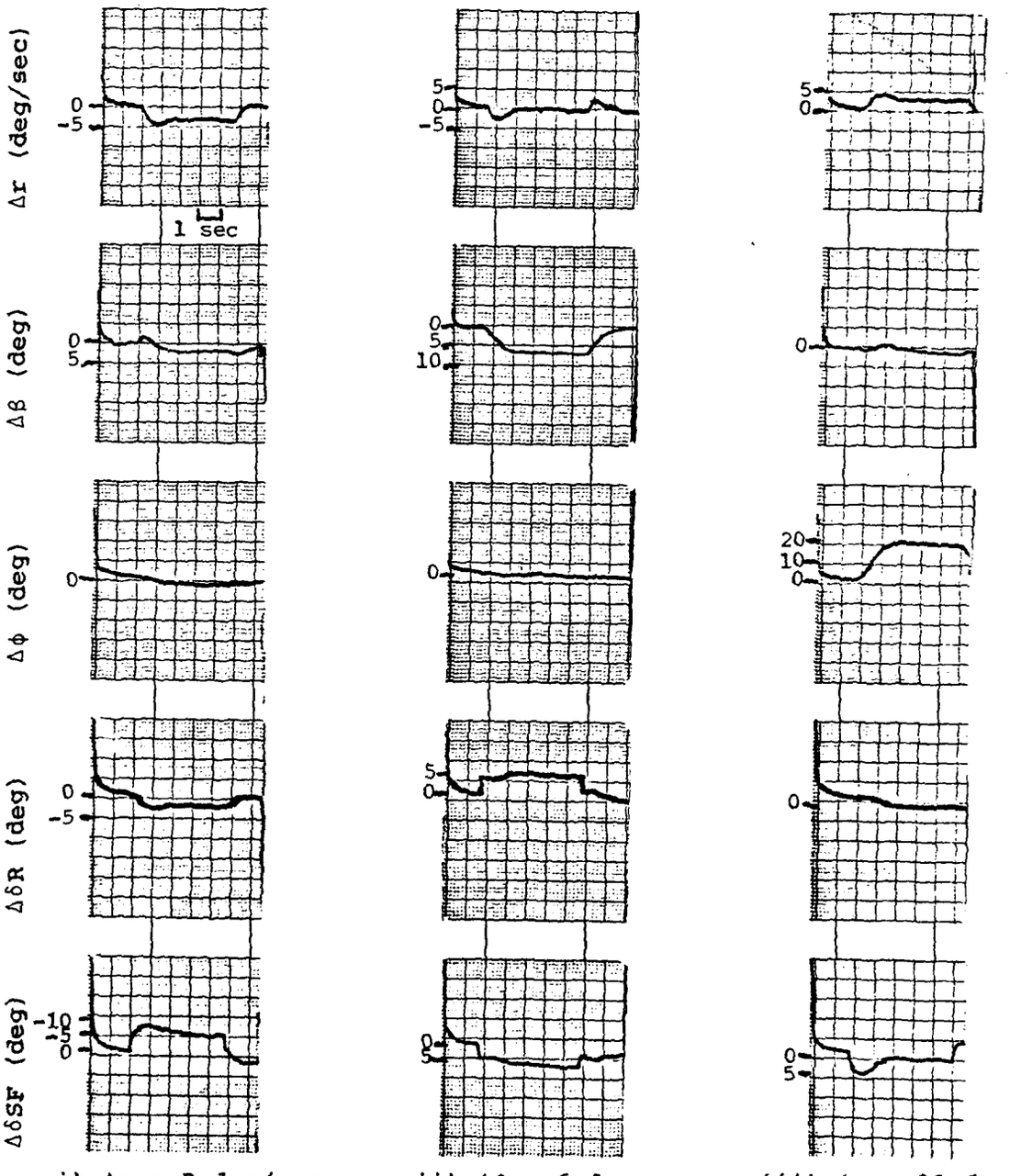

i) Δr_c=-3 deg/sec ii) $\Delta \beta_c$= 6 deg iii) $\Delta \phi_c$= 20 deg, Δr_c= 3.6 deg/sec

f) Mode 08

Figure 4-9. Continued

4-28

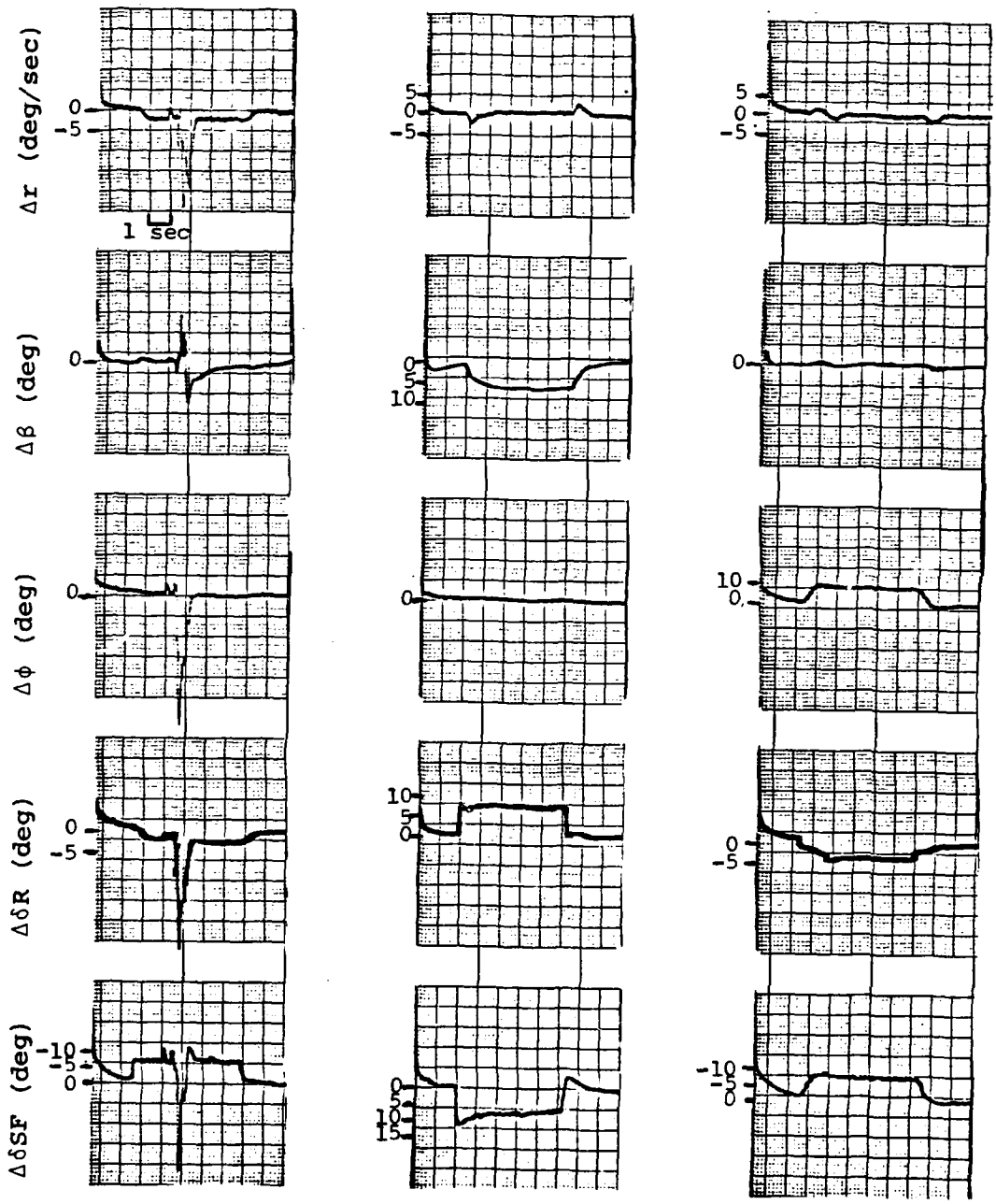

g) Mode 11

Figure 4-9. Continued.

Also, command authority at 105 KIAS with the thumb lever was reduced 40 percent to 8.07 deg, or a lateral velocity of 14.9 KIAS.

A further measure was undertaken in an effort to reduce the noise in the FBW system. Low-pass filters were incorporated with both rate gyros (yaw rate and roll rate). Such a filter already existed in the sideslip feedback circuit. (See Appendix D for all VRA filter values.) The maximum command signal from the thumb controller also was increased from 2.88 volts to 16.14 volts.

The other profile used to evaluate the advanced control maneuvers involved the acquiring of stationary ground targets. The task was severely limited by the necessity that the aircraft remain within the FRL telemetry cone (extending from the antenna atop the FRL to no farther than about 5 miles east and 2000 feet AGL) for data acquisition. Just as limiting was the rudimentary tracking sight installed for the tests. Aligned with the fuselage, the boresight-like device consisted of a small circle drawn on windscreen in front of the test pilot and a "pipper" mounted just above the aircraft's nose. The task began with the pilot acquiring and momentarily tracking--using the flat turn--two prominent landmarks which were located about 5 miles away and 2 miles apart. As the VRA approached the FRL the pilot attempted to perform the same task--this time alternating between two ground targets (about 40 ft apart) next to the building--by using the side-step maneuver.

Pilot A performed the task with Modes 01 and 02 and still commented on the noticeable chatter of Mode 01. As a balance between ride quality and task performance, he settled for a time constant of 0.181 sec in the thumb lever's low-pass filter. Pilot A went on to say that the increased breakout force and positive detent of the thumb switch was helpful.

Pilot B evaluated Modes 02 and 08 in the target acquisition task. The

Mode 08 sidestep was smooth, but because the adverse yaw rate transient required full pedal deflection to maintain heading, he deemed the mode, "not useful". The Mode 02 flat turn was better damped and more precise than that of Mode 08. Less of a yaw rate transient existed in the Mode 02 sidestep, but still, target acquisition was hampered by the pilot's head displacement, caused by the lateral acceleration transient.

Nevertheless, the ability to translate laterally could prove useful for last-second acquisition and tracking. Likewise, the flat turn was beneficial in enabling the pilot to make small heading changes and to constantly maintain sight of both targets. Representative telemetry strip chart recordings of the task are located in Figures 4-10 and 4-11. Yaw rate (which contains a large amount of noise), sideslip, roll angle, rudder deflection, and side force panel deflection are plotted.

Figure 4-10 depicts Mode 01 in the latter part of the long-range acquisition task and then the short-range task. It is seen that the pilot uses the roll-to-turn method for the large heading changes necessary in acquiring a new target at a distance. Since this mode does not incorporate a coordinated turn "interconnect", the pilot commands roll rate with the lateral stick and coordinates the turn with yaw rate through the foot pedals. The figure shows a 25-deg roll angle properly coordinated with about 4.5 deg of yaw rate. The flat turn is only used for fine tuning heading adjustments on the target. The time response concludes showing the sidestep maneuver being used four times in the close-in target tracking. Sometimes full authority is commanded, in which case relatively large control deflections result.

The entire target acquisition profile (100 sec) employing Mode 02 is included in Figure 4-11. The task is accomplished in a manner similar to that used with Mode 01. The pilot coordinates a banked turn himself to acquire the new target and then uses the flat turn for precise tracking.

For the final 21 seconds, a series of lateral translations occurs in the short-range tracking task.

Thus concludes the final phase of the direct side force Micro-DFCS study. In addition to remarks contained in this chapter, Chapter 5 includes further results gained from the flight testing along with concluding remarks concerning the entire investigation.

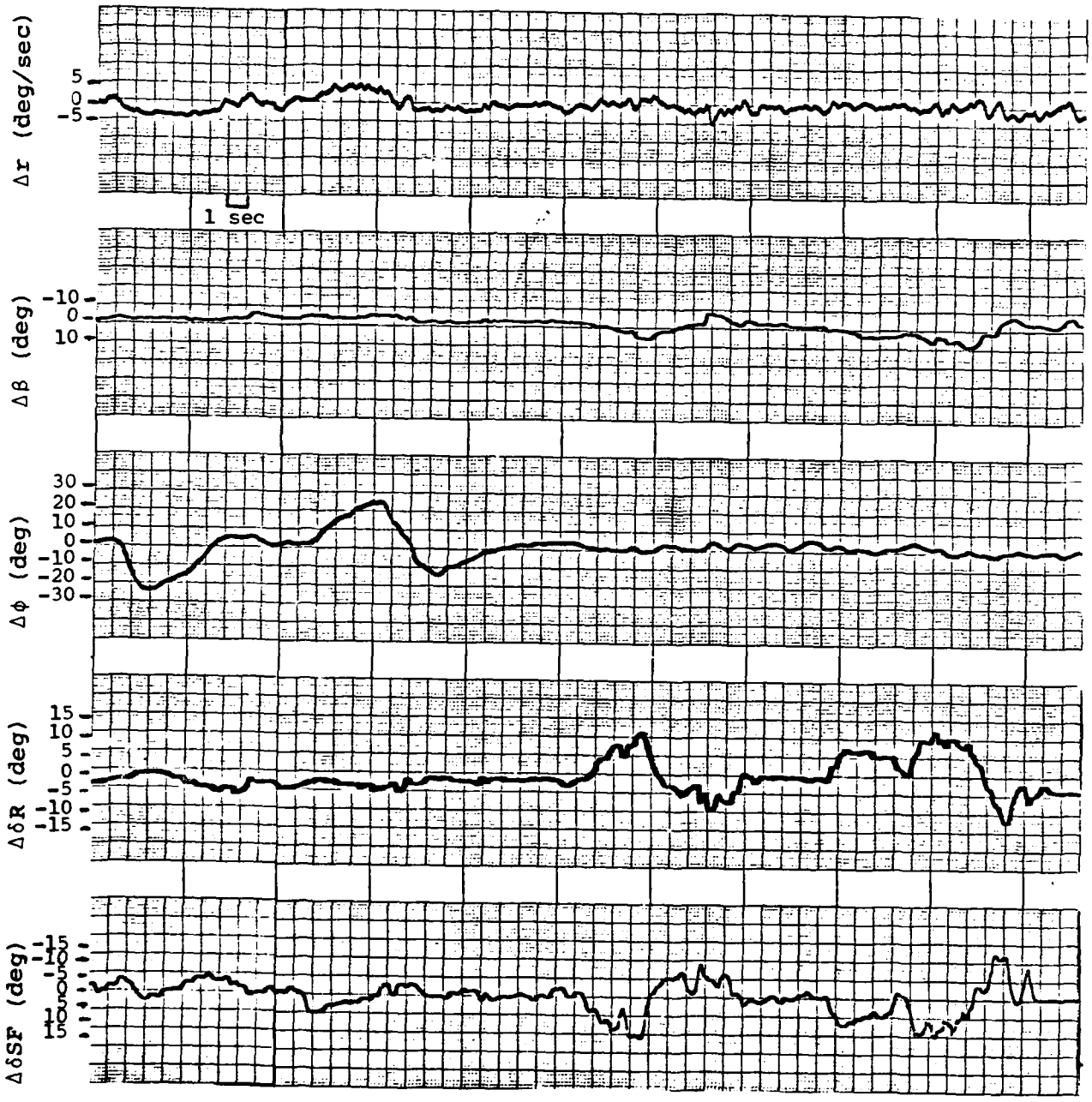

Figure 4-10. Target Acquisition Task Telemetry - Mode 01.

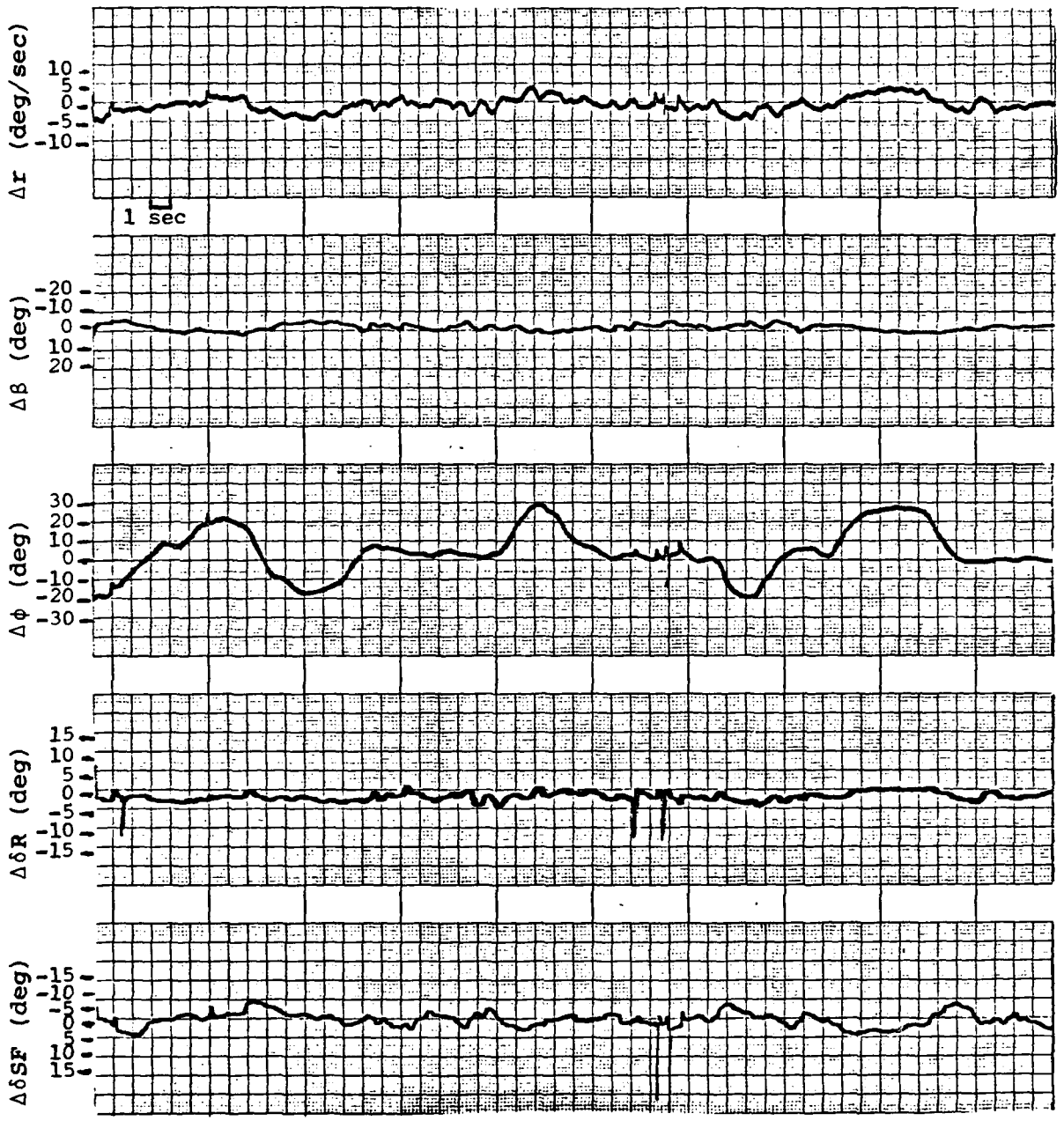

Figure 4-11. Target Acquisition Task Telemetry - Mode 02.

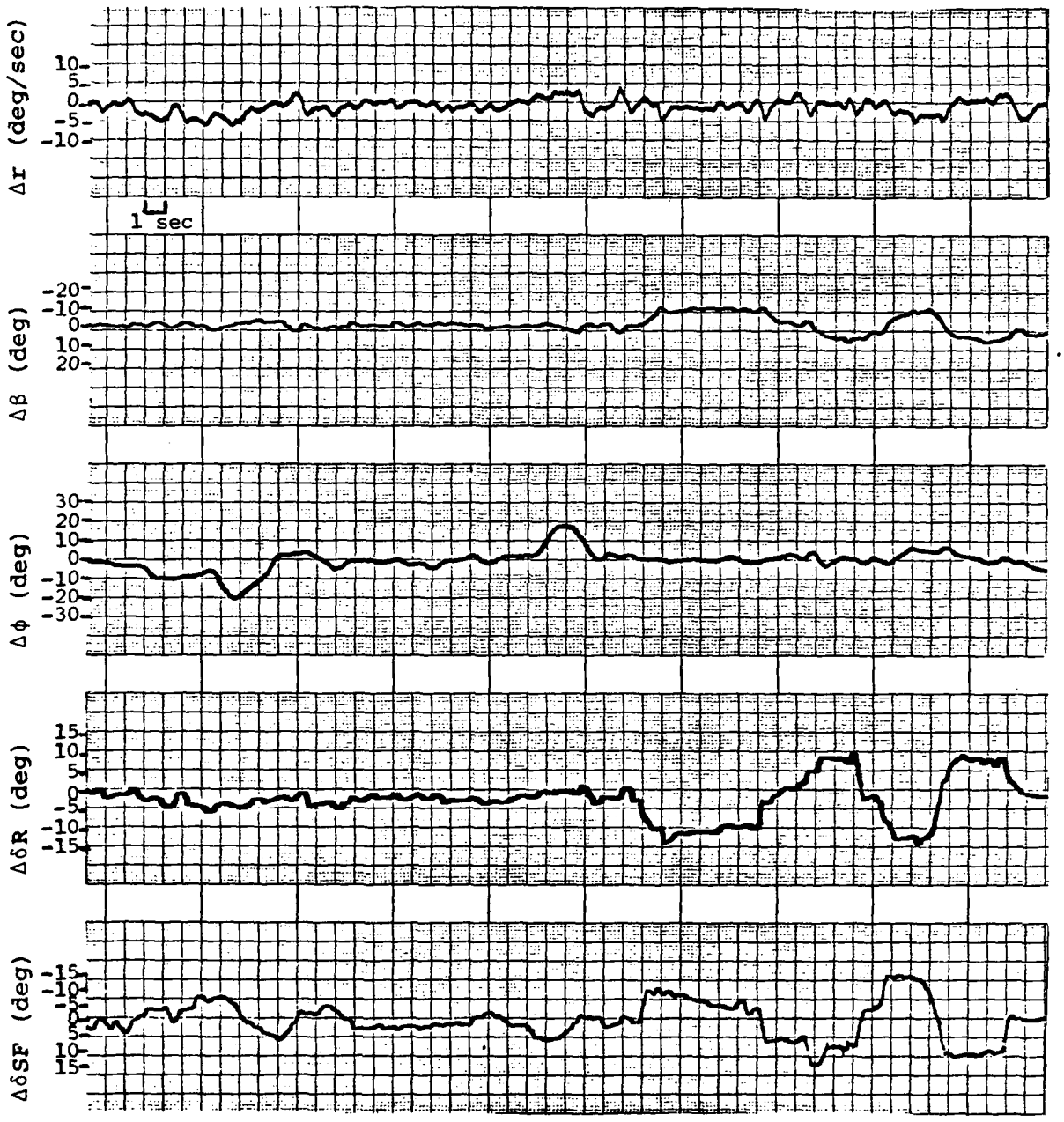

Figure 4-11. Continued.

5. CONCLUSION

This investigation has been concerned with the implementation of a microprocessor-based flight control system aboard an aircraft with a direct side force capability. Advanced maneuvers were developed using Equivalent Stability Derivative Matching and then implemented as a digital command augmentation system in flight. Numerous conclusions can be drawn as a result of the research conducted.

- In developing a CAS, a steady-state response analysis is beneficial and is independent of the control law selected. Care must be used when trying to command a motion whose integral is a state because of the resulting singularity; in this case, a quasi-steady equilibrium analysis must be performed.

- In theory, ESD Matching is a simple but effective control design technique, when dealing with an aircraft that has independent control of all rigid-body degrees of freedom. However, the selection of the model to be followed may be at least as difficult as the determination of weighting matrices associated with a linear-quadratic regulator.

- The flexibility of a digital flight control system based on microprocessor technology was proven. Additions and alterations to the control system were accomplished with simple software modifications, and further time savings, if needed, could still be achieved.

- Any ground test designed for the verification of a control law should include disturbance inputs to more closely reflect the flight test environment. As a corollary, some of the resulting closed-loop stability derivatives, such as N_β, must be stabilizing.

As far as the controller-to-command pairings are concerned, the baseline configuration of rudder pedals to yaw rate, lateral stick to roll, and thumb lever to sideslip, provided the best pilot ratings. The ratings

for the other configurations suffered as a result of their novelty to the pilots. It remains to be seen what type of cockpit manipulator is best for direct side force control, or whether the DSF capability should be blended with the conventional controls. Apparently the answer is task-dependent.

Finally, conclusions concerning each of the three advanced maneuvers designed--flat turn, lateral translation, and roll mode--are presented. (Fuselage pointing, another maneuver available with direct side force, was not tested in flight, but it could prove beneficial since it involves no lateral acceleration.) No flight tests were conducted for the evaluation of air-to-air tracking or the tracking of moving ground targets.

- The inherent difficulty of the flat turn is the steady-state lateral acceleration. This is particularly troublesome during turns that can easily be accomplished conventionally with the aid of bank for coordination. In a maneuver like dive-bombing, where a turn involving roll contributes to the tracking error because of the "pendulum effect", the flat turn has shown great potential. A lack of facilities and equipment prohibited the testing of these types of sophisticated tasks. The mode did prove the importance of flight testing. Unlike studies employing only a fixed-base simulator that concluded the flat turn mode should achieve a lateral acceleration of at least one g (Ref. 6, 9-10), VRA pilots noted that an acceleration of more than about 0.5 g would be counterproductive. It should be noted that human factors improvements over the present test conditions could alter this conclusion. For example, the pilot would be less susceptible to the effects of lateral acceleration if equipped with a contoured seat (to include side-body and head restraints), and a lightweight helmet such as that being developed for military pilots.

- The lateral translation probably showed the most promise of any of the modes tested. It is extremely effective in negating crosswinds, thus alleviating the need for using a crab or wing-low maneuver on final approach and in the flare. The sidestep also displayed promise for making last-second tracking corrections, as in a strafing pass. The limitations of the maneuver are twofold. There is a

tradeoff between speed of response and transient acceleration. It is difficult, however, to express the maximum initial acceleration tolerable because of the inclusion of a pre-filter in the command signal during flight testing. The other limitation of the sidestep is the limited steady-state velocity. At 105 KIAS, the maximum lateral velocity available was 24.3 KIAS, and as such, it was not very noticeable to the pilot until near the "target". Transient lateral acceleration is also affected by this command authority. No air-to-ground task involving moving targets, which is suited to the sidestep maneuver, was attempted.

- Two variations involving the command of roll were tested--a pure roll rate angle, and a roll angle coordinated with yaw rate. The only advantage of commanding roll angle, instead of roll rate, was that the aircraft roll attitude was maintained during wind gusts. The coordinated roll was advantageous because it required only one command input as opposed to two during a conventional turn. Both roll angle variations were degraded by the necessity of displacing the stick laterally for as long as the bank was to be held.

The microcomputer provided a tremendous amount of flexibility to the flight testing of various lateral-directional maneuvers involving the use of side force. So much can be gained by this type of research by both the civilian and military sectors that work must be continued. More sophisticated tasks should be undertaken--this will necessitate the use of better equipment and, probably, a more complex control law.

APPENDIX A

VARIABLE-RESPONSE RESEARCH AIRCRAFT

The Variable-Response Research Aircraft (VRA) is a modified Navion aircraft. It is based at the Flight Research Laboratory (FRL) located on the James Forrestal Campus of Princeton University. The aircraft has been involved in many flight experiments concerning flying qualities, control systems, and human factors.

The main feature of the VRA is the capability to produce independent motion about all six rigid-body degrees-of-freedom. This is accomplished by the inclusion of direct lift flaps and direct side force panels. Each of the two side force panels ia a NACA 0012 airfoil with a surface area of 16.0 square feet. The panels are mounted on the wing as shown in Figure A-1.

The VRA is further modified with hydraulic servos, originally used on the B-58 bomber, to drive the control surfaces. The lateral-directional actuator dynamics are depicted in Table A-1.

Sensors available during flight testing include angular rate gyros and linear accelerometers for all three axes, a vertical gyro, dual angle-of-attack and sideslip-angle vanes, radar altimeter, indicated airspeed, control surface positions, and cockpit control positions. This data can be used for system feedback or telemetered to the FRL ground station.

For safety and efficiency, a two-man crew operates the VRA during flight testing. The cockpit layout is shown in Figure A-2. The safety pilot flys the conventional mechanical system in the left seat and the evaluation pilot operates the fly-by-wire (FBW) system in the right seat.

The safety pilot is responsible for setting up and monitoring the experiment. When the situation dictates, he can disengage the FBW system and regain mechanical control of the aircraft. On the other hand, the evaluation pilot controls the aircraft during the microprocessor-based digital flight control system (Micro-DFCS) operation. His side of the cockpit is adapted for the experiment and includes a center control stick, thumb switches for trim and direct force control, rudder pedals, and sideslip and side force panel position meters in addition to conventional instrumentation. The interface of the two pilots and the Micro-DFCS with the VRA is described in Figure A-3.

Table A-1. VRA Lateral-Directional Actuators

CONTROL	DISPLACEMENT LIMIT (deg)	RATE LIMIT (deg/sec)	BANDWITH (Hz) FLAT RESPONSE	6db ATTENUATION
Rudder	15	70	5	10
Side Force	35	60	2	3
Aileron	30	70	5	10

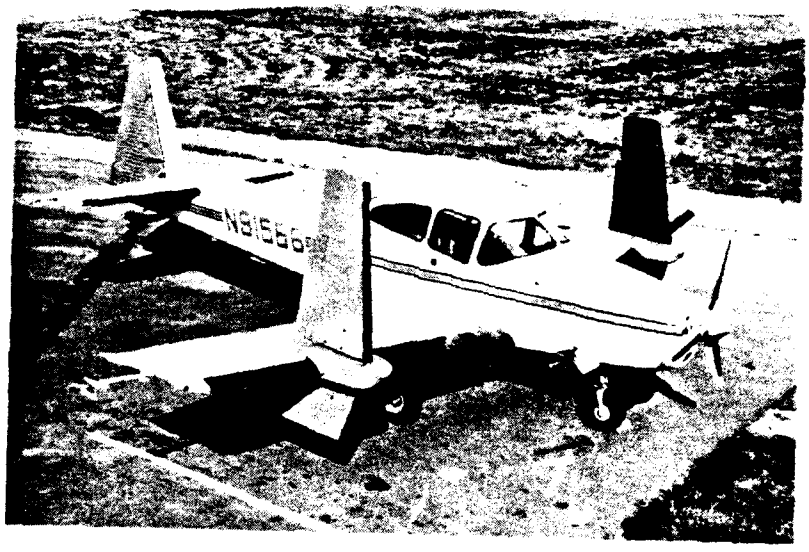

a) Side View

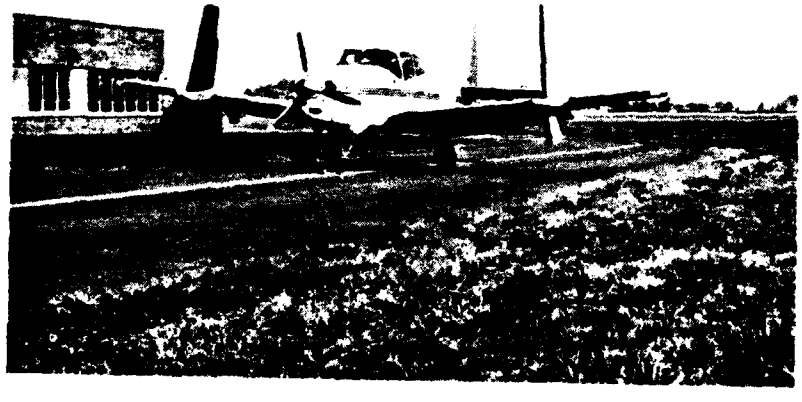

b) Front View

Figure A-1. Variable-Response Research Aircraft.

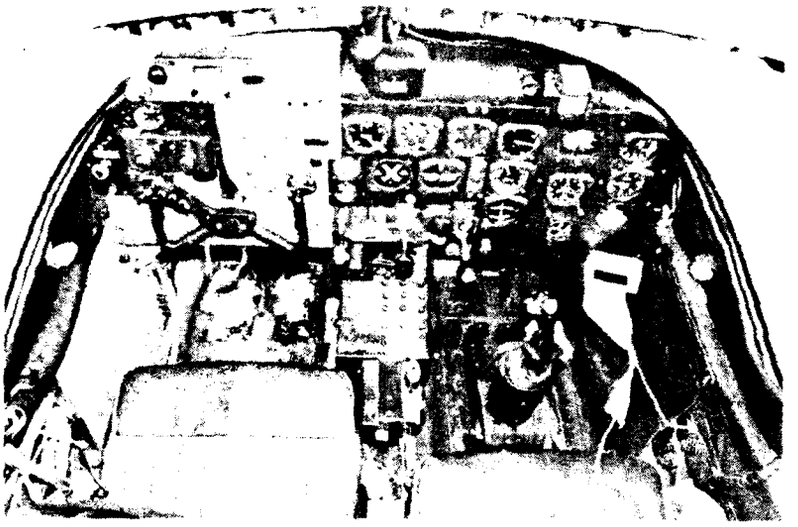

Figure A-2. Cockpit Layout.

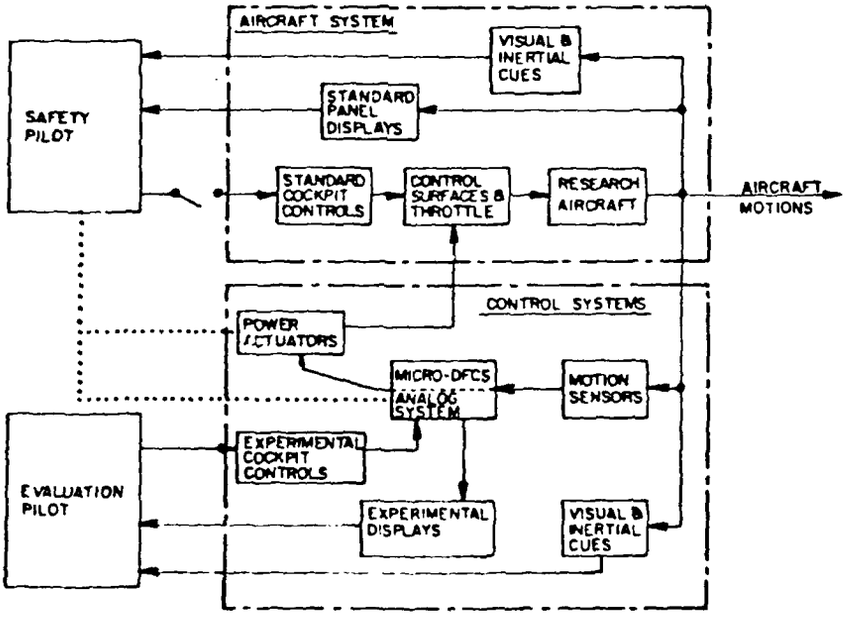

Figure A-3. Systems Interaction with Micro-DFCS.

APPENDIX B

COMPUTER PROGRAMS

The FRL microprocessor laboratory was well-equipped for the writing, debugging, and implementation of computer software required in this study. A description of those items pictured in Figure B-1 (from left to right) follows.

- Oscilloscope--analyzes operation time of microcomputer program when connected to output ports
- Keyboard-printer terminal--enables user to write APL functions and also obtain hard copies of computer programs and output
- Telephone couplers (above terminal)--enables communication between the FRL terminals and the IBM 3033 computer located on the main campus
- FCCU--see Section 4.1
- HT/4 CDU (on FCCU)--see Appendix C
- EP-2A-79 PROM programmer (in front of FCCU)--allows the transfer of memory stored in the microcomputer to an EPROM; in this case, 2716-type 2K (2048 bytes) EPROMs were used, which could be "burned", or altered, several times by the programmer
- Housing Unit--see Appendix C
- Switching box--user-selectable to enable the communication between any of the following: 3033 computer, CRT terminal, and microcomputer
- Keyboard CRT terminal--enables user to communicate with 3033 computer or Z-80A microprocessor

The software necessary for this research is now described.

B.1 APL FUNCTIONS

Most of the work performed in Chapter 2 was accomplished using the APL computer language (APL stands for A Programming Language). APL is ideally suited to the discrete time control equations because of its orientation toward matrix algebra. The APL functions (or programs) devised for this study were stored in the workspace entitled SLG. In addition, the public libraries EIGVAL and LINPLOT were used. The functions contained in SLG are presented in Figure B-2, and briefly described below.

CONTIN---calculates the quasi-steady equilibrium response to command based on continuous time dynamics for comparison with results using DISCRE

DISCRE---calculates the quasi-steady equilibrium response to command based on discrete time dynamics (Eqs. 24 and 25). Results are printed in one-second increments.

ESD------calculates C_B and C_F in the ESD Matching control law using Equations 34 and 35

FCLOOP---calculates F_{CL}, given Φ_{CL}, using Equation 46

GAMMA----calculates Γ using either Equation 11 or 15.

IDENT----creates an identity matrix of size n x n

NRCON----calculates the nonsingular steady-state response to command based on continuous time dynamics for comparison with results using NRDIS

NRDIS----calculates the nonsingular steady-state response to command based on discrete time dynamics (Eq. 22); results are displayed in one-second intervals

PHICL----calculates Φ_{CL} using Equation 47 and then displays F_{CL}; the associated eigenvalues are computed using EIGVAL

STMDYN---calculates Φ using Equation 10

SUDOINV--calculates the pseudoinverse of matrix A using Equation 36

TIMESIM--calculates, and displays in a tabular form, the closed-loop time response of the ESD Matching control law (Eq.38); furthermore, information is stored in matrices for subsequent plotting using LINPLOT

An example of an iteration for selecting a mode based on ESD Matching is presented in Figure B-3. First, a model F matrix (FF2A) is devised based on the method described in Section 2.4-2, and its eigenvalues computed. The determinant is also found to see if a singularity exists. Next, as determined by the command vector choice, the matrix A_M is selected, and the model G matrix (GG2A) computed. H_x and H_u are set so that the pilot's inputs are represented. F105 and G105 contain the VRA stability and control dynamics, respectively, at 105 KIAS. The feedback (CB) and feedforward (CF) matrices of the control law can then be computed. The resulting closed-loop F matrix (FCL), and its eigenvalues, are calculated to ensure a match with the model. The closed-loop steady-state response is computed for each of the three pilot commands to verify the appropriate output. The calculations based on continuous-time and discrete-time dynamics are in agreement. Finally, a time response simulation for each command (only one is shown in Fig. B-3) is generated and stored for subsequent computer plotting on a graphics terminal.

B.2 MICROCOMPUTER PROGRAMS

CAS-6 was written in Assembly Language. The mnemonics then were assembled into machine code for use by the microprocessor. CAS-6 is 6K (6144) bytes long; a smaller assembly language program (150 bytes), named CKSUM, is presented as an example of the program (Fig. B-4).

CKSUM totals (in hexadecimal) the memory contents between the locations MAIN and PEND, inclusive. In CAS-6 this value is used to ensure that no memory is altered during program execution. The first column of the compiled version shown is the memory addresses of the program. The hexadecimal machine code found at these locations is listed in the following three columns. The next column denotes the decimal line number, and the remaining portion of the program is what was typed at the computer terminal. Those lines that begin with a semi-colon are for documentation purposes--an important consideration in microcomputer programs, especially one as large as CAS-6.

Figure B-1. FRL Computer Room.

```
      ∇CONTIN[□]∇
      ∇ CONTIN;TIME;NEW;XSING;ΔF;ΔG;ΔHX;L;NN;NEG;HX1;Z
[1]   ⍝GIVES QUASI-STEADY CONTINUOUS RESPONSE
[2]   ⍝SET BDOT=1 IFF CONTROLLING SIDESLIP RATE
[3]   ⍝INSURE SINGULARITY(IES) IS (ARE)AT BOTTOM OF ΔX
[4]    NN←((⍴,F)×0.5)-1+BDOT
[5]    NEG←¯1-BDOT
[6]    ΔF←(NN,NN)↑F
[7]    ΔG←(NN,3)↑G
[8]    L←(NN,NEG)↑F
[9]    NEW←(NN+3,1)⍴0
[10]   TIME←¯1
[11]   ΔHX←(3,NN)↑HX
[12]   HX1←(3,NEG)↑HX
[13]  LOOP:TIME←TIME+1
[14]   XSING←TIME×(NEG,1)↑DELT
[15]   SMAT←⌸(ΔF,ΔG),[1] ΔHX,HU
[16]   Z←(-L+.×XSING),[1] DELT-HX1+.×XSING
[17]   NEW←SMAT+.×Z
[18]   TIME
[19]   (NN,1)↑NEW
[20]   XSING
[21]   ¯3 1 ↑NEW
[22]   →(DELT[1;1]=1)/0
[23]   →(DELT[2;1]=1)/0
[24]   →(TIME<5)/LOOP
       ∇
```

Figure B-2. APL Functions.

```
      ∇DISCRE[[]]∇
      ∇ DISCRE;NN;NEG;ΔSTM;STM4;LAM;ΔGAM;GAM4;DELX;DELU;I;K;TIME;H
[1]   ⍝GIVES QUASI-STEADY EQUILIBRIUM RESPONSE                    ;OMEGA
[2]   ⍝SET BDOT =1 IFF CONTROLLING SIDESLIP RATE
[3]   ⍝INSURE SINGULARITY(IES) IS(ARE) AT BOTTOM OF ΔX
[4]   NN←((⍴,F)×0.5)-1+BDOT
[5]   NEG←¯1-BDOT
[6]   STM←0.1 STMDYN F
[7]   GAMMA STM
[8]   ΔSTM←(NN,NN)↑STM
[9]   STM4←(NEG,NN-NEG)↑STM
[10]  LAM←(NN,NEG)↑STM
[11]  ΔGAM←(NN,3)↑GAM
[12]  GAM4←(NEG,3)↑GAM
[13]  DELX←((NN-NEG),1)⍴0
[14]  DELU←3 1⍴0
[15]  I←(⍳NN)∘.=⍳NN
[16]  K←¯1
[17]  TIME←0
[18]  ΔHX←(3,NN)↑HX
[19]  OMEGA←(3,NEG)↑HX
[20]  LOOP:K←K+1
[21]  →(K≠10)/LT10
[22]  K←0
[23]  TIME←TIME+1
[24]  LT10:XSING←(STM4+.×DELX)+GAM4+.×DELU
[25]  SMAT←⌸((ΔSTM-I),ΔGAM),[1] ΔHX,HU
[26]  Z←(-LAM+.×XSING),[1] DELY-OMEGA+.×XSING
[27]  NEW←SMAT+.×Z
[28]  DELX←((NN,1)↑NEW),[1] XSING
[29]  DELU←¯3 1↑NEW
[30]  →(K≠0)/LOOP
[31]  TIME
[32]  DELX
[33]  DELU
[34]  →(DELY[1;1]=1)/0
[35]  →(DELY[2;1]=1)/0
[36]  →(TIME<5)/LOOP
      ∇
```

Figure B-2. Continued

```
     ∇ESD[⎕]∇
     ∇ R ESD A;STMV;STMM;GA[illegible];GAMV;F1;G1
[1]   ⍝CALCULATES GAINS--CB AND CF--FOR EQUIVALENT STA[illegible]
[2]   ⍝     DERIVITIVE MATCHING
[3]   ⍝A IS F(MODEL) AND B IS G(MODEL)
[4]   ⍝NOTE:  INITIALIZE F ,G FOR V[illegible]
[5]    STMV←DT STMDYN F
[6]    GAMMA STMV
[7]    GAMV←GAM
[8]    STMM←DT STMDYN A
[9]    G1←G
[10]   F1←F
[11]   F←A
[12]   G←B
[13]   GAMMA STMM
[14]   GAMM←GAM
[15]   G←G1
[16]   F←F1
[17]   CB←(SUDOINV GAMV)+.×STMM-STMV
[18]   CF←(SUDOINV GAMV)+.×GAMM
[19]   LF
[20]   'CB'
[21]   CB
[22]   LF
[23]   'CF'
[24]   CF
[25]   LF
     ∇


     ∇FCLOOP[⎕]∇
     ∇ FCLOOP;SM;R;FACTOR;INDEX;I;IFCL
[1]   ⍝ CALCULATES C,L, F MATRIX FOR STMCL GIVEN
[2]    R←(⍴,STMCL)*0.5
[3]    I←(⍳R)∘.=⍳R
[4]    N←0
[5]    FCL←I-I
[6]    STMI←I
[7]   LO:N←N+1
[8]    STMI←(STMCL-I)+.×STMI
[9]    FACTOR←((¯1)×N+1)×STMI
[10]   IFCL←FCL+FACTOR÷N
[11]   INDEX←(+/|,FCL-IFCL)÷R*2
[12]   FCL←IFCL
[13]   →(N=200)/STP
[14]   →(INDEX>0.00001)/LO
[15]   →[illegible]
[16]  [illegible] NOT C[illegible] [illegible]RIX IN 200 ITERA[illegible]'
[1[illegible]] [illegible]
```

Figure B-2. Continued

```
     ∇GAMMA[⎕]∇
     ∇ GAMMA STM;N;[illegible]TOR;I[illegible];IGAM;R
   ⍝CALCULATES GAMMA [illegible]
   ⍝NOTE; MUST DE[illegible] F,G, [illegible] FUN STMDYN FIRST
     →((|DET F)<0.00[illegible]
   ⍝F NONSINGULAR
     GAM←(STM-I)+.×(⌹F)+.×G
     →0
   ⍝F SINGULAR
    SING:N←1
     R←(⍴,F)*0.5
     FACTOR←IGAM←DT×I
    LO:N←N+1
     FACTOR←(¯1)×FACTOR+.×F×DT÷N
     IGAM←IGAM+FACTOR
     INDEX←(+/|,FACTOR)÷R*2
     →(INDEX>EPS)/LO
     GAM←STM+.×IGAM+.×G
     ∇


     ∇IDENT[⎕]∇
     ∇ I←IDENT N
   ⍝  MAKES IDENTITY MATRIX OF SIZE N
     I←⍳N
     I←I∘.=I
     ∇


     ∇NRCON[⎕]∇
     ∇ NRCON;N;YY
   ⍝GIVES CONTINUOUS S.S. RESPONSE W/ NO 'R'
     N←(⍴,F)*0.5
     SMAT←⌹((F,G),[1] HX,HU)
     YY←((N,1)⍴0),[1] DELY
     SMAT+.×YY
     ∇


     ∇NRDIS[⎕]∇
     ∇ NRDIS;N;YY
   ⍝GIVES STEADY-STATE RESPONSE WHEN THERE'S NO 'R' COMMAND
     N←(⍴,F)*0.5
     STM←0.1 STMDYN F
     GAMMA STM
     [illegible]
     [illegible]
     [illegible]
     [illegible]
```

Figure B-2. Continued

```
      ∇PHICL[□]∇
      ∇ F,PHICL;GAM;PHI
[1]   ⍝CALCULATES CLOSED-LOOP STM AND F MATRICES
[2]   PHI←DT STMDYN F
[3]   GAM←A PHI
[4]   CALC:
[5]   STMCL←PHI+.×GAM+.×CP
[6]   LF
[7]   FCLOOP
[8]   'FCL IS:'
[9]   LF
[10]  FCL
[11]  LF
[12]  'EIGVALS ARE:'
[13]  LF
[14]  0.01 EIGVAL FCL
[15]  LF
      ∇
```

```
      ∇STMDYN[□]∇
      ∇ PHI←DT STMDYN A;F;N;FACTOR;INDEX
[1]   ⍝ CALCULATES TRANSITION MATRIX
[2]   R←(⍴,A)×0.5
[3]   I←(⍳R)∘.=⍳R
[4]   N←0
[5]   PHI←I
[6]   FACTOR←I
[7]   L0:N←N+1
[8]   FACTOR←FACTOR+.×A×DT÷N
[9]   PHI←PHI+FACTOR
[10]  INDEX←(+/|,FACTOR)÷R×2
[11]  →(INDEX>EPS)/L0
      ∇
```

```
      ∇SUDOINV[□]∇
      ∇ R←SUDOINV A
[1]   ⍝CALCULATES PSEUDO-INVERSE OF A
[2]   R←(⌹(⍉A)+.×A)+.×⍉A
      ∇
```

Figure B-2. Continued

```
[1]  ⍝***RUN ESD FIRST***
[2]  ⍝INITIALIZE ΔYD (3 X 1)
[3]  ⍝⍝⍝⍝⍝⍝⍝⍝⍝⍝INITIALIZE⍝⍝⍝⍝⍝⍝⍝⍝⍝⍝
[4]   R←(⍴,F)×0.5
[5]   T←TIM←0
[6]   DELX←((R+1),1)⍴0
[7]   ΔX←(R,1)⍴0
[8]   DELU←ΔU← 3 1 ⍴0
[9]   STM←DT STMDYN F
[10]  GAMMA STM
[11]  'PRINTED TABLE??'
[12] ⍝N FOR NO; Y FOR YES
[13]  →('N'=ANS←⍞)/LOOP
[14]  LF
[15]  LF
[16]  →(R=5)/FIFTH
[17]  ' T    ΔR         ΔE         ΔF         Δϕ         ΔNT        ΔRD
[18]  LINE1                                              ΔSF        ΔAL'
[19]  →LOOP
[20] FIFTH:' T     Δλ         ΔR         ΔΘ         ΔF         Δϕ
[21]  LINE2                    ΔNT        ΔRD        ΔSF        ΔAL'
[22] ⍝⍝⍝⍝⍝⍝⍝⍝⍝⍝⍝⍝CONTROL LAW⍝⍝⍝⍝⍝⍝⍝⍝⍝⍝⍝⍝⍝
[23] LOOP:ΔX←(STM+.×ΔX)+GAM+.×ΔU
[24]  ΔU←(CF+.×ΔYD)+CB+.×ΔX
[25]  ΔAT←((F[(R-2);(R-2)]×ΔX[(R-2);])+G[(R-2);]+.×ΔU)'
[26]  ΔNT←ΔAT÷F[(R-2);R]×57.3
[27] ⍝                              +((F[(R-2);(R-3)]+1)×ΔX[(R-3);])
[28] ⍝STORE FOR PLOTTING
[29]  ΔXTEMP←ΔX[1;]
[30]  →(R≠5)/SKIP
[31] ⍝STORING AND PRINTING FLIGHT ANGLE RATHER THAN YAW ANGLE
[32]  ΔX[1;]←ΔX[1;]+ΔX[3;]
[33] SKIP:DELX←DELX,ΔX,[1] ΔNT
[34]  DELU←DELU,ΔU
[35]  T←T,TIM
[36]  →(ANS='N')/NEXT
[37] ⍝
[38] ⍝OUTPUT
[39]  TIM
[40]  5↑⍉ΔX,[1] ΔNT,[1] ΔU
[41] NEXT:TIM←TIM+DT
[42]  ΔX[1;]←ΔXTEMP
[43]  →(TIM≤TEND)/LOOP
[44] ⍝⍝⍝⍝⍝⍝⍝⍝⍝FINALIZE⍝⍝⍝⍝⍝⍝⍝⍝⍝⍝⍝
[45]  T←1↓T
[46]  DELX← 0 1 ↓DELX
[47]  DELU← 0 1 ↓DELU
[48]  LF
[49]  SPACE,'DONE'
      ∇
```

Figure B-2. Continued.

B-3

```
apl


      V S  A F L

CLEAR WS
      )LOAD SLG
SAVED 22:38:54 09/03/80


      FF2A
 ¯5      5.3    0      0
  0     ¯2      0      0
  0      0     ¯5    ¯12.7
  0      0      1      0
      .01 EIGVAL FF2A
 ¯5        0
 ¯2.5      2.5397
 ¯2.5     ¯2.5397
 ¯2        0
      DET FF2A
1020
      CONST2
 1      0      0.181
 0      1      0
 0      0      0
 0      0      1
      GG2A←¯FF2A+.×CONST2
      GG2A
   5       ¯5.3      0.905
   0        2         0
   0        0        12.7
   0        0         0
      F←FF2A
      G←GG2A
      HX←3 4⍴0
      HU←IDENT 3
      HX
0 0 0 0
0 0 0 0
0 0 0 0
      HU
1 0 0
0 1 0
0 0 1
```

Figure B-3. APL Example.

```
      F105
 ¯0.75     5.3      ¯0.26      0
 ¯1       ¯0.4      0          0.181
  1.16    ¯11.5     ¯6.5       0
  0        0        1          0
      G105
 ¯6.1       2.1      ¯0.222
  0.0935    0.38      0
  0.6       0        21
  0         0         0
```

```
      F←F105
      G←G105
      GG2A ESD FF2A
```

```
CE
   1.1714    ¯0.91858   ¯0.037601  ¯0.10723
   1.8155    ¯3.0628    ¯0.012772  ¯0.44618
 ¯0.078332    0.5083     0.026477  ¯0.63041

CF
  ¯0.4470.     2.0364     ¯0.125
   0.63784     3.8404      0.12255
   0.0023967   0.0073809   0.63517
```

```
      FHICL

FCL IS:

   ¯4.9998          5.2987          ¯0.000071445   ¯0.000075633
   ¯0.000051337     ¯1.9997          0.00017527     0.00016496
    0.0033188       ¯0.015895       ¯5.0111        ¯12.712
    0.0047998       ¯0.023905        0.98358        ¯0.015127

EIGVALS ARE:

 ¯4.9997   0
 ¯2.5131   2.5027
 ¯2.5131  ¯2.5027
 ¯1.9998   0
```

Figure B-3. Continued

```
      DELT←3 1⍟1 0 0
      NRDIS
 1.0000E0
 2.4315E¯17
 6.7598E¯20
¯5.1491E¯19
 1.0000E0
 1.6170E¯17
 3.8563E¯19
      NRCON
 1.0000E0
¯1.5679E¯16
 0.0000E0
 0.0000E0
 1.0000E0
 0.0000E0
 0.0000E0
      DELT←3 1⍟0 1 0
      NRDIS
¯2.8106E¯16
 1.0000E0
¯3.7980E¯19
 1.4062E¯18
¯1.2914E¯17
 1.0000E0
 1.1555E¯18
      NRCON
 1.2578E¯16
 1.0000E0
 0.0000E0
 0.0000E0
 0.0000E0
 1.0000E0
 0.0000E0
      DELT←3 1⍟0 0 1
      NRDIS
 1.8100E¯1
 5.4711E¯18
¯5.9996E¯17
 1.0000E0
 7.3725E¯18
¯8.9542E¯18
 1.0000E0
      NRCON
 1.8100E¯1
¯2.6948E¯17
 0.0000E0
 1.0000E0
 0.0000E0
 0.0000E0
 1.0000E0
```

Figure B-3. Continued

```
      TIMESIM 2
PRINTED TABLE??
Y
```

T	ΔR	ΔB	ΔF	ΔΦ	ΔNT	ΔRD	ΔSF	ΔAL
0	.00000	.00000	.00000	.00000	.00336	⁻.12500	.12255	.63517
0.1	.07122	⁻.00001	.97845	.05412	.00713	⁻.08416	.21522	.62138
0.2	.11441	.00000	1.47468	.17940	.00789	⁻.06567	.23137	.55216
0.3	.14061	.00002	1.63062	.33548	.00707	⁻.05759	.20726	.45585
0.4	.15651	.00003	1.56543	.49492	.00559	⁻.05362	.16578	.35237
0.5	.16615	.00004	1.37284	.64078	.00396	⁻.05073	.12063	.25457
0.6	.17201	.00005	1.12202	.76417	.00248	⁻.04768	.07939	.16969
0.7	.17556	.00005	.86051	.86189	.00127	⁻.04416	.04557	.10088
0.8	.17772	.00005	.61812	.93452	.00037	⁻.04031	.02018	.04851
0.9	.17903	.00005	.41101	.98486	⁻.00023	⁻.03638	.00274	.01119
1	.17983	.00005	.24551	1.01679	⁻.00059	⁻.03265	⁻.00794	⁻.01339
1.1	.18030	.00004	.12137	1.03447	⁻.00076	⁻.02931	⁻.01335	⁻.02786
1.2	.18059	.00004	.03440	1.04179	⁻.00079	⁻.02648	⁻.01496	⁻.03180
1.3	.18077	.00003	⁻.02158	1.04213	⁻.00073	⁻.02421	⁻.01407	⁻.03652
1.4	.18087	.00002	⁻.05333	1.03821	⁻.00063	⁻.02247	⁻.01171	⁻.03490
1.5	.18093	.00002	⁻.06732	1.03210	⁻.00051	⁻.02121	⁻.00868	⁻.03143
1.6	.18097	.00002	⁻.06920	1.02527	⁻.00039	⁻.02036	⁻.00574	⁻.02717
1.7	.18099	.00001	⁻.06356	1.01866	⁻.00027	⁻.01984	⁻.00361	⁻.02286
1.8	.18100	.00001	⁻.05393	1.01284	⁻.00018	⁻.01956	⁻.00010	⁻.01894
1.9	.18100	.00001	⁻.04283	1.00806	⁻.00011	⁻.01946	.00190	⁻.01543
2	.18100	.00001	⁻.03192	1.00438	⁻.00005	⁻.01947	.00341	⁻.01302

```
DONE
```

Figure B-3. Continued.

T CKSUM LISTING

```
0000                      ORG   0D000H         ;STARTING ADDRESS OF PROGRAM
D000            ;;;;;;;;;;;;;;;;;;;;;;;;;;;;;;;;;;;;;;;;;;;;;;;;;;;;;;;;;;;;;;;;
D000            ;    CKSUM ADDS THE CONTENTS OF THE MEMORY LOCATIONS
D000            ; BETWEEN TWO ADDRESSES (MAIN AND PEND), INCLUSIVE.
D000            ; AFTER ACCESSING THIS PROGRAM ('GO TO D000'), INPUT
D000            ; THE STARTING ADDRESS OF THE MEMORY BLOCK TO BE
D000            ; SUMMED; AFTER A CARRIAGE RETURN AND LINE FEED,
D000            ; INPUT THE ENDING ADDRESS OF THE BLOCK.  THE HEX SUM
D000            ; IS DISPLAYED, AFTER WHICH YOU ARE RETURNED TO THE
D000            ; SYSTEM MONITOR.
D000            ;           PROGRAMMER: S.L. GRUNWALD
D000            ;                        8/18/80
D000            ;;;;;;;;;;;;;;;;;;;;;;;;;;;;;;;;;;;;;;;;;;;;;;;;;;;;;;;;;;;;;;;;
D000            ;
003F            CHOR     EQU   003FH          ;CHANNEL 0 OUTPUT IN MONITOR
003B            CHOW     EQU   003BH          ;CHANNEL 0 INPUT IN MONITOR
D000            ;
D000            ;;;;;;;;;;;;;;;;;;;;;;;;;;;;;;;;;;;;;;;;;;;;;;;;;
D000            ; THE STARTING AND ENDING ADDRESSES ARE
D000            ;INPUT AND STORED
D000            ;;;;;;;;;;;;;;;;;;;;;;;;;;;;;;;;;;;;;;;;;;;;;;;;;
D000 0E 02               MVI   C,2            ;NUMBER OF ADDRESSES TO BE INPUT
D002 21 94 D0            LXI   H,MAIN+1       ;LOC. OF MSB OF STARTING ADDRESS
D005 06 02      AGAIN:   MVI   B,2            ;NUMBER OF BYTES TO BE INPUT
D007 CD 86 D0            CALL  CRLF           ;CARRIAGE RETURN, LINE FEED
D00A CD 74 D0   CONT:    CALL  READVAL        ;INPUT FIRST DIGIT
D00D 17                  RAL                  ;MULTIPLY
D00E 17                  RAL                  ;  INPUT
D00F 17                  RAL                  ;     BY
D010 17                  RAL                  ;       16
D011 E6 F0               ANI   0F0H           ;MASK OFF LSB
D013 77                  MOV   M,A            ;STORE IT IN MEMORY
D014 CD 74 D0            CALL  READVAL        ;INPUT SECOND DIGIT
D017 86                  ADD   M              ;ADD TO FIRST
D018 77                  MOV   M,A            ;  AND STORE IN MEMORY
D019 2B                  DCX   H              ;DECREMENT MEMORY ADDRESS
D01A 05                  DCR   B              ;DECREMENT NUMBER OF BYTES
D01B C2 0A D0            JNZ   CONT           ;INPUT LSB
D01E 0D                  DCR   C              ;ELSE, DECREMENT NO. OF ADDRESSES
D01F CA 28 D0            JZ    NEXT           ;DONE WITH INPUT IF ZERO
D022 21 96 D0            LXI   H,PEND+1       ;LOC. OF MSB OF ENDING ADDRESS
D025 C3 05 D0            JMP   AGAIN          ;INPUT ADDRESS
D028            ;;;;;;;;;;;;;;;;;;;;;;;;;;;;;;;;;;;;;;;;;;;;;;;;;;
D028            ; THE NUMBER OF LOCATIONS IN THE BLOCK
D028            ;IS CALCULATED
D028            ;;;;;;;;;;;;;;;;;;;;;;;;;;;;;;;;;;;;;;;;;;;;;;;;;;
D028 11 02 00   NEXT:    LXI   D,0002         ;OFFSET FOR 2'S COMPLEMENT ADD.
D02B 2A 93 D0            LHLD  MAIN           ;LOAD H,L WITH STARTING ADDRESS
D02E 7C                  MOV   A,H            ;MOVE MSB TO A
D02F 2F                  CMA                  ;COMPLEMENT IT
D030 67                  MOV   H,A            ;STORE MSB
D031 7D                  MOV   A,L            ;DO THE
D032 2F                  CMA                  ;    SAME WITH
D033 6F                  MOV   L,A            ;        THE LSB
D034 19                  DAD   D              ;ADD OFFSET TO STARTING ADDRESS
D035 EB                  XCHG                 ;STORE IN D,E
D036 2A 95 D0            LHLD  PEND           ;LOAD H,L WITH ENDING ADDRESS
D039 19                  DAD   D              ;TOTAL NUMBER OF LOCATIONS IN BLOCK
D03A EB                  XCHG                 ;STORE IN D,E
D03B            ;;;;;;;;;;;;;;;;;;;;;;;;;;;;;;;;;;;;;;;;;;;;;;;;;;
D03B            ; THE CONTENTS OF THE BLOCK IS SUMMED
```

Figure B-4. "CKSUM" Microcomputer Program.

```
D03B                    62      ;#########################################
D03B 2A 93 D0           63              LHLD MAIN       ;START AT BEGINNING ADDRESS
D03E EB                 64              XCHG            ;PUT IT IN D,E
D03F 06 00              65              MVI  B,00       ;STORES SUM OF MACHINE CODES
D041 1A                 66      ADDIT:  LDAX D          ;LOAD THE BYTE AT THE ADDRESS
D042 80                 67              ADD  B          ;AND ADD IT TO THE SUM
D043 47                 68              MOV  B,A        ;STORE SUM
D044 13                 69              INX  D          ;INCREMENT ADDRESS POINTER
D045 2B                 70              DCX  H          ;DEC. NO. OF BYTES IN PROGRAM
D046 7D                 71              MOV  A,L        ;CHECK TO SEE IF
D047 B4                 72              ORA  H          ;    ALL DONE ADDING
D048 C2 41 D0           73              JNZ  ADDIT      ;ELSE, KEEP ADDING
D04B                    74      ;#########################################
D04B                    75      ; THE HEX SUM IS DISPLAYED
D04B                    76      ;#########################################
D04B 78                 77              MOV  A,B        ;MOVE FINAL SUM TO A
D04C F5                 78              PUSH PSW        ;SAVE FINAL SUM
D04D 1F                 79              RAR
D04E 1F                 80              RAR
D04F 1F                 81              RAR
D050 1F                 82              RAR
D051 E6 0F              83              ANI  0FH        ;GET JUST MSB
D053 FE 0A              84              CPI  0AH
D055 DA 5A D0           85              JC   FIRST
D058 C6 07              86              ADI  07         ;ADD 37H IF DIGIT > 9
D05A C6 30              87      FIRST:  ADI  30H        ;ELSE, ADD 30H
D05C CD 86 D0           88              CALL CRLF       ;CR AND LF
D05F CD 3B 00           89              CALL CHOW       ;OUTPUT MOST SIG. DIGIT OF SUM
D062 F1                 90              POP  PSW        ;RESTORE FINAL SUM TO A
D063 E6 0F              91              ANI  0FH        ;GET JUST LSB
D065 FE 0A              92              CPI  0AH
D067 DA 6C D0           93              JC   SECOND
D06A C6 07              94              ADI  07
D06C C6 30              95      SECOND: ADI  30H
D06E CD 3B 00           96              CALL CHOW
D071 C3 92 00           97              JMP  0092H      ;JUMP TO SYSTEM MONITOR
D074                    98      ;#########################################
D074                    99      ; SUBROUTINE TO READ THE INPUT FROM
D074                   100      ;THE CONSOLE, AND ECHO IT BACK
D074                   101      ;#########################################
D074 CD 3F 00          102      READVAL: CALL CHOR      ;GET INPUT
D077 E6 7F             103              ANI  7FH        ;MASK OFF BIT 7
D079 CD 3B 00          104              CALL CHOW       ;ECHO INPUT TO CONSOLE
D07C FE 3A             105              CPI  3AH        ;IF INPUT IS NUMERAL, SUBTRACT
D07E D2 83 D0          106              JNC  RETU       ;     30H FROM ASCII REP.
D081 C6 07             107              ADI  7
D083 D6 37             108      RETU:   SUI  37H        ;ELSE, SUBTRACT 37H
D085 C9                109              RET
D086                   110      ;#########################################
D086                   111      ; SUBROUTINE TO OUTPUT A CARRIAGE
D086                   112      ;RETURN AND A LINE FEED
D086                   113      ;#########################################
D086 F5                114      CRLF:   PUSH PSW
D087 3E 0A             115              MVI A,0AH
D089 CD 3B 00          116              CALL CHOW       ;OUTPUT CARRIAGE RETURN
D08C 3E 0D             117              MVI A,0DH
D08E CD 3B 00          118              CALL CHOW       ;OUTPUT LINE FEED
D091 F1                119              POP  PSW
D092 C9                120              RET
D093                   121      ;
D093                   122      MAIN:   DS   2          ;LOCATION OF MAIN
D095                   123      PEND:   DS   2          ;LOCATION OF PEND
D097                   124      ;
D097                   125              END

R# T=0.03/0.19 12:40:24
```

Figure B-4. Continued.

APPENDIX C

MICROCOMPUTER HARDWARE

A description is given of each piece of equipment necessary for the implementation of the Micro-DFCS.

Housing Unit

The unit designed to house and provide power to the microcomputer boards during ground testing is pictured in Figure C-1. This rear view shows the boards along with various connections for peripheral devices. For flight, the computer boards are transferred to an RF-shielded, shock-mounted Flight Control Computer Unit (FCCU).

Monolithic MSC 8004 Single Board Computer

At the heart of the Micro-DFCS is the MSC 8004 central processing board (Figure C-2). This board contains the Zilog Z-80A microprocessor which operates at 4.0 MHz with 8-bit data words (or bytes). The microprocessor allows for 158 different instructions--with a minimum instruction time of 1.0 μsec--and is compatible with the popular Intel 8080 instruction set. Additionally, the chip contains 17 storage registers. Besides the Z-80A, the MSC 8004 contains a substantial amount of memory: 32K (32,768) bytes of RAM and up to 16K (16,384 bytes) of PROM. Other features of the board include: three 16-bit 8253 programmable timers; two 8255 programmable peripheral interfaces, providing a total of 48 parallel I/O lines; an 8214 interrupt controller; an 8251 USART for serial transmission; and an edge connector for interface with the Intel Multibus™.

Although not used during the investigation, the Am 9511 Arithmetic Processing Unit (APU) also is included on the MSC 8004. If operating at 4 MHz, the APU performs math operations twice as fast as the Intel 310

Math board--the unit used during the present work. The APU also provides for trigonometric, logarithmic, and exponential functions. The APU was not incorporated in the current Micro-DFCS because verification tests of its clock and distinct programming format had not been completed.

Intel iSBC 310 High-Speed Math

The iSBC 310 Math board (Figure C-3) reduces the computational time between sampling instants during Micro-DFCS operation. The board performs 14 arithmetic functions an order of magnitude faster than software routines. The functions performed in CAS-6, along with the typical execution time in parenthesese, follow: fixed-to-floating point (84 μsec), floating-to-fixed point (42 μsec), floating point multiply (84 μsec), floating point addition and subtraction (each 33 μsec), and floating point test (7 μsec). In addition to the execution times presented, it typically takes 90 μsec to pass the arguments to the math board and, subsequently, read the result.

Intel iSBC 732 Combination Analog I/O

The iSBC 732 (Figure C-4) is used to interface the VRA's FBW system with the Micro-DFCS. Electric signals from the aircraft's sensors are converted for use in the digital control law and then reconverted for output to the control surfaces. The iSBC 732 has 16 single-ended analog input channels (expandable to 32) for A/D conversion and two D/A converters. The board has a 12-bit resolution capability and a ±10-volt range.

Intel iSBC 724 Analog Output

Augmenting the iSBC 732 is the iSBC 724 Analog Output board (Figure C-5). The board contains 4 D/A converters, also using 12-bit resolution and a ±10-volt range.

Intel iSBC 094 Battery RAM

The iSBC 094 (Figure C-6) board contains 4K (4096 bytes) of RAM that can be jumpered to start at any 4K memory address boundary. After removal

of the 5-volt system power, the on-board RAM remains intact for at least 96 hours because of an on-board rechargeable battery. This feature enables the transfer of memory from the ground-based microcomputer unit to the FCCU used in flight.

Termiflex HT/4 Handheld Control Display Unit

The HT/4 CDU provides the interface between the test pilot and the Micro-DFCS. The unit, operating at a 1200-baud rate, accepts and displays all ASCII characters; however, a two-stroke input is required and the display is limited to two 12-character lines.

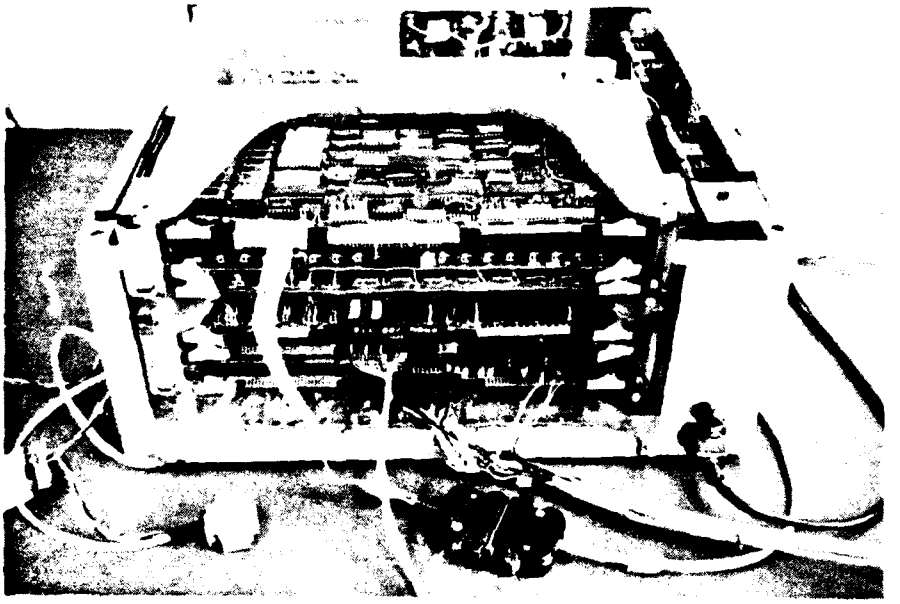

Figure C-1. Rear View of Microcomputer.

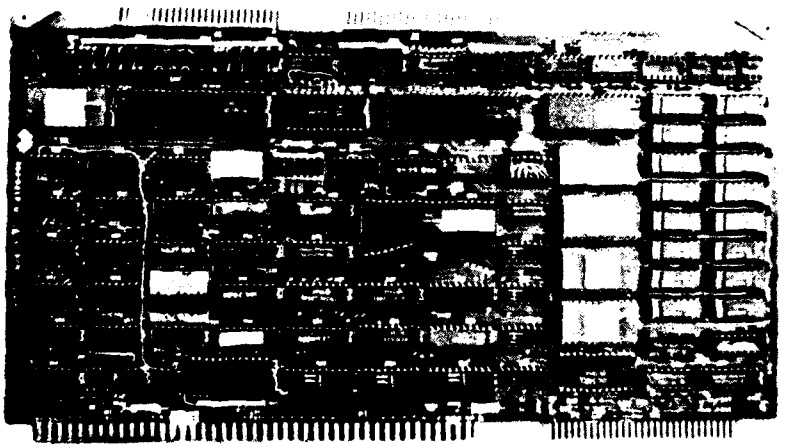

Figure C-2. MSC 8004 Single Board Computer.

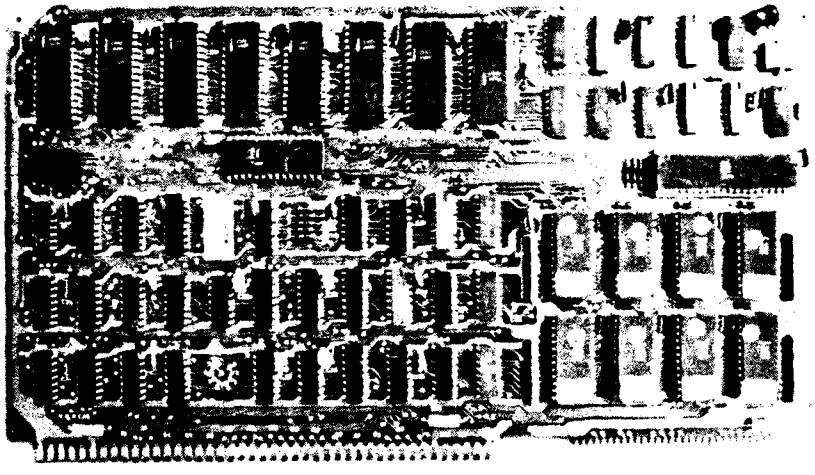

Figure C-3. iSBC 310 High-Speed Math.

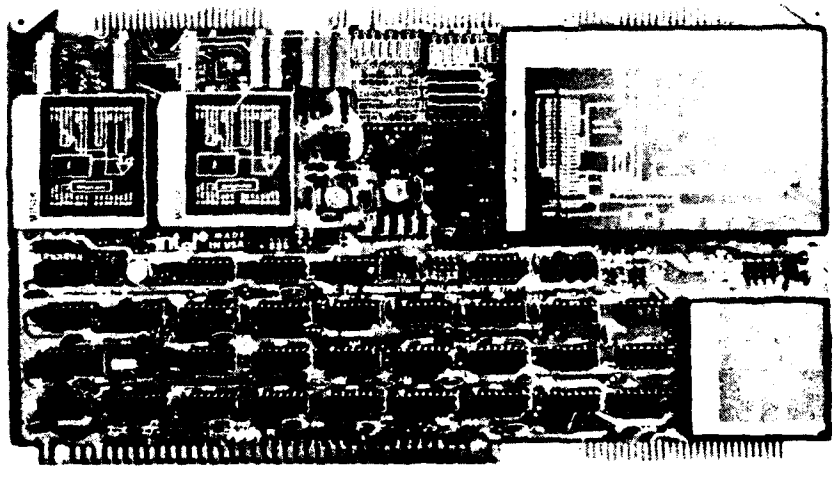

Figure C-4. iSBC 732 Combination Analog I/O.

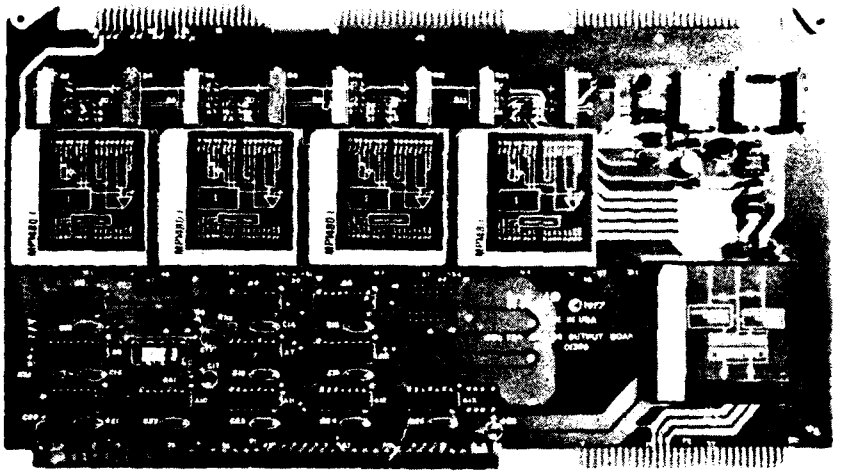

Figure C-5. iSBC 724 Analog Output.

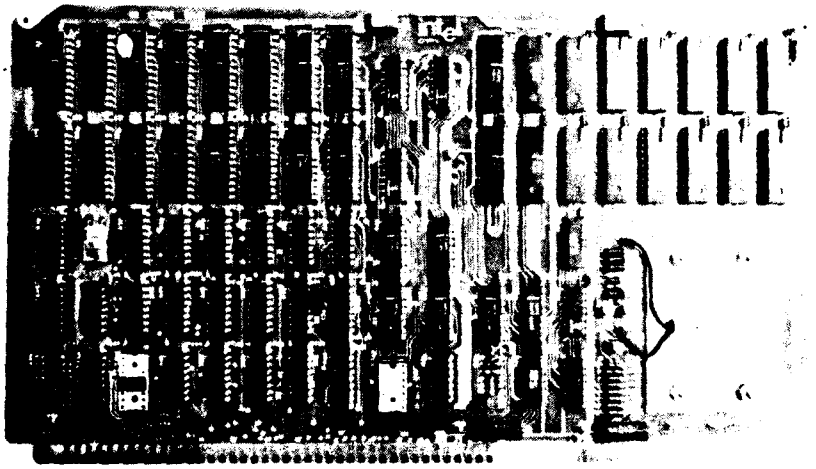

Figure C-6. iSBC 094 Battery Ram.

APPENDIX D

VALUES USED DURING INVESTIGATION

This Appendix is a source for the parameters (scaling, conversions, etc.) encountered during this Micro-DFCS research. Table D-1 depicts the final values.

Table D-1. Pertinant Data

VRA

Stability and Control Derivitives	see Table 2-1
Actuator Dynamics	see Table A-1

TELEMETRY CALIBRATIONS

Signal	Channel	Gain	Scaling
r	4, [illegible]	.659	1V = 5°/s
β	2,24	.420	1V = 5°
P	3,25	.789	1V - 5°/s
ϕ	10,32	.690	1V = 10°
n_y	18	1.22	1V = .1g
δR	14	.809	10V = full deflection
δSF	15	.903	"
δA	37	1.00	"
δP	5,27	.937	"
δS	1,23	.867	"

Table D-1. Pertinant Data (con't)

FILTERS (First Order, Low-pass)

Sensor	τ (sec)
δT	.181 (with C = .3μF)
r	.0188
β	.020
p	.0225

A/D CONVERSIONS

Sensor	Value	Sign Convention (+)
r	- 3.686 deg/sec/V	right
β	+ 2.867 deg/V	trailing edge left
P	+ 4.460 deg/sec/V	right
ϕ	-12.019 deg/V	"
δP	-17.43 deg/full deflection	"
δT	+16.14 "	"
δS	+18.00 "	"

D/A CONVERSIONS

Sensor	Value	Sign Convention (+)
δR	.524 V/deg	trailing edge left
δSF	-.287 "	"
δA	.513 "	right up

AD-A119 084 AIR FORCE INST OF TECH WRIGHT-PATTERSON AFB OH F/G 1/3
COMMAND AUGMENTATION INCORPORATING DIRECT SIDE FORCE CONTROL AN--ETC(U)
MAY 82 S L GRUNWALD
UNCLASSIFIED AFIT/CI/NR/82-39T NL

REFERENCES

1. Stengel, R. F., Seat, J. C., and Miller, G. E., "Digital Flight Control Research Using Microprocessor Technology", ONR-CR-300-003-1, 23 May 1980.

2. Atzhorn, D., "Digital Command Augmentation for Lateral-Directional Aircraft Dynamics", ONR-CR-300-003-2, May 1981.

3. Binnie, W. B. and Stengel, R. R., "Flight Investigation and Theory of Direct Side-Force Control", Journal of Guidance and Control, Vol. 2, No. 6, Dec 1979, pp. 471-478.

4. Jenkins, M. W. M., "Direct Side Force Control for STOL Transport Aircraft", AIAA Paper No. 73-887, Aug 1973.

5. Mercier, D. and Duffy, R., "Application of Direct Side Force Control to Commercial Transport", AIAA Paper No. 73-886, Aug 1973.

6. Sammonds, R. I. and Brunnel, J. W., Jr., "Flying Qualities Criteria for Wings-Level-Turn Maneuvering During an Air-to-Ground Weapon Delivery Task", AIAA Paper No. 80-1628, 1980.

7. Ramage, J. K. and Swortzel, F. R., "Design Considerations for Implementing Intergrated Mission-Tailored Flight Control Modes", in The Impact of Integrated Guidance and Control Technology on Weapons System Design, AGARD-CP-257, Dec 1978, pp. 16-1 to 16-18.

8. Stein, G., Hartmann, G. L., and Hendrick, R. D., "Adaptive Control Laws for the F-8 Flight Test", IEEE Transactions on Automatic Control, Vol. AC-22, No. 5, Oct 1977, pp. 758-767.

9. Carlson, E. P., "Direct Side Force Control for Improved Weapon Delivery Accuracy", AIAA Paper No. 74-70, Aug 1974.

10. Brulle, R. U., Moran, W. A., and Marsh, R. G., "Direct Side Force Control Criteria for Dive Bombing, Volume I - Summary", AFFDL-TR-76-78, Volume I, Sep 1976.

11. Marti, V. M., and Greenquist, S. P., "AFTI-15 Predesign and Preliminary Development of DFCS and HAC-Phase I", AFFDL-TR-79-3017, Part II, Vol. 2, April 1978.

12. Hall, G. W., "A Flight Test Investigation of Direct Side Force Control", AIAA Paper No. 72-94, Jan 1972.

13. Fink, Donald E., "Improved Fighter Capabilities Sought", Aviation Week, July 4, 1977, pp. 56-60.

14. Anon., "Flying Qualities of Piloted Airplanes", MIL-F-8785B(ASG), 7 Aug 1969.

15. Hoh, R. H., Myers, T. T., Ashkenas, I. L., et al., "Development of Handling Qualities Criteria for Aircraft with Independent Control of Six Degrees of Freedom", AFWAL-TR-81-3027, April 1981.

16. Ellis, D. R., and Raisinghani, S. C., "An In-Flight Simulator Investigation of Roll and Yaw Control Power Requirements for STOL Approach and Landing: Development of Capability and Preliminary Results", MAE 1422, Princeton University, April 1979.

17. Fernand, J. M., "Determination of the Stability and Control Derivatives for the Variable-Response Research Aircraft Using a Modified Maximum Likelihood Estimator", M.S.E. Thesis, Princeton Report No. MAE 1401-T, Sept 1978.

18. Dorato, P. and Levis, A. H., "Optimal Linear Regulators: The Discrete-Time Case", IEEE Transactions on Automatic Control, Vol. AC-16, No. 6, Dec 1971, pp. 613-620.

19. Atzhorn, D. and Stengel, R. F., "Design and Flight Test of Lateral-Directional Command Augmentation System", AIAA Paper No. 81-2331, 1981.

20. Blakelock, J. H., Automatic Control of Aircraft and Missiles, John Wiley & Sons, Inc., New York, 1965.

21. Stengel, R. F., "Equilibrium Response of Flight Control Systems", Proceedings of the 1980 Joint Automatic Control Conference, San Francisco, Aug 1980.

22. McRuer, D., Ashkenas, I., and Graham, D., Aircraft Dynamics and Automatic Control, Princeton University Press, 1973.

23. Tyler, J. S., Jr., "The Characteristics of Model-Following Systems as Synthesized by Optimal Control", IEEE Transactions on Automatic Control, Vol. AC-9, No. 4, Oct 1964.

24. Gran, R., Berman, H., and Ross, M., "Optimal Digital Flight Control for Advanced Fighter Aircraft", Journal of Aircraft, Vol. 14, No. 1, Jan 1977, pp. 32-37.

25. Stengel, R. F., "Digital Flight Control Design Using Implicit Model Following", AIAA Paper No. 73-844, Aug 1973.

26. Lebacqz, J. V., and Aiken, E. W., "Optimal Control Techniques for V/STOL Flight Experiment Design", Proceedings of the 1976 IEEE Conference on Decision & Control, Dec 1976, pp. 1017-1022.

27. Stengel, R. F., Broussard, J. R., and Berry, P. W., "Command Augmentation Control Laws for Maneuvering Aircraft", AIAA Paper No. 77-1044, Aug 1977.

28. Stengel, R. F., Broussard, J. R., and Berry, P. W., "Digital Controllers for VTOL Aircraft", IEEE Transactions of Aerospace and Electronic Systems, Vol. AC-22, No. 10, Oct 1977, pp. 758-767.

29. Stengel, R. F., "In-Flight Simulation with Pilot-Center of Gravity Offset and Velocity Mismatch", Journal of Guidance and Control, Vol. 2, No. 6, Nov-Dec 1979, pp. 538-540.

30. Erzberger, H., "Analysis and Design of Model Following Control Systems by State Space Trajectories", Proceedings of the 1968 Joint Automatic Control Conference, June 1968, pp. 572-581.

31. Ben-Israel, A. and Greville, T. N. E., Generalized Inverses: Theory and Applications, J. Wiley and Sons, New York, 1974.

32. Kwakernaak, H., and Siran, R., Linear Optimal Control Systems, J. Wiley & Sons, New York, 1972.

33. Van Dierendonck, A. J., Wynne, M., and Druczynski, L., "An Optimal Model-Following Flight Control System for Manual Control", Thirteenth Joint Automatic Control Conference of the American Automatic Control Council, Stanford, Aug 16-18, 1972, pp. 25-32.

34. Graham, D. and Lathrop, R. C., "The Synthesis of Optimum Transient Response: Criteria and Standard Forms", Transactions of the AIEE, Vol. 72, part II, Nov 1953, pp. 273-288.

35. Broussard, J. R., Berry, P. W., and Gully, S. W., "Synthesis of Digital Controllers for Fighter Aircraft Using Continuous-Time Specifications", Proceedings of the Flight Control Systems Criteria Symposium, Naval Postgraduate School, Monterey, July 1978, pp. 91-111.

36. Harper, R. P., Jr. and Cooper, G. E., "The Use of Pilot Rating in the Evaluation of Aircraft Handling Qualities", NASA TND-5153, April 1969.

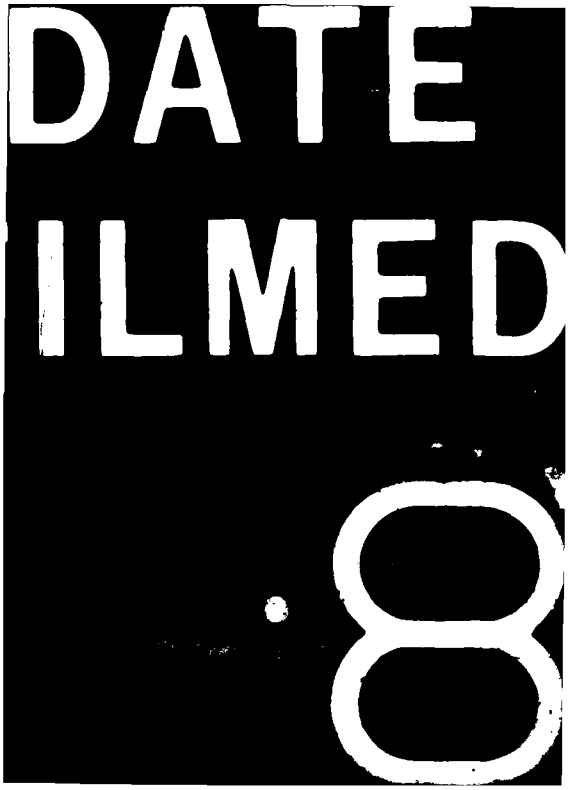
DATE
ILMED
8